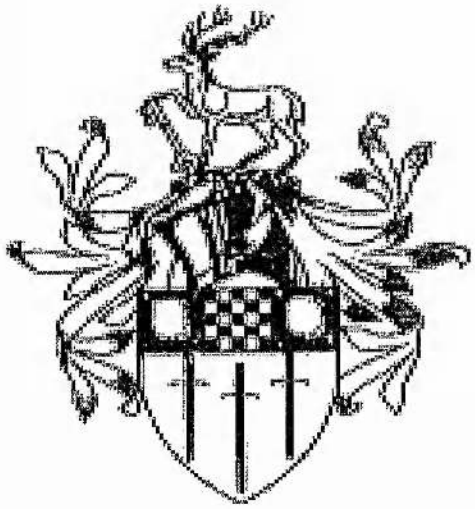

University of Surrey

A Study of Damage Accumulation in a Knitted Fabric Reinforced Composite

by

Carlos Rolando Rios Soberanis

A thesis submitted to the University of Surrey in partial fulfilment of the requirements of the degree of Doctor in Philosophy

The opinions expressed and conclusions reached are those of the author and are not necessarily endorsed by the Department.

March 2002

This work is dedicated to Lupita, Aaron, Christina and Daniela
With all my love because you are the four pillars of my life.
Thank you so much.

ACKNOWLEDGEMENT

I want to express my thanks to the Consejo Nacional de Ciencia y Tecnología (CONACyT) for supporting me with the scholarship 116476/117581.

My thanks go to Dr. K. H. Leong of the Cooperative Research Centre for Advanced Composite Structures Ltd, Australia for supplying the knitted reinforcement and additional papers.

My special gratitude for my supervisors, Dr. Steve L. Ogin, for his support, guidance and suggestions and without whom there would be no project and Constantina Lekakou for her friendship and valuable comments during the realization of this work.

I would like to express all my gratefulness to Reg Wattingham, for spending most of his time in this project; and Mike Parker, for his patience in teaching me some interesting techniques.

Finally, I want to express my sincere thanks to people who work indefatigable doing the administrative labour to ensure the high quality of the students' life. To Derek, Margaret, Shirley, Penny, Julie and Dave a big thank you very much.

ABSTRACT

The use of knitting technology with advanced fibres such as glass, carbon and aramid, to produce near-net-shape fabrics has in recent years received increasing interest from the composite materials community. Knitted fabrics have the potential of being used in engineering structures with complex shapes in conjunction with a suitable liquid moulding technique, such as Resin Transfer Moulding (RTM), due to their excellent drapeability and manufacturability.

During previous studies in textile reinforced composites, an intimate relationship between the fabric architecture and the damage development has been demonstrated. In this work, the quasi-static tensile loading deformation behaviour and the relation between the fabric architecture and damage development have been studied for a weft knitted glass fabric.Tensile properties have been examined and the failure mechanisms have been identified experimentally by analysing the damage process in-situ with a camera and by studying fracture surfaces using scanning electron microscopy (SEM). The acoustic emission technique was used to support the microscopic analysis .

The work has investigated the tensile properties and failure mechanisms of three knitted fabric reinforced composite laminates reinforced with a Milano weft knitted glass fabric. The three composites were (i) a single layer of fabric reinforcing epoxy resin, (ii) a single knitted fabric layer sandwiched between 0^{o} glass fibre unidirectional plies (again with the glass reinforcing epoxy resin), and (iii) the same knitted glass fabric but this time used as the reinforcement in commercially produced high fibre volume fraction composites (using the RTM technique).

The variation of mechanical properties with angle (from wale to course) has been measured for the single layer of the fabric reinforcing epoxy resin by orientating the wale direction of the fabric at different angles. Mechanical properties have been measured for each angular orientation and comparisons were made between them, especially with regard to the planes of final failure.

The single layer composites failed as soon as the first damage was initiated. Hence, to investigate damage accumulation, a novel technique was employed to manufacture a sandwich laminate, which consisted in placing a single knitted fabric layer between 0^{o} glass fibre unidirectional plies. The success of this method is that the accumulation of damage in the knitted architecture was allowed to be studied and some characteristics of crack initiation and crack propagation could be related to the fabric geometry and structure.

Experiments on these model transparent materials have been complemented by tests on two types of commercial knitted fabric composite manufactured by the RTM process. Characterization of these materials under tensile loading has been carried out for monotonic and cyclic loading and the results have been compared with those found for the single layer and the sandwich model material. Various failure mechanisms such as cracking at loop cross-over points, resin matrix cracking, fibre bundle debonding and tensile fracture of fibre bundles in failed specimens were observed. The behaviour of the commercial RTM specimens has been discussed in the light of the results obtained from the model single layer and sandwich specimens.

CONTENTS

ABSTRACT.....I

CONTENTS.....III

CHAPTER 1

INTRODUCTION 1

CHAPTER 2.- LITERATURE REVIEW

2.1.- INTRODUCTION.....3

2.2.- TEXTILE REINFORCEMENTS.....4

2.2.1.- MATS 5

2.2.2.- WOVEN FABRICS.....6

2.2.3.- BRAIDED FABRICS.....7

2.2.4.- STITCHED FABRICS.....8

2.2.5.- KNITTED FABRICS.....10

2.3.- MATRIX CRACKING IN COMPOSITE MATERIALS.....11

2.4.- FIBRE ARCHITECTURE, MECHANICAL BEHAVIOUR AND MODELLING OF KNITTED FABRIC COMPOSITE.....13

2.4.1.- KNITTED FABRIC FIBRE ARCHITECTURE.....13

2.4.2.- MECHANICAL PROPERTIES OF KNITTED FABRIC COMPOSITES.....15
2.4.3.- MODELLING THE PROPERTIES OF UNDAMAGED KNITTED FABRIC COMPOSITES.....19
2.4.4.- DAMAGE ACCUMULATION.....21

2.5.- CONCLUSIONS.....23

FIGURES.....24

CHAPTER 3.- EXPERIMENTAL METHODS

3.1.- INTRODUCTION.....31

3.2.- MATERIALS AND LAMINATE MANUFACTURE.....31
3.2.1.- MANUFACTURE OF TRANSPARENT MODEL KNITTED FABRIC COMPOSITE PANELS.....32

3.3.- SAMPLE PREPARATION FOR MECHANICAL TESTING.....34

3.4.- MECHANICAL TESTING.....35

3.5.- SAMPLE PREPARATION FOR MISCROSTRUCTURAL ANALYSIS.....36

TABLES.....37

FIGURES.....38

CHAPTER 4.- EXPERIMENTAL RESULTS AND DISCUSSION ON THE MODEL MATERIALS

4.1.- INTRODUCTION.....43

4.2.- ARCHITECTURE OF THE KNITTED FABRIC.....44

4.3.- SINGLE LAYER KNITTED FABRIC COMPOSITE PROPERTIES.....45

4.3.1.- MECHANICAL PROPERTIES.....45

4.4.- DAMAGE DEVELOPMENT IN THE MODEL 2X68 TEX SANDWICH COMPOSITES.....47

4.4.1.- MECHANICAL PROPERTIES.....47

4.4.2.- KNITTED FABRIC IN WALE DIRECTION (0°) PARALLEL TO THE 0° PLIES.....48

4.4.3.- KNITTED FABRIC WALE DIRECTON AT 30° TO OUTER PLIES.....50

4.4.4.- KNITTED FABRIC WALE DIRECTON AT 45° TO OUTER PLIES.....51

4.4.5.- KNITTED FABRIC WALE DIRECTON AT 60° TO OUTER PLIES.....52

4.4.6.- KNITTED FABRIC AT 90° TO THE OUTER PLIES.....54

4.5 - COMPARISON OF RESULTS FOR DIFFERENT ANGLES OF THE KNITTED FABRIC IN THE MODEL SANDWICH MATERIAL.....55

4.6.- CYCLIC TESTS OF MATERIALS TO DIFFERENT STRAINS.....58

4.6.1.- CYCLIC LOADING OF SANDWICH LAMINATE SPECIMENS IN WALE DIRECTION (0°) PARALLEL TO THE 0° PLIES.....58

4.6.2.- CYCLIC LOADING OF 0° PLY AND CROSS-PLY COUPONS....60

4.6.3.- COMPARISON OF CYCLIC LOADING TEST RESULTS FOR SANDWICH, UNIDIRECTIONAL AND CROSS-PLY COMPOSITES.....61

4.7.- RESUME AND DISCUSSIONS.....62

TABLES.....65

FIGURES.....68

CHAPTER 5.- EXPERIMENTAL RESULTS AND DISCUSSION ON THE COMMERCIAL MATERIAL (RTM)

5.1. INTRODUCTION.....114

5.2. STRESS-STRAIN RESULTS FOR KNITTED FABRIC COMPOSITES RTM MANUFACTURED 115

5.2.1. KNITTED FABRIC WALE DIRECTION AT 0° TO THE LOADING DIRECTION.....115

5.2.2. KNITTED FABRIC WALE DIRECTION AT 30° TO THE LOADING DIRECTION.....117

5.2.3. KNITTED FABRIC WALE DIRECTION AT 45° TO THE LOADING DIRECTION.....118

5.2.4. KNITTED FABRIC WALE DIRECTION AT -45° TO THE LOADING DIRECTION.....118

5.2.5. KNITTED FABRIC WALE DIRECTION AT 60° TO THE LOADING DIRECTION.....119

5.2.6. KNITTED FABRIC WALE DIRECTION AT 90° TO THE LOADING DIRECTION.....120

5.3. COMPARISON OF RESULTS FOR DIFFERENT ANGLES IN THE RTM MATERIAL.....120

5.4. CYCLIC TESTS OF RTM MATERIALS TO DIFFERENT STRAINS...123

5.4.1. KNITTED FABRIC WALE DIRECTION PARALLEL TO THE LOADING DIRECTION.....123

5.4.2. KNITTED FABRIC WALE DIRECTION AT 30^0 TO THE LOADING DIRECTION.....125

5.4.3. KNITTED FABRIC WALE DIRECTION AT 45^0 TO THE LOADING DIRECTION.....125

5.4.4. KNITTED FABRIC WALE DIRECTION AT -45^0 TO THE LOADING DIRECTION.....125

5.4.5. KNITTED FABRIC WALE DIRECTION AT 60^0 TO THE LOADING DIRECTION.....126

5.4.6. KNITTED FABRIC WALE DIRECTION AT 90^0 TO THE LOADING DIRECTION (LOADING IN THE COURSE DIRECTION).....126

5.5. COMPARISON OF RESULTS FOR CYCLIC TESTS AT DIFFERENT ANGLES IN THE RTM MATERIAL.....127

5.6. CYCLIC TESTS AT FIXED PEAK CYCLIC STRAINS.....129

5.7. DISCUSSION OF THE IMPLICATIONS OF THE CYCLIC TEST DATA.....130

5.8 SUMMARY.....132

TABLES.....134

FIGURES.....137

CHAPTER 6.- RELATIONSHIP BETWEEN FABRIC ARCHITECTURE AND CRACKING DAMAGE DEVELOPMENT

6.1. INTRODUCTION.....169

6.2. DAMAGE DEVELOPMENT IN MODEL SANDWICH LAMINATE MATERIAL.....169

6.3. RELATIONSHIP BETWEEN KNITTED FABRIC ARCHITECTURE, DAMAGE AND COMPOSITE CROSS-SECTIONS FOR THE MODEL SANDWICH LAMINATE MATERIAL.....171

6.4.- RELATIONSHIP BETWEEN KNITTED FABRIC ARCHITECTURE, DAMAGE AND COMPOSITE CROSS-SECTIONS FOR THE RTM MATERIAL.....173

6.5.- SUMMARY.....174

FIGURES.....176

CHAPTER 7.- CONCLUSIONS AND FURTHER WORK

7.1.- CONCLUSIONS.....189

7.2.- FURTHER WORK.....192

REFERENCES.....194

CHAPTER 1
INTRODUCTION

Considerable research has been directed at understanding the behaviour of composites made using textiles in an attempt for these materials to gain wider industrial acceptance. Over the years, the textile manufacturing industry has developed the ability to produce net-shaped fabrics using highly automated techniques such as stitching, weaving, braiding and knitting. In the manufacture of preforms for advanced composite materials, textile technology has been under intensive investigations due to the potential of these materials to produce low-cost high quality structures with improved mechanical performance.

Among these textile techniques, knitting is particularly suited for the manufacture of composites with complex three-dimensional shapes, since structures with complex shapes can be very difficult and expensive to manufacture using standard prepreg or wet lay-up technology. Knitted fabric can be stretched to a high degree and thus can be formed into the desired complex shape prior to resin infiltration to produce the composite component. This advantage of the knitted fabric (i.e. the ability to be shaped) is due to its fibre structure. However, when the fabric is stretched, distortion of the looped fibre architecture in the direction of stretching occurs which may also affect the final performance of the composite component. The highly looped fibre architecture dictates the mechanical properties of the final composite because these properties are greatly affected by the loop length and loop density. Although the knitting loops can be extremely complicated, they always follow a repetitive pattern; hence repetitive volume elements can be identified. It is interesting to observe that different knitting structures will have different degrees of symmetry. The final composite properties are also dependent on factors such as volume fraction that can be altered with the number of fabric layers employed to make the component.

With increasing interest in knitted fabric composites, many investigations have been oriented to analyse the mechanical properties and to compare them with other textile reinforcements. In general, it has been shown that, although knitted fabric composites do not possess the same high tensile properties as many other composites, they have high impact damage resistance; hence they can be considered for crashworthy structural members in automobiles or in the fabrication of elements of protection, such as helmets.

Composites based on knitted fabrics are relatively a new class of composite materials and extensive mechanical analysis has not yet been carried out, particularly in this area of damage development and quantification. It is very important to know the failure process of this kind of composite material in order to predict its behaviour and improve its properties. This project aims to investigate the development of damage in a typical knitted fabric reinforced composite using a model material which enables damage progression to be observed directly. The results are related to additional work carried out on a commercially produced knitted fabric composite.

Some actual analysis and examinations carried out by researchers in the composite field are considered to cover the information available in the literature review. The experimental procedures and the novel method for laminating knitted cloth are also described in detail as well as the results obtained from the experiments carried out.

The structure of the thesis is as follows. In Chapter 2, the literature review presents a brief review of composite materials and a review of work on knitted fabric composites. Chapter 3 considers all the aspects for the manufacturing and the mechanical and microstructural evaluation of the samples of knitted fabric composites. Chapter 4 includes the results and discussion for the damage behaviour obtained for the model material. The results for the engineering material (RTM) and its damage progression and comparisons are discussed in Chapter 5, while detailed information about the crack-structure relationship derived by microscopy evaluation is presented in Chapter 6. Finally, conclusions and further work are shown at the end.

CHAPTER 2

LITERATURE REVIEW

2.1. INTRODUCTION

Composites are formed by the combination of two materials in which one of these materials is named the reinforcing phase, is presented in the form of fibres, sheets, textiles or particles and is embedded in the other material, named the matrix phase. Generally reinforcing materials are strong with low densities while the matrix is usually a ductile or tough material. If the composite is well designed and manufactured correctly, it will combine the strength of the reinforcement with the toughness of the matrix to achieve a combination of desirable properties that are not found in the single conventional material. However, composite materials do not always exhibit their theoretical strength since micro-flaws can be found in them. On the other hand, fibres can show dramatic enhancement in strength compared to the bulk material, therefore composite materials can benefit by the superior properties of these fibres, being protected by the matrix from environmental and physical damage, and allowing the transfer of load to fibres.

Composites can be produced with a wide range of combinations due to the variety of available reinforcement and matrix materials as well as the ability to mix them in a broad range of volume fraction in order to take advantage of the most desirable characteristics of each constituent. Therefore, composite materials offer low density, corrosion resistance and good insulation properties, in addition to high strength and stiffness. They have won wide acceptance in several areas of the industry, from consumer products to space research. Several introductory texts for composite materials can be found in the literature (eg. Daniel and Ishai, 1994; Harris, 1999; Matthews and Rawlings, 1994, amongst others).

This Chapter is divided into two sections. Firstly, a general introduction concerning composite materials reinforced with textiles is presented. Secondly, a broad revision of the mechanical behaviour of knitted fabric composites is discussed. Finally, the comments included will demonstrate the relevance of this specific project in the materials field.

2.2. TEXTILE REINFORCEMENTS

Nowadays the textile industry has developed advanced technologies that allow the fabrication of fabrics with complex structures and geometries which provide them with particular properties. Several factors can interact in the manufacturing of fabrics such as the distribution of fibres in two or three dimensions as well as combinations of different types of fibres in the same textile (named commingled textile). Fabrics can be manufactured by different techniques depending on the architecture they will have at the end. Such techniques lead to knitted, woven and non-woven reinforcements. Material composites reinforced with textiles have been widely investigated in the last three decades and in recent years they have received increasing interest from the composite materials community. Figure 2.1 illustrates some examples in which textile-based composites have been used. Textile technology is becoming highly applied in a wide range of new applications that it is replacing current metal technology in several fields even modifying old traditional composite manufacture processes such as autoclave and pre-pregging. The main reason is the potential of the textile-based composite materials for reducing manufacturing costs and improving processability as well as having minimum material wastage and reducing production time. On the other hand, their mechanical properties can be tailored to increase and improve their engineering performance. In the last years of the 20^{th} century, conferences devoted to composite materials had burgeoning sessions on textile reinforcements (Ogin, 2000).

Among the wide range of fibre reinforcements (mats, braided, stitched, knitted, etc) woven fabrics for polymeric matrices are considered to be an established application, but many others are still the subject of recent research projects. For instance, a knitted glass fabric drawn over a mould and injected with resin (using RTM technique) has been used to manufacture a door component for a helicopter in order to replace the ordinary processing route based on autoclave processing of carbon fibre/epoxy resin pre-preg material (Leong et al, 1997)

Generally, for structural and engineering applications, the main properties which are normally taken into account are stiffness, strength and resistance to damage/crack growth. The intention of the next sections is to give a brief introduction to textile-reinforced composite materials employing several types of reinforcements.

2.2.1. MATS

Mats are non-woven fabrics that provide equal strength in all directions. These fabrics come in two distinct forms: chopped and continuous strand. Chopped mats contain randomly distributed fibres that are held together with a chemical binder. Inherently weaker than continuous strand mats, chopped-strand mats provide low-cost plastic reinforcement. Chopped mat is used primarily in hand lay-up, continuous laminating and some closed moulding applications.

Continuous-strand mat is formed by swirling continuous strands of fibre onto a moving belt. The mat is finished with a chemical binder that holds the fibre in place. Continuous strand mat is primarily used in compression moulding, resin transfer moulding and pultrusion applications as well as to fabricate performs and stampable thermoplastics. Extremely lightweight mats are often used as surfacing veils. Having a very open (non-dense) fibre arrangement, these mats are designed to accept a high ratio of resin to fibre, thereby producing a thick and smooth resin-rich finish (Schaffer, 1999).

2.2.2. WOVEN FABRICS

Woven fabrics are fabricated on looms in a wide variety of weights, weaves and widths. Bi-directional woven fabrics provide good strength in the 0 and 90 degree directions. They also allow faster composite fabrication compared to using two laminates and applying one in each direction. However, woven fabrics provide lower tensile strength than separate unidirectional fibre laminates because fibres are crimped as they pass over and under one another (Marsden, 1996).

Several different weaves are used for bi-directional fabrics. In plain weave, each fill yarn or roving alternately crosses over and under each warp fibre. Other weaves, such as harness satin and basket weave, allow the yarn or roving to cross over and under multiple warp fibres at a time. These weaves tend to be more pliable and conform more easily to curved surfaces. Woven roving is a thick fabric that is used for heavy reinforcement, especially in hand lay-up operations. Due to its relatively coarse weave, woven roving wets quickly and is relatively inexpensive. Exceptionally fine fibreglass fabrics can also be produced. One use for these fine fabrics is for reinforcing printed circuit boards. Hybrid fabrics can be constructed with different glass types, strand compositions or fabric types. For example, high-strength strands of S-type glass or small diameter filaments may be used in the longitudinal direction while less costly strands are woven across the fabric. Alternatively, stitching the two types of fabric together may create a hybrid of woven and mat fabrics.

The mechanical behaviour of composites reinforced with woven fabric is an indication of the properties of the fibre and the fibre architecture (i.e. fibre orientation and distribution). For example, Raju et al (1990) found a reduction in the modulus for carbon/epoxy laminates moving from 8-harness (73 GPa) to 5-harness (69 GPa). The tensile strengths presented in woven composites are also slightly lower than that exhibited by the nonwoven equivalents. Bishop (1989) made comparisons between woven composites and unidirectional equivalent laminates and found a reduction in the tensile strength of 23%. On the other hand, glass reinforced woven fabrics display lower mechanical properties compared with carbon fibres due to the lower value in the modulus for glass fibres.

Fujii et al (1993) cited Young's modulus and tensile strength values for a plain weave glass/polyester (V_f=33%) of 17 GPa and 231MPa, respectively, while Boniface et al (1993) reported similar values for an eight-harness glass/epoxy composite, i.e. 19 GPa and 319 MPa respectively (V_f=37%).

Under tensile loading of woven fabric reinforced composites damage development is characterised by matrix cracking in the off-axis tows at strain well above about 0.3-0.4% (a description of matrix cracking is given later, section 2.3). The majority of investigations performed on damage development have considered biaxial fabrics loaded in the warp direction. In the woven fabric, weft bundles act as initiation sites and when the load or strain is increased, the density of cracks is augmented; this can sometimes strongly resemble the 90 ply cracks which are presented in cross-ply laminates (Marsden, 1996). The Young's modulus reflects the accumulation of cracks in the composite material by a gradual decrease in its value. In carbon woven composites the matrix cracking can lead to considerable delamination in the region of the crimps in adjacent tows which subsequently reduce the mechanical properties (Gao et al, 1999a).

2.2.3. BRAIDED FABRICS

Braided materials are generally more expensive than woven materials due to a more complex manufacturing process. However, braided fabrics typically offer greater strength per fabric weight. The strength comes from three or more yarns intertwined with one another without twisting any two yarns around each other. Braids are continuously woven on the bias and have at least one axial yarn that is not crimped in the weaving process. This arrangement of yarns allows for highly efficient load distribution throughout the braid (Furness, 1999). Either flat or tubular configurations are available as braids. Flat braids are used primarily for selective reinforcement, such as strengthening specific areas in pultruded parts. Tubular braid can be pultruded over a mandrel to produce hollow cross sections in a variety of parts such as windsurfer masts and lamp and utility poles. Due to decreasing manufacturing costs, braiding is becoming more competitive with other fabrics.

For example, Naik et al (1994) tested a two-dimensional carbon fibre braided /epoxy composite manufactured with a number of fibre architectures while the fibre volume fraction was kept constant (V_f = 56%) overall. They observed that a modest increment in longitudinal modulus (from 60 GPa to 63 GPa) occurred in moving from a braid architecture of (0/±70) to (0/±45), with a much larger fall in the transverse modulus (from 46 GPa to 19 GPa)

It seems that no studies of damage accumulation in braided fabric composites exist yet in the literature. However their energy-absorbing characteristic makes them very attractive to be used as composites reinforcement. Therefore they can be used specially in energy absorbing structures for crash situations due to their ability to be tailored in order to increase their absorbing capabilities (Herszberg et al, 1997).

2.2.4. STITCHED FABRICS

The basic promise of stitched fabrics is to put the glass fibres exactly where they are needed. These fabrics are created by placing yarns into the desired alignment and stitching them together. This process allows great flexibility in yarn alignment because the yarns can be laid in practically any arrangement, including orienting all strands in one direction. Moreover, the proportion of yarn in any direction can be selected at will (Spencer, 1998).

Because the yarns lay on top of each other rather than crossing over and under one another, more of the yarn's inherent strength is utilised. The absence of fibre crimping also creates a more pliable fabric than would normally be achieved by a similar weight woven fabric. Due to the wide variety of yarn orientations and fabric weights, stitched fabrics can be tailored to particular requirements. Stitched fabrics have been widely used preferentially in making composites with a defined geometry in order to increase energy-absorption capacity.

Stitching composites are seen as a direct approach to improve the through-the-thickness strength of the materials in order to improve the mechanical properties. Eventually, significant enhancement will be observed in their damage tolerance and particularly the compression after impact behaviour, where the material fails due to micro-buckling in the vicinity of a delamination. In its simplest form, stitching adds one further production step with the use of a sewing machine to introduce lock stitches in the through-thickness. The stitching can be applied on unimpregnated fibres or fibres in the pre-preg form, although the later is generally avoided due to excessive fibre damage. By this way, stitching can be manufactured with carbon, glass or aramid fibre yarns (Ogin, 2000). In their more sophisticated form, chain or tricot stitches can be employed to fabricate a fabric consisting of warp (0°), weft (90°) and (optionally) bias ($\pm\theta$) yarns which are held together by the warp-knitted stitches that usually consist of a light polyester yarn. At the end, the resulting fabric is called a non-crimp fabric (NCF) or a multiaxial warp-knit fabric (MWK).

An advantage of the NCF is that its mechanical properties are superior to the equivalent fibre volume fraction of woven roving reinforcement material. For instance, it was found that the Young's modulus and the tensile strength of a biaxial NCF glass reinforced polyester, V_f = 33%, was 21 GPa and 264 MPa respectively which are values some 13% and 20% higher than those found for a plain woven reinforced composite of equivalent fibre volume fraction (see section 2.2.2. above). On the other hand, concerning damage development, non-crimp fabric laminates seem to behave very similarly to laminates based on unidirectional fibres due to the fibres in each layer of the non-crimp fabric laminate being parallel. However, there is some evidence to show that matrix cracking preferentially initiates at the inter-loops of the knitted yarn which holds the fabric together (Ogin, 2000).

2.2.5. KNITTED FABRICS

In the textile industry there is a large range of reinforcement structures that can be classified as knitted which can be employed in the composites manufacture. In general, these fabric architectures may differ in appearance but they are all made up of interlocking loops of yarn. Knitted fabric possess excellent drapability that makes them to be considered in the manufacture of composite parts of complex shapes (e.g. parts with double curvatures) without excessive cutting, joining and post-consolidation machining (Figures 2.2 and 2.3). Knitted fabric reinforced composites can be manufactured by almost all traditional processes such as lamination, resin transfer moulding (RTM) and pultrusion. The tailorability of these composites is varied and depends on the knitted fabric type and architecture to suit specific structural requirements. The fabric themselves are normally manufactured through modern techniques developed by the textile industry and several knitting geometry configurations are possible to achieve. Since the fabric yarns are oriented in a repeating series of intermeshing loops, the direction of the fibres is changing continuously in three dimensions. Therefore, the fibre volume fraction is relatively low in the whole composite due to large matrix regions which cannot be avoided during the manufacture processes. Most of the knitted fabric reinforced composites are based on either thermoset or thermoplastic rigid polymer matrices; however some studies (e.g. Ramakrishna et al, 1999) have been carried out using elastomers.

The major manufacturing advantages of knitted fabric reinforced composites, then, are the possibility of producing net-shape/near-net-shape preforms, on the one hand, and the exceptional drapability/formability of the fabric which allows for forming over shaped tools of complex shape, on the other. However, the advantages which the knitted fabric architecture brings also lead to disadvantages, namely reduced in-plane stiffness and strength of the composites due to the relatively poor use of the mechanical properties of the fibres (glass, carbon or aramid) (Ogin, 1998).

The material used in this work is a knitted fabric composite and so it is appropriate to discuss the fibre architecture and mechanical properties of knitted fabric composites in some detail. However, an important feature of the behaviour of the knitted fabric composites is the development of matrix cracking damage. Hence, before turning to the properties of knitted fabric composites, a brief review is given in the next section of matrix cracking and its effect on composite properties.

2.3. MATRIX CRACKING IN COMPOSITE MATERIALS

In recent years, matrix cracking has received the most attention among the various types of damage which can be presented in composite materials. Matrix cracking occurs in materials due to the overloading in tension, fatigue cycling, thermal cycling or bending and it is observed in all types of conventional composite laminates which contain off-axis plies. In many structural applications, matrix cracking is the first type of damage presented at a stress raiser, such as a notch, or an impact damage site. In some components such as vessels and pipes it can lead directly to component failure since linkage of intra and inter-laminar matrix cracking paths can lead to weepage. On the other hand, the strain magnification local to the cracks can lead to premature fibre fracture in adjacent plies. Matrix cracking is of particular importance in this work since this type of failure is present in a wide variety of textile fabric reinforced composites. Therefore, it is important to point out the main experimental observations on matrix cracking, and to begin by discussing matrix cracking in laminates with simple fibre architecture, such as cross-ply laminates made from unidirectionally reinforced composite plies.

Generally, as observed in transverse ply, matrix cracking is the first type of failure to occur under both tensile static and fatigue loading in a multi-directional laminate. In these laminates, the strain at which the cracking initiates is affected by factors such as the transverse ply thickness and stiffness of the neighbouring plies. The crack density (number of cracks per length) increases when the applied laminate stress or number of cycles under fatigue loading is augmented, and eventually it reaches a saturation density at high stresses or long fatigue life.

Fibre/matrix debonding is considered to be the cause of transverse ply cracking which is improved by strain magnification in the matrix between fibres to an extent which depends on the separation of the local fibres. At higher strains, the debonds link up to form a flaw, which subsequently develops into transverse ply crack spanning the fill thickness of the transverse ply and width of the laminate. Boniface (1989) has shown, for example, crack initiation begins at the edge and the crack grows across the laminate as the applied stress is increased. Such cracks are generally observed in regular spacingand the increment in the density up to a characteristic limiting value is normally about the same as the thickness of the ply. At further stresses, near to fracture, damage evolves in additional failure mechanisms such as longitudinal cracks (or splits) followed by micro delaminations at the intersections of transverse and longitudinal cracks (Chareweicz, and Daniel, 1986).

The properties of the 90° ply and subsequently of the whole composite are seriously affected by transverse matrix cracking. In fact, many of the mechanical parameters of the laminate are affected such as Young's modulus, Poisson's ratio, coefficient of thermal expansion, residual strain and bending stiffness (Ogin, 1999). Most of the studies on the effects of matrix cracking on composite properties have been concerned with laminates based on unidirectionally reinforced plies and few studies have focused on textile composite materials. However, Gao et al (1999a) used a woven CFRP material and it is important to summarise briefly here the results for the changes in Young's modulus, Poison's ratio and residual strain as a consequence of matrix cracking damage.

Gao et al (1999a) tested woven fabric CFRP laminates under quasi-static loading and observed matrix cracking initially in the crimp regions of the laminates, followed by delaminations near the crimps. The damage accumulation was monitored by using detailed microscopy combined with dye-penetrant X-radiography and acoustic emission and it was related to the applied strain. The Young's modulus of the CFRP laminates was dominated by the 0^0 plies, so that the modulus was insensitive to accumulating matrix cracks in the 90^0 direction.

It is important to mention that investigations carried out by Marsden (1996) on GFRP laminates have shown that the Young's modulus of woven glass fibre fabric laminates reduces the same way as in cross-ply laminates, as matrix cracks accumulate. The Poisson's ratio observed in woven fabric GFRP laminates, however, reduced by up to 30% in a six-layer laminate when loaded to a strain near to failure. Smith and Wood (1990) obtained similar results concerning the changes in Poisson's ratio with increasing crack density for GFRP cross-ply laminates. Finally, woven fabric GFRP laminates tested by Gao et al (1999a) presented a large increment in residual strain (by up to 350με) which reflected the variation in the length of the coupon due to the relaxation of the residual thermal stresses originated by matrix cracking. Earlier research carried out by Bassam et al (1998) obtained similar results of increased residual strain with increasing crack density.

Having outlined briefly matrix cracking and its consequences in composite laminates, particularly in woven fabric laminates, the next sections are concerned with a discussion of the properties and modelling of knitted fabric composites, a type of composite in which matrix cracking has been observed previously.

2.4. FIBRE ARCHITECTURE, MECHANICAL BEHAVIOUR AND MODELLING OF KNITTED FABRIC COMPOSITES

2.4.1. KNITTED FABRIC FIBRE ARCHITECTURE

Knitted fabrics are made by the interlocking of loops of fibre bundles (Figure 2.4). They are categorised into two main types, namely warp knitted fabrics and weft knitted fabrics, based on the yarn feeding and knitting direction. Weft knitting is characterised by loops forming through the feeding of the weft yarn at right angles to the direction in which the fabric is produced. Warp knitting, on the other hand, is characterised by loops forming through the feeding of the warp yarns, usually from warp beams, parallel to the direction in which the fabric is produced. Generally, weft knit structures are less stable and, hence, stretch and distort more readily than warp knit structures, so that they are also more formable (Leong et al, 1997).

Knitted loops are arranged in rows and columns, roughly equivalent to the weft and warp of woven structures and termed *courses* and *wales,* respectively. A *course* is a horizontal row of loops produced by adjacent needles during the same knitting cycle. A *wale* is a vertical column of loops produced by the same needle knitting at successive knitting cycles and thus intermeshing each new loop through the previous loop. The wale direction is stiffer, whereas in course direction the flexibility is higher. Since the loop structure is so important to the fabric architecture, there is a rather complex set of descriptions for the loop shapes and parts of it. Of particular importance in this work are the needle, sinker and sides (or legs) of the loops. A schematic diagram of these features is shown in Figure 2.5.

The architecture of knitted fabrics involves many important factors which contribute to its final behaviour. For example, loop length is the fundamental unit of the knitted structure while loop shape determines the dimensions of the fabric; this shape depends upon the yarn used and the finishing treatment that the fabric has received. In addition to the rather simple weft and warp structures shown in previous Figure 2.4 more complex styles can be obtained. Among these, knitted Milano rib fabric has been widely investigated (Bannister and Herszberg, 1995; Leong et al, 1997b; Nguyen et al 1997). This fabric is the subject of this work so it is worthwhile providing a description of its fibre architecture at this point.

The Milano weft rib structure affords good control on the natural extensibility of the loops and, hence, produces a relatively stable fabric. Each complete repeat of the Milano structure consists of three courses- two rows of single threads, knitted together by a row of 1x1 rib. Consequently, the resultant fabric is balanced, i.e. both the face and the back surfaces are identical in construction and, therefore, in appearance. Figure 2.6a shows a two dimensional representation of the basic Milano weft-knitted structure and Figure 2.6b shows the traditional notation for this knitted fabric. The notation shows that in rows (or courses) 2 and 3 the fibre tows are knitted only in one face either front or back, while in row 1 (the rib thread) the tows hold together the two faces (rows 2 and 3).

The rib tows (course 1) have a cord appearance because the face loop wales tend to move over and in front of the reverse loop wales. As the face loops have a complementary reverse loop on the other face, the 1x1 rib fabric has the appearance on each face of a plain fabric until stretched to reveal the loop wales on the other face (Figure 2.7). The other feature of the Milano architecture is the float stitch (Figure 2.8) which is where the yarn bypasses (or floats past) a loop (Spencer, 1989). Figure 2.9 shows at low magnification one face of the Milano knitted fabric used in this investigation.

The knitted fabric architecture plays a vital role in the mechanical behaviour of the composite material and it is this behaviour which is considered next.

2.4.2. MECHANICAL PROPERTIES OF KNITTED FABRIC COMPOSITES

The properties of a knitted structure are largely determined by the dependence of each stitch on its neighbours on either side, above and below it. Naturally, when used to reinforce a matrix, the properties of the resulting composite are influenced by both the fabric and the matrix. Huang and Ramakrishna (2000) have recently pointed out the relatively poor mechanical properties of knitted fabric composites compared to other types of composites. In general, knitted composites achieve a Young's modulus which is only about 25% that of unidirectional material and 50% that of woven material, for equivalent fibre volume fractions. The figures for strength are about 12% and 50%, respectively.

In general terms, the mechanical properties of knitted fabric composites are anisotropic and depend on factors such as the number of layers of fabric, the stitch density, the knit architecture, the fibre volume fraction and the degree of fabric stretching prior to making the composite.

Ramakrishna and Hull (1994) showed the general stress-strain behaviour in tension of knitted fabric composites. They tested composites made up of one layer and two layers of weft-knit carbon fibre fabrics embedded in an epoxy matrix. They found that the curves were linear up to low strain (about 0.3%), whether tested in the course or wale directions, followed by a "knee" in the stress-strain curve for specimens tested in the wale direction while the samples tested in course direction failed at this point at low strains. This discontinuity ("knee") was followed by a "softening" of the stress-strain behaviour, i.e. there was a large reduction in the slope of the curve in many cases falling to zero. In addition they observed that after the knee, the stress-strain curve for the sample tested in wale direction became serrated and they demonstrated that these serrations were originated to the appearance of transverse damage in forms of crack across the specimen width, normal to the testing direction. However in most tests of knitted fabric composites containing more that one layer of fabric such serrations are not observed. In fact, in the investigation carried out by Ramakrishna et al (1997a) where a single layer, plain weft-knit glass-epoxy specimen was used neither the wale nor the course specimen showed serrations in the stress-strain curve. A difference from the research by Ramakrishna and Hull (1994) was that a very small non-linearity was observed prior to failure and small matrix cracking was present.

Typical stress-strain curves for knitted fabric reinforced composites made up of several layers of fabrics are shown in Figure 2.10 (Anwar et al, 1997). The tendency for the slope of the stress-strain curve to reduce, sometime to zero, has been called "pseudo-plasticity" by some authors (e.g. Leong et al 1997). In fact, the curves show similar characteristics to those observed by Ramakrisha and Hull (1994) but without the serrations. However, as a difference to that work, some researchers (Gommers and Verpoest, 1995; Leong et al, 2000) have found that the stress-strain curve of glass/epoxy knitted fabric composites was non-linear even at strains smaller than 0.3%. The observation by Ramakrishna and Hull (1994) on the transition between the low strain behaviour and the high-strain behaviour concluded that this seems to be the point at which debonding and matrix cracking occurred for the carbon fibre/epoxy resin weft knitted fabric composites which they tested

Differences are also clear between knitted fabric composites tested in the wale or course direction. For example, Anwar et al (1997) and Leong et al (1997b) have demonstrated that weft knitted fabric epoxy composites possess superior mechanical properties in the wale direction than in the course direction. Anwar et al (1997) tested three different Milano rib fabric composites manufactured with E-glass fibres and Derakane epoxy vinyl ester resin with fibre volume fractions of about 53%. They found that, in samples tested in the wale direction the tensile strengths were about 50% higher (e.g. 122 MPa compared to 83 MPa) and the Young's modulus was about 14% higher (e.g. 14.9 GPa compared to 13.2 GPa) than in those tested in the course direction., respectively. Similar relation was found for the strains to failure whose values were some 20% to 70% higher (e.g. 2.4 % compared to 1.4%). As might be expected, increasing the fibre volume fraction improves both the modulus and strength of knitted fabric composites, but this effect is much more noticeable in tension mode (Leong et al, 1997b). On the other hand the stress-strain curves for samples tested in compression in wale and course directions are very similar. This is a consequence of the importance of the matrix in compression arising from the highly curved fibre architecture (Ogin, 2000). Hence, in wale and course directions the compression strengths are usually approximately the same and only increased by about 15% as the fibre volume fraction increased from 29% to 50% (Leong et al, 1997b)

Since wale and course directions are the principal axes in the knitted fabric, most investigations have focused on the properties in these main orientations. However many other researchers have carried out analyses on the properties as a function of angle. Gommers et al (1998a) investigated the variation of Young's modulus and tensile strength with angle and these composites had fibre architectures which produced large variations in tensile strength and Young's modulus. In addition the variations with angle were not always symmetrical about the wale direction of the cloth due to the fact that the fibre architecture was also not symmetrical about this direction.

The poor tensile and compression properties of knitted fabric composites are not reflected in the impact properties or the mechanical properties after impact. Verpoest et al (1997) have shown that in knitted fabric composites the damage area was greater than in woven fabric composites for the same absorbed impact energy.

It has been suggested that the curved fibres in the knitted fabric are able to bridge the cracks initiated by the impact and also are slightly stretched before being fully loaded. Bannister and Herszberg (1995) also found similar results for a glass fibre composite absorbing a higher proportion of incident impact energy than woven glass fabric composites.

In addition, the compressive strength after impact was retained better for increasing impact energies for the knitted fabric. Such observations have been confirmed by many workers. For example Hamada et al (2000) compared knitted fabrics with roving cloth for reinforcement of large scale composite structures. Although the mechanical properties were observed to be better in the roving cloths composites, the knitted fabric composites again showed better energy absorption. Other studies (e.g. Yu et al, 2000; Cox et al, 2000) confirm such observations.

Finally, it should be pointed out that the poor tensile properties of knitted fabric composites can be improved in a number of ways. Firstly, the linear density of the loops can be increased (Sugun et al 2000). The knitted fabric used in their work was made by reinforcing the course direction by E-glass yarns between successive rows of loops to improve the properties in this direction. Similar work has been carried out by Naveen et al (2000) who demonstrated that by tailoring the course direction with added E-glass yarns between successive rows of loops, the strengths obtained were higher than the corresponding standard woven fabric composite laminate.

2.4.3 MODELLING THE PROPERTIES OF UNDAMAGED KNITTED FABRIC COMPOSITES

In principle, it should be possible to predict, the Young's modulus of knitted fabric composites, on the basis of the geometry of the loop structure, the fibre volume fraction, and the fibre and matrix properties. However when viewed in detail, the problems are complex (Verpoest et al., 1997). First an accurate and appropriate description of the loop structure is required, and of the yarn orientations within them. Such a description will need to be three-dimensional. Second, the stiffness of a unit cell of the structure could be calculated taking advantage of the symmetry elements of the loop structure. Of course this assumes that such symmetry exists even approximately. Ramakrishna and Hull (1994b) carried out one of the earliest attempts to model the mechanical properties of knitted fabric composites. Their model was based on the proportion of fibres oriented at various angles in the fabric geometry and obtained good agreement for the modulus but not for the tensile strength. They suggested that the failure of their model for the strength was due to bending stresses in fibre bundles bridging cracks in the matrix.

In all cases of modelling the properties of knitted fabric composites, a model of the fibre geometry is required. Figures 2.11a and 2.11b show examples of a 'representative volume element' (RVE) for modelling a plain knitted fabric and a Milano rib knitted fabric (Huang and Ramakrishna, 2000). The RVE is, in fact, extracted from the unit cell of the fabric structure, when that cell displays symmetry. Hence, although the RVE or sub-cell contains the essential geometry and properties which are modelled, it is easier to visualize the unit cell itself, which can be defined as the smallest unit repeated in the fibre architecture. In other words, it is the building block of the material. Figure 2.12 shows a typical unit cell used for modelling plain weft knitted fabric composites. Several factors affect the size of the unit cell, for example, the fibre yarn diameter and the number of fabric loops per unit length in the wale or course direction. However in many cases, the loops are not symmetrical about the wale direction (Gommers et al, 1998c). In that case, the fibre geometry requires careful reconstruction from microscopical measurements of composites sections in three dimensions.

Obviously, as the complexity of the fabric increases, the complexity of the RVE increases. Having established the RVE for a particular knitted structure, the approach is then to derive the stiffness of the various parts of the RVE and to combine them in an appropriate way.

In the work of Ramakrishna (1997b) the tensile properties of a plain weft-knit glass fibre fabric reinforced epoxy composite were modelled in the wale and course direction. Elastic properties were predicted by using a "cross-over" model based on representing the loop geometry as arcs of a circle and modelling the arc stiffness using laminated plate theory. In all models, the crossing-over of the yarns presents difficulties: in the model of Ramakrishna (1997b) the cross-over consists of fibre and resin rich regions. Unfortunately, the approach of Ramakrishna (1997b) required the introduction of an arbitrarily chosen additional parameter to achieve good agreement between predictions and experimental values.

Ramakrishna and Hamada (1997) attempted to predict tensile failure mechanisms and tensile properties using a three-dimensional finite element model, again comparing the results with the experimental results. They found a discrepancy between the predicted and experimental values which was attributed to the fact that the fibre bundles bridging the fracture plane may not be aligned perfectly in the loading direction. This is similar to the difficulties which Ramakrishna and Hull (1994a) found when modelling their knitted carbon fabric/epoxy laminates (see above).

Finally, Huang and Ramakrishna (2000) tested different modelling approaches based on representative volume elements and found that the approach of Ruan and Chou (1998)resulted in the best agreement between experiment and prediction for Young's modulus. Ruan and Chou (1998) represented the RVE as infinitesimal segments connected in series. The stiffness of each segment was combined in series. The prediction of modulus for a weft-knitted fabric composite was found to be within 12% of the experimental measurement and the prediction of tensile strength was within 13%.

On the other hand, Huysmans et al (1998) has taken a significantly different approach for modelling the properties of knitted fabric composites. In this approach the yarn architecture was reduced to a sequence of segments. These segments were treated using the Eshelby method for modelling inclusion in the matrix. The predicted elastic modulus was found to be in good agreement with the experimental data.

2.4.4. DAMAGE ACCUMULATION

As it has been mentioned above, previous work has demonstrated that knitted fabric reinforced composites can show an accumulation of matrix cracks under load. Indeed, apart from fracture of the yarns, this is the main type of damage shown by such composites.

Leong et al (1997) found that glass fibre/epoxy knitted fabric reinforced composites, containing between six and twelve layers of fabric, showed an accumulation of cracks under load in both the course and wale directions, and that the cracking patterns were different in detail for these two directions. For specimens tested in the wale direction, cracking was in the form of isolated cracks. In the course direction, adjacent microcracks combined to form larger cracks. They also attempted to relate the cracking damage to the fabric architecture, but this was impossible in laminates which were fabricated from multiple layers of fabric and were not transparent.

There are a large number of potential sites for crack initiation in knitted composites. For example, observations in weft-knitted composites tested in the wale direction (Anwar et al, 1997) suggest that cracks initiate from debonds which form around the needle and sinker loops in the knitted architecture. However, for testing in the course direction, crack initiation was believed to occur from the sides (or legs) of the loops.

Ruan and Chou (1998) tested single layers of weft-knitted reinforced glass-fabric epoxy composites. They observed sudden final fracture of the samples occurring immediately after the first sign of tiny surface cracks and whitening of the matrix. Later investigation of the fracture surfaces suggested that fracture initiated at the yarn/matrix interface. Similar conclusions were reached by Ramakrishna and Hamada (1997). Their investigations of fracture surfaces suggested that debonding of the fibre bundles occur at those portions of the knit loops which are oriented normal to the loading directions. Microcracks initiate from these debonded sites, it was suggested, and propagate normal to the testing direction and into the resin rich regions of the composite.

Studies made by Anwar et al (1997) revealed that the final fracture of the composite appeared to have occurred in the planes of lowest fibre content for specimens tested in the wale as well as in the course directions. This coincides with matrix fractures at the legs of the loops for wale-tested specimens and at the needle-sinker loops for the course-tested specimens. It was further suggested that the microcracks generated from the debonded sites propagated through the adjacent resin rich areas within the knit structure.

Current understanding of the development of failure in a knitted fabric composite has been summarised well by Huysmans et al (2001). Debonding occurs around fibre bundles oriented perpendicular to the loading direction around the knee observed in the stress-strain curve. These debonds grow along the yarn interface and into resin rich regions becoming matrix cracks. The growth and coalescence of debonds leads to a microscopic crack bridged by unbroken yarns. If the number of yarns in the composite is large, failure then is dominated by the yarn strength. The drawback of such description of failure is that it has been obtained from observing fracture surfaces rather than being based on observations of the progressive failure of knitted fabric composites.

2.5. CONCLUSIONS

Although many important studies have been carried out on knitted fabric composites in order to understand and determine their properties and behaviour, knitted composites are still considered a new field in reinforced material composites. For instance it has been demonstrated that under tensile loading, the typical stress-strain curves of knitted fabric composites may be of different appearance depending on the type of material (fibre architecture), the loading direction and the number of layers of the composite. In addition many investigations have shown that damage accumulation in the form of matrix cracking is an important characteristic of the mechanical behaviour. However, it is important to mention that all of the work carried out to date on damage accumulation has concentrated on loading the composites in either wale or course directions and no attempts has been made to analyse the relationship of the damage initiation and propagation to fabric architecture for other angular orientations

Further, most of the studies on damage accumulation have been carried out either on single layer composites, which fractured as soon as the first damage initiated in the material, or in multilayer composites, for which information on the progression of damage had to be derived from the fracture surfaces after final fracture had occurred. It is important to mention as well that such experiments were carried out using opaque resins as matrix system; therefore, the analysis of relating cracking damage to the knitted fabric architecture was more difficult to observe.

The work to be described here presents a novel method of observing damage accumulation in a knitted fabric composite using a single knitted fabric layer sandwiched between unidirectional glass fibre layers to produce a transparent laminate. The aim of this investigation is to characterise the initiation of damage using this technique and to relate the development of the damage to the fabric architecture for a range of angles. The insight gained will then be applied to mechanical testing results derived from testing a commercial knitted-fabric composite plaque.

FIGURES

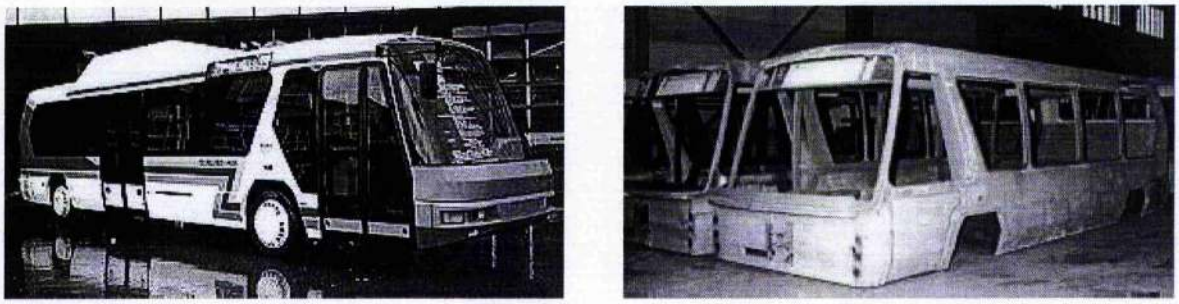

a)

b)

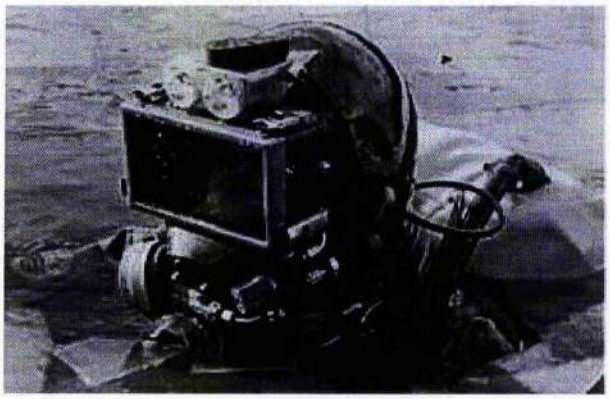

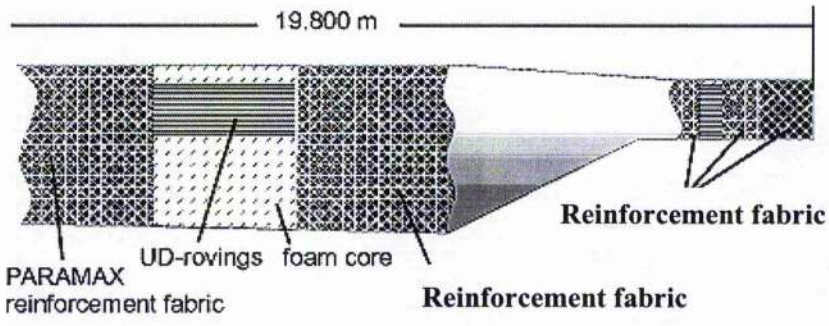

c)

Figure 2.1.- a) Vehicle-bodies made of textile composite material have less weight than the usual ones. They lead to less fuel consumption and are corrosion—resistant. b) Helmets. c) Wind rotors.

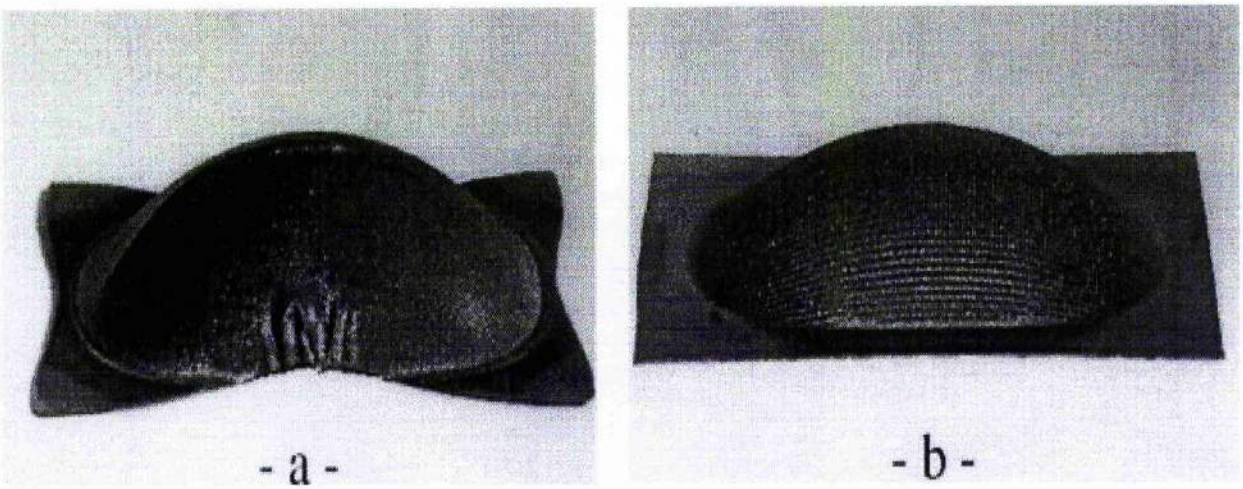

Figure 2.2.- Double curved parts elaborated using (a) woven fabric, (b) knitted fabric.

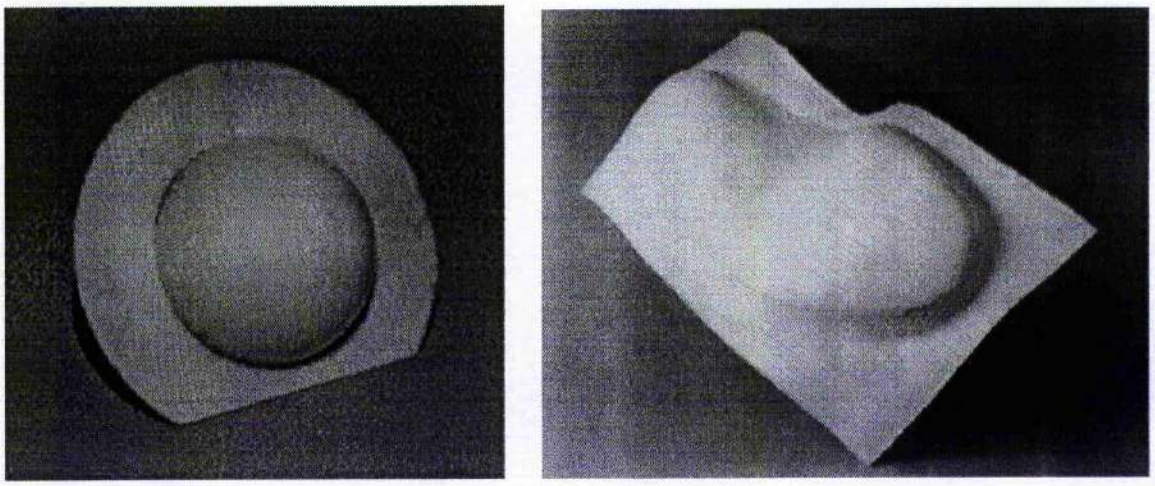

Figure 2.3.- Sample parts made of knitted fabric: (a) Dome, (b) Shoe sole.

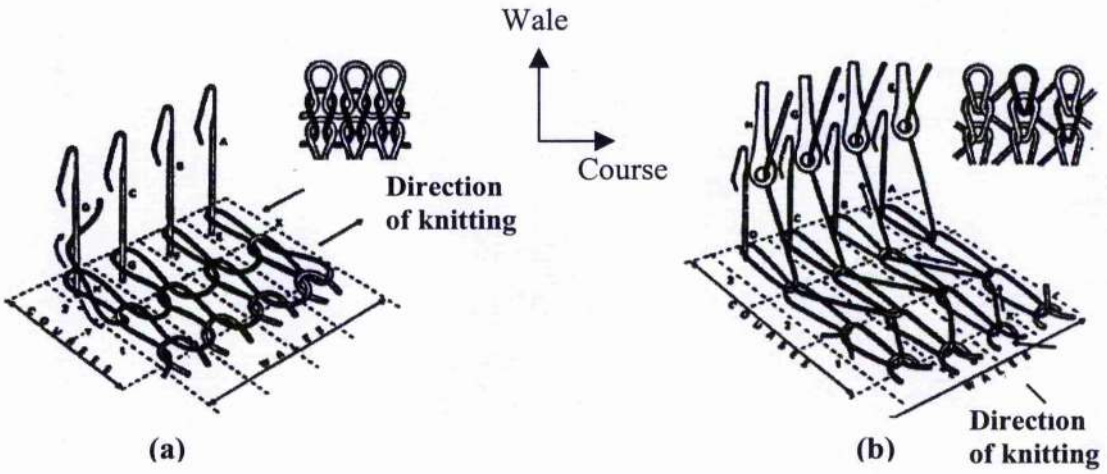

Figure 2.4.- Schematic diagrams showing the wale and course components of a knitted fabric (a) weft knitting, and (b) warp knitting.

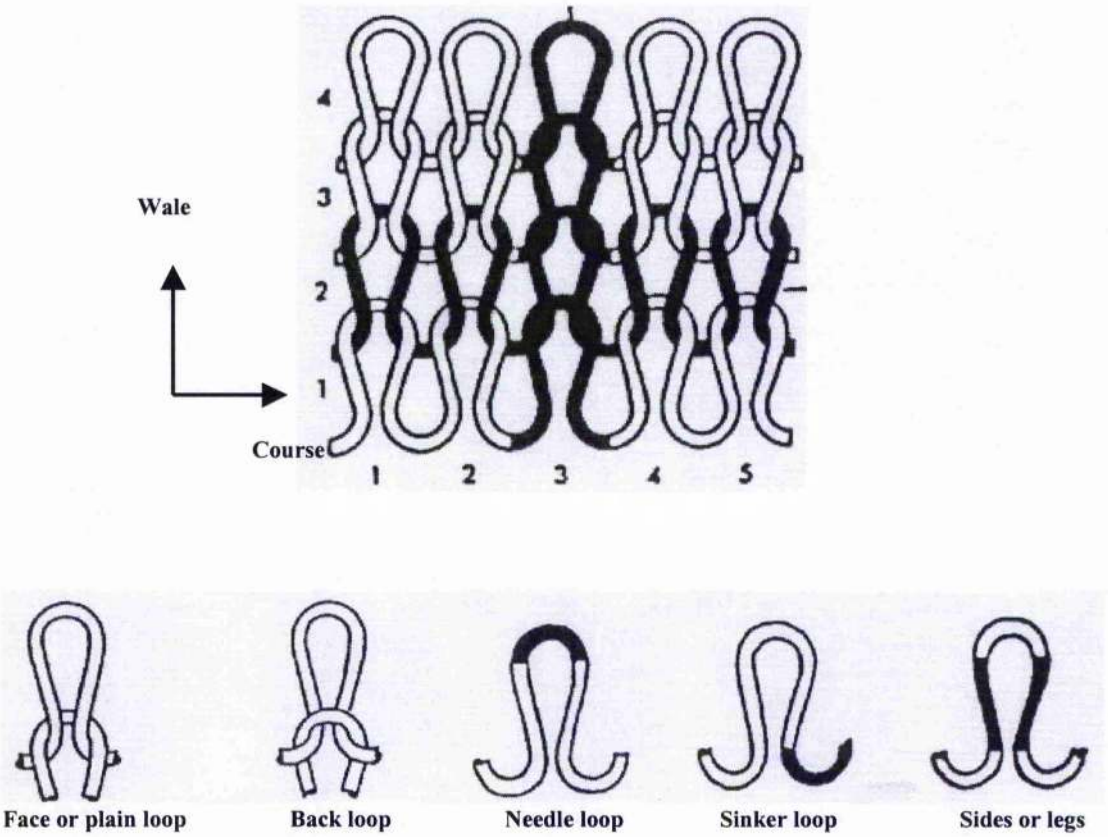

Figure 2.5.- Schematic diagram of knitted plain fabric.

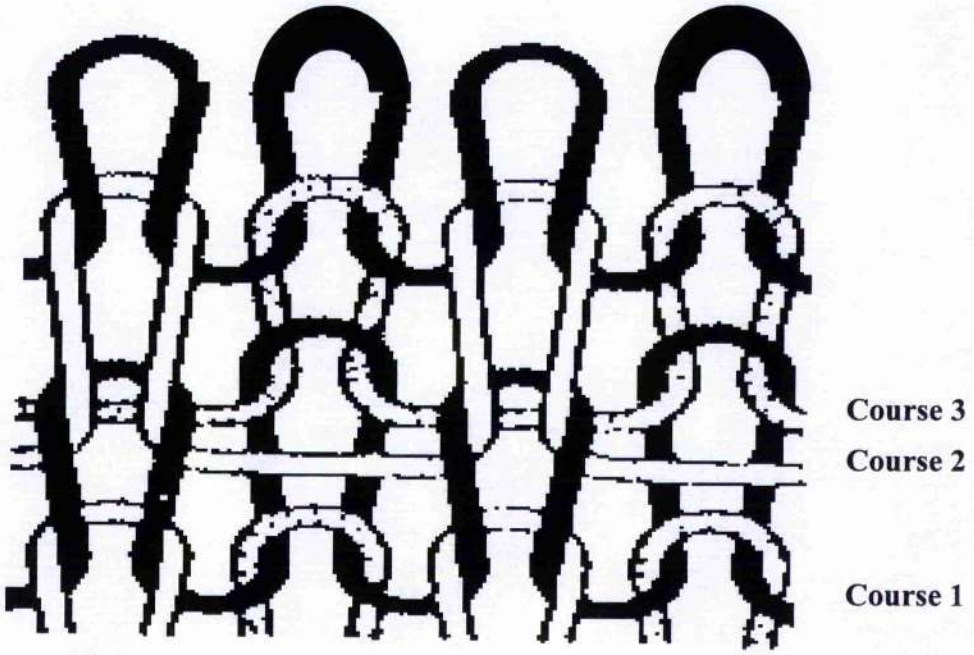

2.6a

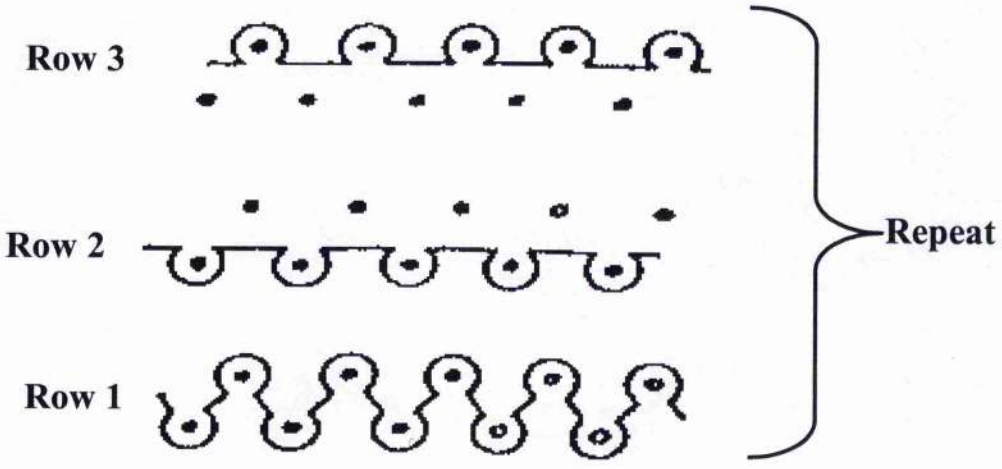

2.6b

Figure 2.6.- Milano knitted fabric architecture.

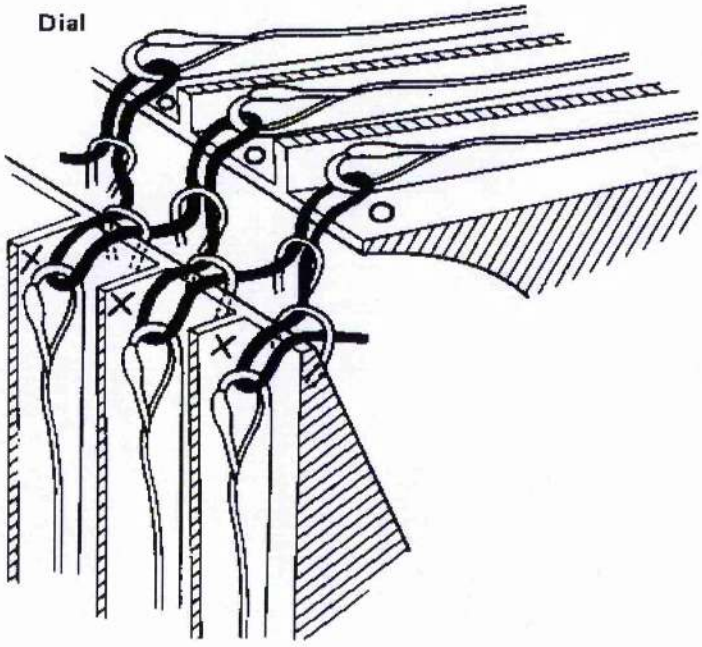

Figure 2.7.- Rib is normally knitted with two sets of latch needles. (After D. J. Spencer, 1989)

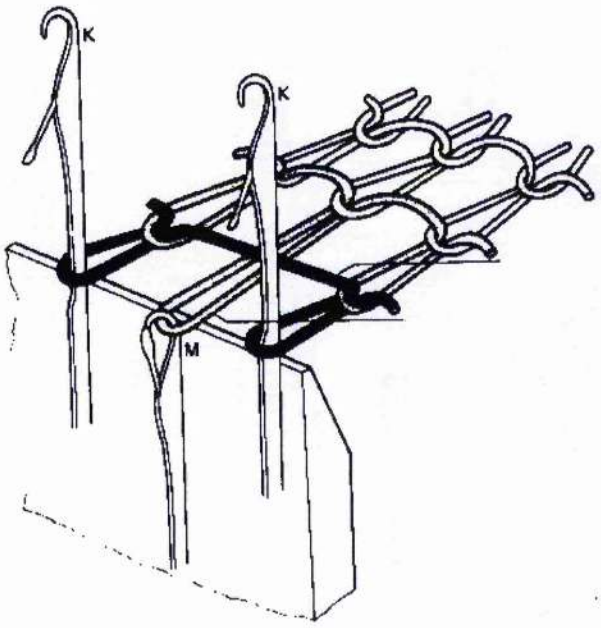

Figure 2.8.- Schematic of a float stitch in knitted fabric. (After D. J. Spencer, 1989)

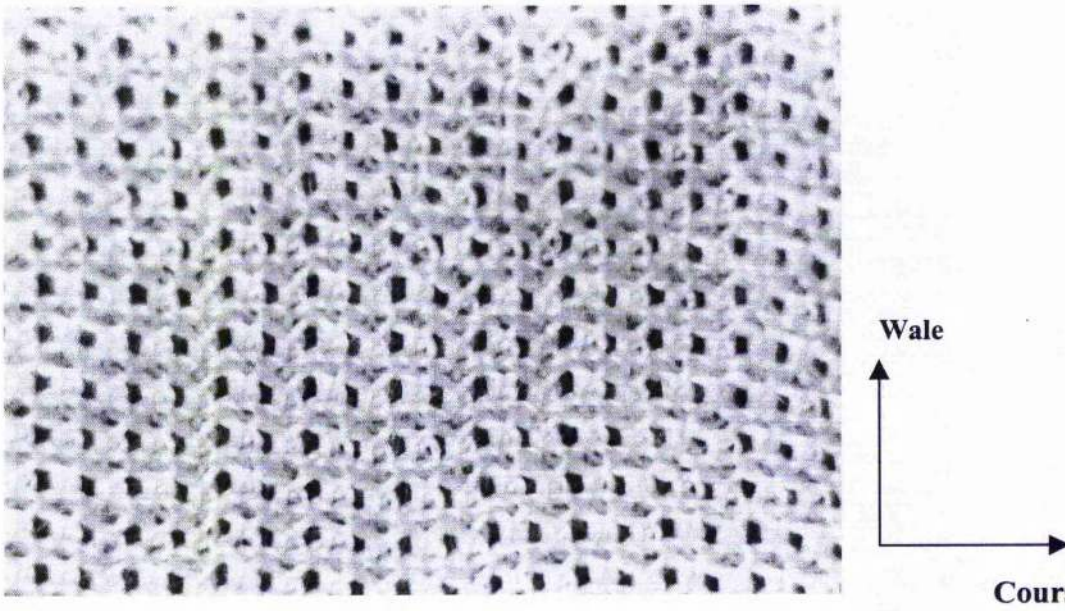

Figure 2.9.- Milano knitted fabric

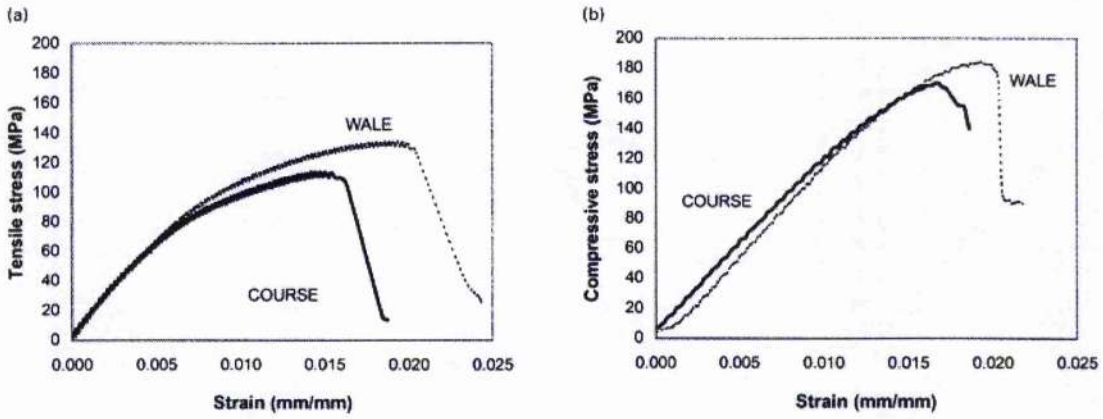

Figure 2.10.- Typical stress-strain curves for rib-knit composites (a) tension and (b) compression, loadings. (After Anwar et al, 1997).

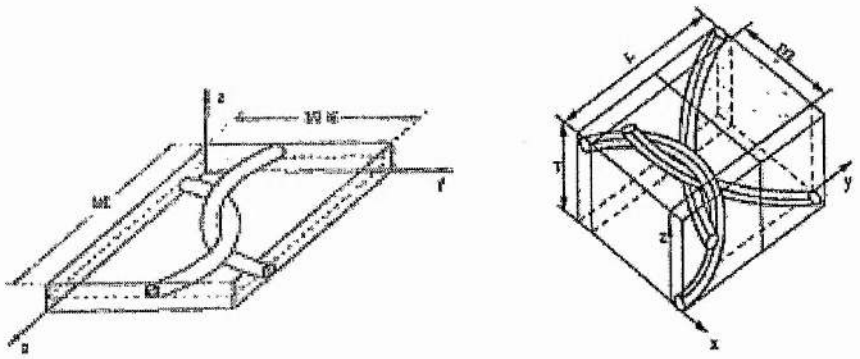

(a) (b)

Figure 2.11.- Diagrams used for modelling (a) a plain knitted fabric and (b) Milano rib knitted fabric. (After Huang and Ramakrishna, 2000)

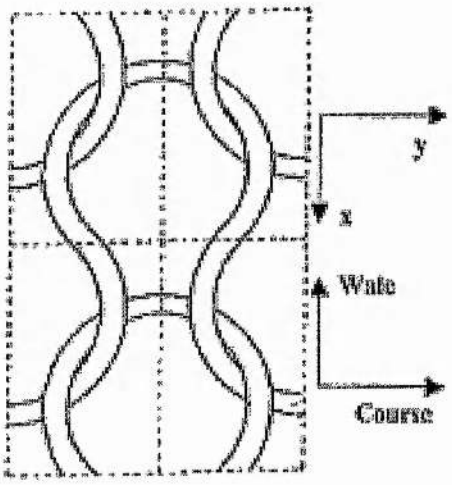

Figure 2.12.- Schematic representation of a unit cell of plain-knit fabric. (After Ramakrishna 1997)

CHAPTER 3

EXPERIMENTAL METHODS

3.1. INTRODUCTION.

This chapter describes the fabrication and testing of the knitted fabric reinforced composite used in this work giving details of the processes for producing a single layer composite and a "sandwich" composite. The "sandwich" composite consists of a single layer of knitted fabric between two 0° plies of continuous unidirectional material. The "sandwich" used here is a new method for investigating damage accumulation in the knitted materials. It was required for two reasons. Firstly the commercially produced specimens evaluated in this work were not transparent making difficult to analyse damage development. Secondly, the model single layer glass/epoxy composite failed suddenly with the first crack. The added 0° plies of unidirectional reinforcement allowed the damage behaviour to be observed hence multiple cracking in the knitted fabric was able to evaluated and monitored. In addition to specimen fabrication, experimental testing techniques are also described.

3.2. MATERIALS AND LAMINATE MANUFACTURE

The Milano weft-knitted fabric (described in section 2.6.1) produced from E-glass yarns of 2x68 tex was the knitted fabric to be investigated. In addition to these fabrics, which were supplied by the Cooperative Research Centre for Advanced Composites Structures Limited (CRC-ACS, Australia) a number of knitted fabric reinforced panels with 4 or 5 layers of knitted fabric were also supplied. The panels were manufactured at CRC-ACS using the RTM method.

3.2.1. MANUFACTURE OF TRANSPARENT MODEL KNITTED FABRIC COMPOSITE PANELS.

The manufacture of the model panels is detailed here. The "sandwich" panel is described first followed by the simpler single layer panels. Knitted fabrics 350 mm x 350 mm size were cut and marked showing the loop direction in order to be able to identify the principal axes (wale and course) after laminate processing. The knitted fabric was fixed into a steel frame and the frame was placed in a filament winder in order to wind unidirectional glass fibre reinforcement around the cloth to produce a sandwich panel. Figure 3.1 shows a glass tow being wound around the frame where the knitted cloth was fixed in the middle. After removal from the frame the glass fibres were impregnated with an epoxy resin following a hand lay up process (Figure 3.2). Model sandwich laminates were made with the knitted fabric oriented at different angles by varying the direction of the fabric with respect to the 0^{o} plies. The angles used were 0^{o} (i.e. wale direction of knitted fabric parallel to unidirectional outer plies), 30^{o}, 45^{o}, 60^{o} and 90^{o} (i.e. course direction of knitted fabric parallel to unidirectional outer plies) as shown in Figure 3.3.

Samples were cut from these laminates parallel to the unidirectional outer plies. In order to determine the properties of the 0^{o} outer plies, a laminate without the knitted cloth (i.e. a 0^{o} unidirectional fibre laminate) was also manufactured.

The matrix resin formulation for all the model laminates was as follows: epoxy resin, Astor Stag Epoxide resin 300 (400 g); curing agent, Astor Stag N.M.A., (240 g); accelerator, ancamine K61B (16 ml). The constituents were mixed thoroughly together for a few minutes, and then the resin was placed, for around 45 minutes into a vacuum oven at a preheated temperature of 46^{o} – 50 ^{o}C in order to de-gass it. After this, the resin was ready to be used for making the sandwich laminates.

Full wetting of the fibres was achieved by placing the uncured laminate inside a vacuum chamber (Figure 3.4) for about 20 minutes before squeezing out any excess resin and entrapped air bubbles. The laminate was cured between thick glass plates under 80 kg weight, as follows:

Temperature	Time
70°C	40 min.
100°C	3 hrs
28°C	30 min.

The resin system was chosen because it readily wets glass fibres and it is sufficiently transparent to enable microcracking to be seen. This transparency improves the ease of observing any damage within the laminate during and after mechanical testing. The manufacture of the single knitted layer composite (without the 0° ply reinforcement) was carried out following the same process as described above except that the cloth was not placed in a frame, nor reinforced by winding.

Two different panels of a commercial material, supplied by CRC-ACS Australia, made by Resin Transfer Moulding (RTM) process were tested in order to compare the behaviour of the model material with a commercial composite. The panels were manufactured using the same knitted glass fabric. Five layers of Milano fabric 2x68 tex were used for one panel and the second panel had four layers. The difference between the fabrics was in the linear density. The fabric used in the five-layer panel had a linear density of 742 g/m^2 and the fabric used in the four-layer panel had a linear density of 940 g/m^2. Derakane 411-350 epoxy–based vinyl ester resin was chosen because it has an exceptionally low resin viscosity and has been specially designed for the resin transfer moulding (RTM) process.

3.3. SAMPLE PREPARATION FOR MECHANICAL TESTING

The manufacturing technique used for the model laminates produced panels which were 250 mm x 250 mm. Samples of 230 mm x 20 mm were cut from the panels using a water cooled 600-grit diamond saw and they were end tagged using aluminium tags of 50 mm length (Figure 3.5). Two strain gauges were bonded to each sample in order to obtain longitudinal and transversal strains (Figure 3.5 and 3.6).

The fibre volume fractions were obtained for all model material panels using the matrix burn-off technique as follows. Four samples (approximately 20 mm x 20 mm) were cut from four different places of the laminate. Each sample was weighed before being placed in a ceramic crucible and covered with a lid. The weight of the crucible and the lid were known. The crucibles were placed in a muffle furnace at a temperature of 600°C for approximately 3 hrs.

After this time, the resin was completely burnt away and the crucibles were set aside to cool. Once cool, the crucibles were reweighed. The densities of the glass (ρ_f) and resin (ρ_m) were 2.56 g/cm^3 (2560 kg/m^3) and 1.21 g/cm^3 (1210 kg/m^3) respectively. The volume fraction (V_f) of the glass fibres in the composite was calculated using the equation below:

$$V_f = \frac{\dfrac{(C-B)}{\rho_f}}{\left[\dfrac{(A-C)}{\rho_m}\right] + \left[\dfrac{(C-B)}{\rho_f}\right]}$$

where A is the mass of the crucible and the sample (pre burn-off), B is the mass of the crucible, C is the mass of the crucible and the glass fibres (post burn-off), ρ_f is the density of the fibres and ρ_m is the density of the matrix. Once the fibre volume fraction had been calculated for all four samples they were averaged to obtain the mean fibre volume fraction of the laminate.

On the other hand, the calculation of fibre volume fraction for the commercial composite (RTM) was carried out using the following formula:

$$V_f = \frac{W_{areal} n}{\rho_f t}$$

which is based on the volume occupied by the yarns divided by the total volume occupied by the fabric (Rozant et al. 2000), where W_{areal}, n, ρ_f and t, are the areal density of the fabric, the number of the fabric layers, the fibre density and the composite thickness respectively.

3.4. MECHANICAL TESTING

An Instron 1196 machine (Figure 3.7) was used for mechanical testing and crack development. The output of the strain gauge, Vishay boxes and the load cell was connected to a data logging system. The cross-head speed for all tests was kept constant at 0.5 mm/min.

In-situ photographs of damage development were taken using a Nikon F-301 mm camera fitted with a Tamrom SP 90 mm extension tube. The camera was mounted on a tripod and placed in front of the Instron testing machine with the (transparent) samples illuminated from the rear. Photographs were taken before loading at intervals during the test and after failure in order to observe crack accumulation and quantify crack densities.

During testing, acoustic emission was monitored as a guide to damage initiation. There were three acoustic transducers in the system used in these experiments. One was the signal transducer, which was placed in the centre of the gauge length of the coupon. The other two were placed near the ends of the coupon. These guard transducers filter out unwanted noise from the grips of the tensile testing machine.

A computerised acoustic emission system (AECL 2100.M) has been used to monitor stress waves as a result of generation and growth of defects. The transducers were attached to the specimen surface with insulation tape using Vaseline as a coupling agent. AE signals were detected by the sensor and sent to a pre-amplifier and amplified by 60 db gain. These signals were amplified for a further 20 db by using the gain control in the main module. Most of the external noise (spurious signals) had peak amplitude levels below 40 db (Ramakrishna and Hull, 1994). Preliminary analysis was performed to establish the best threshold value, which was found to be 0.6 V, allowing the sensor to collect only those events whose signal exceeded this value.

The processing unit was set to count the number of acoustic events in 0.1 s intervals. The AE output from the processing unit was connected to the data logger for simultaneous recording with the other monitored parameters (i.e. load, strains). *

3.5. SAMPLE PREPARATION FOR MICROSTRUCTURAL ANALYSIS

In many cases sections from the tested samples were cut out using the diamond saw, mounted in epoxy resin and polished in order to obtain information about damage initiation and cracking development in relation to the knitted fabric architecture. Samples were taken both parallel and perpendicular to the loading direction and sometimes at angles to these directions (Figure 3.8). The mounted specimens as shown in Figure 3.9 were polished following the procedure shown in Table 3.1. The first four stages were carried out using grain paper allowing a deep cleaning of the sample surface; the remaining four stages were executed with polishing plates in order to achieve micro-cleaning and to produce a good quality specimen surface.

Photographs of the sections were taken using an optical microscope with an incorporated camera.

* Values were plotted as acoustic emission count rates

TABLES

Table 3.1.- Procedure for sample polishing in epoxy composites. The Table shows details of the eight polishing stages.

Stage	**1**	**2**	**3**	**4**
Grade	500	1200	2400	4000
Lubricant	water	water	water	water
Speed	300 rpm	300 rpm	300 rpm	300 rpm
Pressure	60	60	60	60
Time	1 min	1 min	1 min	1 min

Stage	**5**	**6**	**7**	**8**
Paper type	DP-DUR	DP-DUR	DP-DUR	OP-chem
Grade	6 μ	3 μ	1 μ	¼ μ
Lubricant	blue	blue	blue	OPS
Speed	150 rpm	150 rpm	150 rpm	150 rpm
Pressure	60	60	60	60
Time	4 min	4 min	4 min	30 s.

FIGURES

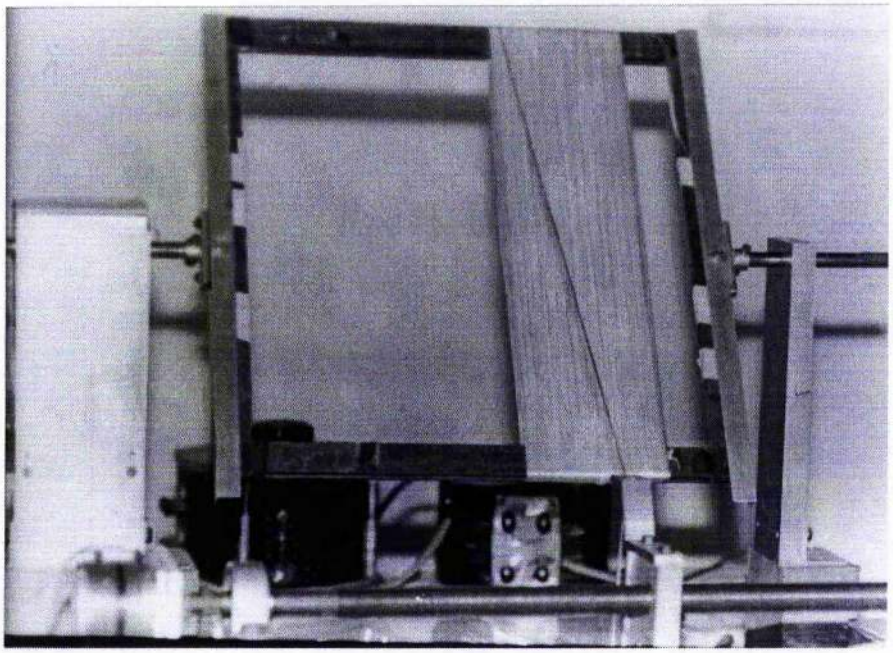

Figure 3.1.- Frame in the winding system showing 0° fibres being wound

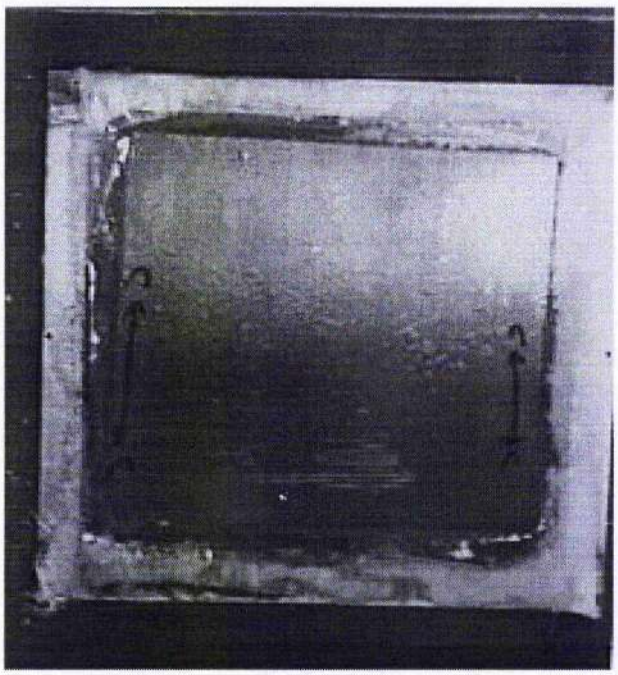

Figure 3.2.- Model material panel.

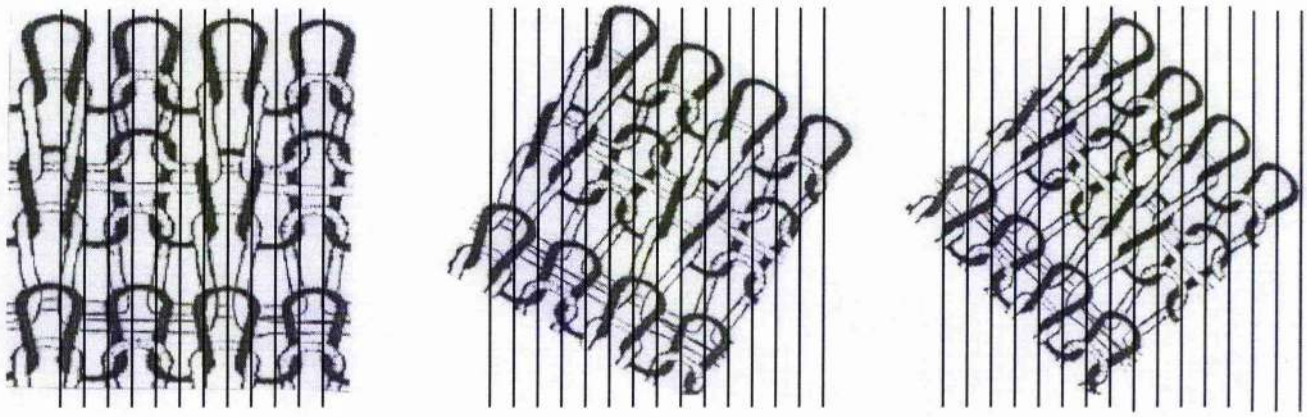

0 ° (Wale) **30 °** **45 °**

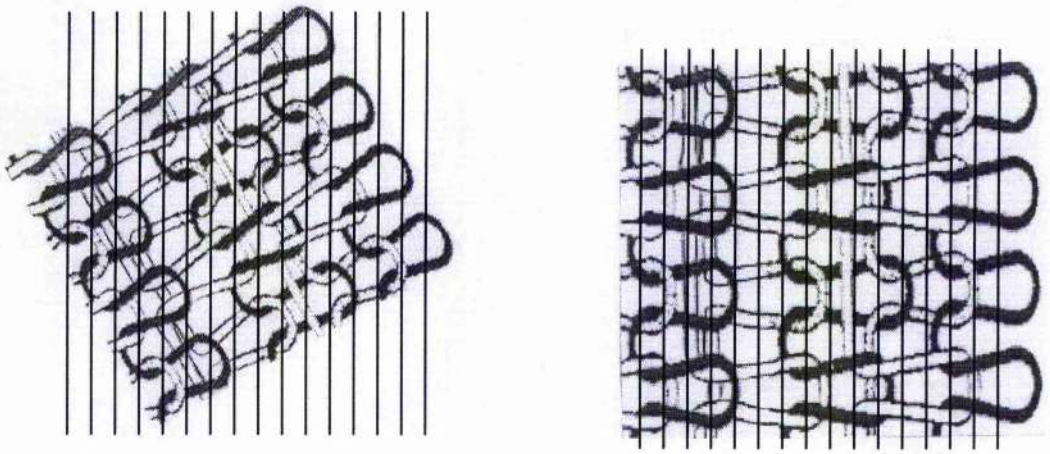

60 ° **90° (Course)**

Figure 3.3.- Angular orientations of the knitted fabric in relation to the unidirectional (0°) outer plies in the "sandwich" laminates.

Figure 3.4.- Vacuum system for resin impregnation.

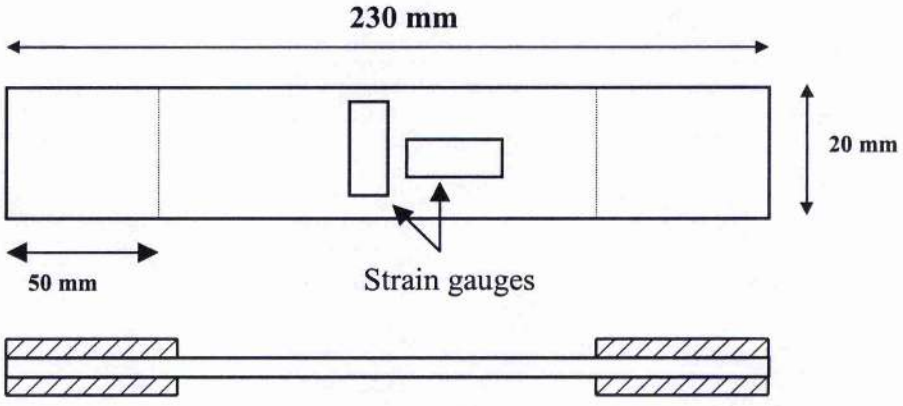

Figure 3.5.- View of the specimen prepared for mechanical testing.

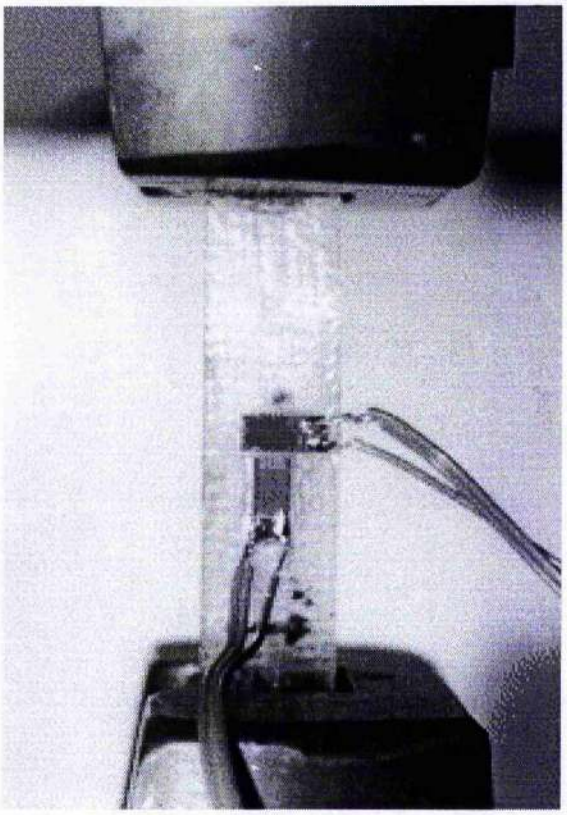

Figure 3.6.- Specimen mounted between the grips of the mechanical testing machine ready to be tested.

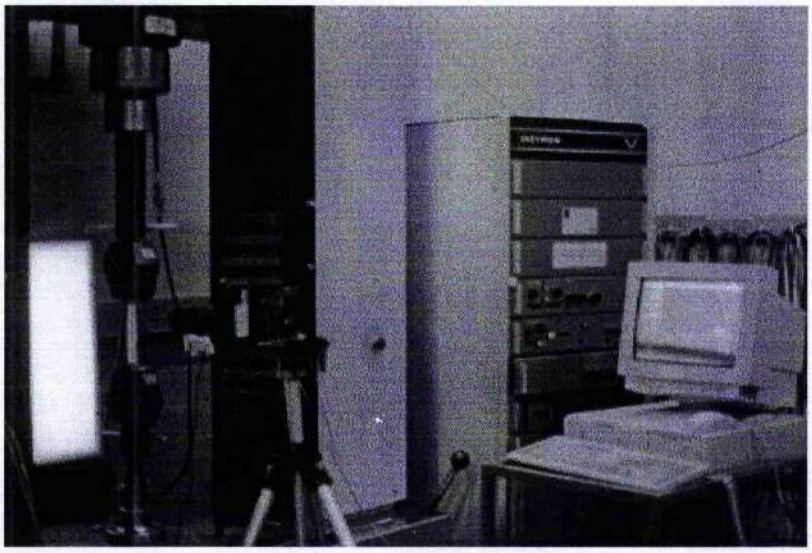

Figure 3.7.- View of the Instron machine used for mechanical testing and the camera used for in-situ photography.

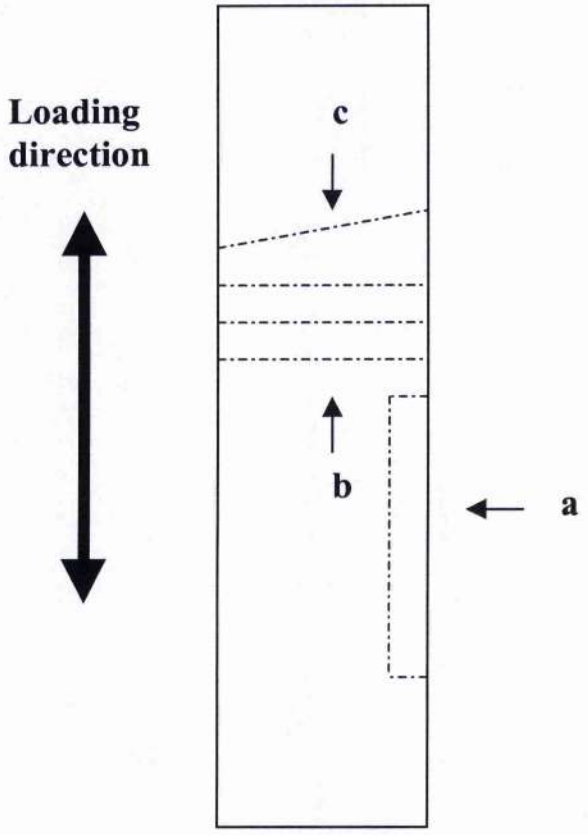

Figure 3.8.- Pieces taken from the samples in both the wale and the course direction for polishing: a) parallel to load direction. b) perpendicular to load direction. c) angular. Arrows indicate the surface that was polished and microscopically analysed.

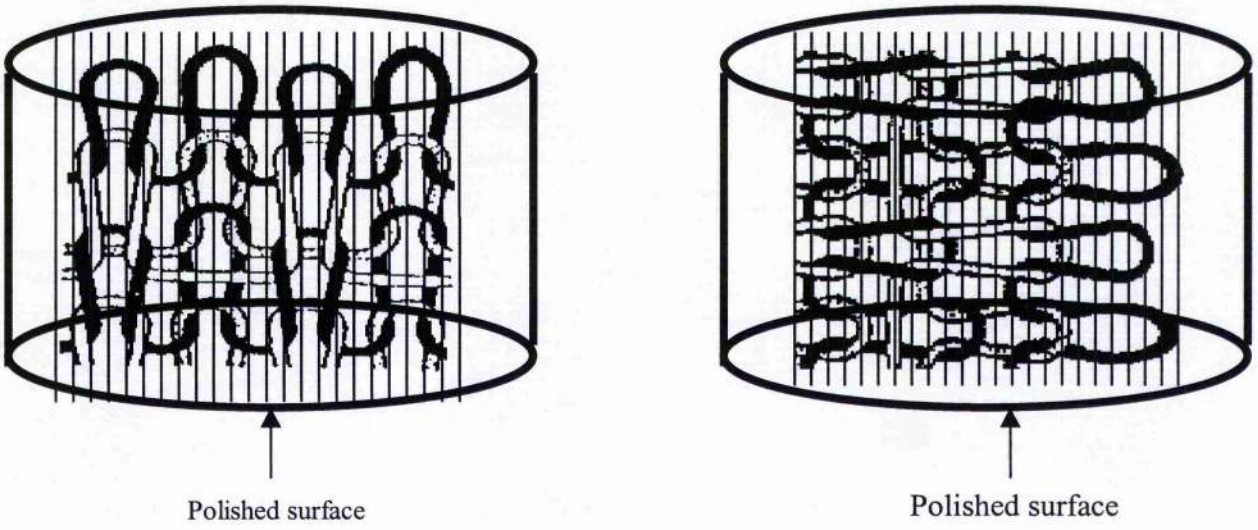

Figure 3.9.- Specimens embedded in epoxy resin for polishing.

CHAPTER 4

EXPERIMENTAL RESULTS AND DISCUSSION ON THE MODEL MATERIALS

4.1. INTRODUCTION.

The experimental results obtained on the model material investigated during this research are presented in this chapter. In the first place, the structure of the knitted fabric is described followed by the results on the single knitted layer/epoxy composite using the 2x68 tex fabric. Secondly, after outlining the mechanical behaviour of this material, and the difficulties encountered in analysing damage propagation due to the premature failure of the material, results on a model sandwich laminate made up of unidirectional glass fibre 0° plies, with the knitted fabric between the outer plies are discussed. These results include tests on the 0° plies alone and tests where the knitted fabric within the sandwich laminate is oriented at different angles to the loading direction. A detailed microstructural relationship between fabric geometry and cracking behaviour is discussed, the acoustic emission technique being used to support the investigation of crack initiation and accumulation. Finally a method is introduced for extracting, from the results on the sandwich panels, the behaviour of the knitted fabric layer itself. These results together with tests on the cyclic behaviour of the material enable some conclusions to be drawn about the mechanical behaviour of the knitted fabric layer during damage accumulation.

4.2. ARCHITECTURE OF THE KNITTED FABRIC.

A photograph of the Milano knitted fabric used in this study is shown in Figure 4.1a. The front and rear faces of the cloth are identical, hence only one face is shown. The basic dimensions of the cloth architecture are shown on it. A two-dimensional representation of the fabric architecture is shown again in Figure 4.1(b). It is clear that the two dimensional illustration is a useful representation of the structure but cannot show the three-dimensional complexity of the geometry. Essential dimensions of the fabric are marked in the figure.

The properties of a knitted structure are largely determined by the interdependence of each stitch with its neighbours on either side, above and below it. This is the main reason why many researchers (e.g. Huang et al, 1998; Ramakrishna, 1997; Ruan et al, 1997) have characterised the loops themselves. In this work, a geometrical analysis was carried out on loops of the Milano knitted fabric (2x68 tex) used here to determine the fibre orientations. The method used was similar to that of Verpoest et al (1997) and Gommers et al (1998a). They carried out a detailed three-dimensional analysis of the fabric architecture of a range of fabrics structures to establish the proportion of fibres at various angles in the fabric. A shorter two-dimensional study of the 2x68 knitted fabric was carried out in this investigation. Measurements were made by taking photographs of 8 loops from a single layer knitted fabric composite. An example of a loop is shown in Figure 4.2. The loops were divided into equivalent length straight segments (Figures 4.3 and 4.4) and then the angle of each section was determined with respect to the nominal wale direction of the fabric.

A histogram was constructed (Figure 4.5) which shows the fraction of fibre at various angles to the wale direction of the fabric. The results show a high proportion of fibres within about 25° of the wale direction (0°) and that the loop architecture is approximately symmetric about this direction. An extremely time-consuming three-dimensional study would be necessary to determine accurately the three-dimensional fibre architecture. In line with most other studies of knitted fabric composites, such a determination was not carried out here.

Verpoest et al (1997) found similarly symmetric loops for certain types of knitted fabrics they investigated, although some fabrics were not even approximately symmetric about the wale direction. In accordance with their results, it is to be expected that the modulus and strength of the knitted fabric composites will be higher in this direction.

4.3. SINGLE LAYER KNITTED FABRIC COMPOSITE PROPERTIES.

The results of tests on the single layer 2x68 tex knitted fabric composite will now be outlined. As described in Chapter 3, this laminate consists of a single 2x68 tex knitted cloth reinforcing epoxy resin. No additional reinforcement was present. Coupons were tested at angles of -45°, 0°, 30°, +45°, 60° and 90° where the 0° and 90° represent the wale and course directions (Figure 4.6). Acoustic emission (AE) was used to detect damage onset in order to analyse cracking initiation and propagation, and at least four coupons were tested at each angle. The fibre volume fraction for the single layer knitted fabric panels was found to be 13.0±0.1%.

4.3.1. MECHANICAL PROPERTIES

Typical stress-strain curves for all the angles tested can be seen in Figures 4.7 to 4.12. At least four coupons were tested for each direction. In these plots, the left-hand axis shows stress and the right-hand axis shows acoustic emission (AE) event counts. It should be noted that a small tensile offset, introduced during tightening of the grips occurs for all specimens.

All the stress-strain results show a small non-linearity. Such a non-linearity has been noted in previous investigations (Ramakrishna, 1997; Ramakrishna and Hamada, 1997; Ruan and Chou, 1998) although these authors mention a linear portion at very low strains. This may indeed be the same here for strains less than 0.1%. As observed in the work of Ruan and Chou (1998) on glass fabric/epoxy composite samples, the coupons tested here failed suddenly and catastrophically when the first damage initiated, with the consequence that there was no acoustic emission activity recorded until very close to failure.

The mechanical properties (Young's modulus, Poisson's ratio, tensile strength and strain to failure) for all the coupons tested are shown in Table 4.1 (average values and standard errors are shown) and all the results are shown graphically in Figures 4.13 to 4.16. It is clear from the results that the Young's modulus and tensile strength are both higher close to the wale direction as would be expected from the analysis of the loop shapes (Figure 4.3). On the other hand the Poisson's ratio variation and strain to failure are reasonably independent of the angle.

Examples of fractured specimens for each angle are shown in Figures 4.17 to 4.22 and higher magnification images of the fracture area can be seen in Figures 4.23 to 4.28. For the wale direction (0°), the fracture surface connects the needle of the loops in the crack direction. This can be clearly seen in Figure 4.23 where the needle of the courses 2 and 3 can be seen in the fracture surface, together with the fracture tows of course 1 (rib). The 30° specimen shows similar behaviour to the wale direction, cracks running parallel to the needle of the loops producing fracture surfaces inclined at 60^0 to the loading direction of the knitted fabric (Figure 4.18). Again the needle loops can be seen parallel to the course direction in the fracture area. A change in the fracture path was observed for the +45° and -45° specimens. Here the cracks tend to follow the legs of the loops (Figures 4.19 and 4.20) where they do not grow transversally in the specimen. Figures 4.25 and 4.26 show photographs of legs of the loops, which have been fractured as the cracks formed the fracture surface. In both the 60° and course direction (90°), the cracks again developed parallel to the sides or legs of the loops (Figures 4.21, 4.22, 4.27 and 4.28). For all angles, failure of the composites did not always lead to complete separation. The fracture surfaces were frequently connected by unbroken loops of bridging tows as seen, for example, in Figure 4.28.

Almost all of the single layer composite samples in all the orientations tested failed without any prior indication of damage, either visual damage (in the form of cracks) or damage recorded by the acoustic emission equipment (the only exception to this was the 0° (wale direction) and the 30° specimens in which very small amounts of AE were registered just prior to fracture).

As will be seen later (Chapter 5), the commercial composites tested in this work based on the same fabric failed at strains of about 2%, substantially higher than the strain to failure recorded here for single layer composites (typically 0.8%). Further, it is well known that commercial knitted fabric composites can show multiple matrix cracking prior to failure (see section 2.4.2 and 2.4.4 in the literature review). In order to be able to investigate damage accumulation prior to failure, the knitted fabric layer was sandwiched between 0° plies.

4.4. DAMAGE DEVELOPMENT IN THE MODEL 2X68 TEX SANDWICH COMPOSITES.

The previous section has shown that single layer knitted fabric composite samples were unable to show cracking development due to sudden fracture occurring as soon as damage initiated. Hence, sandwich laminates were made by winding unidirectional glass fibres over the 2x68 tex knitted fabrics as described in section 3.1. Observation of damage accumulation was facilitated by the transparent nature of the composite, which allowed the plan view damage development to be observed during testing by in situ photography. For all the sandwich laminates the average fibre volume fraction was measured obtaining a value of $29.0 \pm 0.2\%$.

4.4.1. MECHANICAL PROPERTIES

The sandwich laminates were used to investigate damage accumulation and hence their mechanical properties were not of particular significance. However for completeness Table 4.2 shows the mechanical properties of all the orientations tested and Figures 4.29 to 4.32 show Young's modulus, Poisson's ratio, tensile strength and strain to failure. Of interest here are the values of Poisson's ratio, which were up to 20% lower than in the single layer laminates, and the strain to failure. All the strains to failure of the sandwich composites are about 2% since the final failure of these laminates is controlled by the failure of the outer 0° plies. The stress-strain curve of the 0° plies alone was measured and the strain to failure was found to be about 2% (see later: Figure 4.80).

Another feature which should be noted is that the Young's modulus of the sandwich laminate is highest for a fabric orientation of 30°, although as in the single-layer composite specimens, there is little difference in the modulus between 0^0 and 30^0

In the following section, the behaviour of the sandwich composite specimens under load is described. Coupons were tested with the knitted fabric at angles of 0°, 30°, 45°, 60°, and 90°.

4.4.2. KNITTED FABRIC IN WALE DIRECTION (0°) PARALLEL TO THE 0° PLIES

Figures 4.33 and 4.34 show typical stress-strain curves for sandwich samples with the knitted fabric wale direction parallel to the 0° plies. The stress-strain curve is linear up to almost 1.0% strain when the first cracks appear in the sample. Figure 4.37 shows the development of cracking (i.e. crack density) with increasing strain. Immediately after the first cracks appear, a "knee" becomes visible in the stress-strain curve. At a higher strain of about 1.5% another "knee" appears.

Acoustic emission signals give additional information with respect to the damage development. A small number of acoustic emission events are observed between 0.80% and 0.95% strain. This is in advance of the development of the cracks and is related to crack initiation at cross-over points in the knitted fabric architecture (evidence for this is clearer at the other angles; see later). Next, in a range of 1.1% to 1.2% strain, the first significant cracks appear producing many more AE events.

Figure 4.35 and 4.36 show the ratio of transverse strains to longitudinal strains plotted as a function of the longitudinal strain. Those graphics suggest that the value of the Poisson's ratio is constant up to the strain at which the significant damage initiates, detected by acoustic emission at around 1.00% strain. At this point the Poisson's ratio value displays a decrement.

Crack density measurements enable the sequence of crack development to be identified. The crack density, which is defined as the number of cracks per unit length of the sample, was measured by drawing five lines at regular spacing on photographs of the cracks and measuring the number of intersections. The crack density as a function of strain is shown in figure 4.37. Cracks initiate at a strain of about 1.1% to 1.2% (as mentioned earlier) and above this strain, the rate of increase of crack density with strain is roughly uniform up to a strain of about 1.4%.

Beyond this strain the rate of increase of crack density reduces. The initial rate up to about 1.4% strain corresponds to the development of a fairly uniform crack pattern with a crack spacing of 4 mm as can be seen in figure 4.38. Beyond this strain further cracking produces a spacing of 2 mm. Indeed very few extra cracks are added between a strain of about 1.9% and failure (at about 2.2%), so that the crack density curve seems to show a plateau at a crack density of about 0.5 mm^{-1}. However, occasionally, additional cracks do form between the 2 mm cracks.

The cracking pattern which develops is intimately connected with the fabric architecture. Detailed discussion of this is reserved for a later chapter (Chapter 6), but figure 4.39 gives an indication of the sequence of events. The first sign of damage develops at the loop cross-over sites, represented by A (see section 4.4.2 for clearer evidence of this suggestion). Significant cracks appeared firstly in the plane where the float stitch of course 2 and 3 are together (represented by the dashed lines in Figure 4.37) possibly due to the strain magnification caused by adjacent tows. These cracks have a spacing of 4 mm, which is the dimension of the repetitive unit in the knitted fabric. When these sites have been used, then at a higher strain cracks develop where the rib holds threads 2 and 3 (represented by dotted lines), giving a final crack spacing of 2 mm, which is the wale direction dimension of a single loop.

4.4.3. KNITTED FABRIC WALE DIRECTION AT 30° TO OUTER PLIES

Figures 4.40 and 4.41 show stress-strain curves for samples for which the inner knitted fabric layer is at 30° to the outer 0^0 plies (loading is parallel to these outer plies). Linearity is observed at low strain up to about 1.2% strain when matrix cracks appear in the sample. At higher strain a second "knee" appeared in the samples, but this was not as prominent or consistent as for 0° specimens. In the same stress-strain curves the AE signal is displayed in order to relate the AE behaviour with the crack initiation and propagation. As can be seen from figures 4.40 and 4.41, AE indicating precracking damage begins at strains of about 0.80% - 0.90%, which is similar to that found in 0° specimens.

Figures 4.42 and 4.43 show the ratio of transverse strains to longitudinal strains plotted as a function of the longitudinal strain. Similarly to the curves observed in 0°, the decrement in the Poisson's ratio is related with the appearance of the significant cracking damage. The first AE signals named as predamage are not significant to disturb the curve greatly. The precracking damage occurs at the loop cross-over points and can clearly be seen in Figure 4.45 at strains above 1.00% as black spots on the photograph. The "knee" after the linearity appears at 1.2% (similar to the 0° fabric case) which is due to the development of many cracks.

Crack density is shown in Figure 4.44 where the curve behaviour is similar to that observed for 0°. There is an abrupt increment up to 1.2% strain and then a slight drop in density and then starts with an apparent uniform increment until failure. Figure 4.46 shows the sequence of cracking development with increasing strain. At low strains it is possible to see the microcracking in cross-over sites (labelled A in the figure) which are the crack initiation sites. As the strain increases, transverse cracks grow from these sites perpendicular to the loading direction. At higher strains a cracking pattern emerges parallel to the course direction of the knitted fabric.

This cracking pattern runs parallel to the direction of the cross-over points (represented by A in Figure 4.46) and is formed by accentuated cracking around the loops of the fabric where the loops are perpendicular to the loading direction. From these crack initiation sites, as already stated above, transverse cracks grow across the coupons, perpendicular to the loading direction. At higher strains the accumulating damage leads to a pattern of cracks dominated by transverse cracking (represented by B), such that the accentuated cracking around the loops forms a pattern in the course direction of the fabric. The accentuated cracking occurs around the head or needle of the loops and the pattern which forms has a spacing of 4 mm (see Figure 4.45). This spacing is the distance of the repeating unit of the fabric (see Figure 4.1).

4.4.4. KNITTED FABRIC WALE DIRECTION AT 45° TO OUTER PLIES

Figures 4.47 and 4.48 show stress-strain curves for samples tested with the knitted fabric at 45^0 to the outer 0^0 plies. The linearity can be observed up to about 0.85% strain and then a "knee" appears due to cracking accumulation. Here there is no prominent second "knee" in the stress-strain curve. AE begins at about 0.6% - 0.75% strain and crack accumulation from about 0.75% strain.

Figure 4.49 and 4.50 show the ratio of transverse strains to longitudinal strains plotted as a function of the longitudinal strain. It is evident the change on the ratio due to the cracking damage, for this case the significant damage was detected at lower strains than the 0^0 and 30^0 at about 0.8% strain. The change in crack density with strain is shown in Figure 4.51. The crack density increases uniformly with increment of strain up to about 1.50% strain when the crack accumulation rate slows.

Figure 4.52 shows the cracking behaviour sequence at different strains from predamage to near failure. Again at low strains the precracking damage at loop cross-over points can be seen as tiny black spots on the photographs (especially at 1.25% strain). Transverse cracks appear in the sample to again be initiated from these cross over sites. At high strains the cracks try to follow the path of the loops, as for the 30^0 specimens, again creating a pattern with a 4 mm spacing at 2% strain.

Cracking behaviour is explained using Figure 4.53. Again the first damage occurs at the cross-over points (represented by A). At higher load, matrix cracks grow perpendicularly to the load direction from initiation sites, forming an irregular crack pattern (represented by B). At the same time a regular pattern emerges (as observed at 30°) due to accentuated cracking around the head or needle of the loops. As before, this pattern (represented by C in figure 4.53), has a spacing of 4 mm, though now it lies at 45^0 to the loading direction.

It might be expected that since there are cross-over pints for every loop, that the pattern which emerges due to the accentuated cracking around the needles of the loops should have a spacing of 2 mm. However, it was found that this accentuated cracking occurs along those planes in the fabric where the float stitch of course 2 and 3 are held together by the rib course. This occurs every 4 mm. The geometry of the accentuated cracking pattern can also be described in another way. It is as if the regular cracking pattern of the 0° specimen at a strain of 1.30% (Figure 4.36) is rotated clockwise through 45° to produce the accentuated 4 mm spacing at a strain of 2.00% (Figure 4.52)

4.4.5. KNIITED FABRIC WALE DIRECTION AT 60° TO OUTER PLIES

Figures 4.54 and 4.55 show the stress-strain curve for samples tested at 60°. In this case, the linearity can be observed up to 0.85% - 0.90% strain and then the same "knee" indicating significant cracks, appears at this strain. An AE signal was recorded at slightly lower strains for predamage in comparison with the others angles. The number of acoustic emission events grew gradually and uniformly with strain up to failure.

Figure 4.56 and 4.57 show the ratio of transverse strains to longitudinal strains plotted as a function of the longitudinal strain. The variation of Poison's ratio is accentuated with the main cracking damage as observed before. This discrepancy of the ratio can be related with the AE signals detected.

Crack density is plotted in Figure 4.58 showing the increment of cracks in relation to the strain. This curve is similar to that observed in 90° (course direction; see later, section 4.4.5). The transverse cracks in this case appear to branch with the consequence that the number of cracks per unit length is higher than for previous angles (0^0, 30^0 and 45^0).

Figure 4.59 shows the cracking behaviour sequence at different strains. At a strain of 0.75% the initiation sites, which are again the cross-over points, can be identified as tiny black spots on the photographs. For the previous angles, the transverse cracks which initiate from the cross-over points led to a clear pattern due to the accentuation of the cracks at the needles of the loops. A slightly different pattern can be seen in this case. The cracks formed at 60° are accentuated and seem to track the legs of the loops which have a 2 mm spacing (shown previously by C in Figure 4.1a)

Cracking behaviour is explained using Figure 4.60. As observed from the AE signals, predamage starts at about 0.65% – 0.75% strain in the form of cracking at the loop cross-over sites (represented by A), (it is difficult to see the sites clearly at this angle in Figure 4.51). At this angle, all these sites are sites where cracks potentially can grow. When the load is increased, cracks appear from these points, coalescing to develop transverse cracks across the sample. The cracks form an irregular pattern as they follow the loops (represented by B), and finally, the cracks form a regular pattern at 60° following the legs of the loops in the wale direction (this pattern can be seen in Figure 4.51). The pattern has a spacing of 2 mm since the legs of the loops are spaced 2 mm apart (represented by C). These dimensions are shown in Figure 4.1a.

4.4.6. KNITTED FABRIC AT 90° TO THE OUTER PLIES

In this orientation, the fabric is being loaded parallel to the course direction. . Typical stress-strain curves can be seen in Figures 4.61 and 4.62 where linearity can be appreciated up to 0.7% -0.8% strain. The first damage observed is again in the form of microcracks at the loop cross-over points. This can just be seen at a strain of 0.9% in Figure 4.66.' Matrix cracking appeared at a strain of about 0.8% producing a small knee in the stress-strain curve. During loading in this direction, branched-like cracks were observed perpendicular to the load direction. The first damage observed is again in the form of microcracks at the loop cross-over points. This can just be seen at a strain of 0.9% in Figure 4.56. Matrix cracking appeared at a strain of about 0.8% producing a small knee in the stress-strain curve while the acoustic emission signal seems to be uniformly increasing up to near fracture.

The ratio of transverse strains to longitudinal strains plotted as a function of the longitudinal strain is shown in Figure 4.63 and 4.64. Again it is possible to identify the cracking damage initiation and propagation by observing the variation of the ratio. Figure 4.65 shows the cracking density in the course direction in which a constant increase is observed due to the nature of the cracks. The crack density increases fairly uniformly since cracks are able to propagate and grow following the legs of the loops. As the cracks curve to follow the needle, or head, of the loops, they cross a loop and hence take on a branched appearance. The cracking development sequence can be seen in Figure 4.66. At low strains, cracking at the cross-over points is visible, again as black spots in the photographs (represented by A). In this orientation, it is easy for the developing matrix cracks to link up as they grow. Hence, the crack density increases fairly uniformly.

Figure 4.67 shows a schematic of crack formation. The crack initiation points are represented by A, where the yarns are joined together (cross-over). All these sites coalesce to propagate the cracks along the sample perpendicularly to load direction by running on the sides or legs of the loops.

4.5 COMPARISON OF RESULTS FOR DIFFERENT ANGLES OF THE KNITTED FABRIC IN THE MODEL SANDWICH MATERIAL

The first comparisons which can be made for the damage initiation and propagation for the various fabric angles is the difference between the single layer behaviour and the behaviour observed on the fabric in the model sandwich laminate. Table 4.3 summarises the single layer samples failure and, for the model sandwich coupons, both the initiation of predamage strain range and the matrix cracking onset strain range. Comparisons done between the single layer failure strains and the sandwich laminate predamage strain show that these correspond fairly well. Therefore, as suggested earlier, the onset of predamage in the single layer material leads immediately to the failure of these samples for all angles. Hence the value of the sandwich laminate technique used to investigate the development of damage is immediately clear.

The influence of the knitted fabric architecture in determining the damage development in the composites has been also shown in the results. The identification of the predamage as occurring in the cross-over points in the knitted fabric architecture was identified and determined by the transparency of the coupons, together with the employment of the acoustic emission (AE) technique. It was demonstrated that the most important sites for predamage occur in the fabric planes where the float stitch of courses 2 and 3 are held together. In all the samples, the development of the matrix cracks was observed to initiate at these cross-over points perpendicular to the load direction and independently of the angular orientation. However, it is important to note that the macroscopic cracking behaviour of these sandwich laminate coupons is dominated by the stiff outer 0° plies and as a result the matrix cracks do not follow the knitted fabric architecture completely (in the commercial composites to be discussed in the next chapter, the cracking behaviour is not affected in the same way). It was observed that in the sandwich specimens which have the wale or course direction parallel to the 0° outer plies and 90° fabric angles, matrix cracking would be expected to follow the wale or course direction. Therefore, for these particular cases, the development of the matrix cracking damage is not affected in the same way by the outer 0° plies.

Although the development of matrix cracking is affected in the off-axis specimens by the outer 0^0 plies, the fabric architecture still exerts an effect on the cracking damage. For the 30^0 and 45^0 sandwich laminate specimens, the accentuated cracking which develops at high strain occurs around the needle, or head of the loops in the fabric architecture. Careful observations identified that for samples tested at 30^o the accentuated cracks appeared in the majority of the loops, however, for samples at 45^o this accentuated cracking corresponds to the plane where course 2 and 3 are drawn together by the rib course which occurs every 4 mm. On the other hand, for the 60^0 sandwich specimens, the accentuated cracking develops along the legs of the loops and the legs of the loops have a spacing which is much smaller (about 2 mm). The consequence is that the crack densities achieved in the 60^0 and 90^0 specimens, where cracking is affected by the legs of the loops, are higher. Figure 4.68 shows that whereas crack densities in the 60^0 and 90^0 specimens approach 1.5 mm^{-1}, they do not exceed 0.8 mm^{-1} for the other angles.

Table 4.3 also shows that, in general, the strain for the onset of matrix cracking increases as the angle of the fabric increases away from the 0^0 outer ply directions. A simple technique has been developed here which enables a clear comparison to be made between the onset strain for cracking in the sandwich coupons for different angles. The technique makes use of the rule-of-mixtures expression applied to the 0^0 layers and the knitted fabric layer of the sandwich coupons. For the model sandwich composites, the rule-of-mixtures gives the stress for the model composite, σ_c, as

$$\sigma_c = \sigma_{(0)} V_{(0)} + \sigma_{(k)} V_{(k)} \qquad (4.1)$$

where $\sigma_{(0)}$ is the stress in the outer 0^0 plies, $\sigma_{(k)}$ is the stress in the knitted fabric layer, $V_{(0)}$ is the volume fraction of 0^0 plies in the model composite and $V_{(K)}$ is the volume fraction of the knitted fabric layer in the model composite. Assuming that the outer 0^0 plies behave in a linear elastic manner then

$$\sigma_{(0)} = \varepsilon E_{(0)} \qquad (4.2)$$

where $E_{(0)}$ is the Young's modulus of the 0^0 plies and ε is the strain applied to the model composite. Substitution gives the stress in the composite to be

$$\sigma_c = \sigma_{(k)} V_{(k)} + \varepsilon E_{(0)} V_{(0)} \qquad (4.3)$$

Solving for $\sigma_{(K)}$, the stress in the knitted fabric layer, gives

$$\sigma_{(k)} = \frac{\sigma_c}{V_{(k)}} - \frac{V_{(0)} E_{(0)}}{V_{(k)}} \varepsilon \qquad (4.4)$$

This equation allows the knitted fabric layer stress, $\sigma_{(K)}$, to be found for increasing values of the composite strain, ε.

Derived stress-strain curves for the knitted fabric layer in the model sandwich laminate using equation 4.4 are displayed in Figures 4.69 to 4.73 for all the angles tested for the model sandwich material. In deriving these results, the volume fraction of the knitted layer and 0^0 plies is calculated from the thicknesses of the layers measured from edge sections. When the Young's modulus of the 0^0 plies is taken to be 40 GPa then the initial slope of all the stress-strain curves corresponds to a Young's modulus of about 6 GPa, which is close to the measured moduli of all the single layer knitted composites (see Table 4.1). Equation 4.4 is quite sensitive to the value of $E_{(0)}$, and the value of 40 GPa was chosen to give the best fit. Using this method, the strains for the onset of matrix cracking appear in all the curves in Figures 4.69 to 4.73 as a sharp discontinuity. Also, it is clear that the precracking damage, ie the damage which occurs at the loop cross-over points before matrix cracking begins, does not affect the derived stress-strain curves. Only the matrix cracking damage produces such an effect. The results from Figures 4.69 to 4.73 confirm that the onset of matrix cracking damage occurs at smaller values of the applied strain as the loading direction for the fabric changes from the wale to the course directions. In other words, it is easiest to initiate matrix cracking in specimens loaded in the course direction.

The matrix cracking damage is an important feature of damage accumulation but it was decided to investigate whether the matrix cracking was associated with significant fibre or tow fracture. Small pieces of sandwich laminate specimens were removed from fractured specimens of wale and course sandwich laminates, with the samples taken well away from the fracture planes of the specimens. The polymer matrix of these pieces was burnt-off using the same technique as used for obtaining the fibre volume fractions. Microscopical investigation of the remaining glass tows showed no indication of fibre breakage, and certainly no tow fracture, even though the specimens had failed at these strains at another location within the specimen. Hence, it can be concluded that fibre tows remain intact to high strains during quasi-static tensile loading. In order to investigate whether the role of the fibre tows could be further understood, it was decided to subject the coupons to cyclic loading experiments which are presented in the next section.

4.6. CYCLIC TESTS OF MATERIALS TO DIFFERENT STRAINS.

Three types of model sandwich specimen were used for these experiments at orientations 0°, +45° and 90°. In addition, both unidirectional (ie 0^0 plies alone) and a cross-ply laminate were tested for comparison. In each case, the specimens were loaded to an applied strain of 0.6%, unloaded and then reloaded to a strain of 1.0%, unloaded and reloaded to a strain of 1.5%, before finally being unloaded and then reloaded to failure. Both the stress, strain and acoustic emissions were recorded during the tests.

4.6.1. CYCLIC LOADING OF SANDWICH LAMINATE SPECIMENS IN WALE DIRECTION (0°) PARALLEL TO THE 0° PLIES

The material at this angle exhibits linearity when loaded and unloaded to a strain of 0.6% as can be seen in Figure 4.74. As found previously for these specimens (Figure 4.34), no damage occurs until a strain above about 0.8% is applied, and hence no acoustic emission was recorded.

The specimen was unloaded completely and the stress-strain behaviour is almost completely linear elastic. The specimen was then reloaded to a strain of 1% and it can be seen that AE activity began at a strain of about 0.8% as found previously. Interestingly, during unloading the specimen again shows an almost completely linear elastic response down to the zero stress/zero strain. This shows that the damage developed at the loop cross-over points has a negligible effect on the stress-strain behaviour. The development of matrix cracking damage occurred as before at about 0.95% strain, and when the applied strain had reached 1.5%, a significant amount of cracking had occurred (see, for example, Figure 4.37). The AE activity increased dramatically during crack development, as found before. Unloading the specimens this time produced a permanent residual strain of about 0.06%. The development of this residual strain as a consequence of matrix cracking damage is the same as found by Bassam et al (1998) in cross-ply laminates. It is due to the release of the compressive thermal strains in the 0^0 plies. These develop due to the mismatch in the coefficients of thermal expansion between the central layer (which is here a knitted fabric composite) and the outer 0^0 plies. The specimen was then reloaded to failure and Figure 4.74 suggests that during reloading the AE activity began at a strain of about 1.3%, even though the specimen had previously been loaded to a strain of 1.5%.

The results can be plotted in a different way to make the interaction between stress, strain and AE activity clearer. Figure 4.75 shows the stress plotted against the cumulative strain during the cyclic tests. This simply means that the strain seen by the specimen is summed, with the unloading strains treated as if they were positive. The peaks in Figure 4.75 represent the specimen being loaded to the successively higher strains of 0.6%, 1.0%, 1.5% and then to failure. The results show that there was very little AE activity for loading to 1.0% strain, but substantial activity for loading to 1.5% strain, and then to failure. A number of interesting observations can be made with the aid of this plot. The third peak represents an applied strain of 1.5% and is labelled A_1. If a perpendicular line is drawn from A_1 to the cumulative strain axis, then it is clear that while the specimens are being unloaded, AE activity continues for an unloading strain of about 0.2%.

Now, if a horizontal line is drawn from A_1, it intersects the final loading line at point A_2. If, again, a perpendicular line is drawn from A_2 to the cumulative strain axis, it is clear that AE activity begins before the specimen has reached the previous peak stress value represented by point A_2.

Very similar results are found for the 45^0 and 90^0 specimens. The specimens with the knitted fabric at 45^0 show a stress-strain curve for a peak strain of 1.0% and then unloading which is not linear elastic but shows a small hysteresis. Otherwise all the observations made above about the 0^0 specimens are repeated for these angles, ie the development of the residual strain and the behaviour of the AE. The results are shown in Figures 4.76 to 4.79. In figures 4.77 and 4.79, the same construction for points A_1 and A_2 is shown. Again, for these angles, AE activity continues during unloading (from point A_1) for a strain of about 0.2% and begins again during loading by a strain of about 0.2% prior to reaching point A_2 on the stress-strain curve.

To investigate whether these observations are significant, further tests were carried out on unidirectionally reinforced coupons (ie 0^0 plies alone) and cross-ply coupons.

4.6.2 CYCLIC LOADING OF 0^0 PLY AND CROSS-PLY COUPONS

A lamina made up of only unidirectional glass fibres (0^0 plies) and a cross-ply laminate were manufactured and analysed in order to obtain some AE data from cyclic loading experiments on these specimens.

Figures 4.80 and 4.81 show the mechanical testing and AE data for the cyclic tests on the unidirectional material. The specimen was loaded to strains of 0.6%, 1.0% and 1.5% as in the tests on the model sandwich material of section 4.6.1. Surprisingly, Figure 4.80 shows that there was some AE activity recorded even at quite low strains, although the majority of the AE activity occurred at strains above about 1.7% and near to failure at about 2% strain.

The Young's modulus and principal Poisson's ratio were found to be 29.5±0.5 GPa and 0.33, which are both reasonable for unidirectional glass fibre/epoxy with a fibre volume fraction which was measured to be 38±1 %. For the unidirectional material, the same construction can be made linking the peak stress at an applied strain of 1.5% (labelled point A_1) to the stress when the specimen was being reloaded to failure (Figure 4.81). However, in this case, the amount of AE activity during unloading from A_1 is very small, and the amount of AE before point A_2 is also very small; in each case the AE activity might extend for a strain of about 0.05%, compared to 0.2% in the case of the sandwich coupons.

The results for the crossply laminates tested in a similar way are shown in Figures 4.82 and 4.83. Again samples were tested to different strains (0.6%, 1.0% and 1.5%), and then to failure. The stress-strain curve of Figure 4.82 shows that during loading to a strain of 0.5%, the first cracks initiated at a strain of about 0.35%, giving a characteristic 'knee' in the stress-strain curve. Constructing the points A_1 and A_2 on the stress-cumulative strain curve of Figure 4.83, it would appear that, as in the case of the unidirectional material, the amount of AE activity during unloading from A_1 is small, and the amount of AE before point A_2 is also small. In this case, the AE activity might extend for a strain of about 0.1% beyond point A_1 during unloading, and about 0.1% in advance of point A_2, compared to 0.2% in the case of the sandwich coupons.

4.6.3.- COMPARISON OF CYCLIC LOADING TEST RESULTS FOR SANDWICH, UNIDIRECTIONAL AND CROSS-PLY COMPOSITES

The behaviour of the sandwich laminate specimens and the cross-ply composite laminates was similar in a number of ways. Firstly, in both cases, the stress-strain curves were linear-elastic up to the onset of matrix cracking. Once matrix cracking had developed, then unloading the specimens produced a residual strain in both cases due to the relaxation of the thermal residual strains.

The AE results, however, showed some possible differences. In the case of the knitted-fabric sandwich laminates, after matrix cracking has initiated, the AE appears to continue as the laminate is unloaded for a strain of about 0.2%. Additionally, during unloading and reloading, the AE begins at a lower stress than the peak stress in the previous loading cycle. This lower stress corresponds to a strain of about 0.2% less than the strain at which the previous peak stress was achieved.. Although similar AE effects were found in the cross-ply laminates, the comparable strain range appeared much smaller (about 0.1%). In the case of the unidirectional laminate, the effect was almost completely absent.

Burning away the matrix in fractured sandwich laminate coupons showed that there had been no fibre fracture or tow fracture. Hence, it seems likely that the knitted fabric loops bridge the matrix cracks which develop in the knitted fabric layer. It is therefore possible that the AE effects mentioned in the previous paragraph are due to the pulling out of tows across the matrix cracks. Possibly the tows are debonding from the matrix and sliding in the debonded region. Such an effect would produce the AE effects observed during both loading and unloading. Similar, though much less clear effects were observed in the cross-ply laminates, although in this case, bridging fibres may be the cause. The method for displaying the results, using the cumulative strain, has revealed these differences. However, more work is required to carefully define the differences in the behaviour of the cross-ply laminates and the sandwich laminates with the knitted fabric layer.

4.7. RESUME AND DISCUSSIONS

Unidirectional reinforcement of the knitted fabric layer in a sandwich-like composite has been shown to be an excellent option in order to appreciate the damage behaviour in the textile layer. The model sandwich laminates allowed the measurement and analysis of the damage progression in the knitted fabric composite layer, to determine the damage initiation sites and to comment on the development of damage in relation to the fabric architecture.

It was found that the majority of the single layer composite samples tested in all angular orientations failed without any prior indication of damage, either visual or recorded by the acoustic emission equipment. Stress-strain curves showed a small non-linearity independently of angular orientations. Samples tested at 0^{o} and 90^{o} directions fractured perpendicular to the load direction while the other angles (30^{o}, $+45^{o}$. -45^{o}, and 60^{o}) were affected by the orientation of the knitted fabric. On the other hand, the sudden fracture of the samples was solved by winding the unidirectional glass fibres which allowed the observation of the failure mechanism through coupon. The first appreciable registration of damage in the tensile samples was observed to be the cross-over points as a microdebonding in the fibre-matrix interface, which appear at low strains as predemage regardless of the angular orientation. Although the failure mechanism was dominated by the outer 0^{o} plies, the influence of the knitted fabric architecture at different angular orientations was evident by dictating the cracking development in the material.

From the tensile test of model materials, vital information about the cracking behaviour in accord to the angular dependence was obtained where the two main orientations, wale and course direction, were observed to be dominant during the angular test, which at the end determined the path of the cracks in the fabric structure, as well as in the amount of cracks as observed in the crack density curves. Mechanical parameters of the model materials samples were dominated by the unidirectional reinforcement, therefore the values are not too different.

The locations of the cracks in the samples tested in all angles were initially relatively random, but as loading progressed, a more regular pattern was emerging and the spaces between the cracks are more uniform. Leong et al (1997) found similar cracking behaviour in their samples. Fracture of the samples involves yarn/matrix interfacial debonding, resulting in smooth fracture paths, which follows the path of the yarn loops and bridging yarn breakage and pull-out, resulting in rugged fracture paths. Ruan and Chou (1998) described similar observations of their fractured samples.

Figure 4.84 shows photomicrographs of tensile specimens in wale and course direction where fibre bundle debonding and resin cracking from the debonded sites are evident. In both cases fracture appeared to have occurred in the planes of lowest fibre content for both specimens. Similar results were obtained by Anwar et al (1997). Investigations of fracture surfaces suggest that debonding of fibre bundles occurs at those portions of knit loops which are oriented normal to the loading direction.

Derived stress-strain behaviour for the model material gave information about the performance of the knitted cloth alone when the composite is loaded in tensile mode. There was found certain similarity between the stress-strain curve of the derived data and that obtained from the single layer tensile tests. Discrepancy in the behaviour was found when the material is loaded in both wale and course directions and the other angles due to the knitted fabric architecture as it is going to be explained in the next chapter.

Cyclic tests demonstrated variations in the stress-strain curve due to damage accumulation in the knitted fabric composites. The appearance of significant number of cracks alters the linearity of the curve and develops more acoustic emission signals.

TABLES

Table 4.1.- Mechanical parameters for single 2x68 knitted layer composite

Angle	#	E	ν	UTS (MPa)	εf (%)
0°	1	6.6	0.39	51.6	0.80
	2	6.7	0.38	53.0	0.79
	3	6.8	0.37	51.5	0.80
	4	6.3	0.37	53.8	0.89
Average		***6.6 ±0.1***	***0.37± 0.01***	***52.5 ±0.6***	***0.82 ±0.03***
30°	1	6.1	0.37	49.8	0.84
	2	6.6	0.38	45.4	0.74
	3	6.9	0.36	51.9	0.80
	4	6.4	0.38	50.0	0.79
Average		***6.5 ±0.2***	***0.37± 0.01***	***49.3 ±1.2***	***0.79 ±0.02***
-45°	1	5.6	0.37	44.3	0.75
	2	5.3	0.38	46.9	0.58
	3	5.9	0.39	47.3	0.76
	4	5.7	0.36	48.8	0.86
Average		***5.6 ±0.1***	***0.38±0.01***	***46.8 ±0.9***	***0.74 ±0.06***
+45°	1	6.4	0.36	49.2	0.71
	2	6.1	0.38	48.2	0.77
	3	5.8	0.34	52.4	0.93
	4	6.3	0.38	45.7	0.75
Average		***6.2 ±0.1***	***0.37±0.01***	***48.9 ±1.4***	***0.79 ±0.06***
60°	1	5.8	0.36	35.8	0.61
	2	6.8	0.4	48.4	0.77
	3	5.5	0.31	45.6	0.83
	4	5.4	0.33	49.2	0.85
Average		***5.9± 0.3***	***0.35 ±0.02***	***44.8 ±3.1***	***0.77 ±0.05***
90°	1	4.0	0.33	29.2	0.80
	2	3.9	0.33	27.2	0.71
	3	3.8	0.33	28.3	0.74
	4	4.2	0.35	26.7	0.64
Average		***3.9 ±0.01***	***0.33± 0.01***	***27.9 ±0.6***	***0.72 ±0.03***
Volume fraction = 13±0.1%					

Table 4.2.- Mechanical parameters for a 2x68 knitted layer reinforced composite (Model material)

Angle	#	E	ν	UTS (MPa)	εf (%)
0°	1	18.9	0.33	331.1	2.1
	2	17.7	0.33	314.7	2.1
	3	18.3	0.32	290.8	2.0
	4	17.6	0.31	335.5	2.1
Average	***x***	***18.1 ± 0.3***	***0.32± 0.01***	***318 ± 10.1***	***2.1***
30 °	1	19.2	0.31	379.2	2.2
	2	18.9	0.31	369.3	2.2
	3	19.5	0.32	356.3	2.1
	4	19.3	0.29	359.8	2.1
Average		***19.2 ± 0.1***	***0.31± 0.01***	***366 ± 5.14***	***2.2***
+45 °	1	16.6	0.28	345.6	2.0
	2	15.7	0.29	319.5	2.0
	3	16.5	0.28	336.9	2.1
	4	16.6	0.32	303.1	2.1
Average		***16.4 ± 0.2***	***0.29± 0.01***	***326.3 ± 9.43***	***2.1***
60 °	1	14.9	0.33	364.8	2.0
	2	15.3	0.30	376.8	2.0
	3	14.3	0.32	380.4	2.1
	4	15.7	0.32	398	2.0
Average		***15.5 ± 0.3***	***0.32± 0.01***	***380 ± 6.9***	***2.0***
90°	1	13.7	0.33	363.9	2.2
	2	16.2	0.34	339.2	2.1
	3	15.8	0.32	358.8	2.2
	4	15.4	0.29	324.4	2.0
Average		***15.28 ± 0.6***	***0.32 ± 0.01***	***346.6 ± 9.1***	***2.1***
Volume fraction = 29±0.2%					

Table 4.3.- Variation of data taken from acoustic emission technique to five samples at each angle (Model material).

Angle	Predamage strain (%)	Crack onset strain (%)	Single layer failure strain
Wale (0°)	0.80 – 0.95	0.95 – 1.05	0.82
30°	0.75 – 0.90	0.90 – 1.00	0.79
45°	0.65 – 0.70	0.75 – 0.85	0.74/0.79
60°	0.65 – 0.75	0.80 – 0.85	0.77
Course (90°)	0.65 – 0.85	0.80 – 0.90	0.72

FIGURES

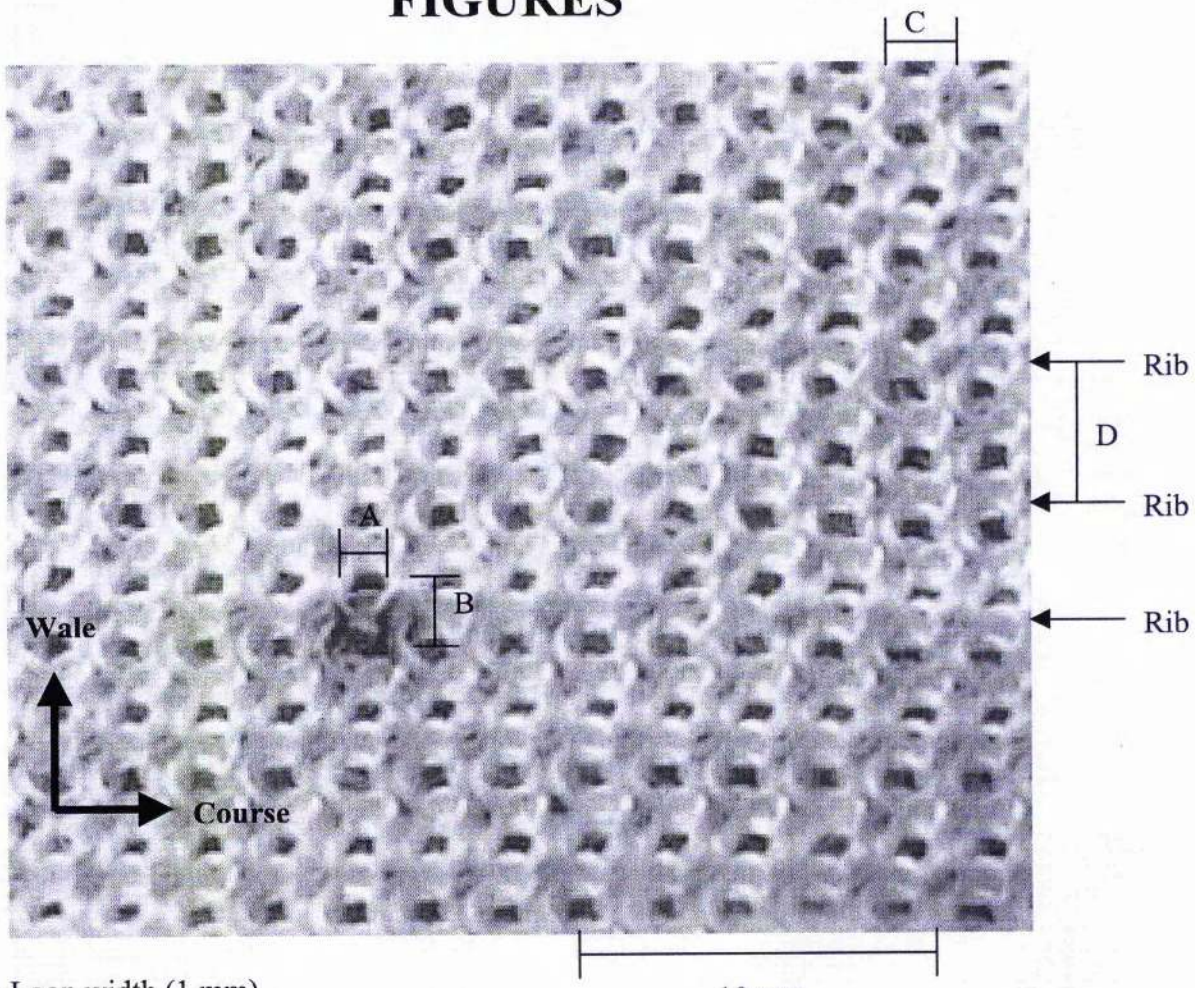

A= Loop width (1 mm)
B= Loop length (2 mm)
C= Distance between ribs in wale direction (2 mm).
D= Repetitive unit length (4 mm)

(a)

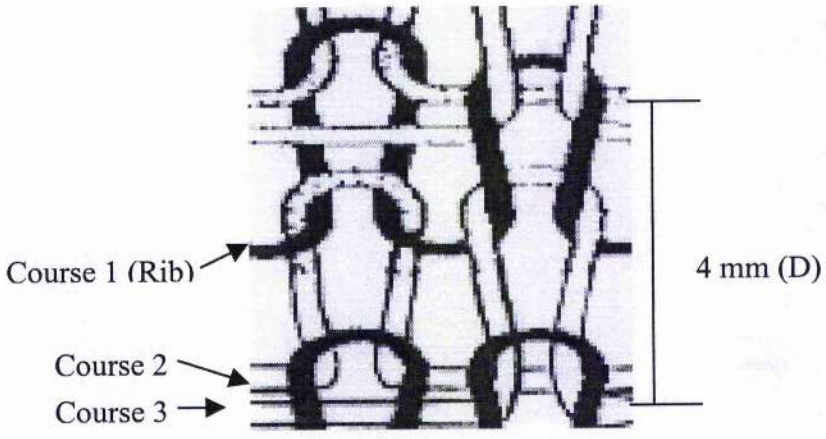

(b)

Figure 4.1.- Milano weft Knitted fabric. (a) A loop (near A and B) has been inked for clarity; (b) A two-dimensional view of the repetitive unit of the fabric architecture

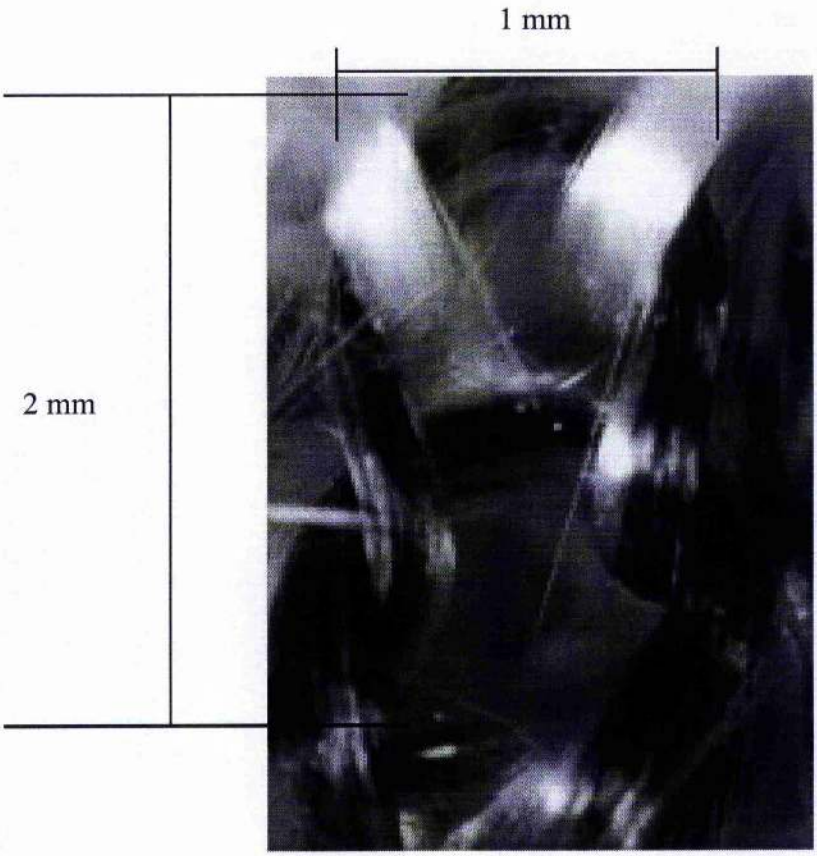

Figure 4.2. Single loop f the knitted fabric.

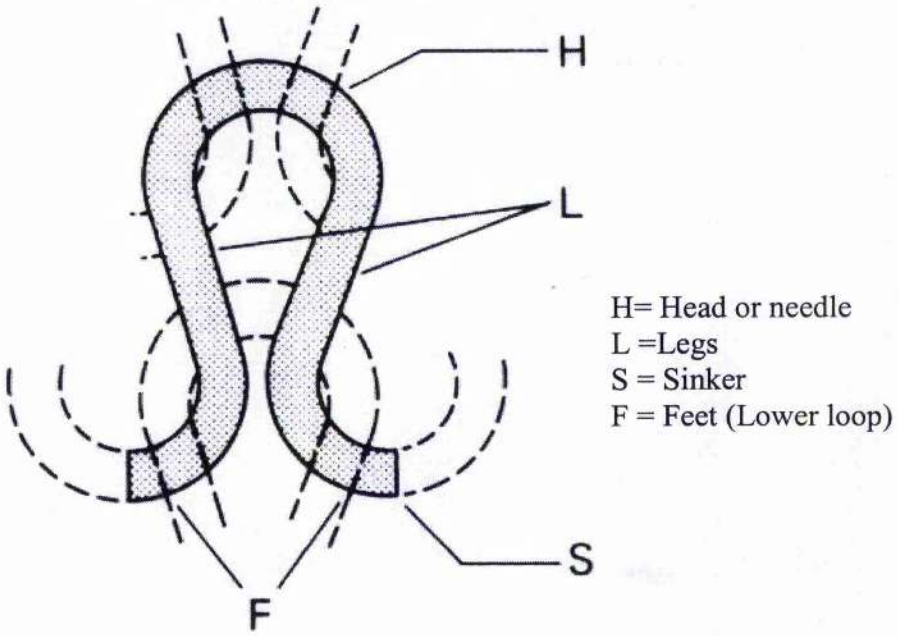

Figure 4.3.- Knitted fabric single loop and terminology.

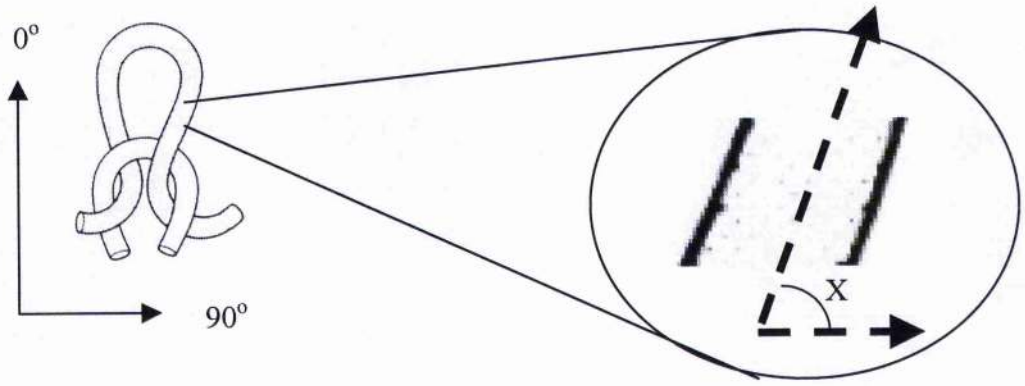

Figure 4.4.- Measurements for determination of fibre orientation.

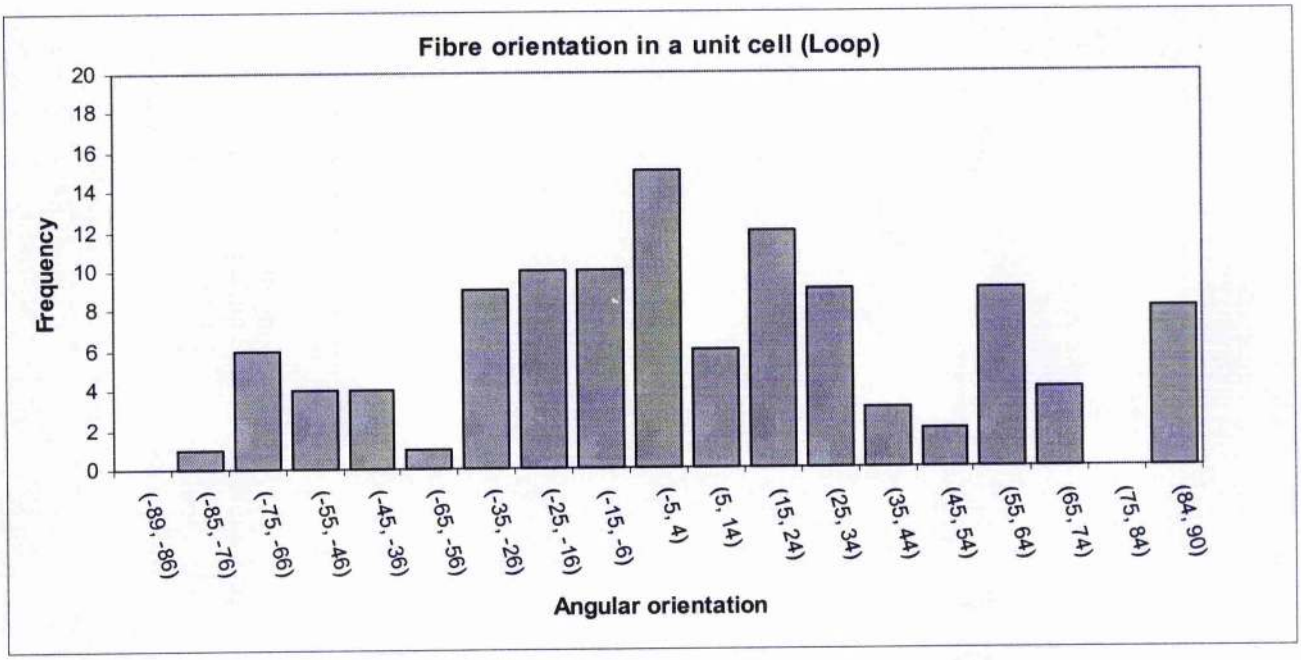

Figure 4.5.- Histogram representing the angular orientation of the fibres in the loop.

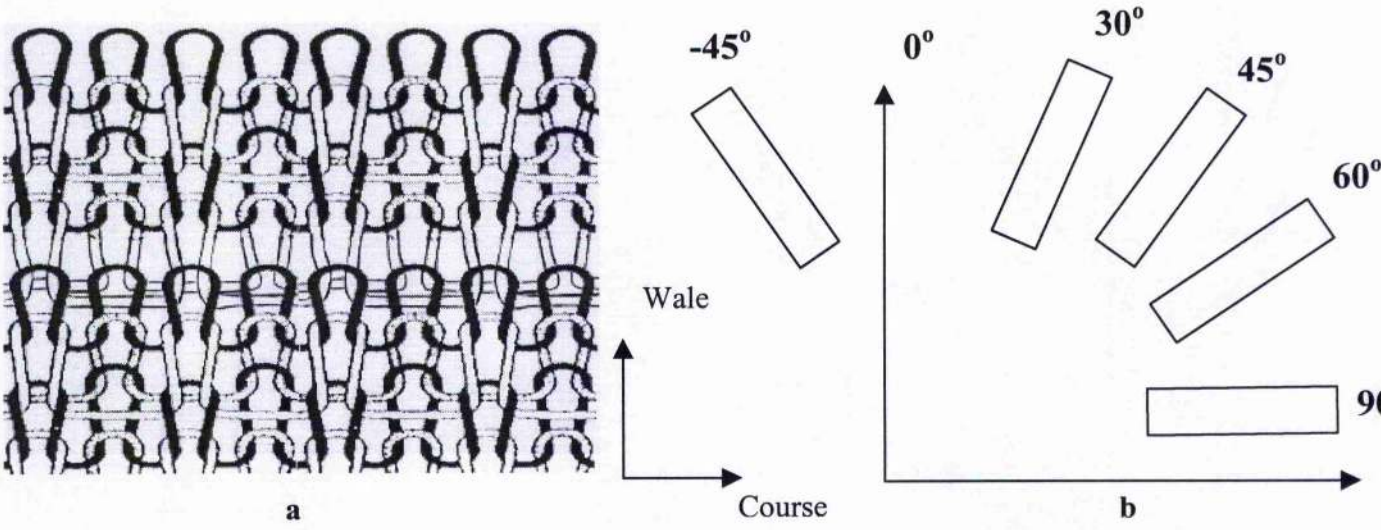

Figure 4.6.- (a) Wale and course directions of the knitted fabric, (b) angular orientations of coupons for single layer tests.

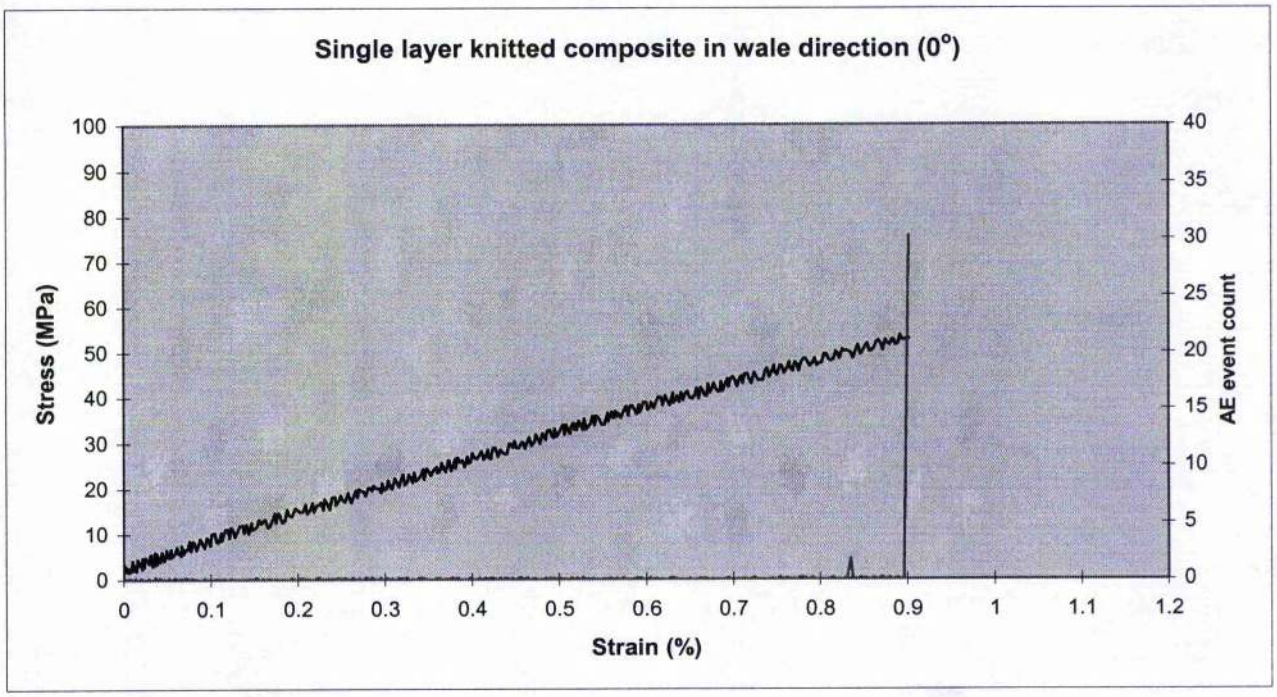

Figure 4.7.- Stress-strain curve for single layer sample in 0° direction.

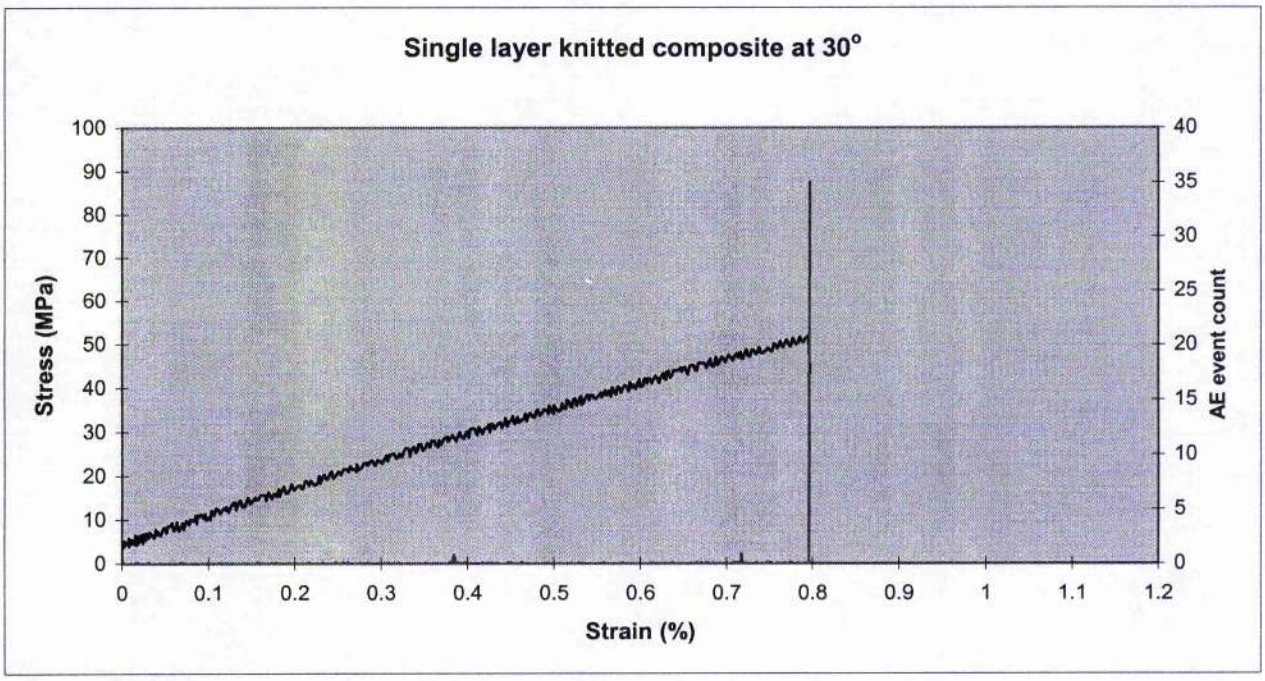

Figure 4.8.- Stress-strain curve for single layer sample in 30° direction.

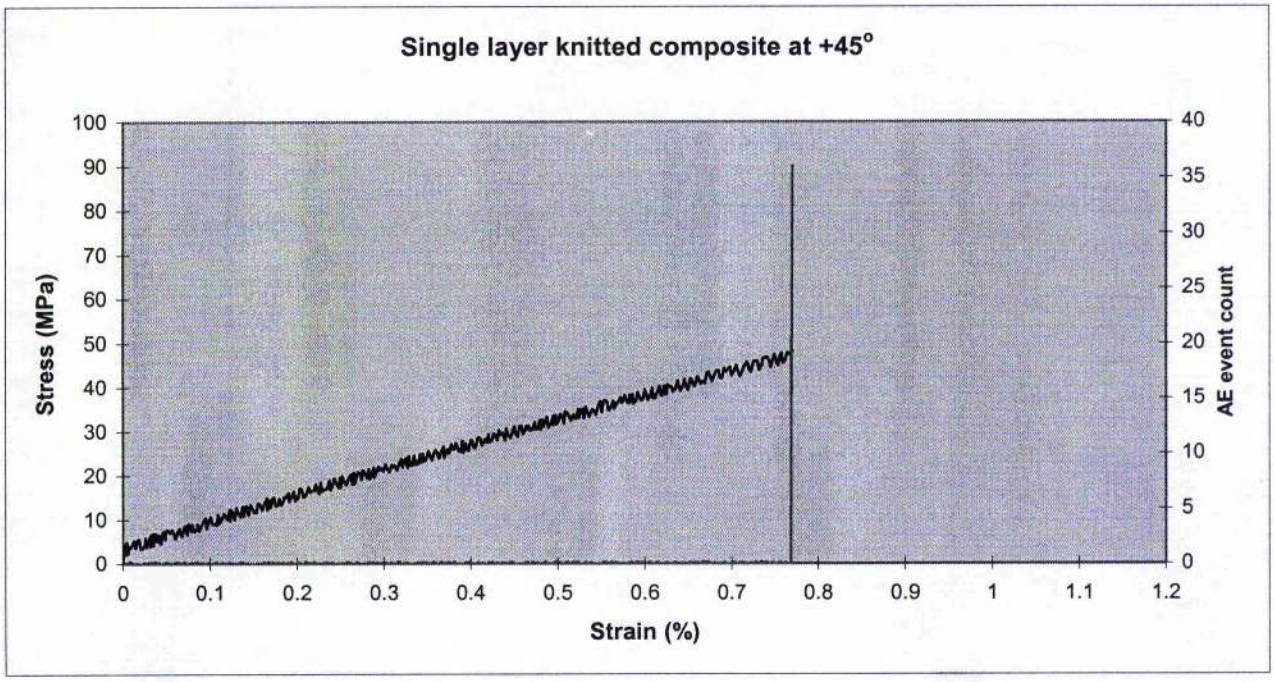

Figure 4.9.- Stress-strain curve for single layer sample in +45° direction.

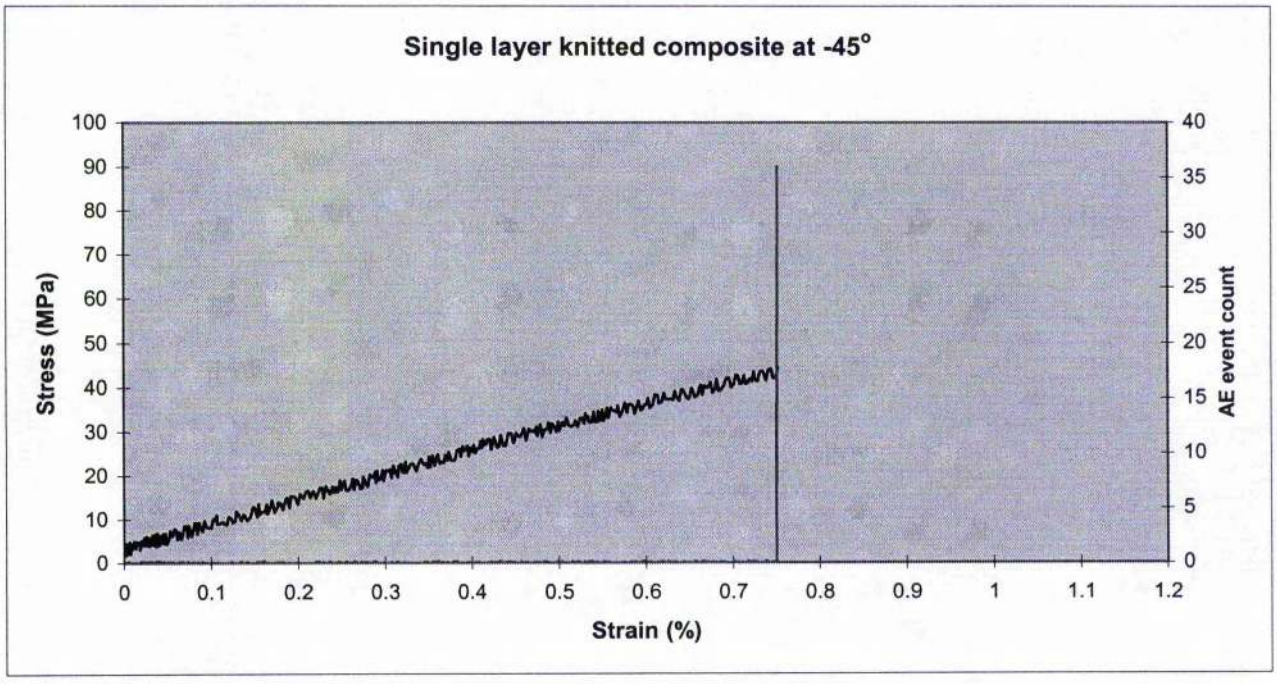

Figure 4.10.- Stress-strain curve for single layer sample in -45° direction.

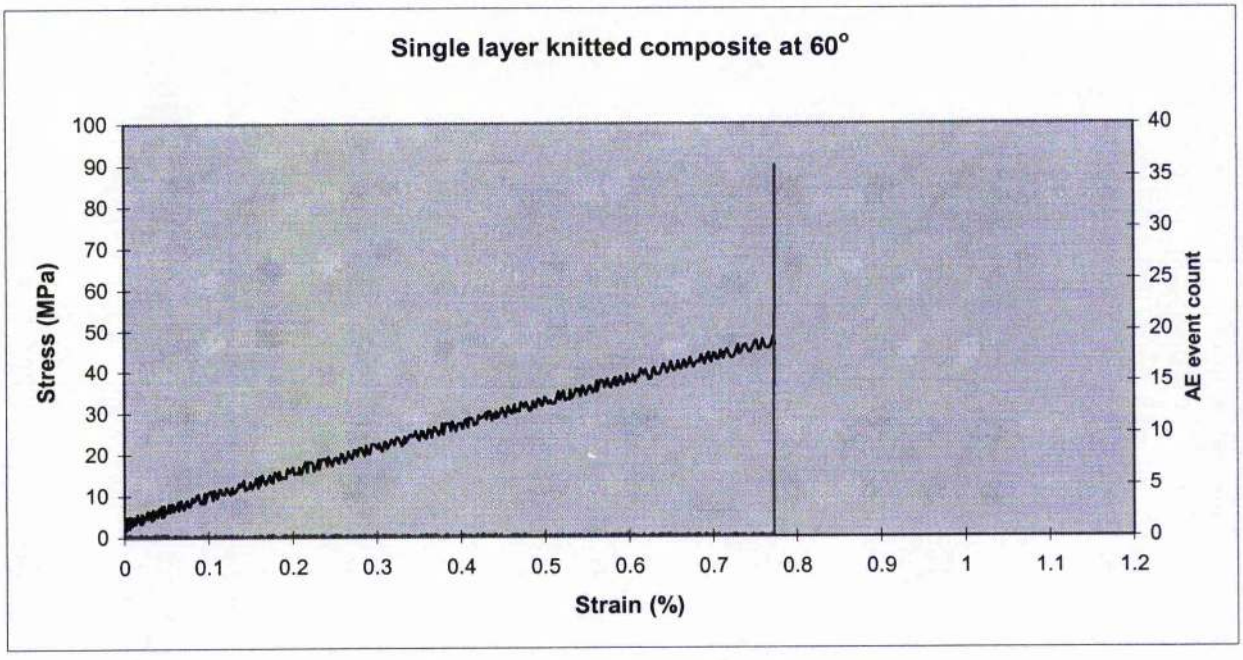

Figure 4.11.- Stress-strain curve for single layer sample in 60° direction.

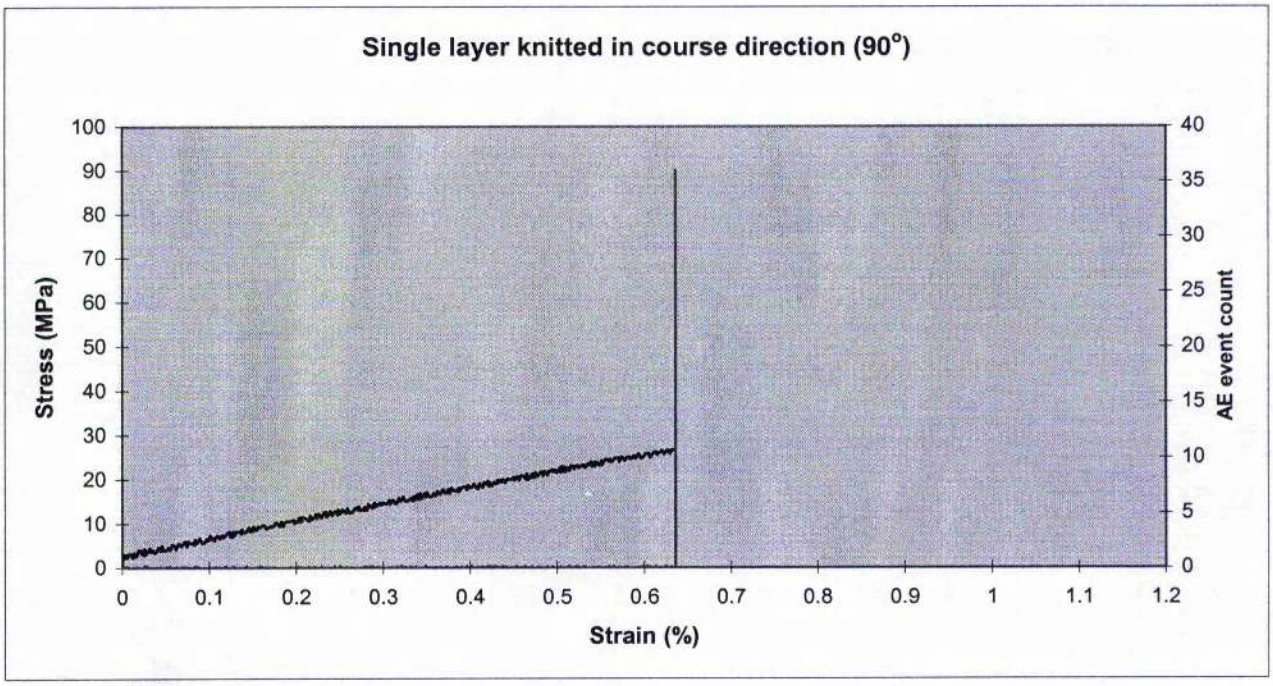

Figure 4.12.- Stress-strain curve for single layer sample in 90° direction.

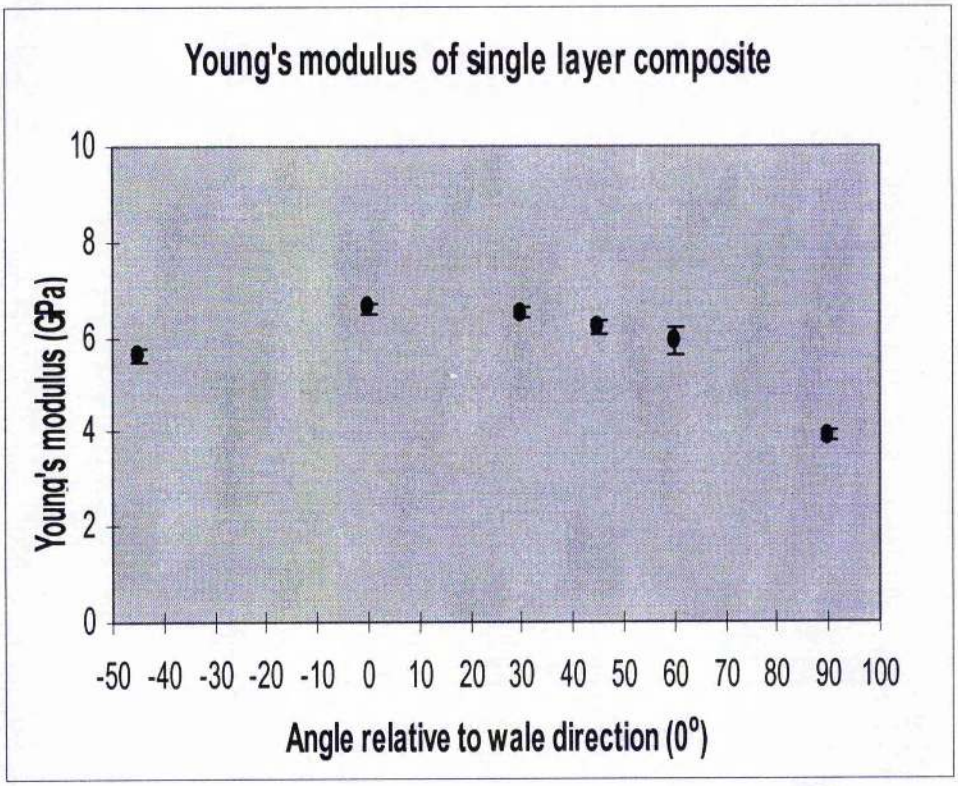

Figure 4.13.- Young's modulus of single layer 2x68 knitted fabric composite as function of angle. For some angles, the uncertainty is smaller than the symbol.

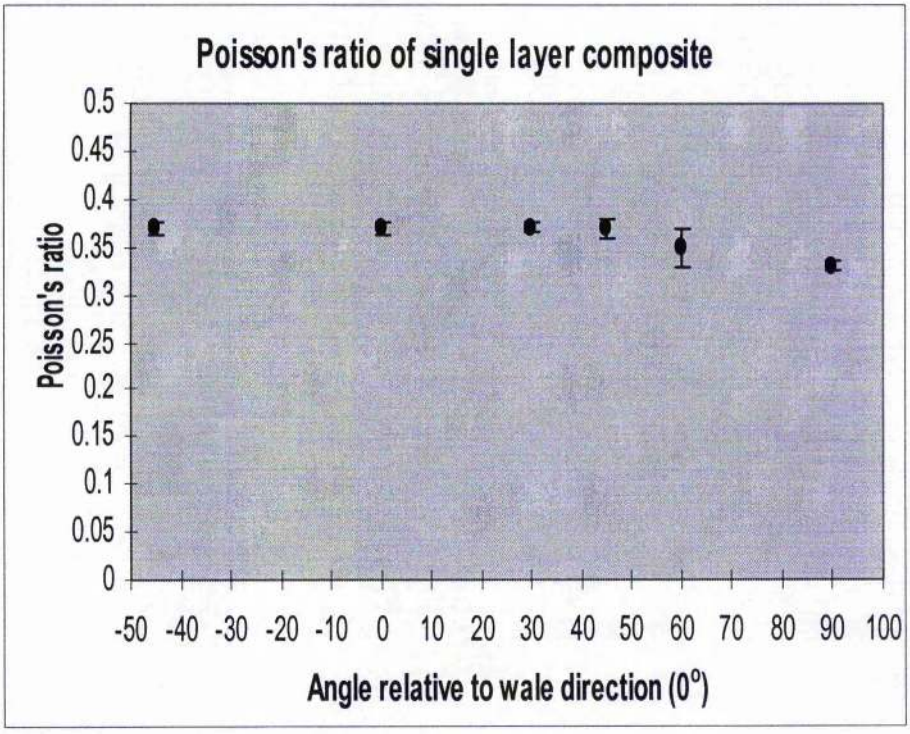

Figure 4.14.- Poisson's ratio of single layer 2x68 knitted fabric composite as function of angle. For some angles, the uncertainty is smaller than the symbol.

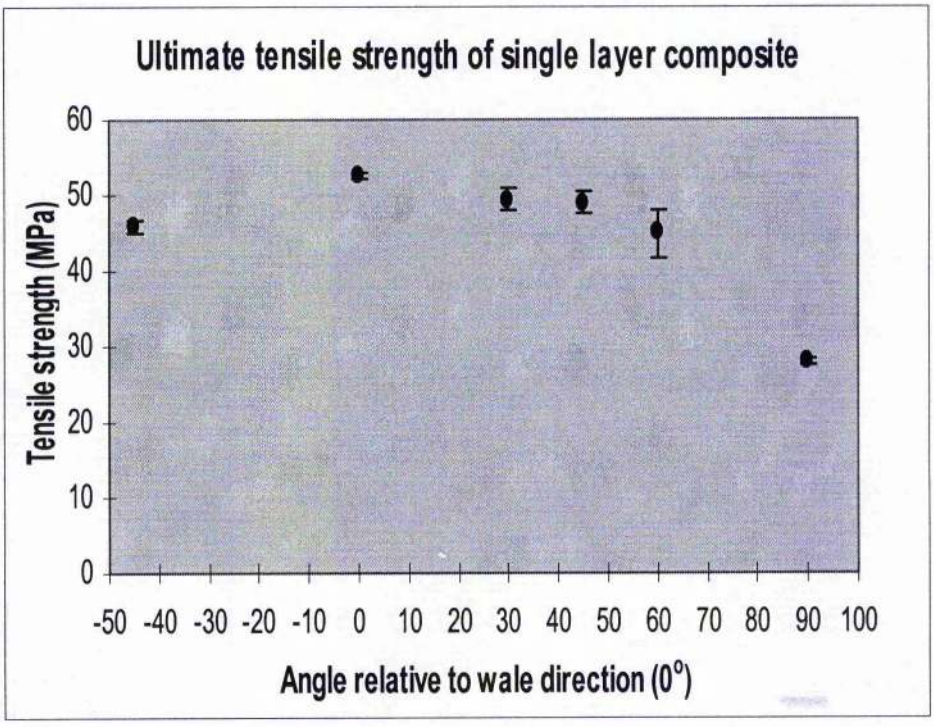

Figure 4.15.- Ultimate tensile strength of single layer 2x68 knitted fabric composite as function of angle. For some angles, the uncertainty is smaller than the symbol.

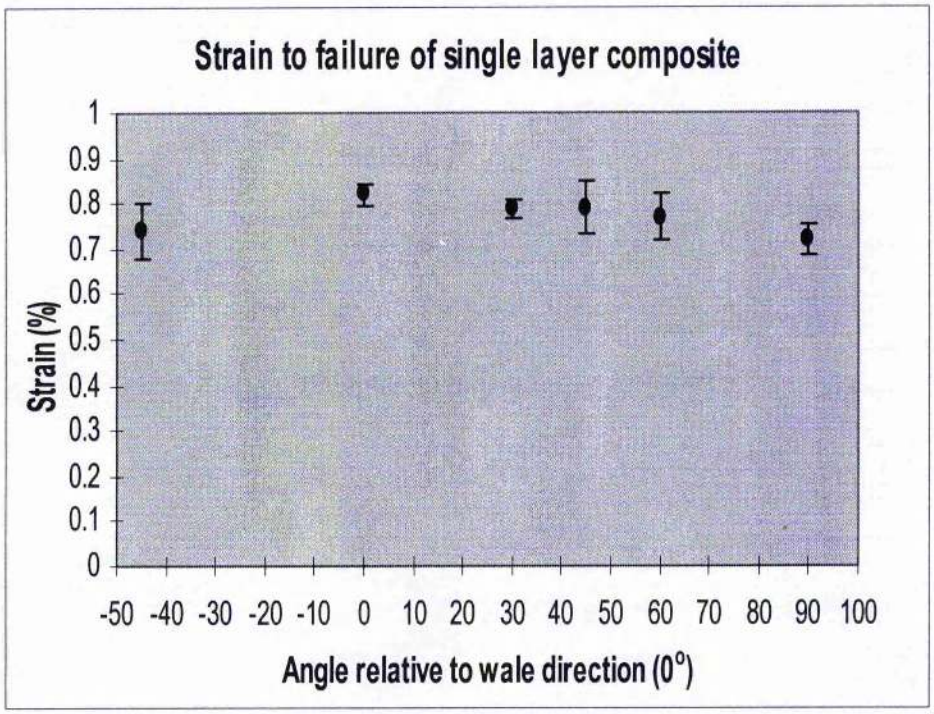

Figure 4.16.- Strain to failure of single layer 2x68 knitted fabric composite as function of angle. For some angles, the uncertainty is smaller than the symbol.

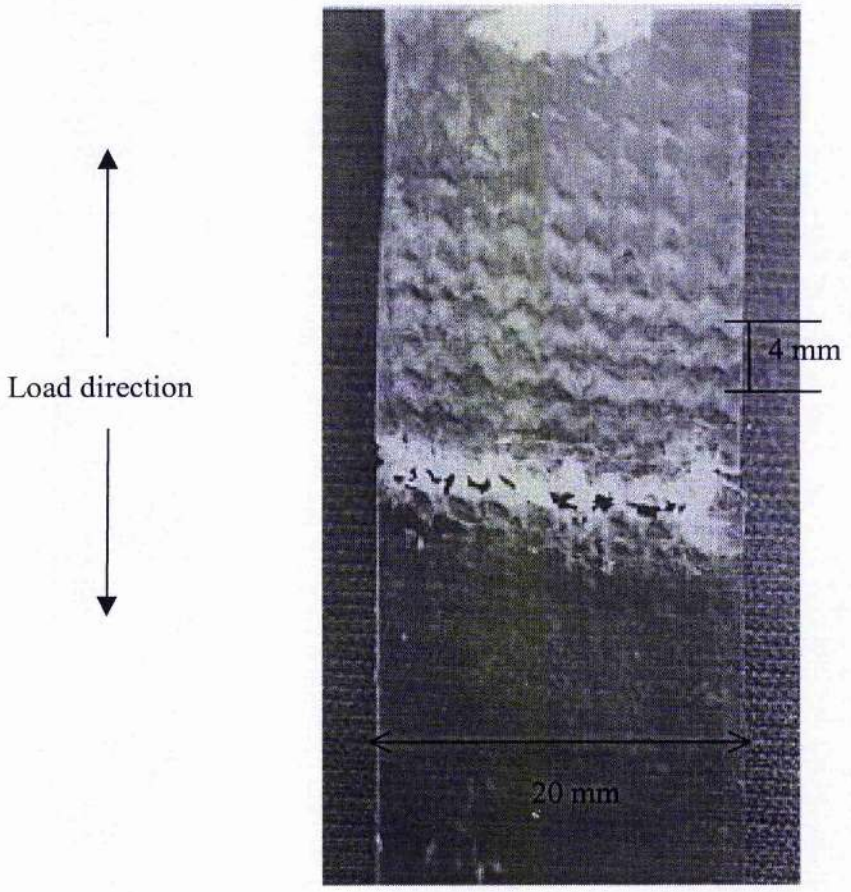

Figure 4.17.- Fractured specimen tested in the 0° (wale) direction.

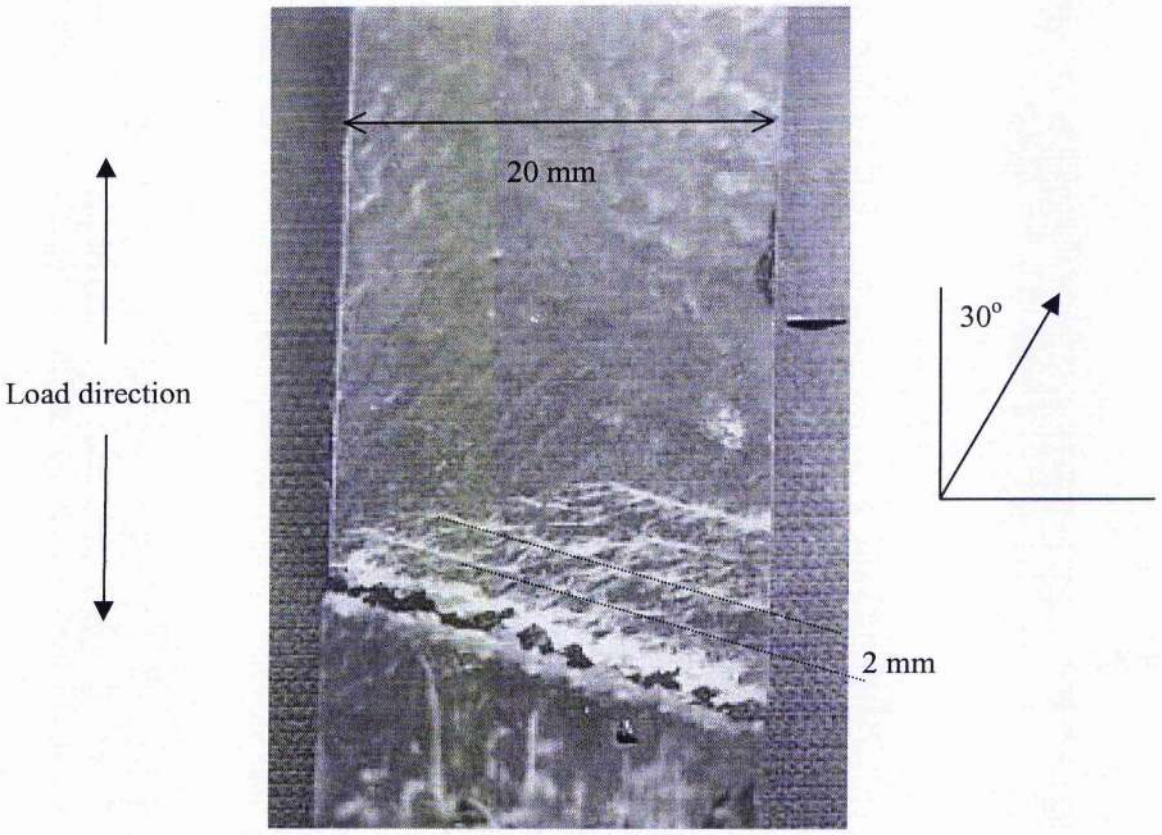

Figure 4.18.- Fractured specimen tested in the 30° direction.

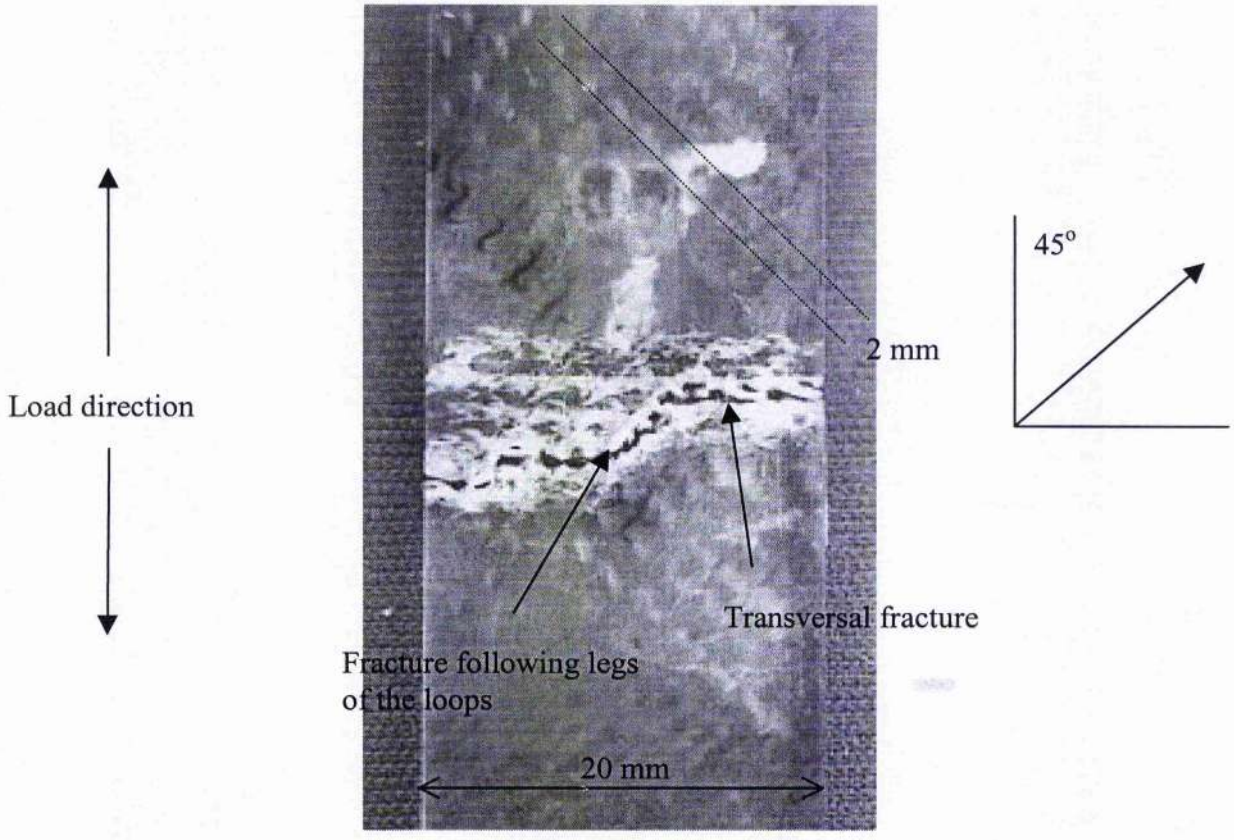

Figure 4.19.- Fractured specimen tested in the +45° direction.

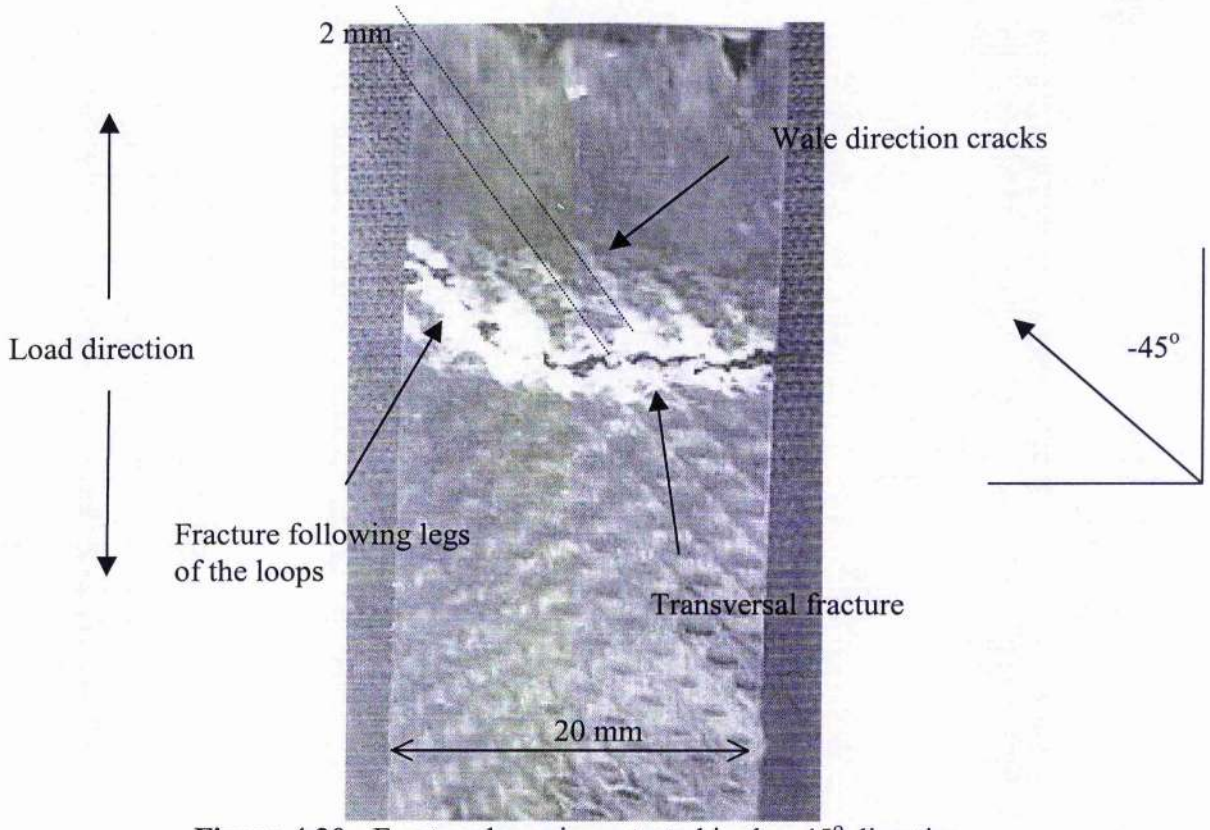

Figure 4.20.- Fractured specimen tested in the -45° direction.

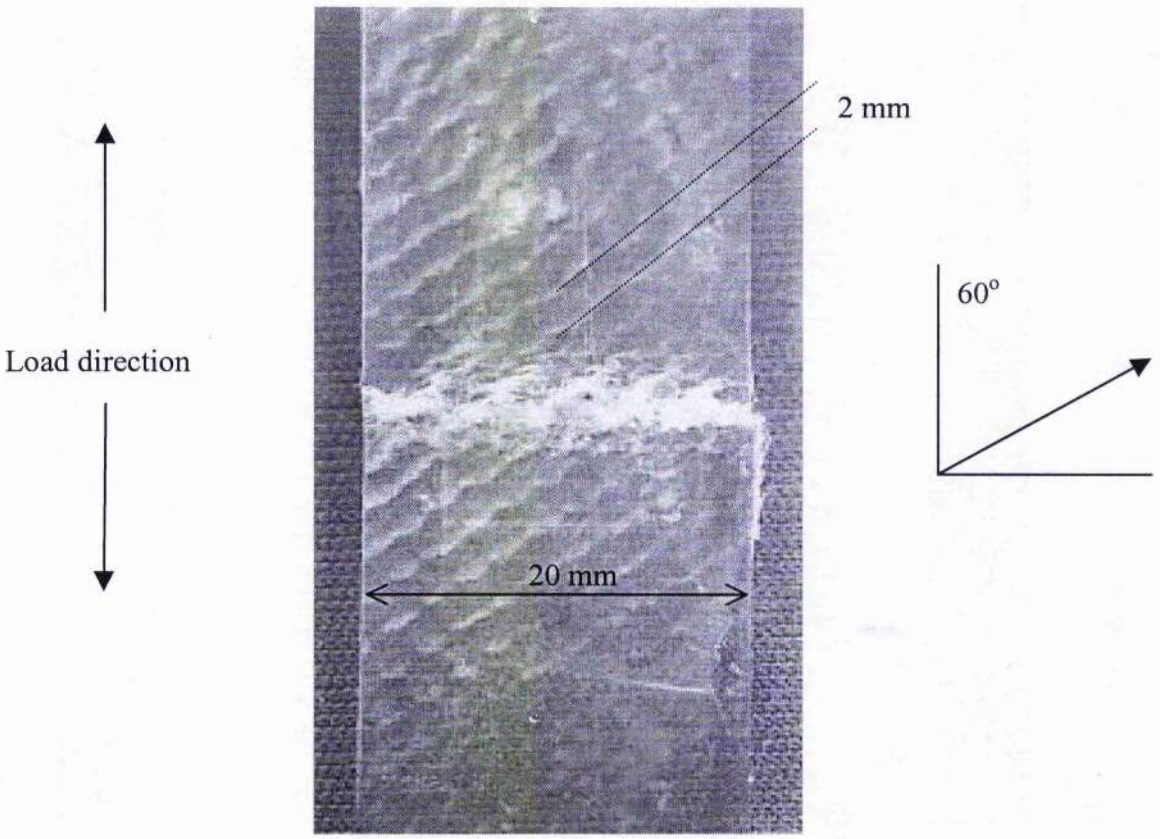

Figure 4.21.- Fractured specimen tested in the 60° direction.

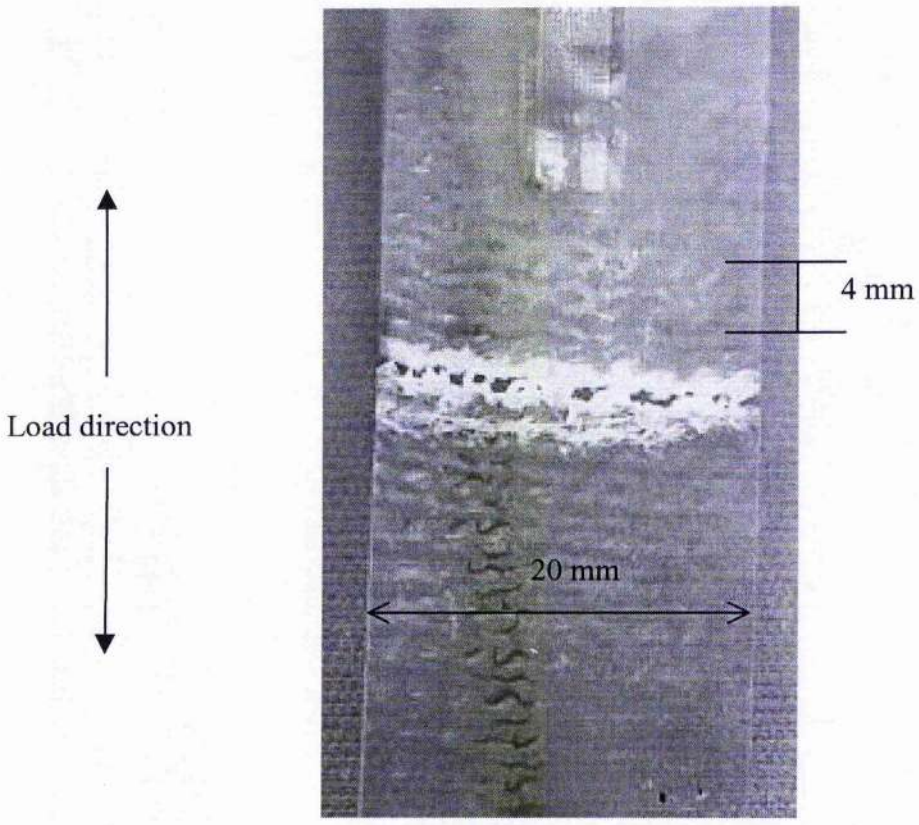

Figure 4.22.- Fractured specimen tested in the 90° (course) direction.

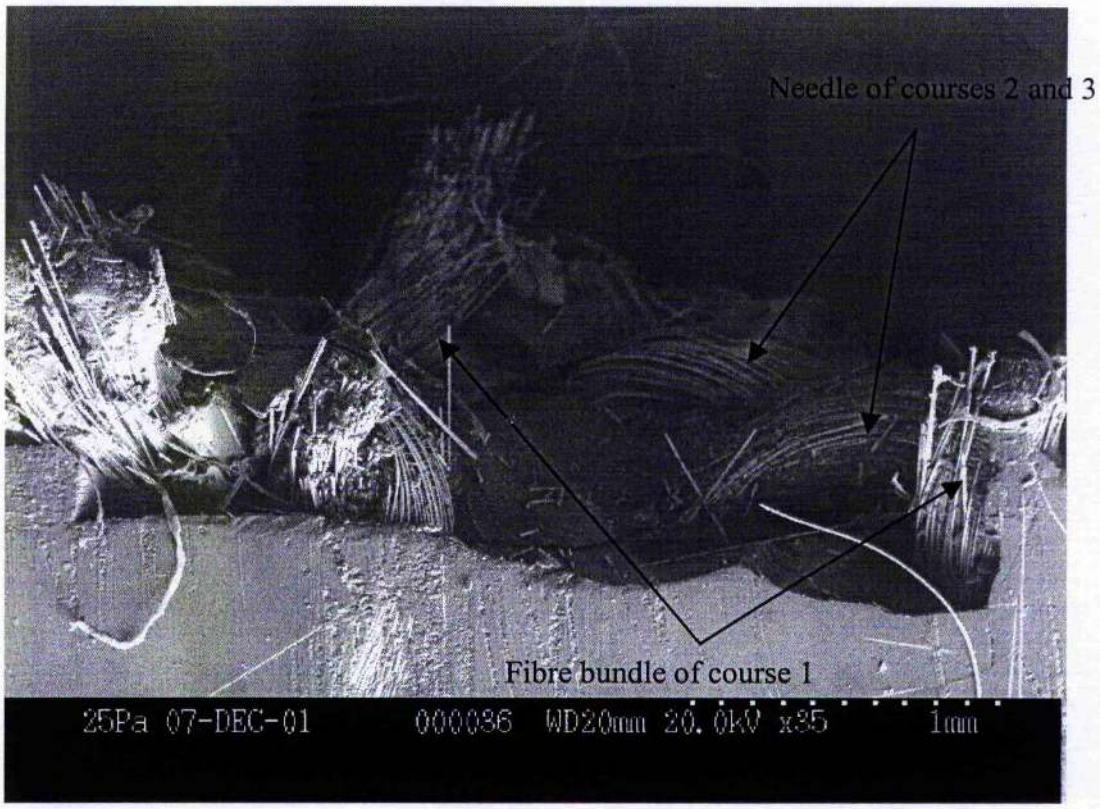

Figure 4.23.- Fractured surface of single layer sample tested in the 0° (wale) direction.

Figure 4.24.- Fractured surface of single layer sample tested in the 30° direction.

Figure 4.25.- Fractured surface of single layer sample tested in the +45° direction.

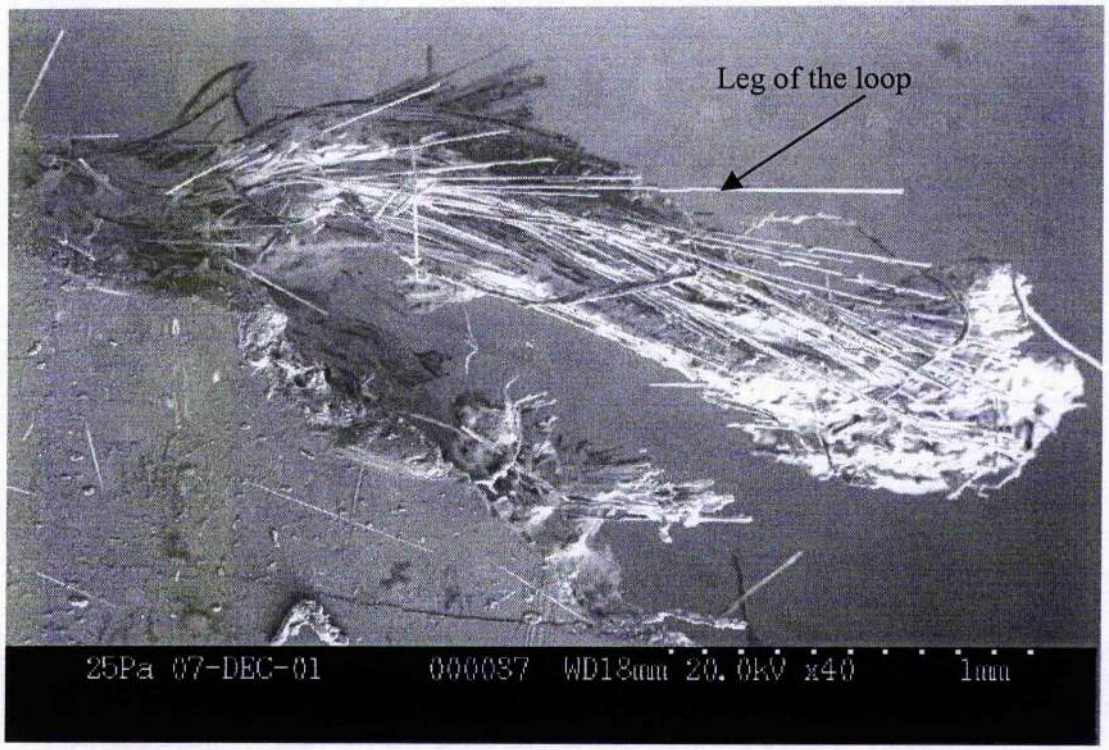

Figure 4.26.- Fractured surface of single layer sample tested in the -45° direction.

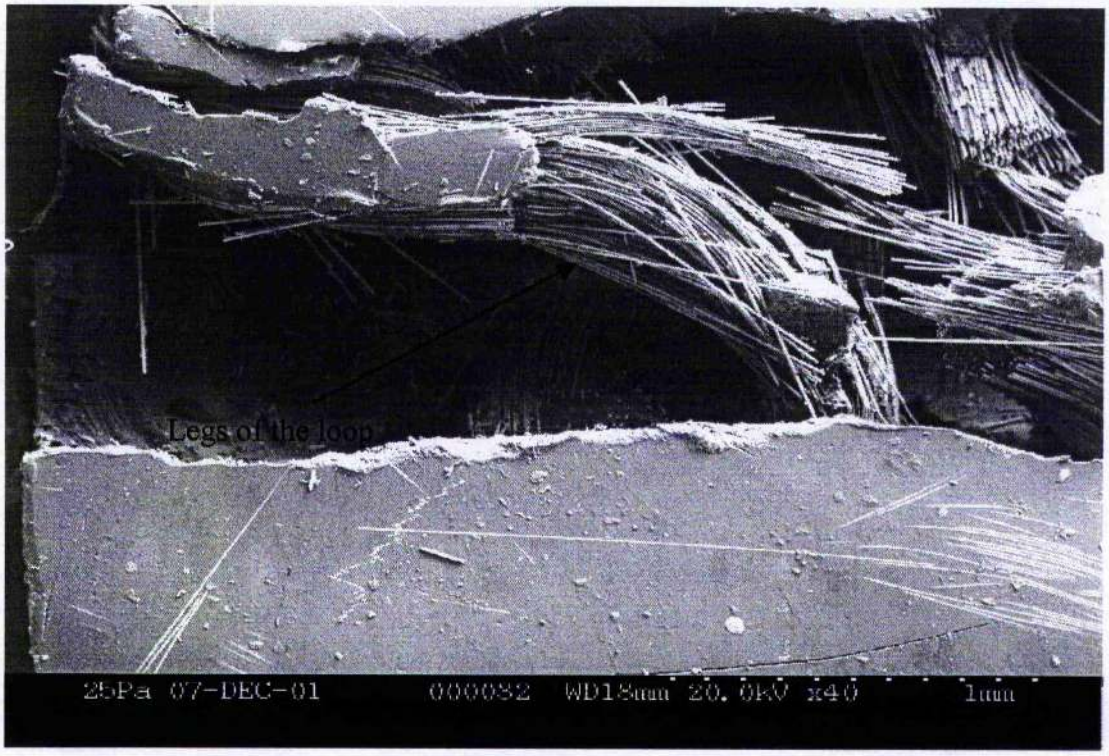

Figure 4.27.- Fractured surface of single layer sample tested in the 60° direction.

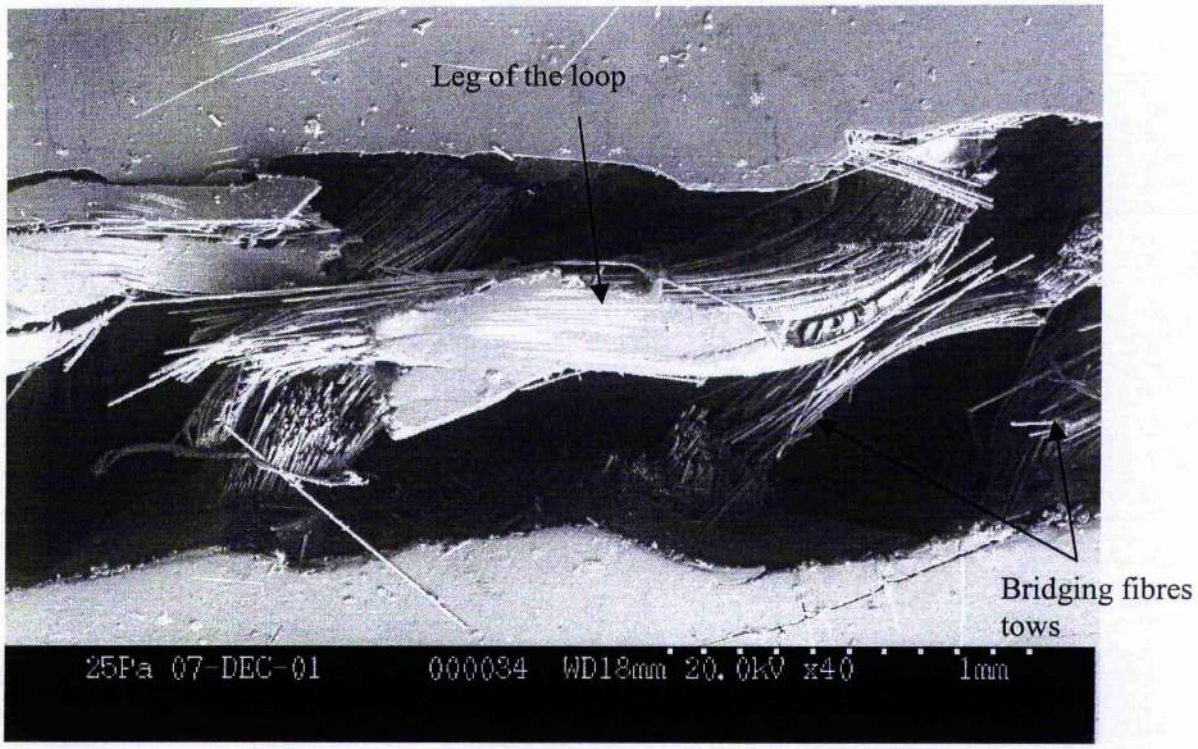

Figure 4.28.- Fractured surface of single layer sample tested in the 90° (course) direction.

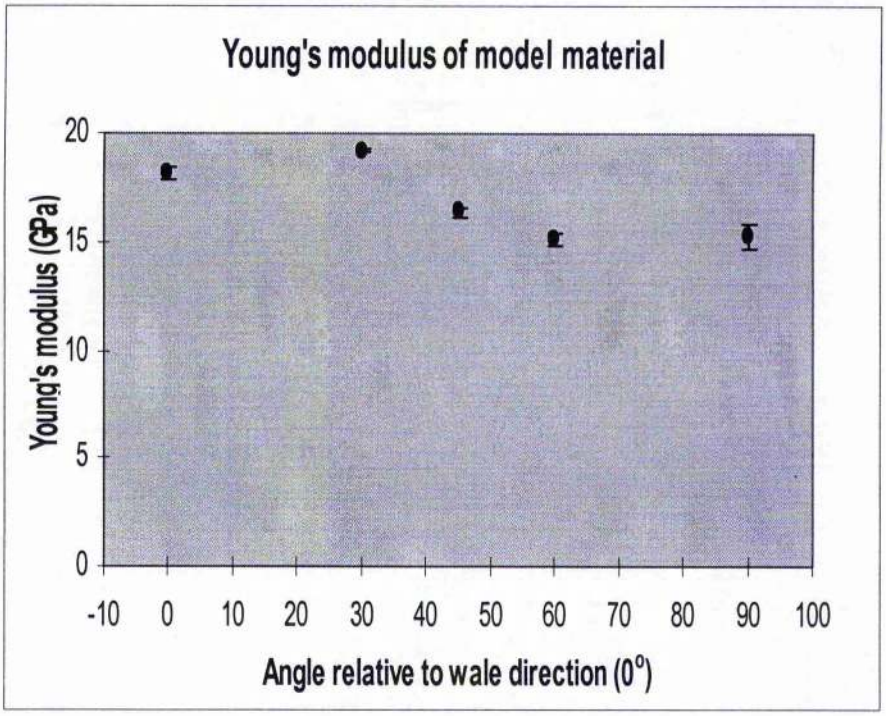

Figure 4.29.- Young's modulus of 2x68 model material as function of angle. For some angles, the uncertainty is smaller than the symbol.

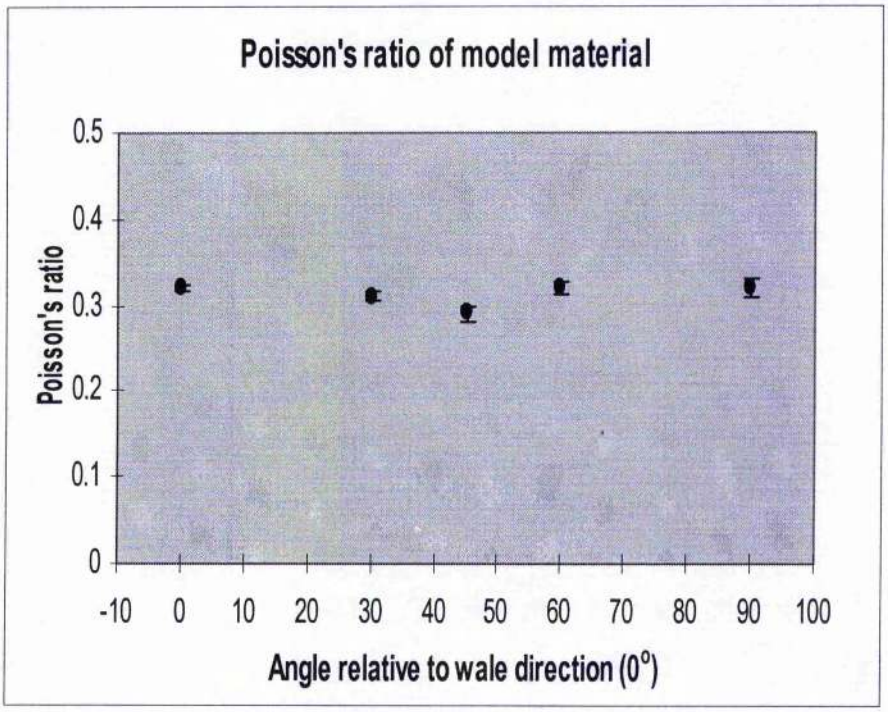

Figure 4.30.- Poisson's ratio of single 2x68 model material as function of angle. For some angles, the uncertainty is smaller than the symbol.

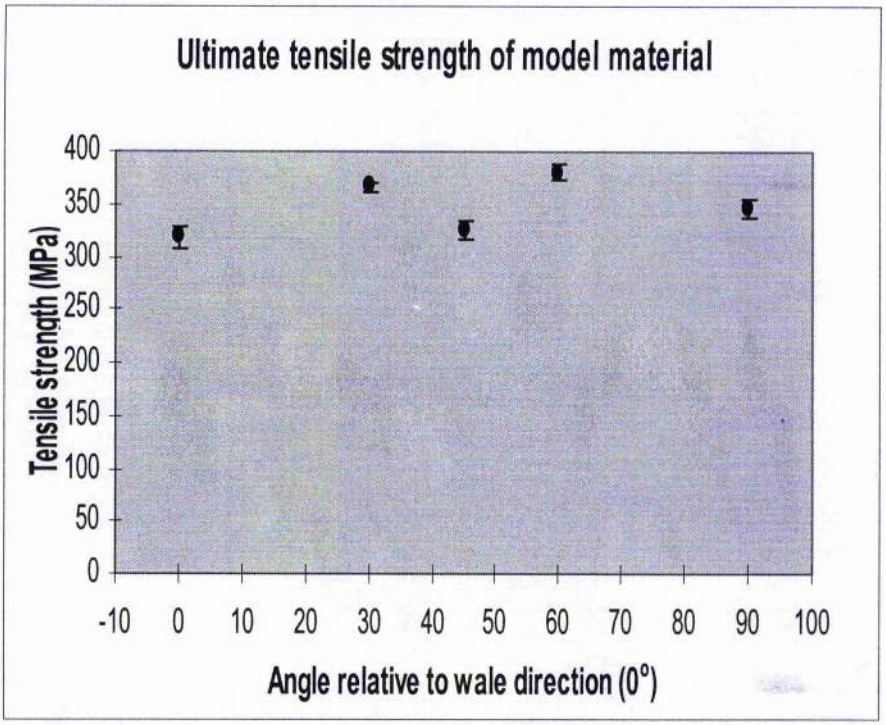

Figure 4.31.- Ultimate tensile strength of single 2x68 model material as function of angle. For some angles, the uncertainty is smaller than the symbol.

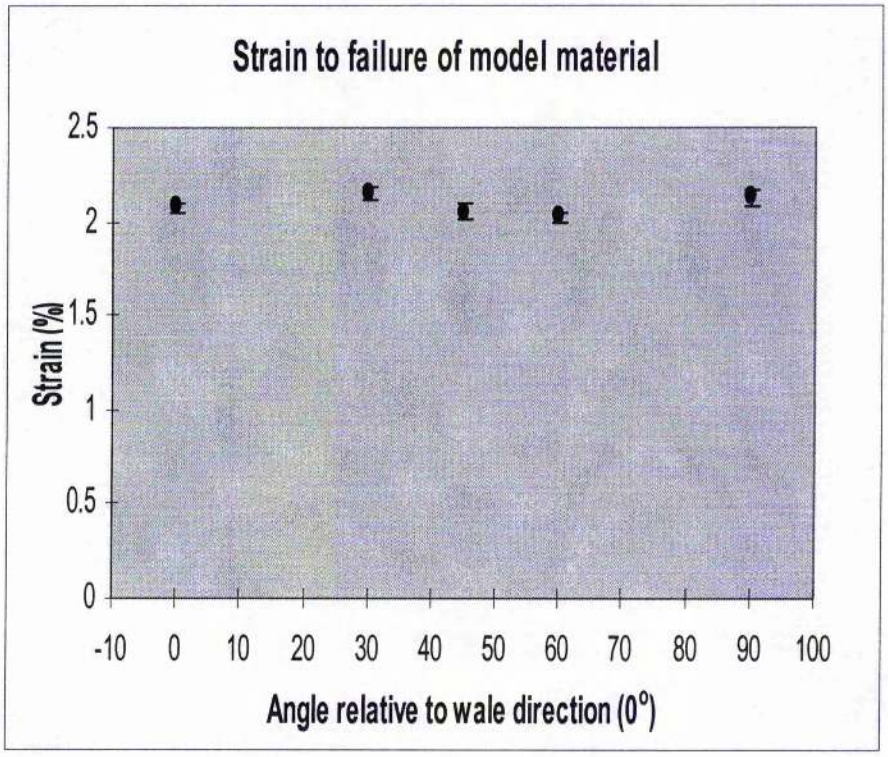

Figure 4.32.- Strain to failure of single 2x68 model material as function of angle. For some angles, the uncertainty is smaller than the symbol.

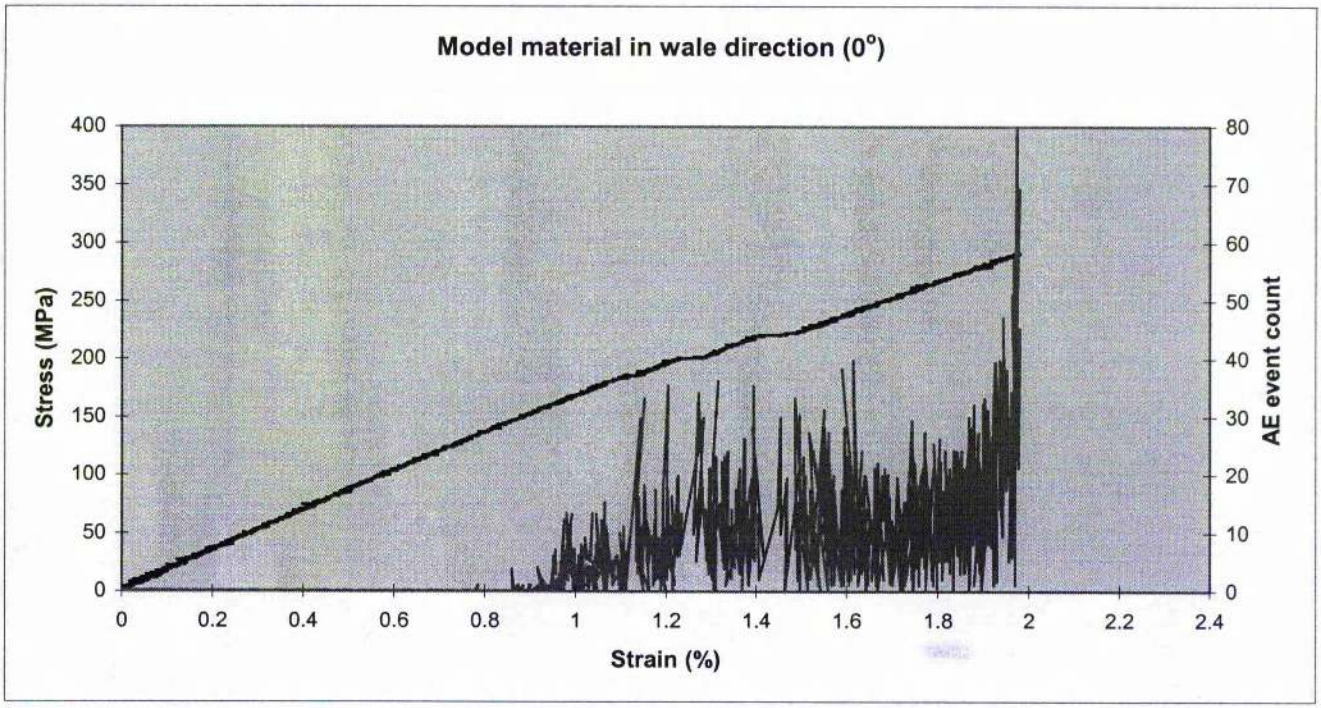

Figure 4.33- Stress-strain curve and acoustic emission event counts for the model sandwich laminate with the fabric layer in the 0° direction.

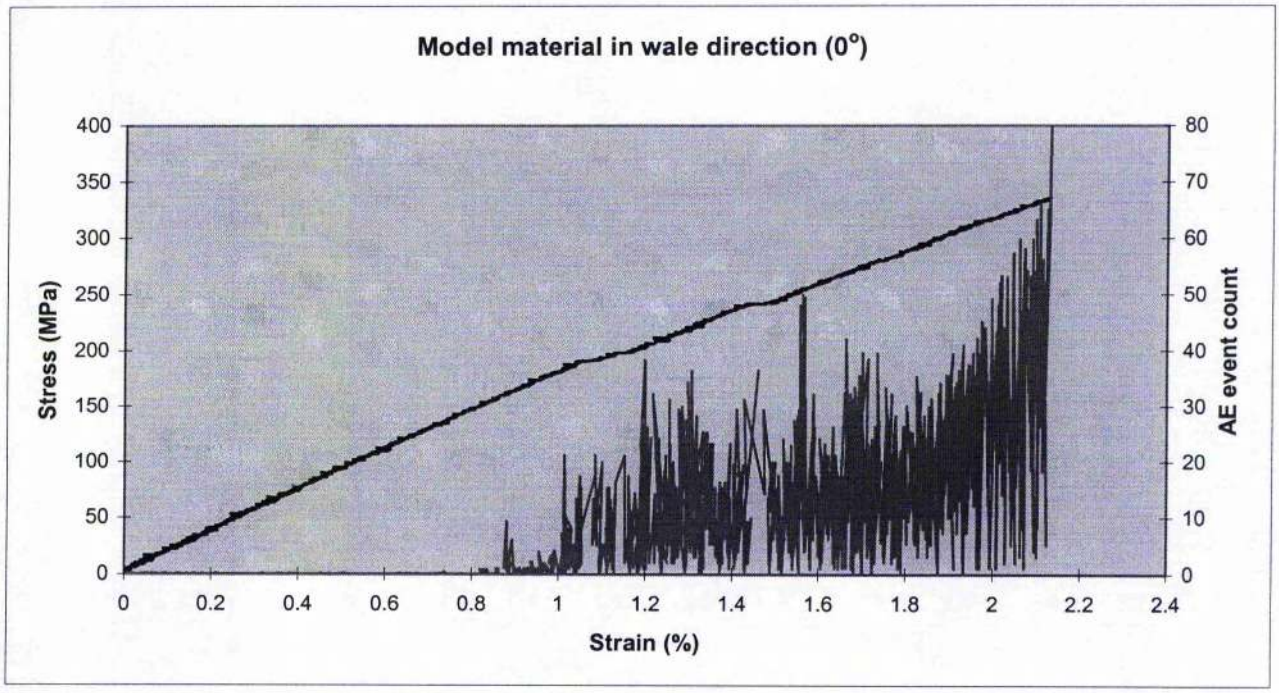

Figure 4.34- Stress-strain curve and acoustic emission event counts for the model sandwich laminate with the fabric layer in the 0° direction.

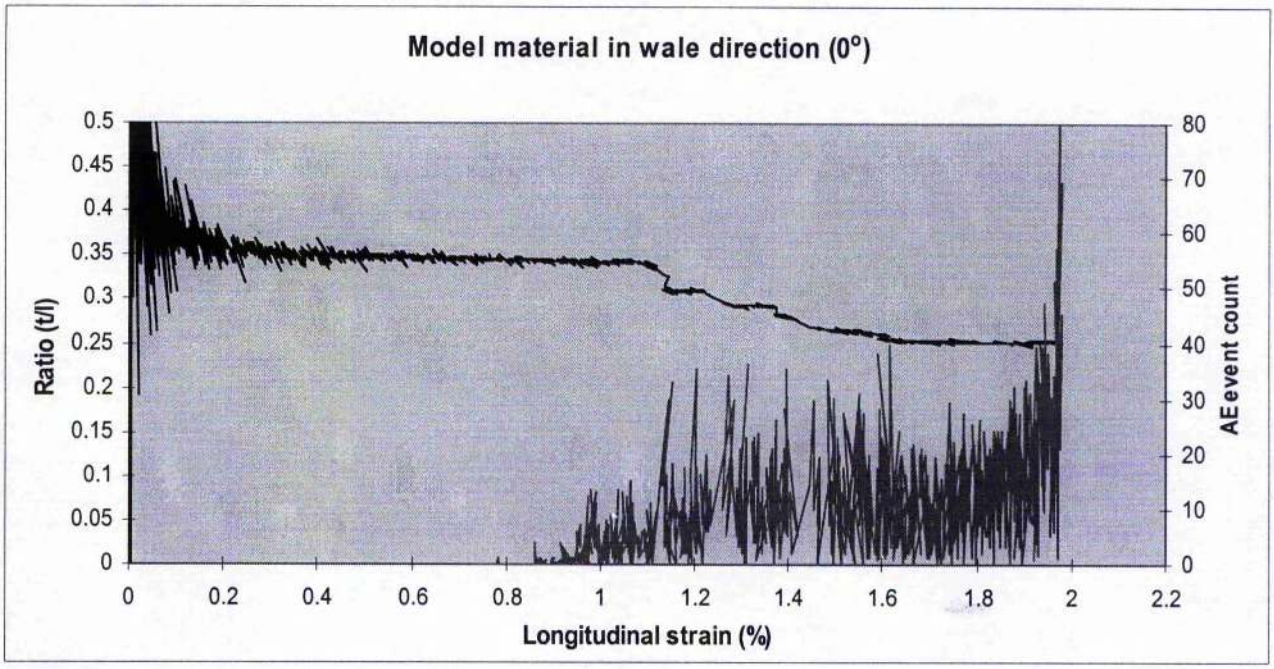

Figure 4.35.- Behaviour of the negative of the ratio of the transverse strain to the longitudinal strain, ie the Poisson's ratio –(t/l), as a function of the longitudinal strain for the model sandwich laminate with the fabric layer in the 0° direction

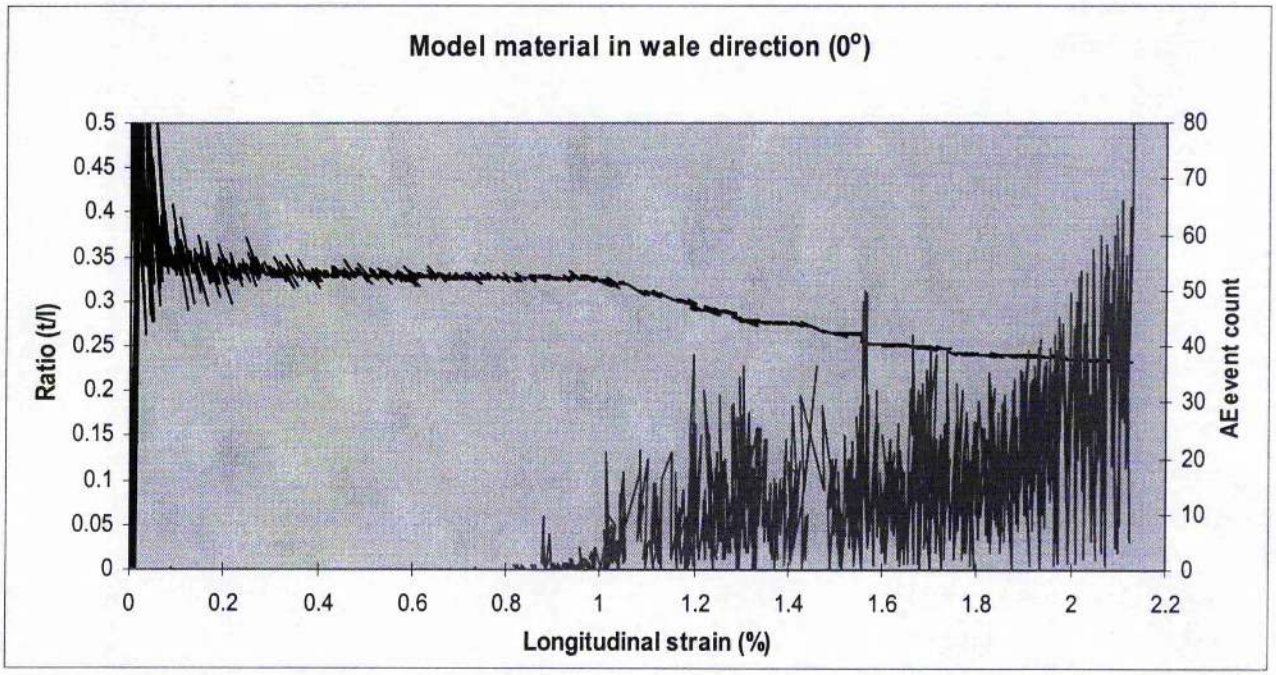

Figure 4.36.- Behaviour of the negative of the ratio of the transverse strain to the longitudinal strain, ie the Poisson's ratio –(t/l), as a function of the longitudinal strain for the model sandwich laminate with the fabric layer in the 0° direction

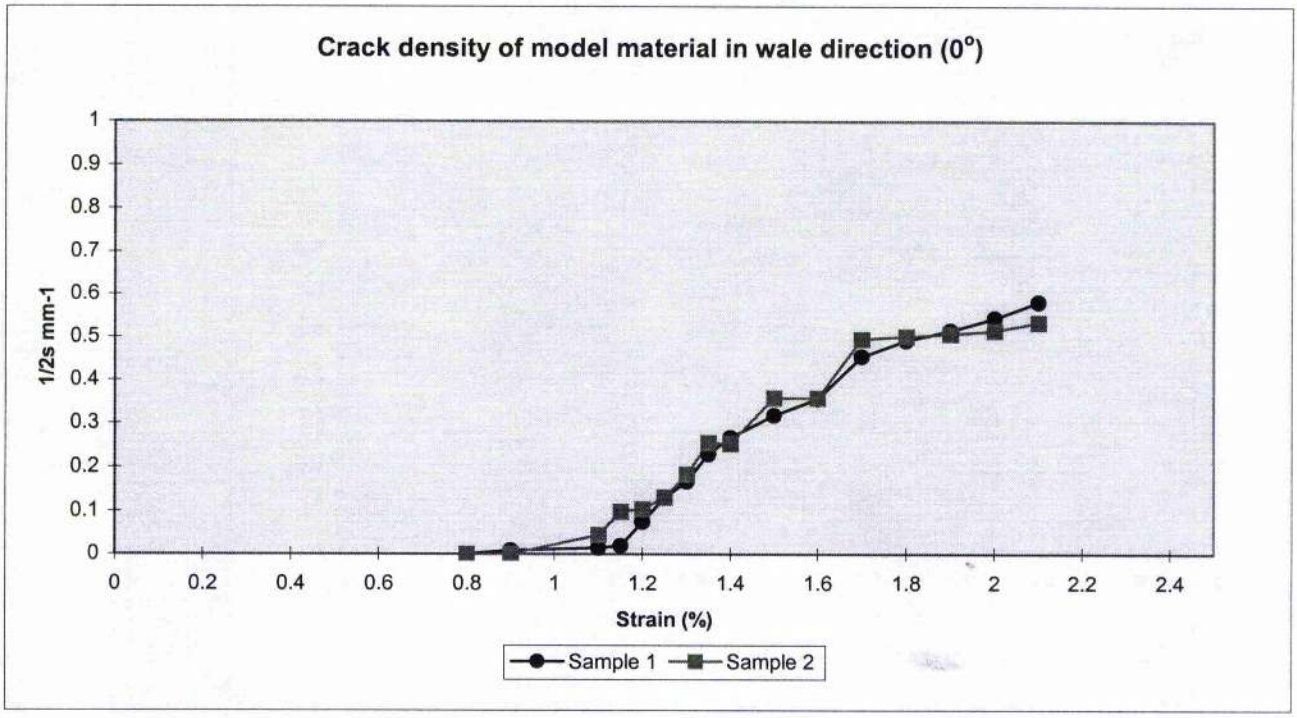

Figure 4.37.- Crack density-strain curve for the model sandwich laminate with the fabric layer in the 0° direction.

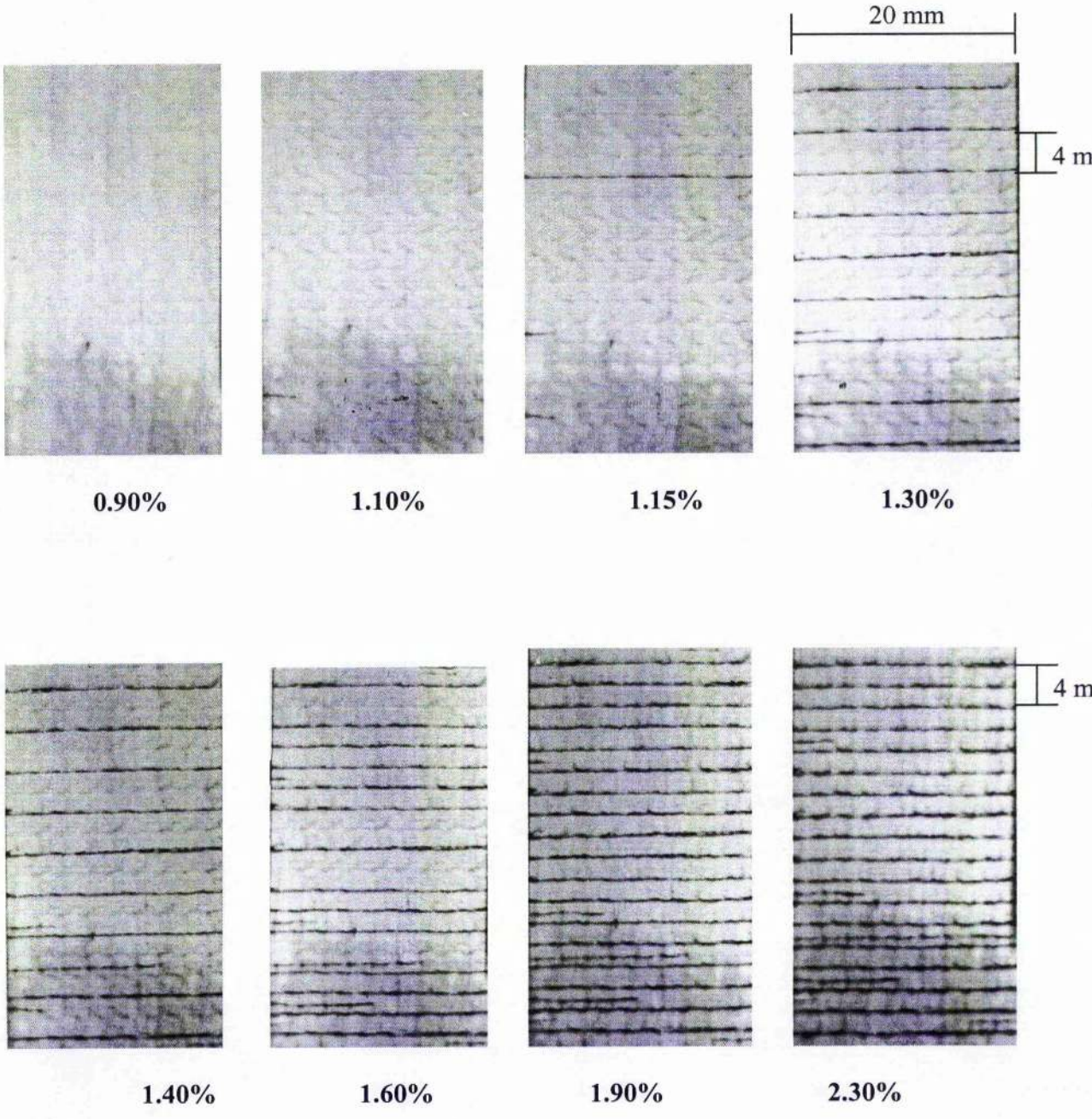

Figure 4.38.- Crack development for the model sandwich laminate with the fabric layer in the 0^{o} direction Applied strains are indicated.

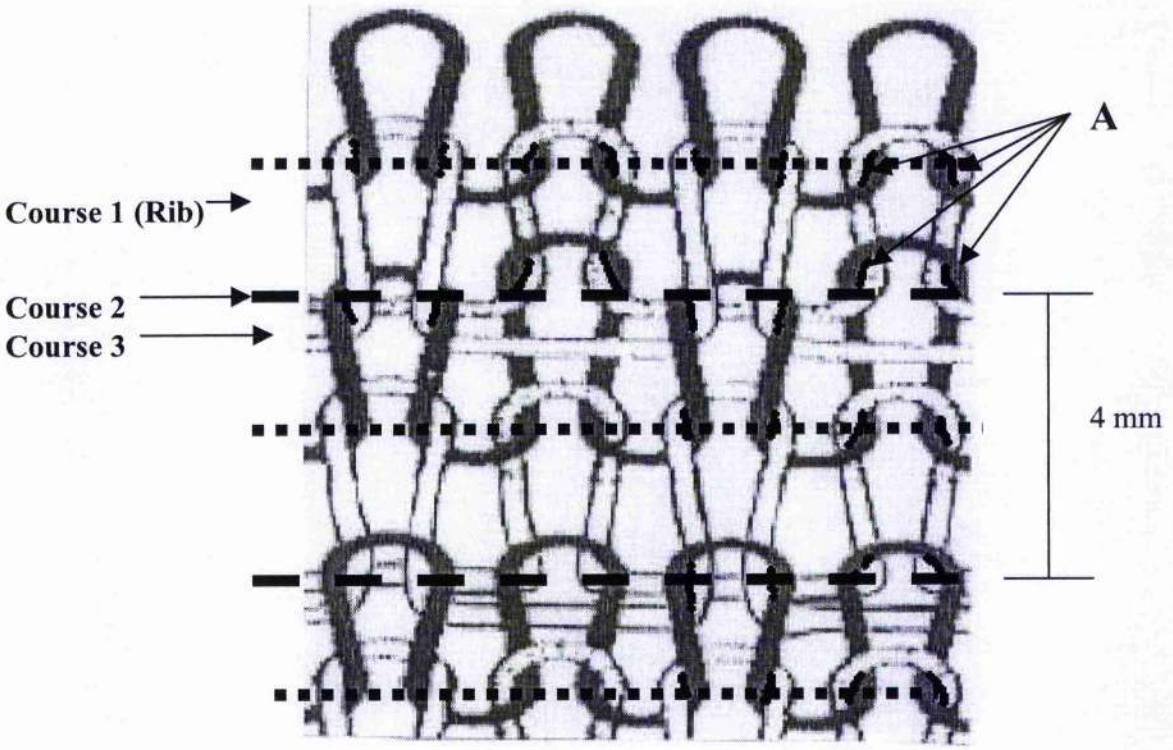

Figure 4.39.- Schematic diagram showing crack development for the model sandwich laminate with the fabric layer in the 0° direction.

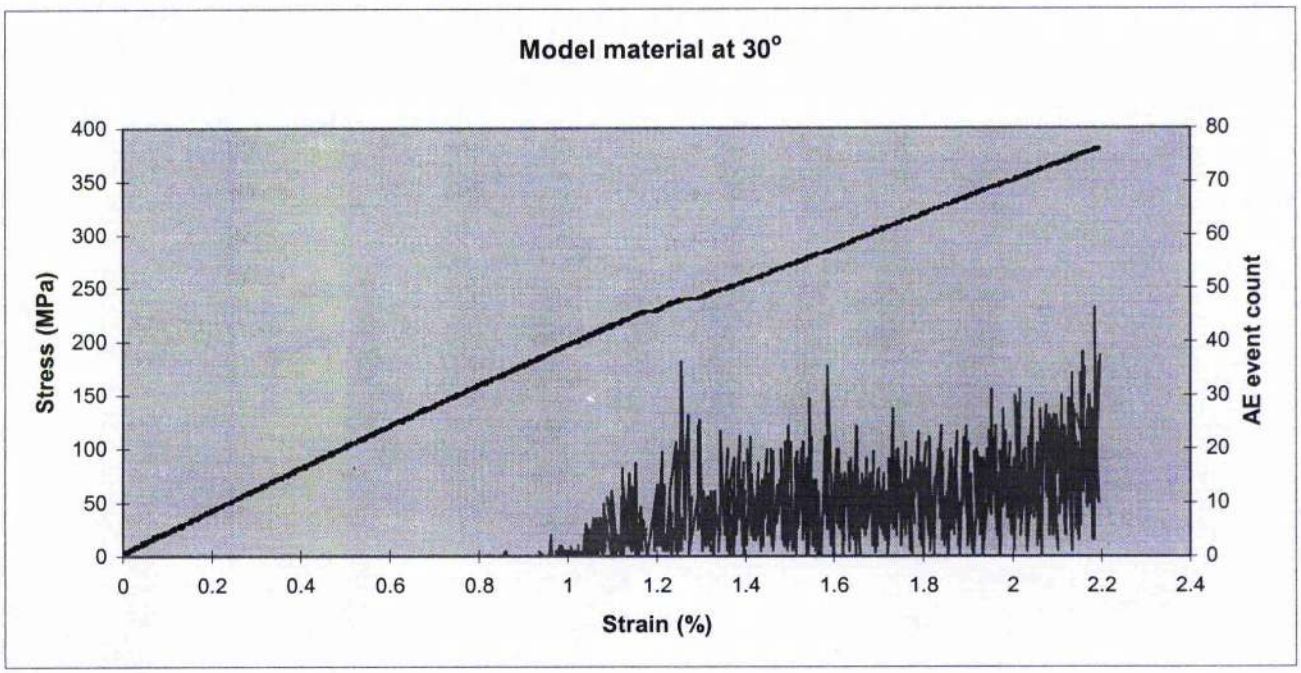

Figure 4.40- Stress-strain curve and acoustic emission event counts for the model sandwich laminate with the fabric layer in the 30° direction.

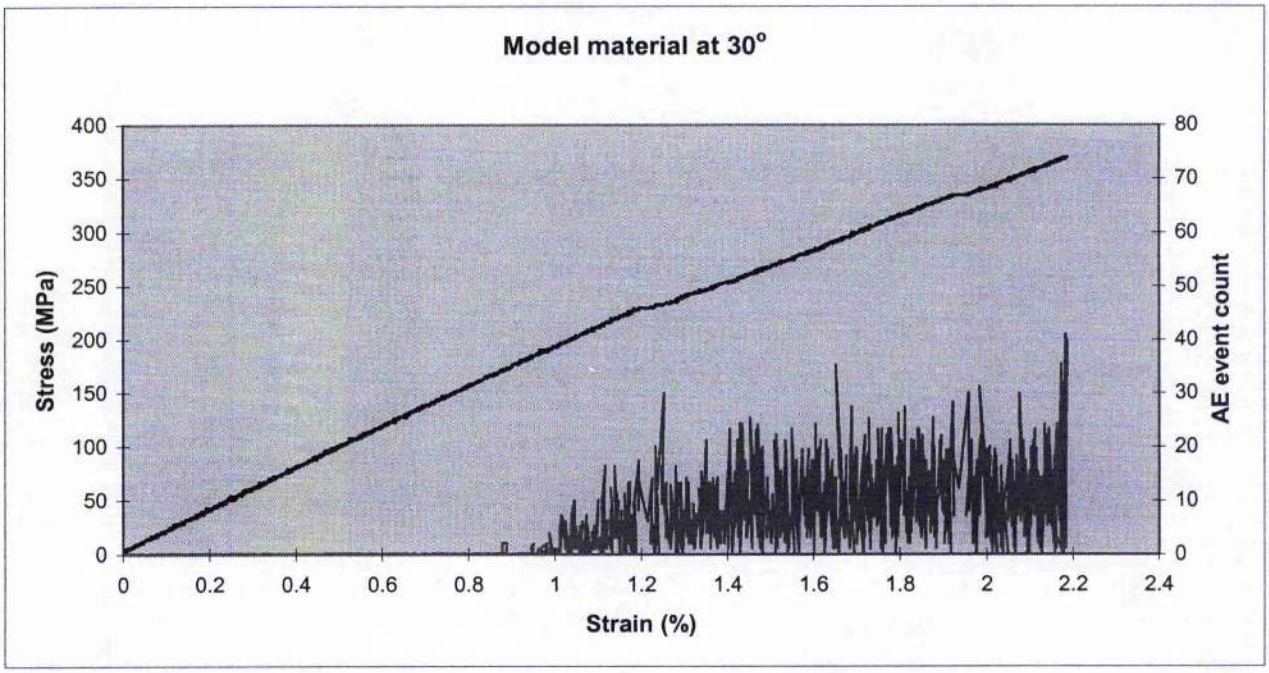

Figure 4.41- Stress-strain curve and acoustic emission event counts for the model sandwich laminate with the fabric layer in the 30° direction.

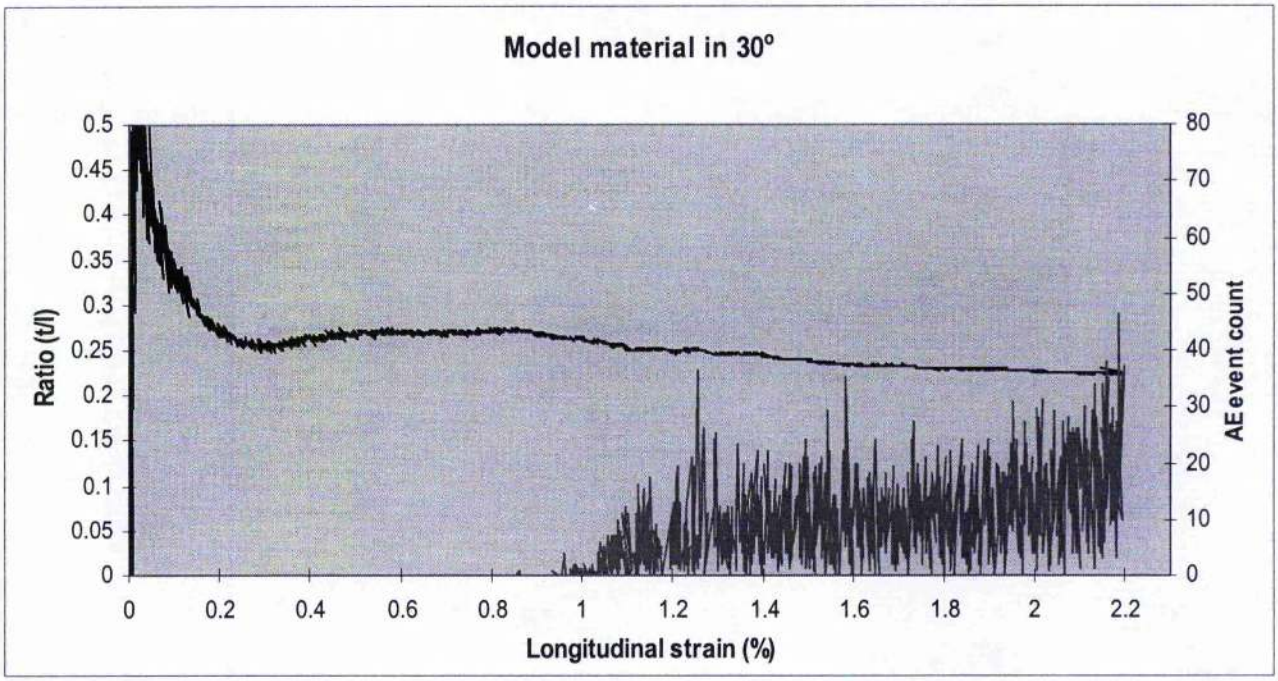

Figure 4.42.- Behaviour of the negative of the ratio of the transverse strain to the longitudinal strain, ie the Poisson's ratio –(t/l), as a function of the longitudinal strain for the model sandwich laminate with the fabric layer in the 30° direction.

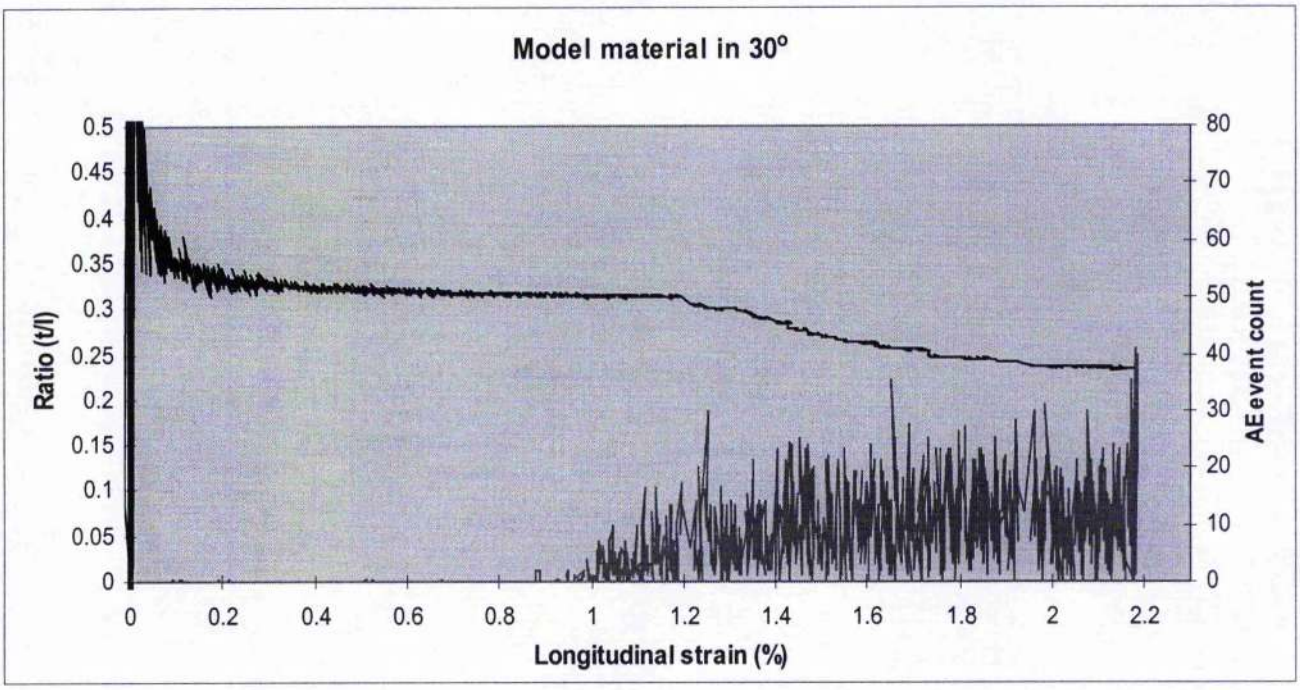

Figure 4.43.- Behaviour of the negative of the ratio of the transverse strain to the longitudinal strain, ie the Poisson's ratio –(t/l), as a function of the longitudinal strain for the model sandwich laminate with the fabric layer in the 30° direction

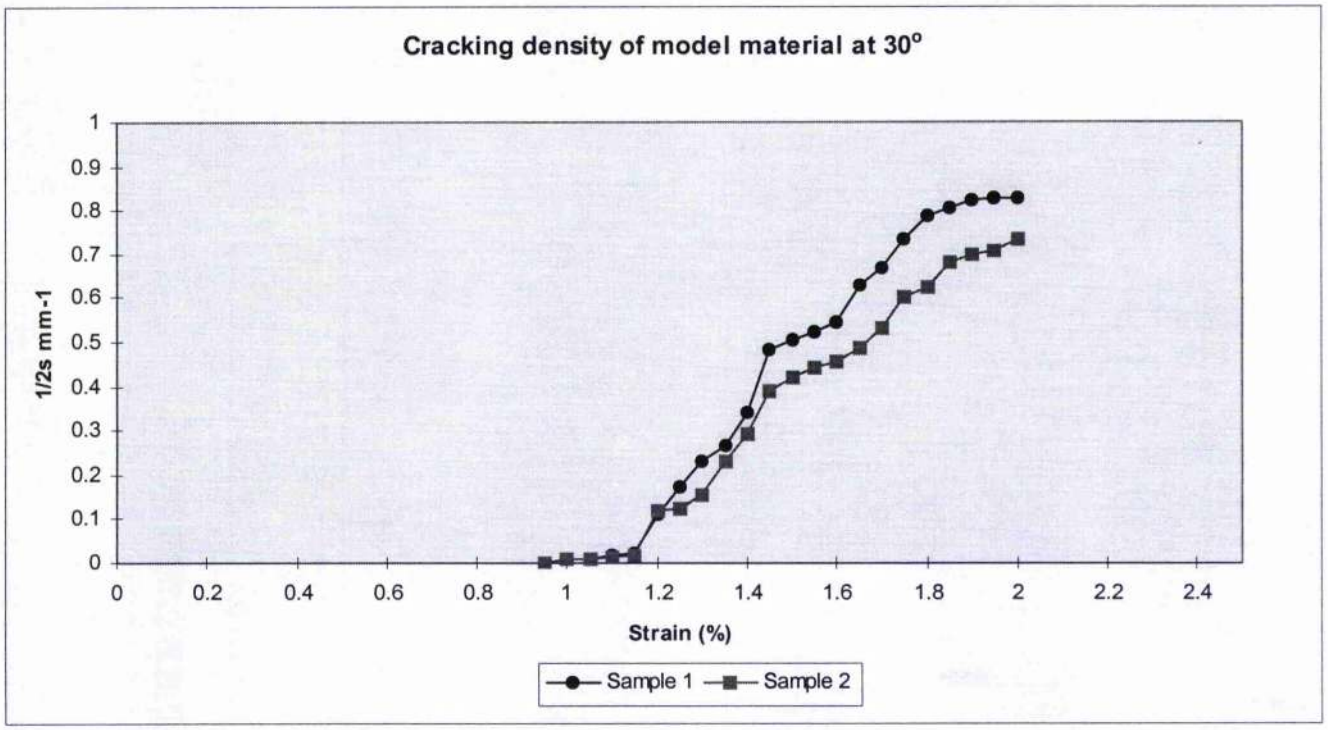

Figure 4.44.- Crack density-strain curve for the model sandwich laminate with the fabric layer in the 0° direction.

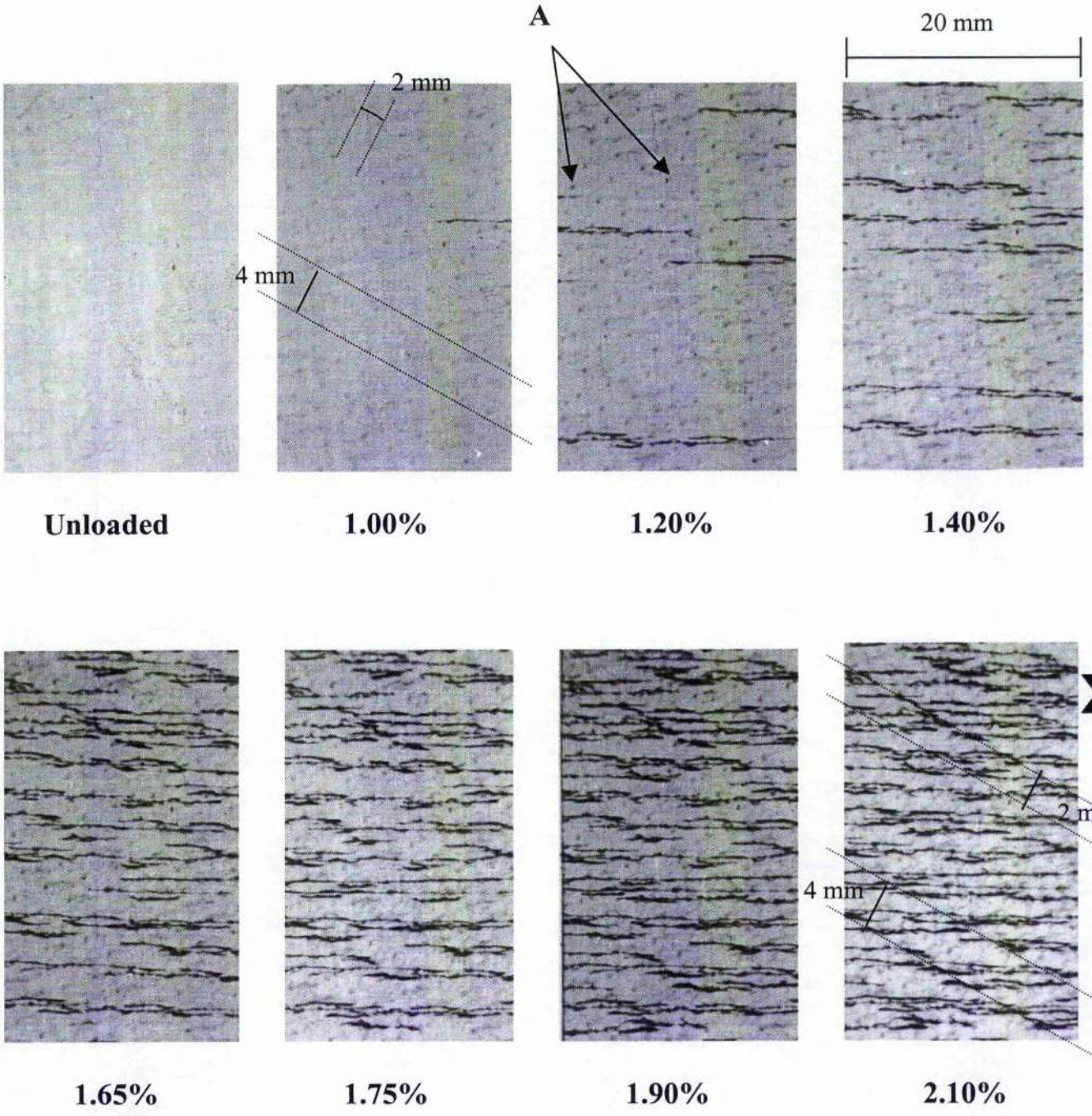

Figure 4.45.- Crack development for the model sandwich laminate with the fabric layer in the 30° direction Applied strains are indicated.

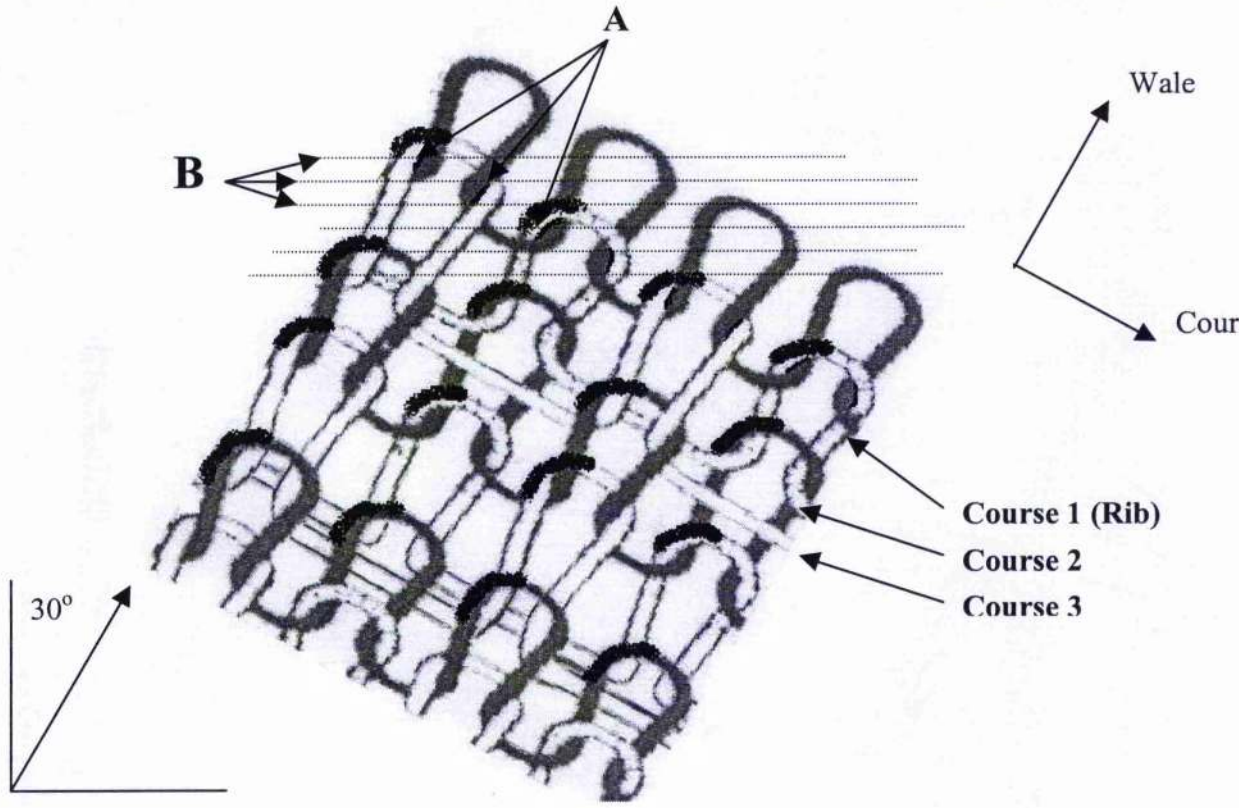

Figure 4.46.- Schematic diagram showing crack development for the model sandwich laminate with the fabric layer in the 30° direction.

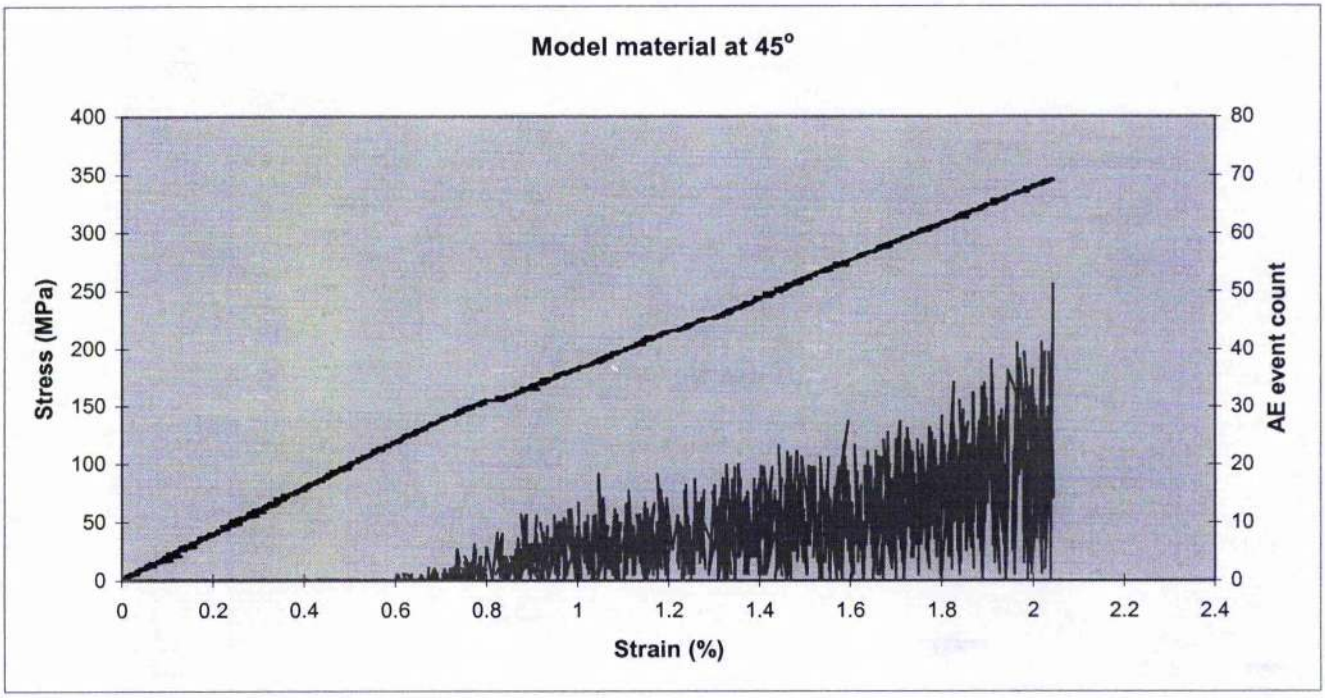

Figure 4.47- Stress-strain curve and acoustic emission event counts for the model sandwich laminate with the fabric layer in the +45° direction.

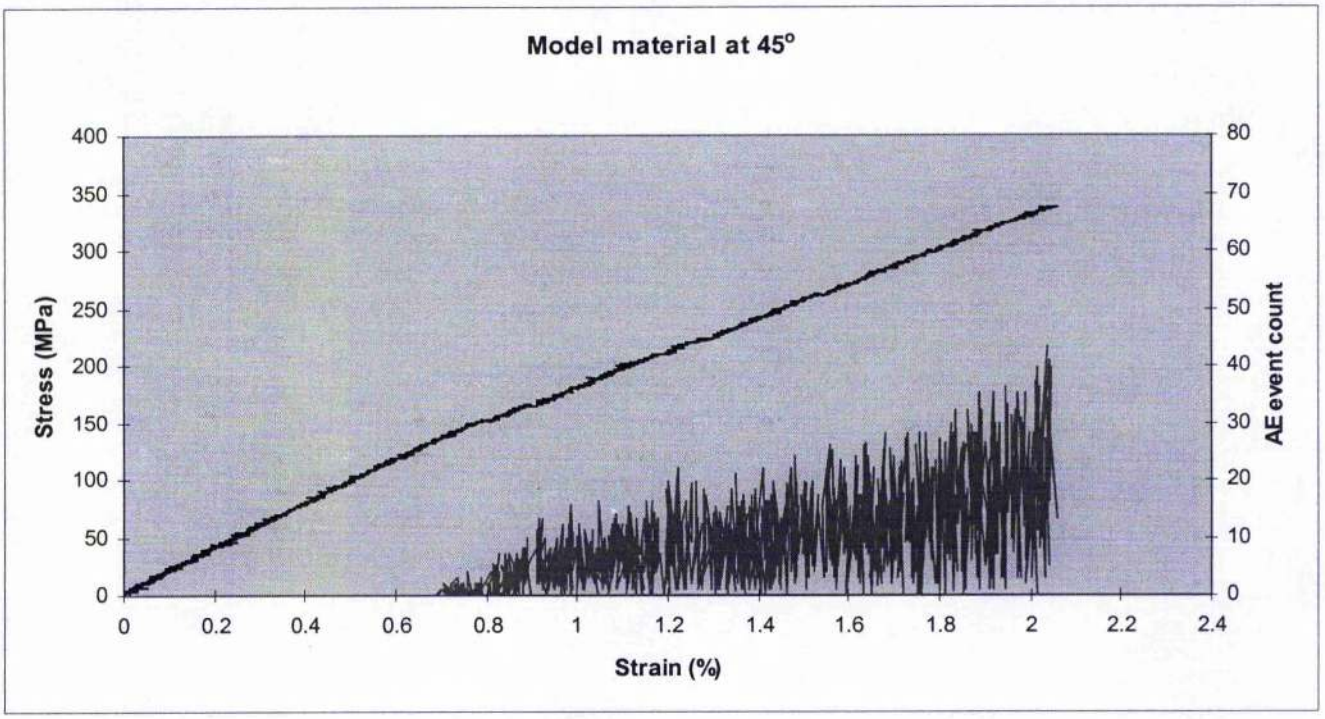

Figure 4.48- Stress-strain curve and acoustic emission event counts for the model sandwich laminate with the fabric layer in the +45° direction.

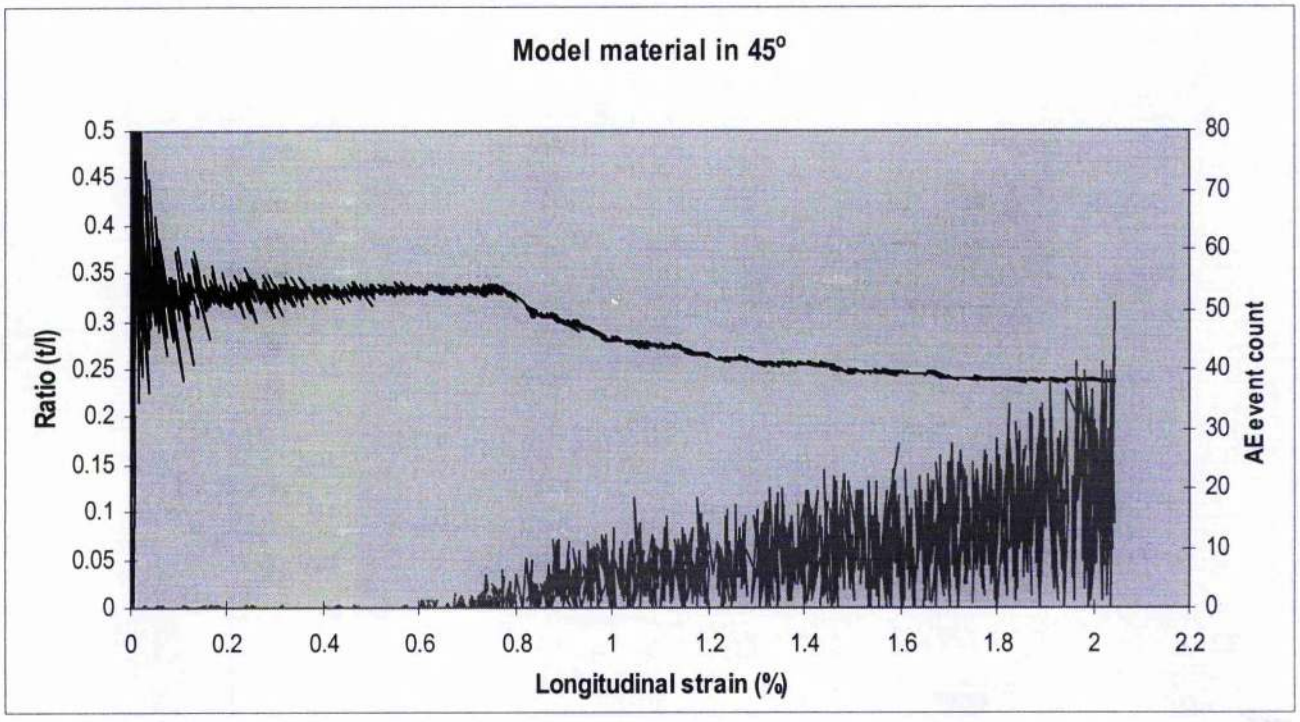

Figure 4.49.- Behaviour of the negative of the ratio of the transverse strain to the longitudinal strain, ie the Poisson's ratio –(t/l), as a function of the longitudinal strain for the model sandwich laminate with the fabric layer in the +45° direction

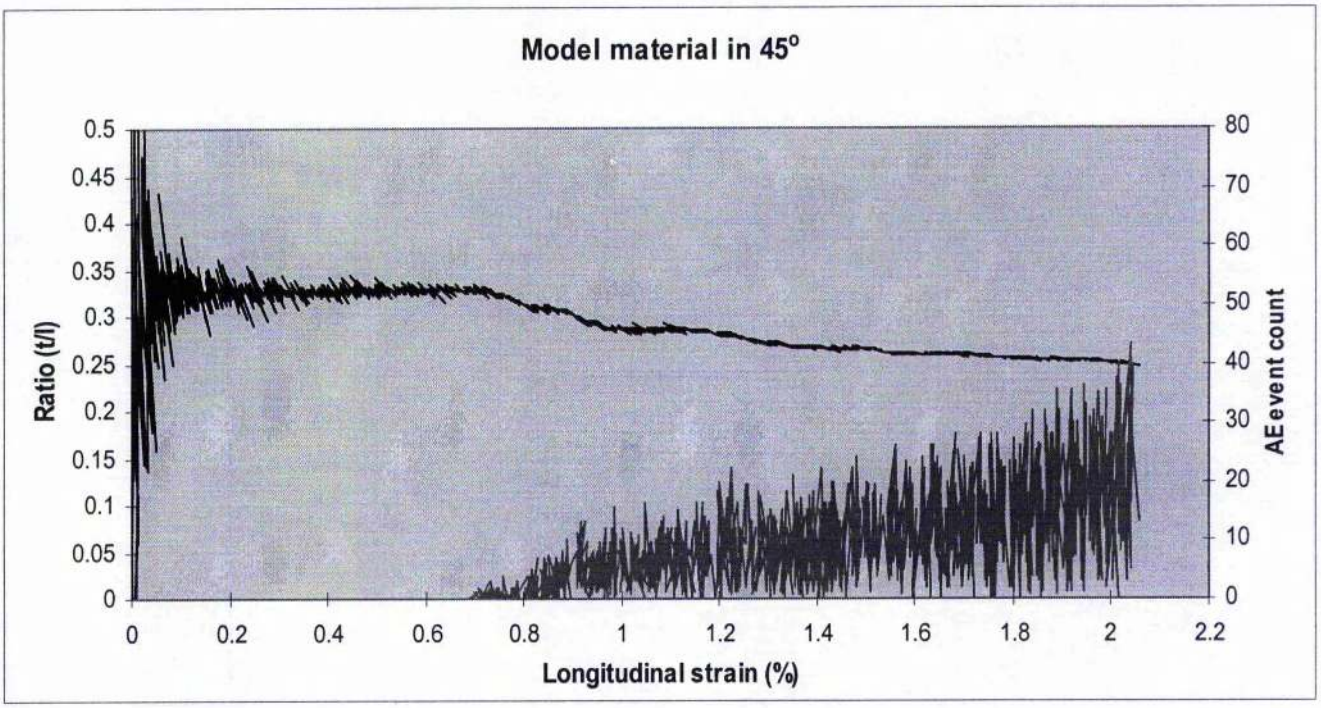

Figure 4.50.- Behaviour of the negative of the ratio of the transverse strain to the longitudinal strain, ie the Poisson's ratio –(t/l), as a function of the longitudinal strain for the model sandwich laminate with the fabric layer in the +45° direction

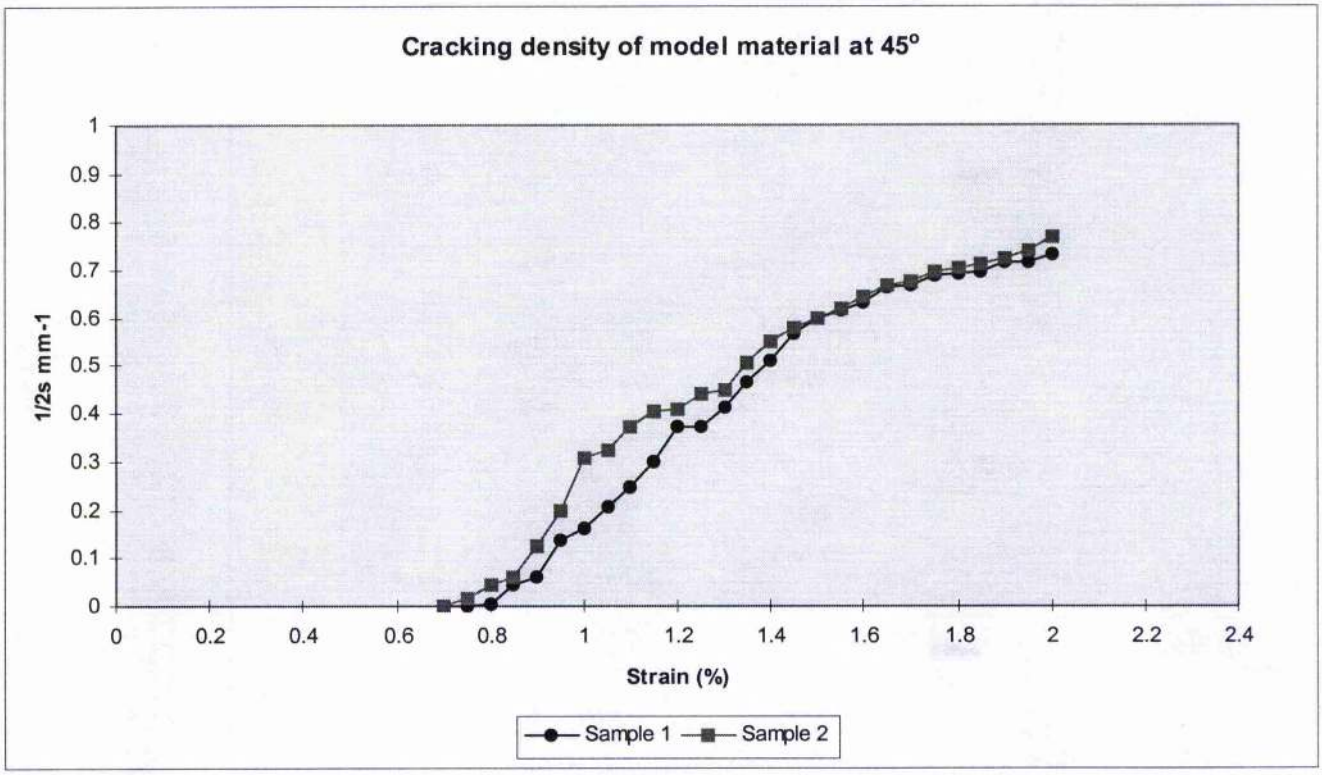

Figure 4.51.- Crack density-strain curve for the model sandwich laminate with the fabric layer in the +45° direction.

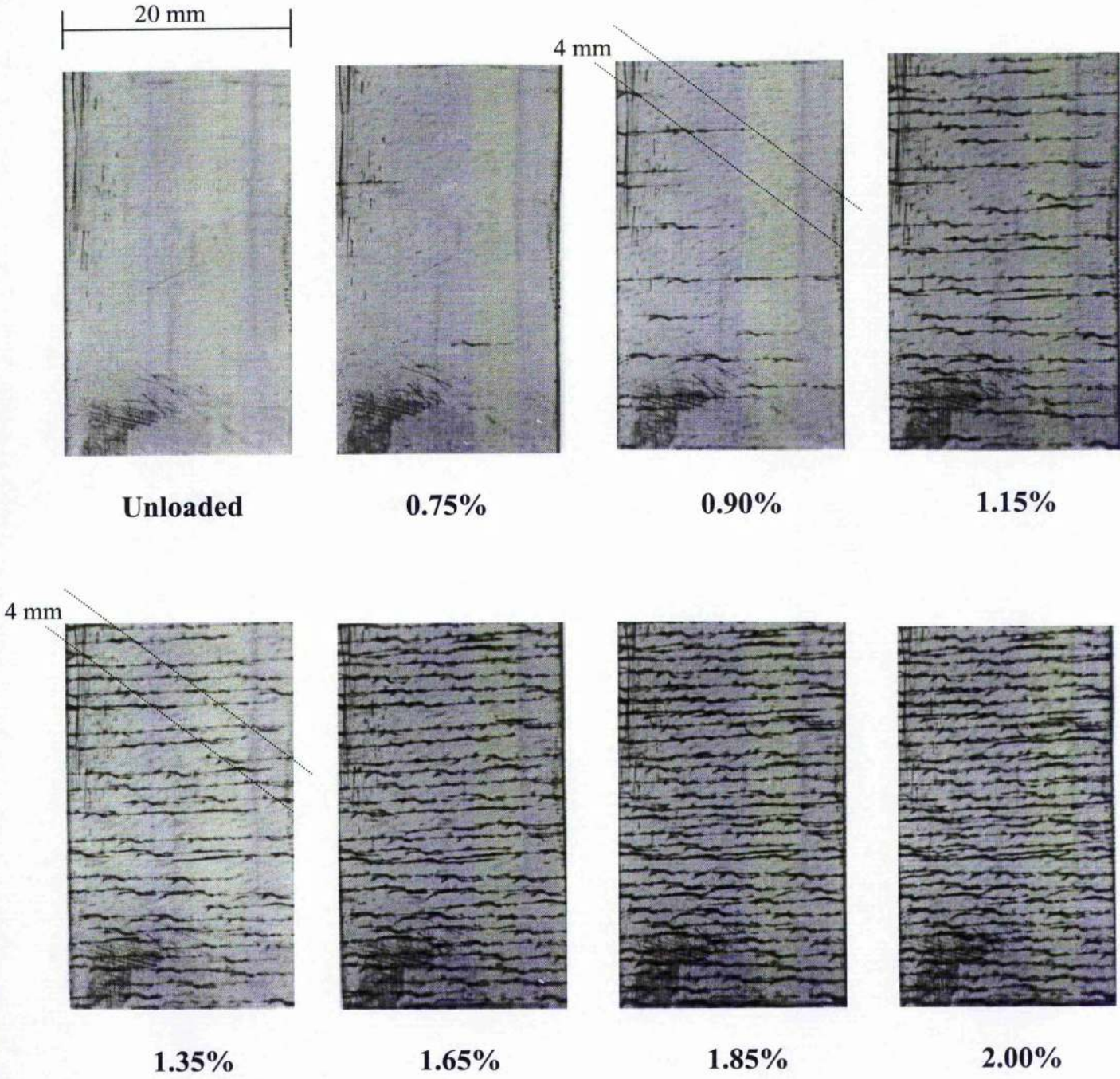

Figure 4.52.- Crack development for the model sandwich laminate with the fabric layer in the +45° direction Applied strains are indicated.

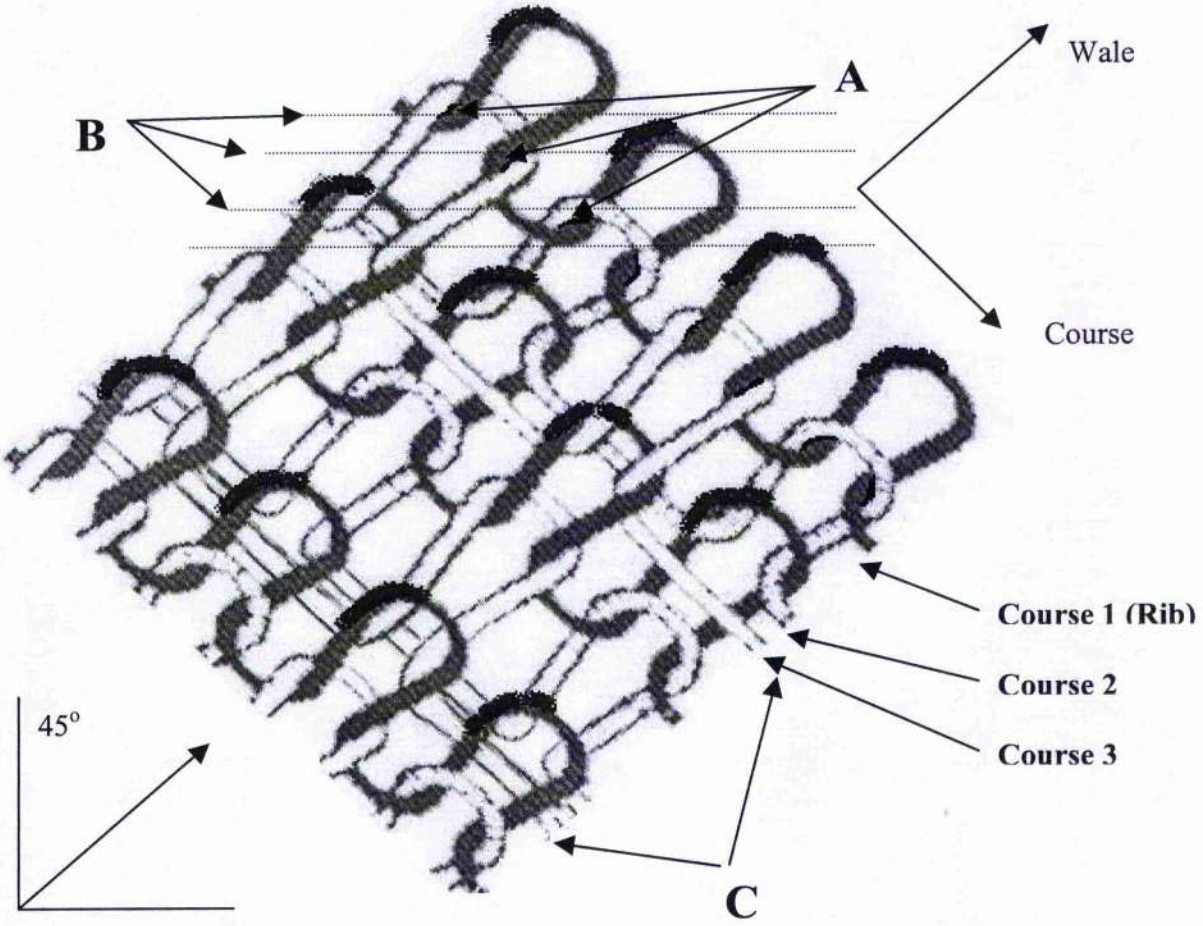

Figure 4.53.- Schematic diagram showing crack development for the model sandwich laminate with the fabric layer in the +45° direction.

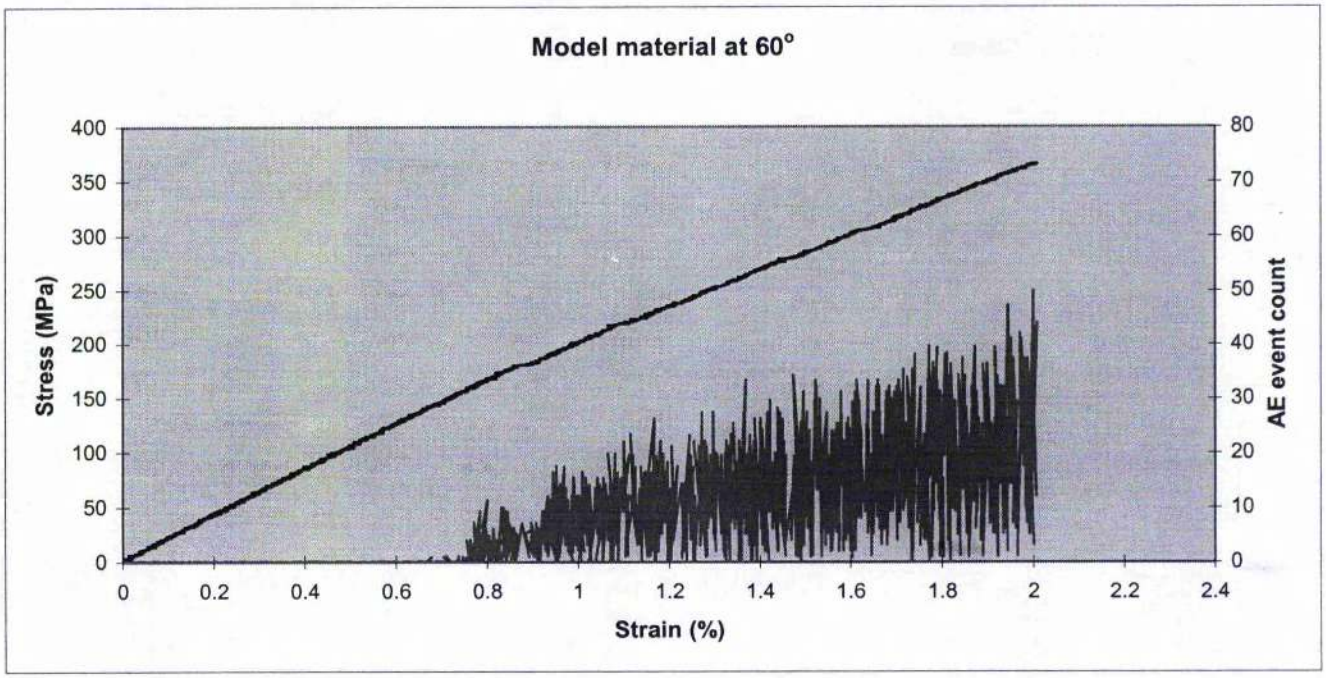

Figure 4.54- Stress-strain curve and acoustic emission event counts for the model sandwich laminate with the fabric layer in the 60° direction.

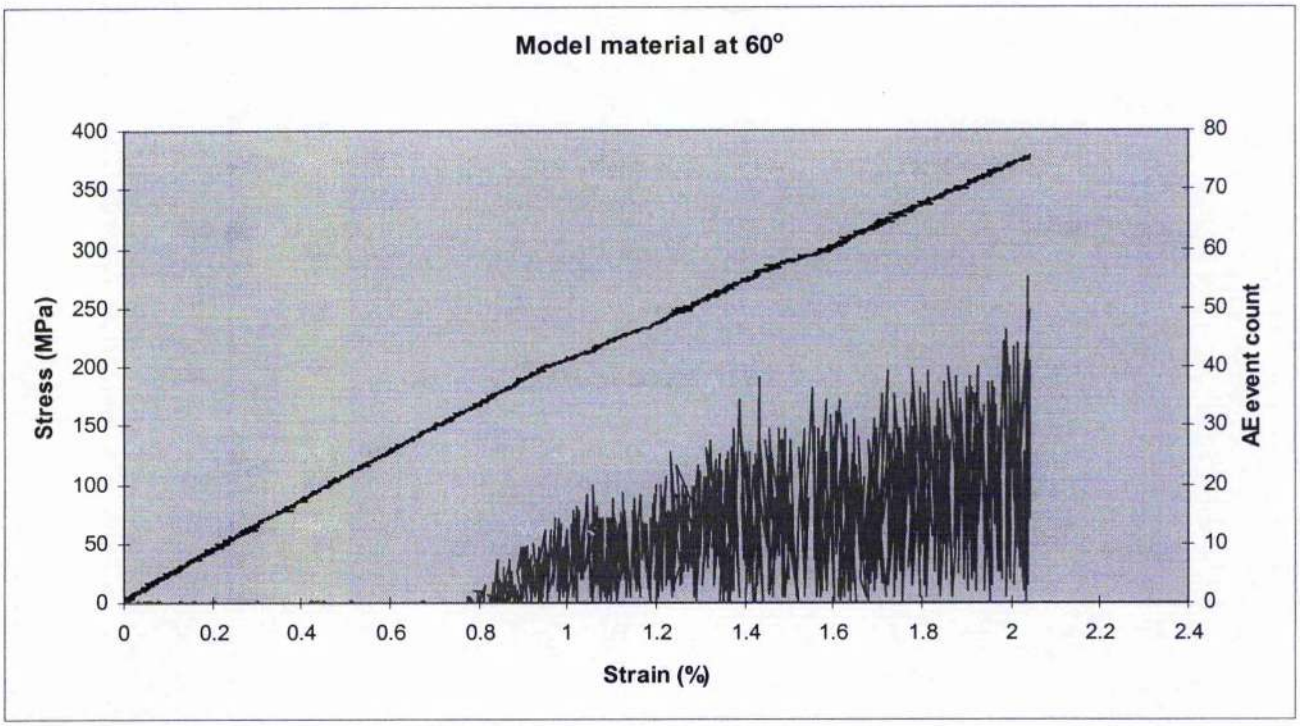

Figure 4.55- Stress-strain curve and acoustic emission event counts for the model sandwich laminate with the fabric layer in the 60° direction.

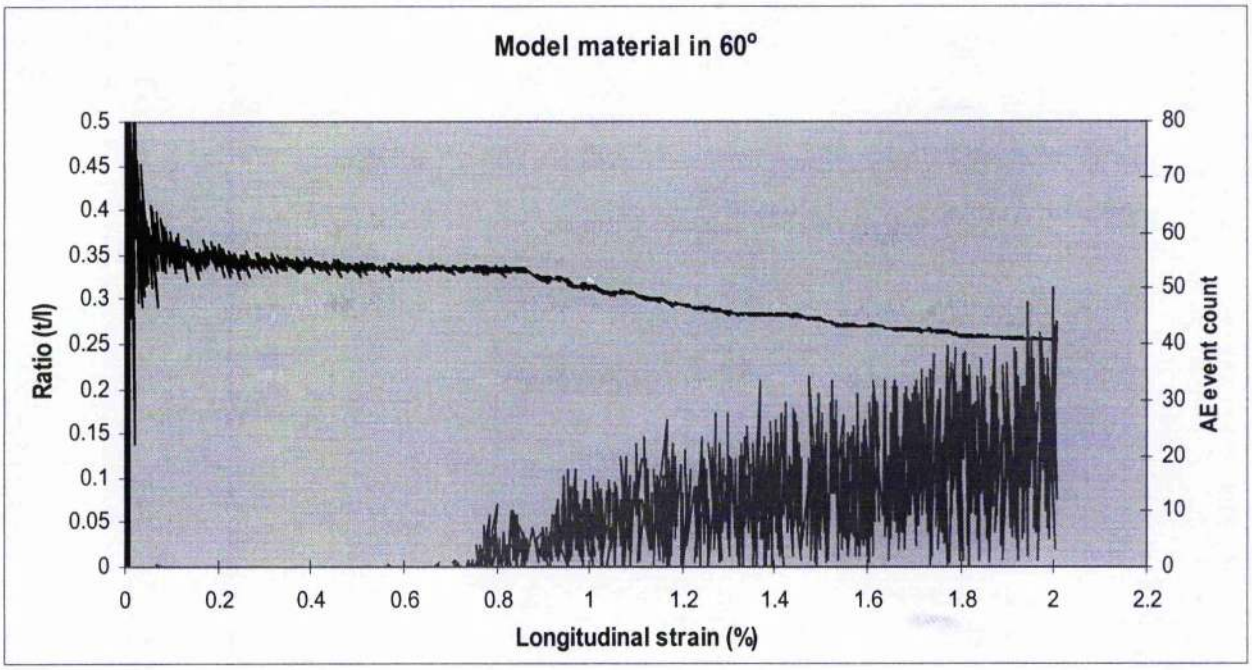

Figure 4.56.- Behaviour of the negative of the ratio of the transverse strain to the longitudinal strain, ie the Poisson's ratio –(t/l), as a function of the longitudinal strain for the model sandwich laminate with the fabric layer in the 60° direction

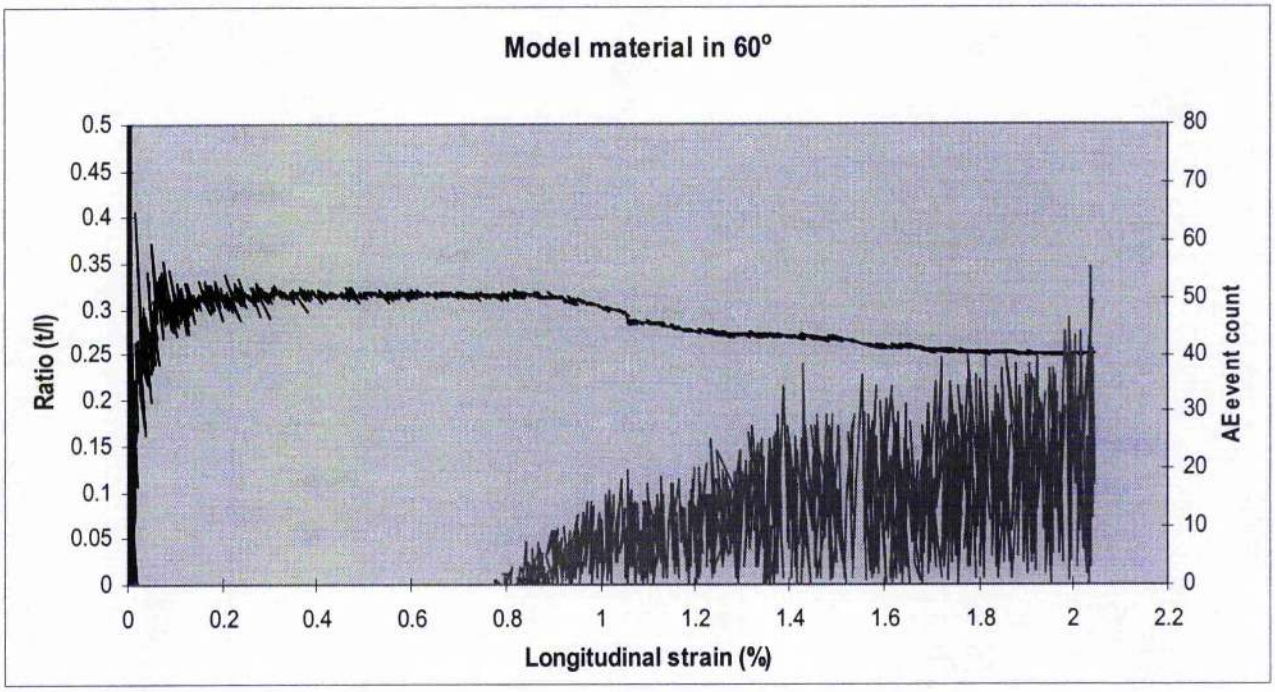

Figure 4.57.- Behaviour of the negative of the ratio of the transverse strain to the longitudinal strain, ie the Poisson's ratio –(t/l), as a function of the longitudinal strain for the model sandwich laminate with the fabric layer in the 60° direction

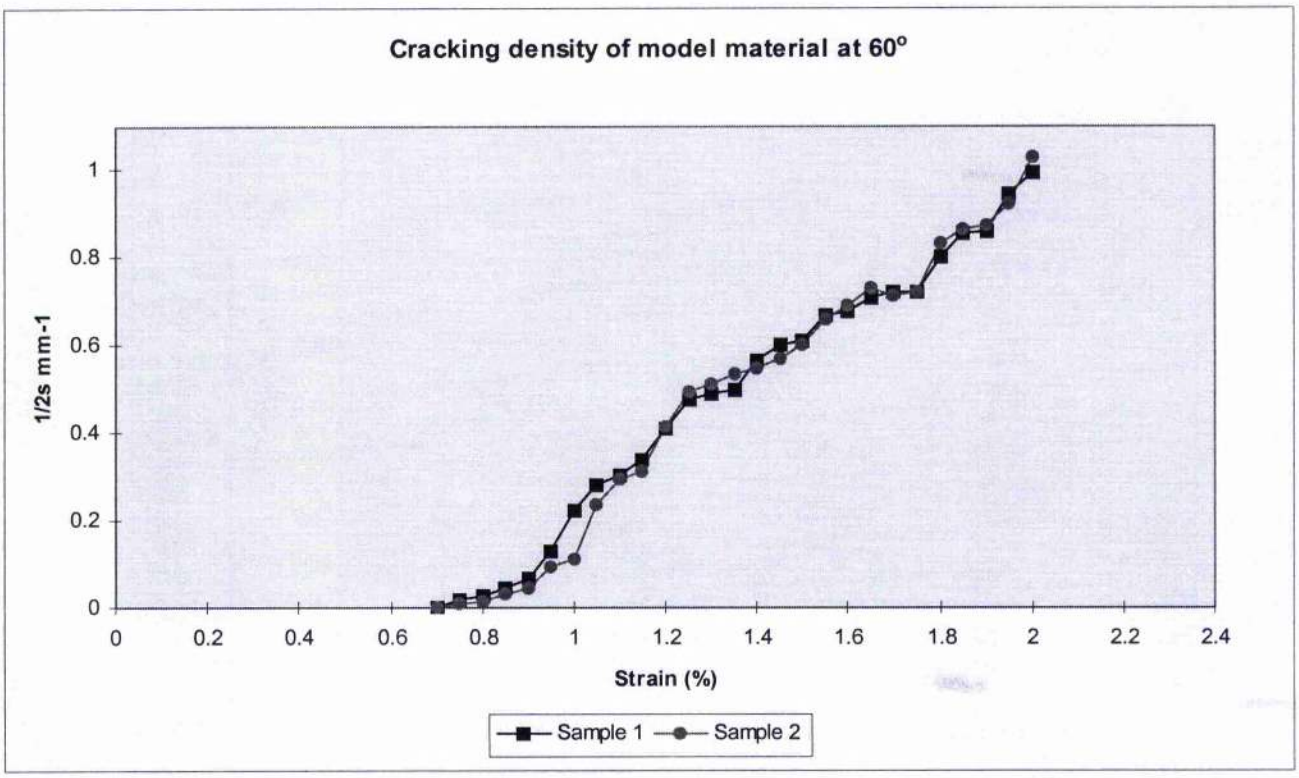

Figure 4.58 Crack density-strain curve for the model sandwich laminate with the fabric layer in the 60° direction.

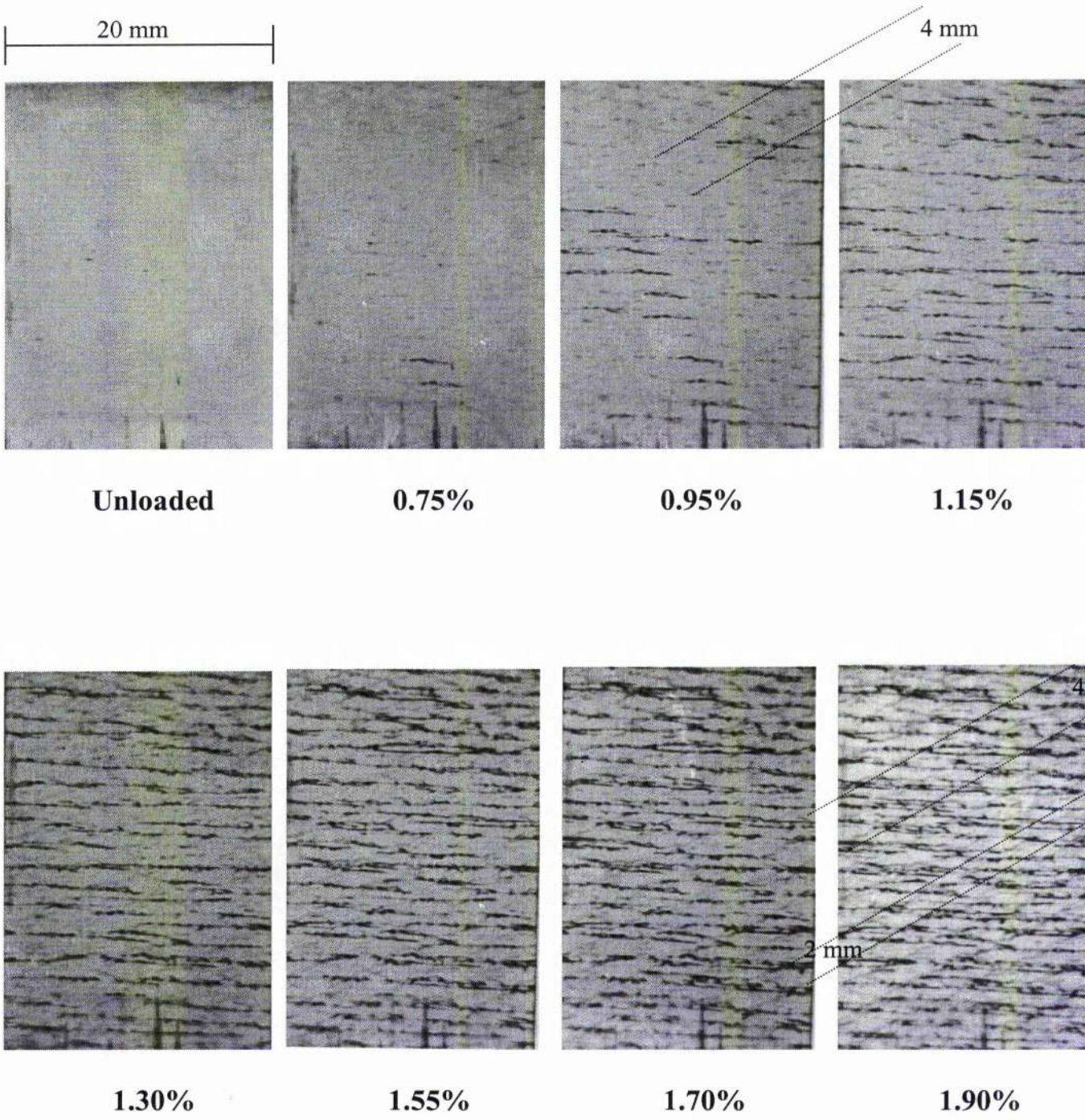

Figure 4.59.- Crack development for the model sandwich laminate with the fabric layer in the 60° direction Applied strains are indicated.

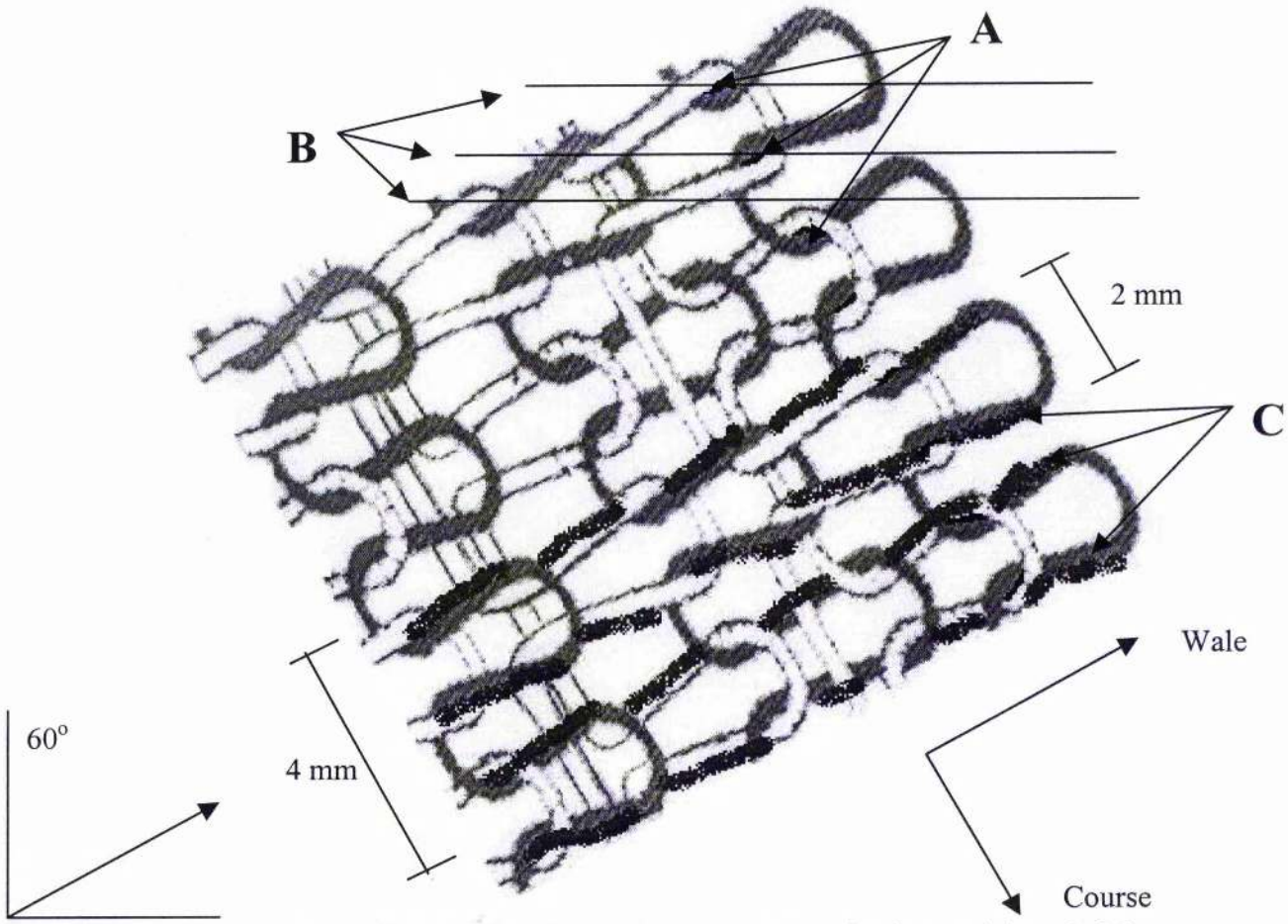

Figure 4.60.- Schematic diagram showing crack development for the model sandwich laminate with the fabric layer in the 60° direction.

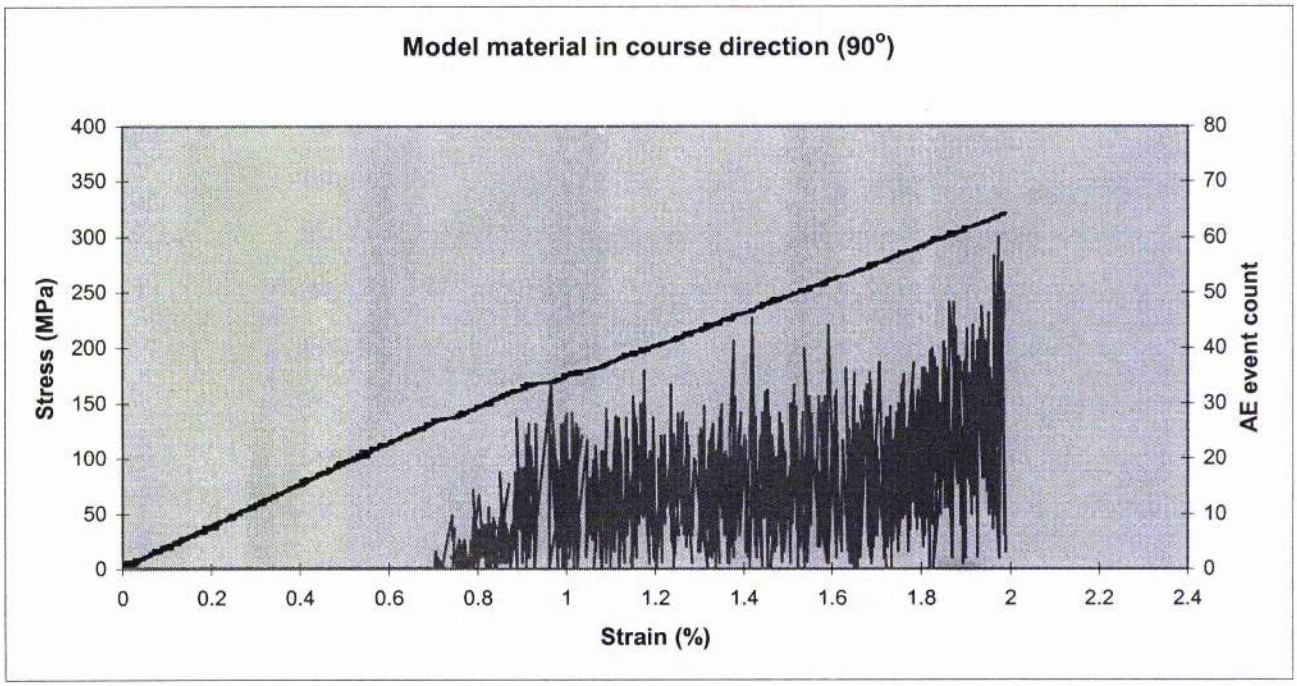

Figure 4.61- Stress-strain curve and acoustic emission event counts for the model sandwich laminate with the fabric layer in the 90° direction.

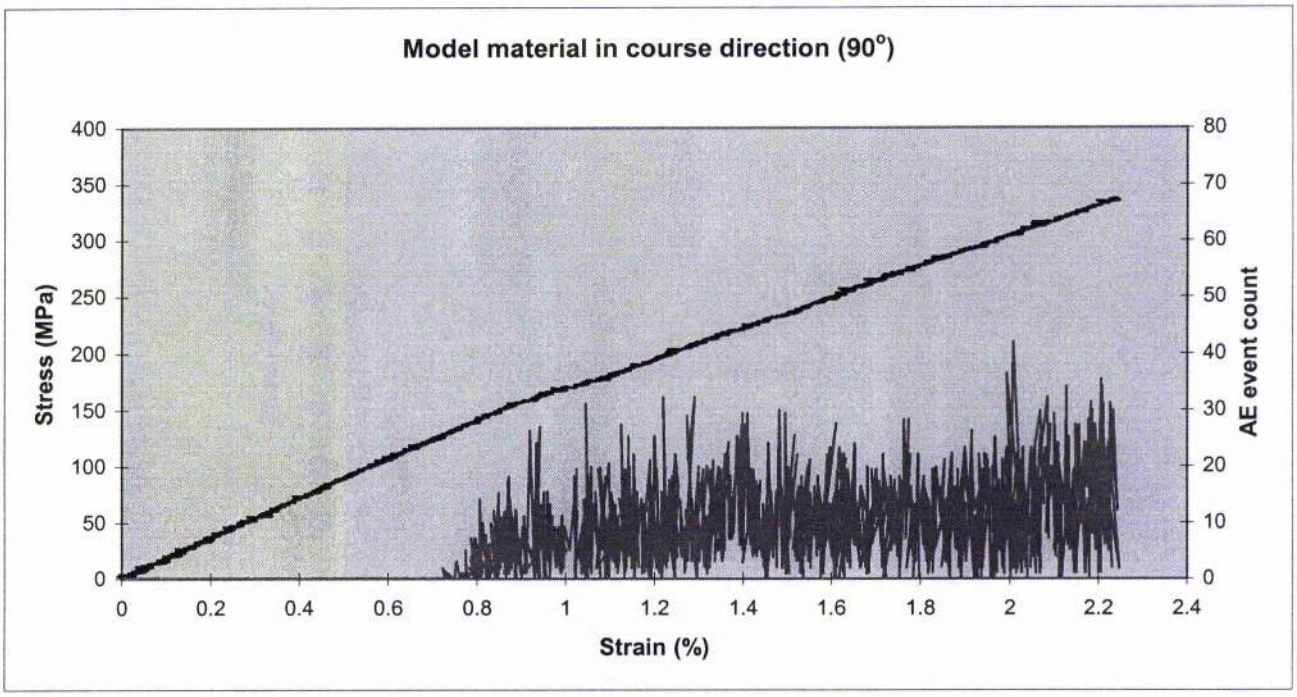

Figure 4.62- Stress-strain curve and acoustic emission event counts for the model sandwich laminate with the fabric layer in the 90° direction.

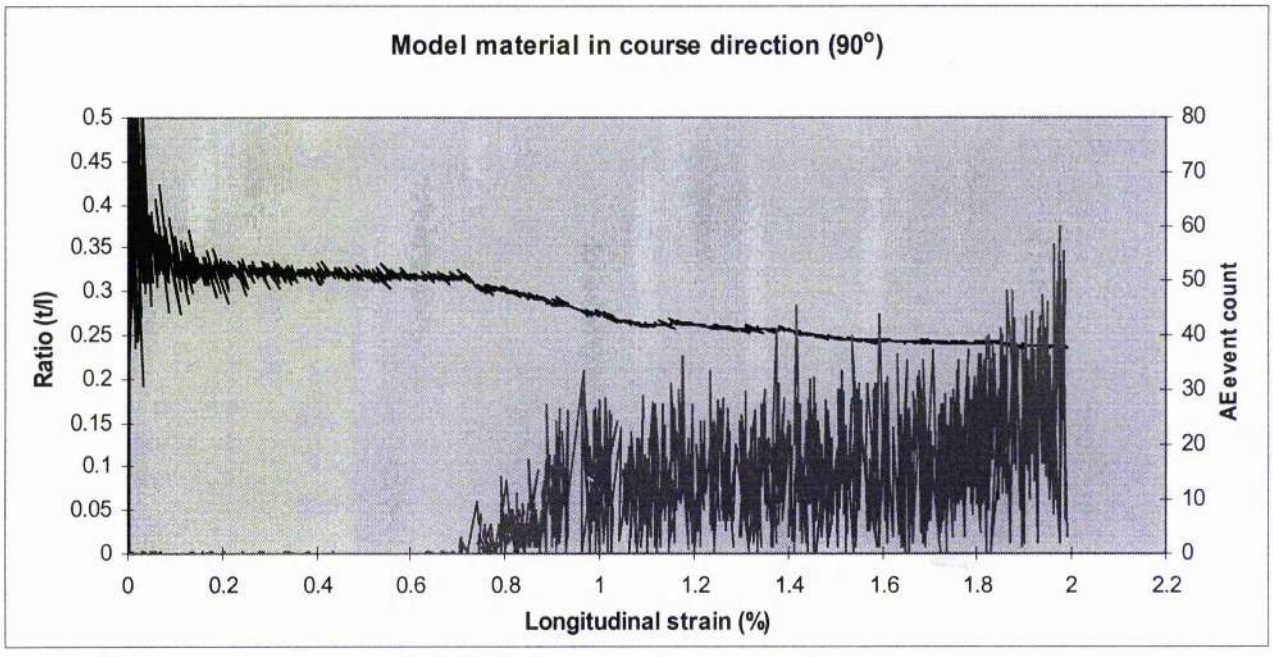

Figure 4.63.- Behaviour of the negative of the ratio of the transverse strain to the longitudinal strain, ie the Poisson's ratio –(t/l), as a function of the longitudinal strain for the model sandwich laminate with the fabric layer in the 90° direction

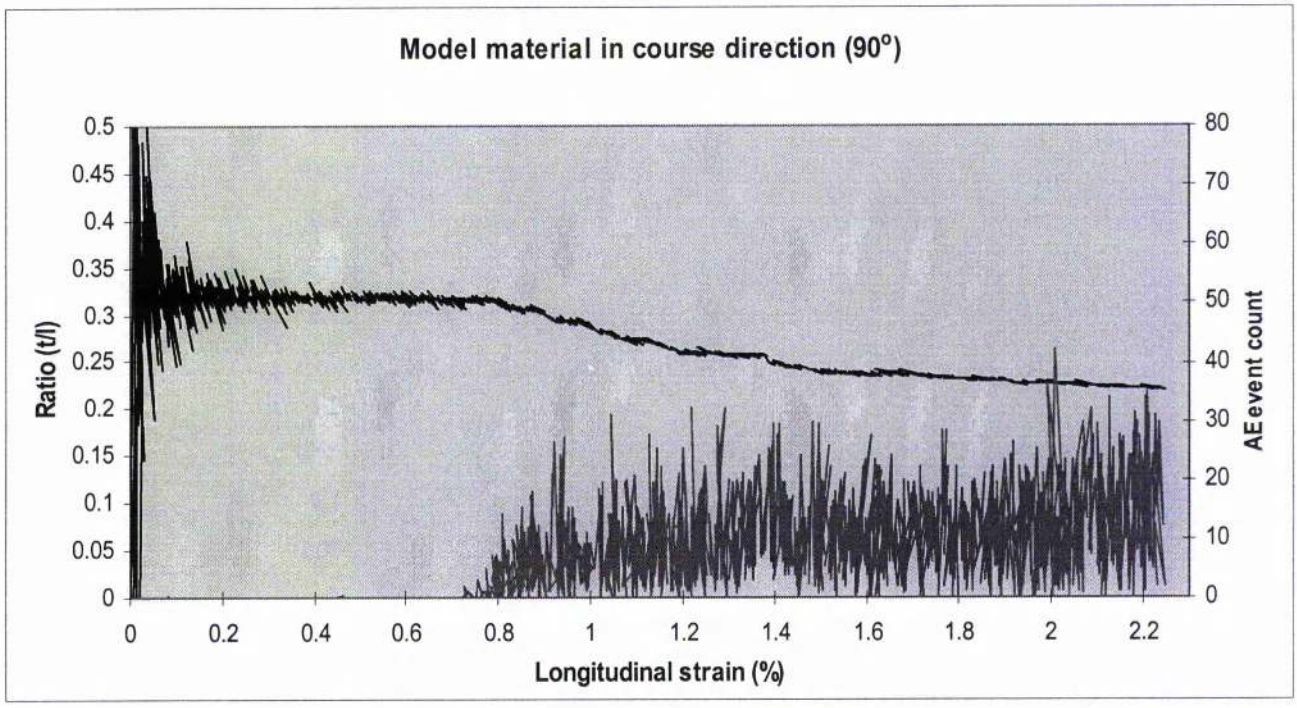

Figure 4.64.- Behaviour of the negative of the ratio of the transverse strain to the longitudinal strain, ie the Poisson's ratio –(t/l), as a function of the longitudinal strain for the model sandwich laminate with the fabric layer in the 90° direction

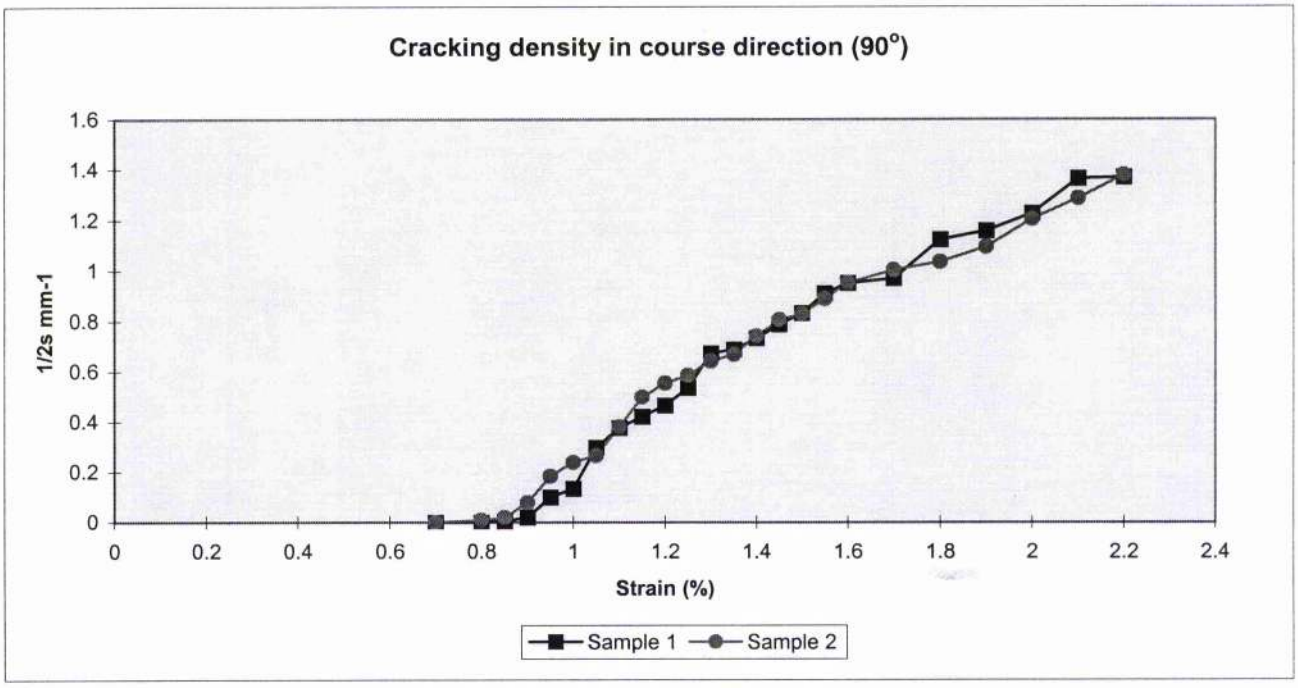

Figure 4.65.- Crack density-strain curve for the model sandwich laminate with the fabric layer in the 90° direction.

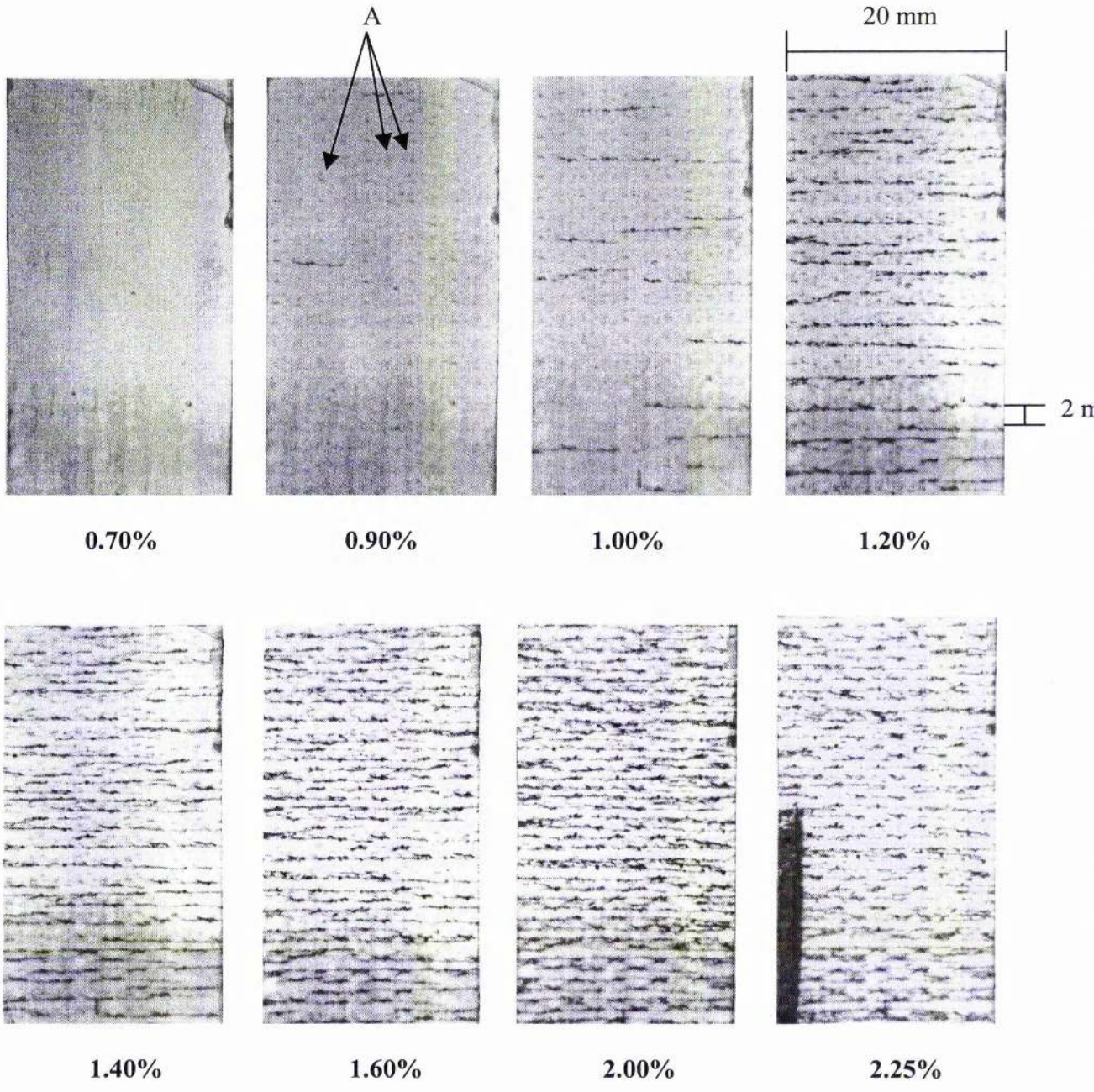

Figure 4.66.- Crack development for the model sandwich laminate with the fabric layer in the 90° direction Applied strains are indicated.

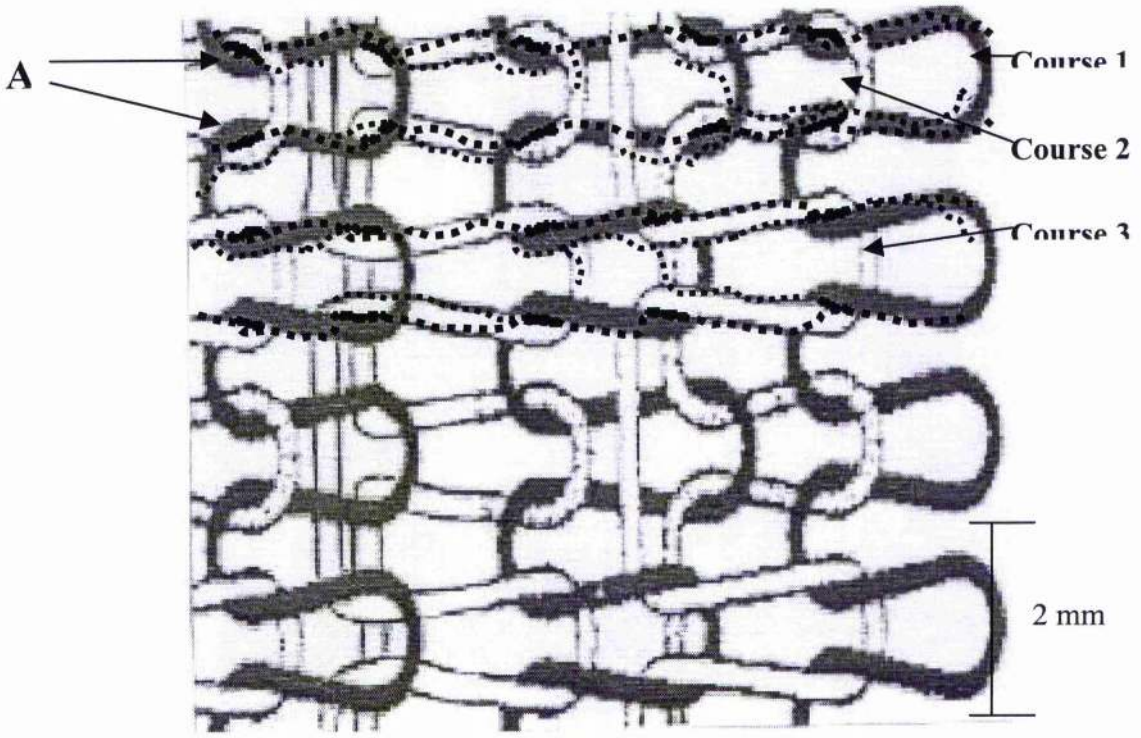

Figure 4.67.- Schematic diagram showing crack development for the model sandwich laminate with the fabric layer in the 0^{o} direction.

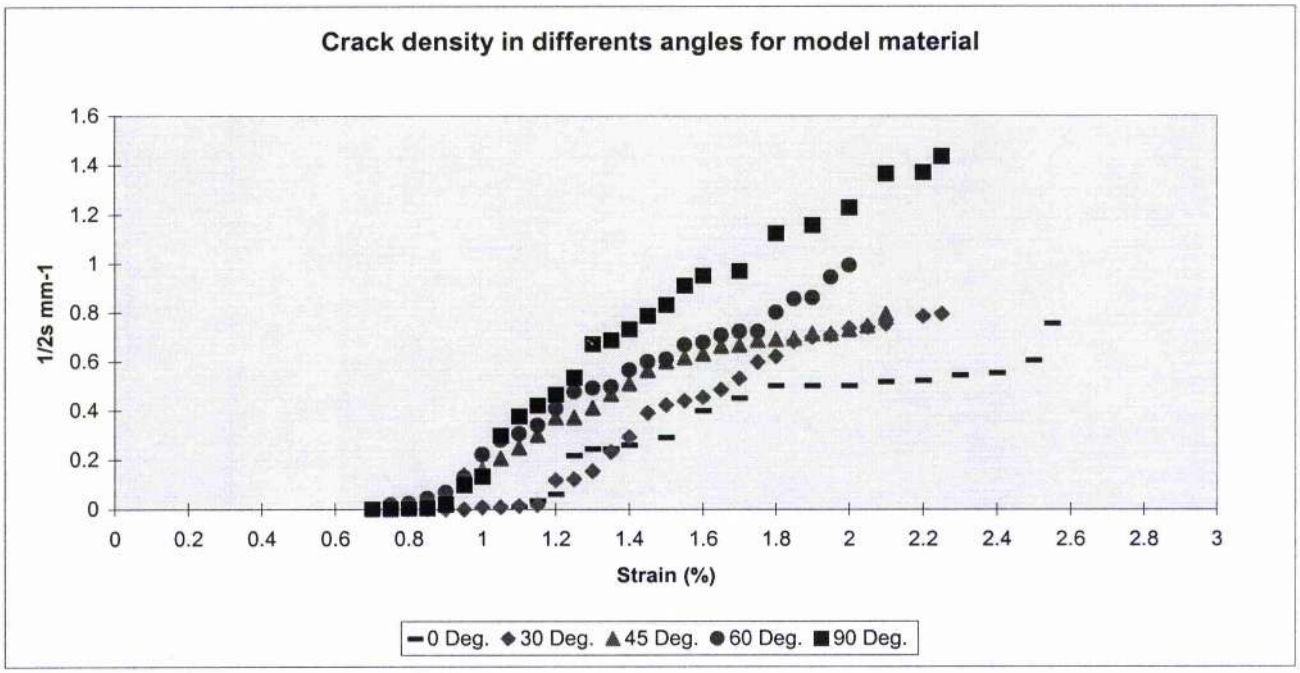

Figure 4.68.- Crack density versus strain curves for the model sandwich laminates in all angular orientations.

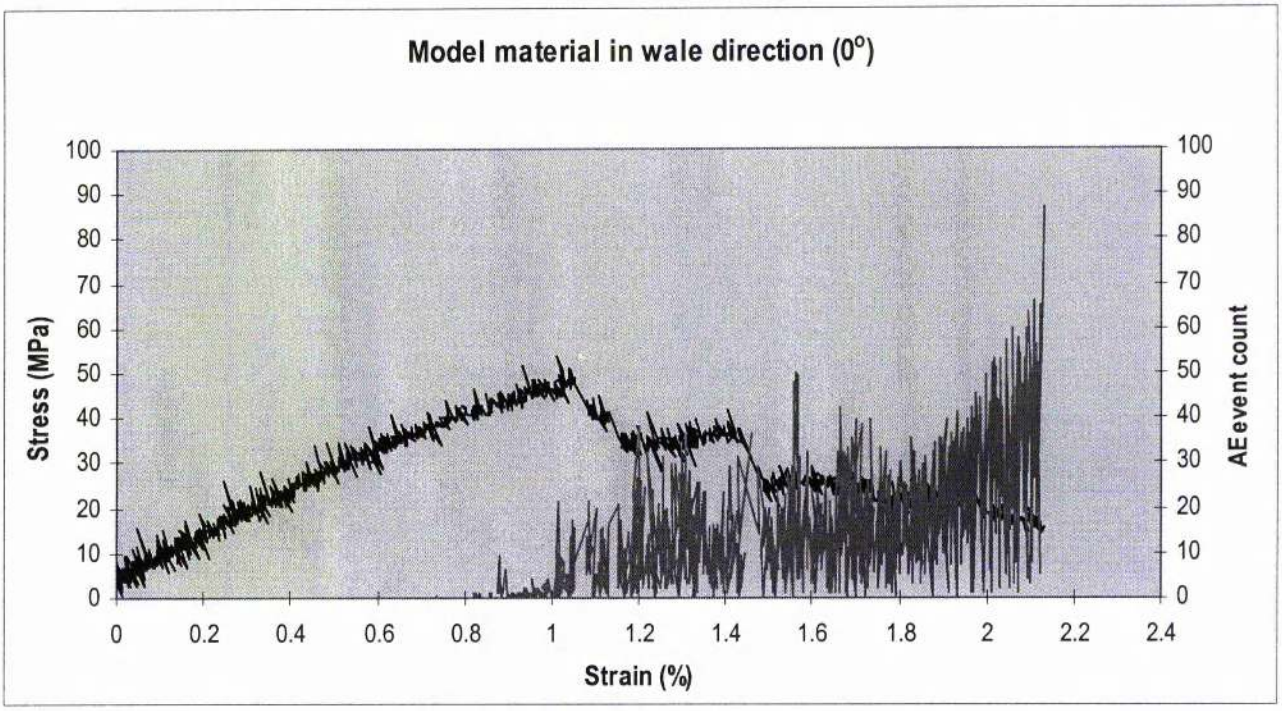

Figure 4.69.- Curve of derived knitted fabric stress in loading direction vs. strain for model material sample in 0° (Wale direction).

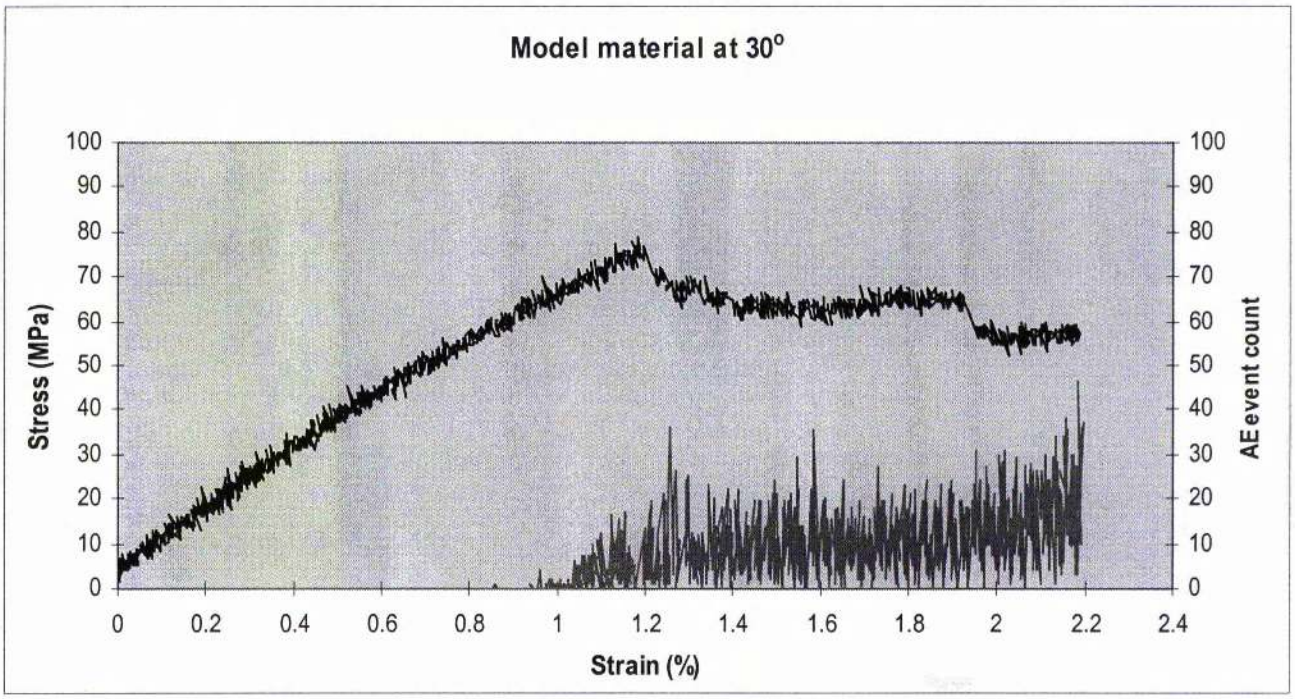

Figure 4.70.- Curve of derived knitted fabric stress in loading direction vs. strain for model material sample in 30°.

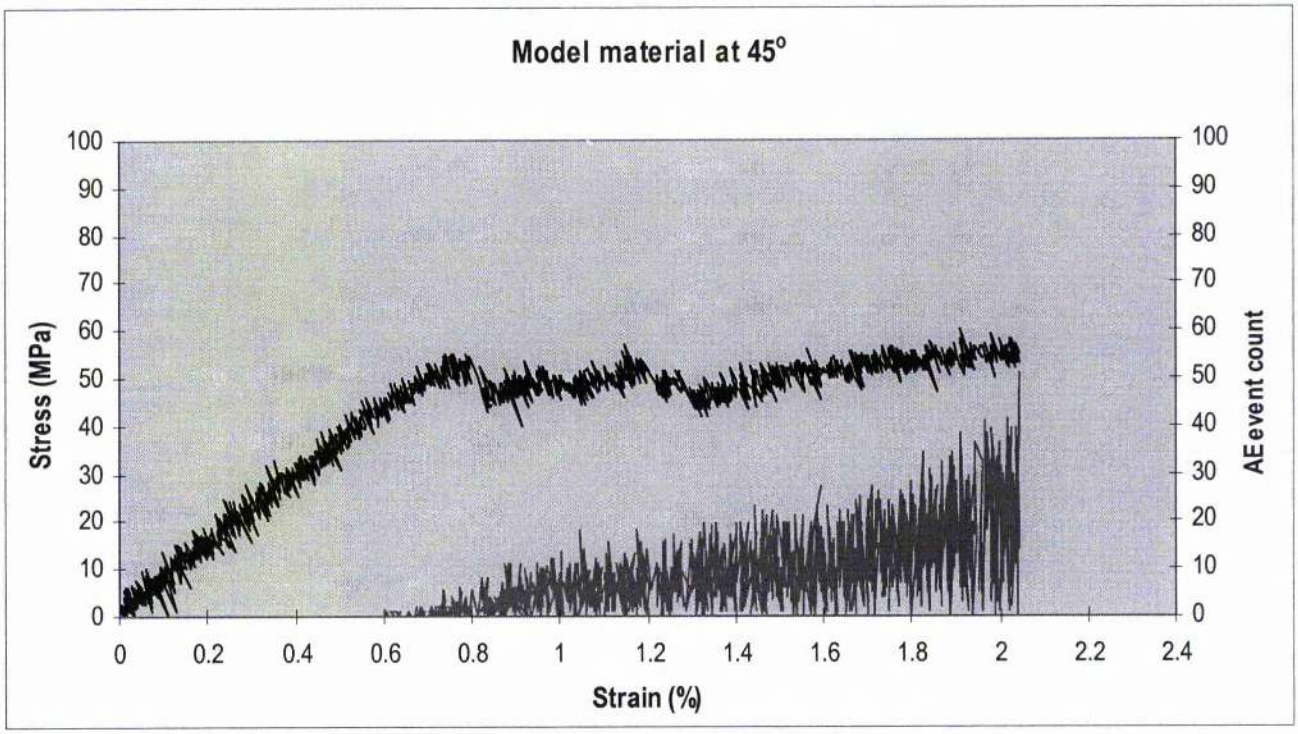

Figure 4.71.- Curve of derived knitted fabric stress in loading direction vs. strain for model material sample in 45°.

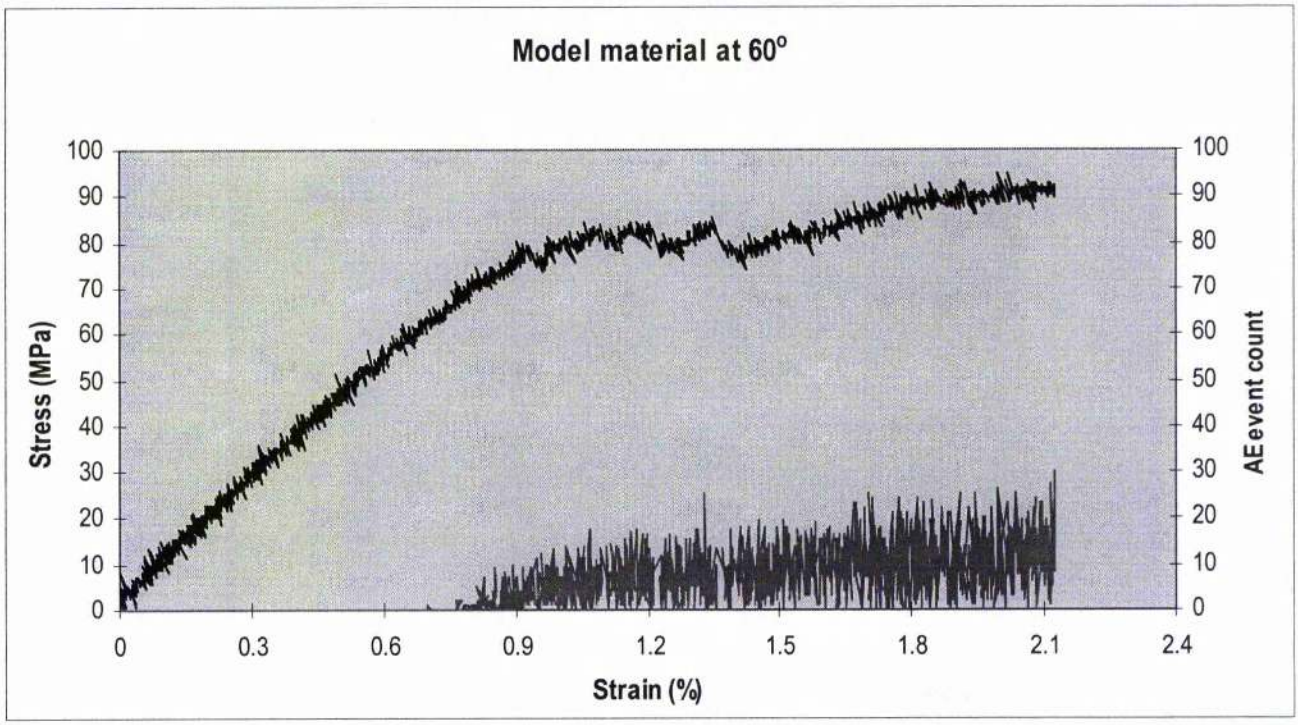

Figure 4.72.- Curve of derived knitted fabric stress in loading direction vs. strain for model material sample in 60°.

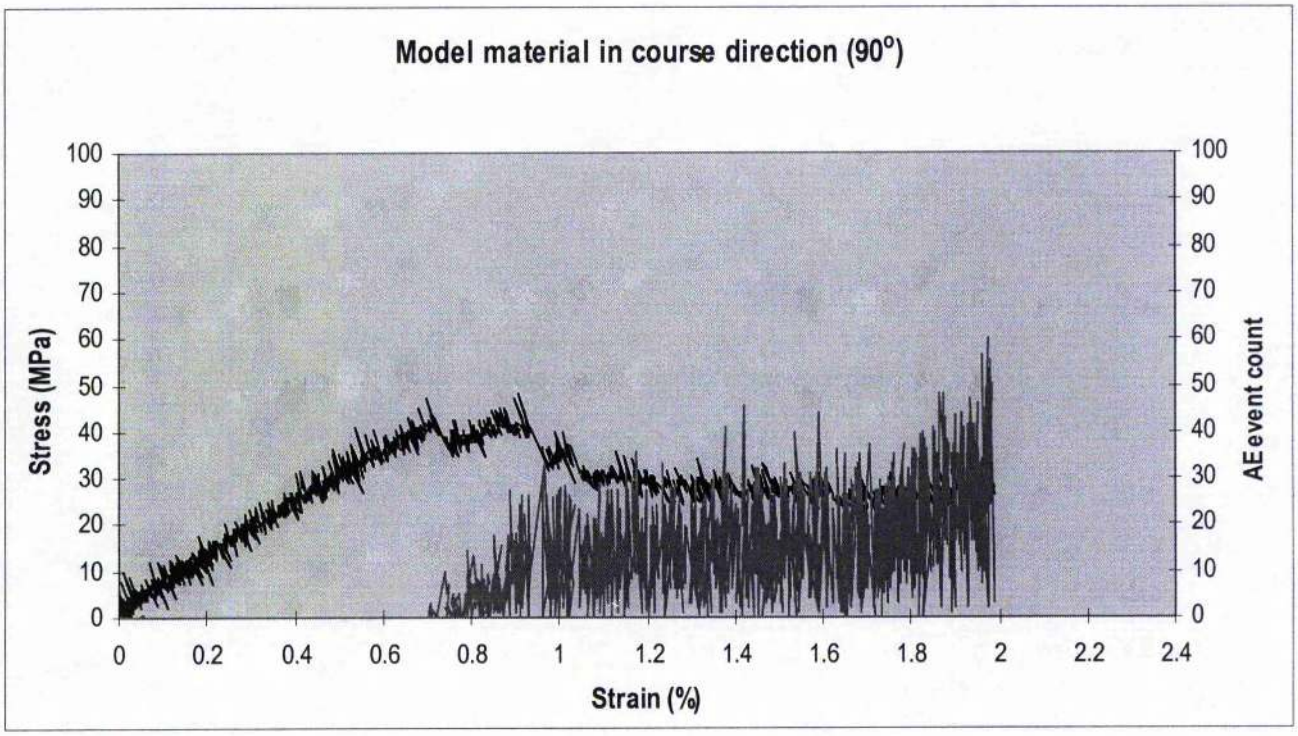

Figure 4.73.- Curve of derived knitted fabric stress in loading direction vs. strain for model material sample in 90° (Course direction).

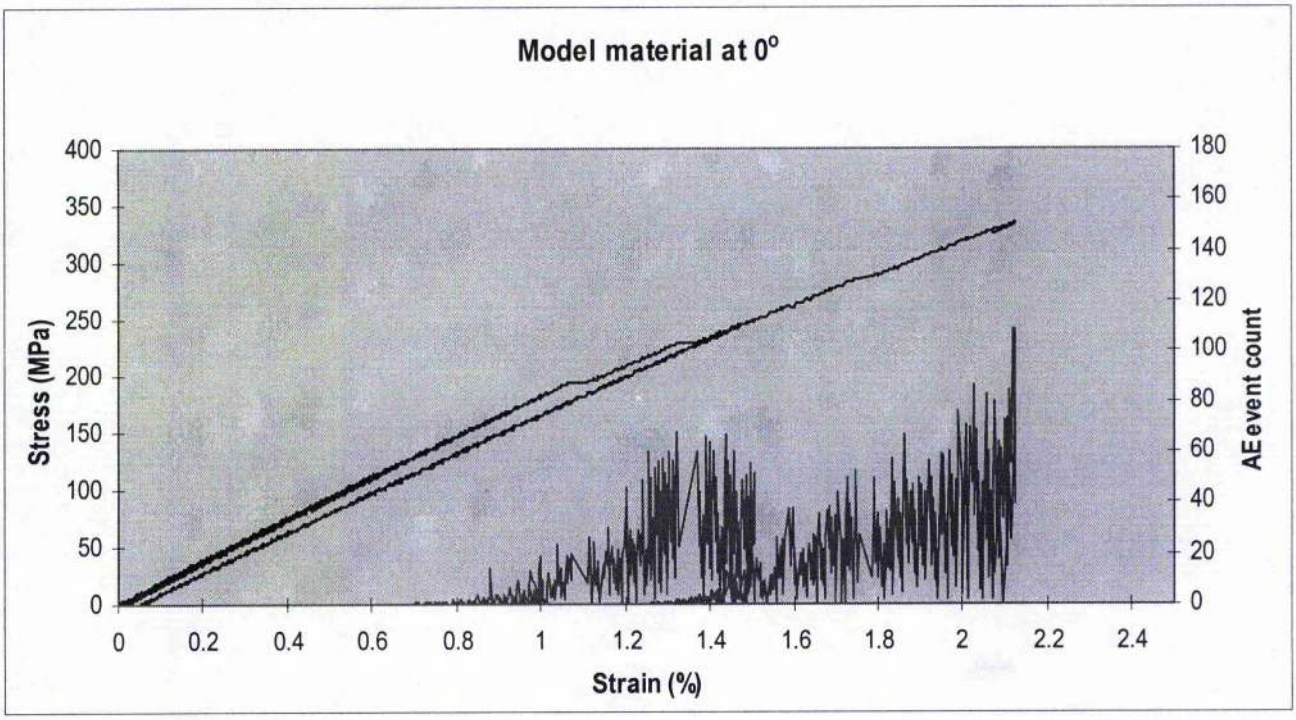

Figure 4.74.- Stress vs. strain curve in cyclic test for model material at 0° (Wale direction).

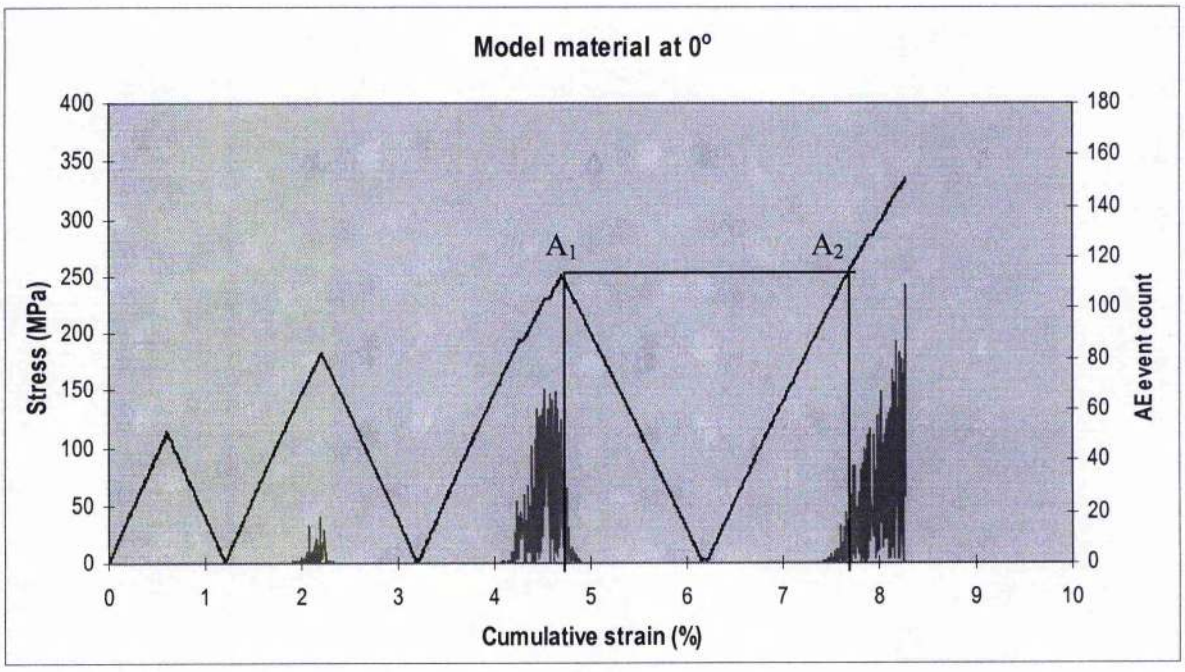

Figure 4.75.- Stress vs. cumulative strain curve in cyclic test for model material at 0° (Wale direction).

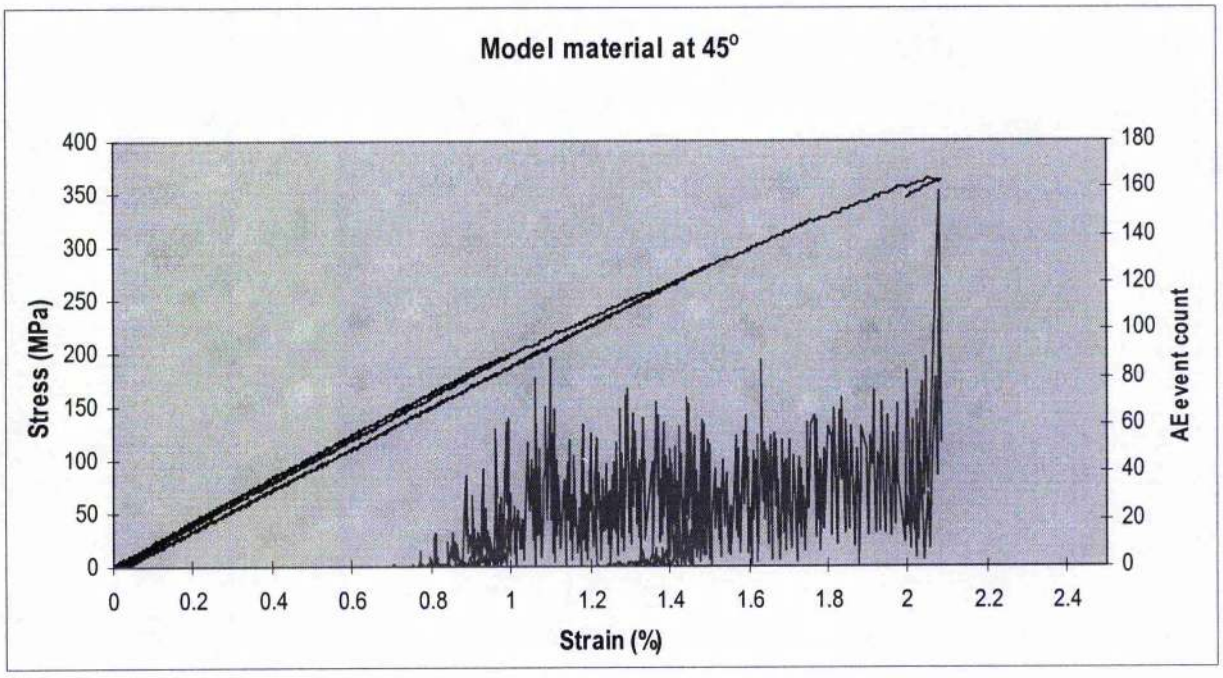

Figure 4.76.- Stress vs. strain curve in cyclic test for model material at 45°

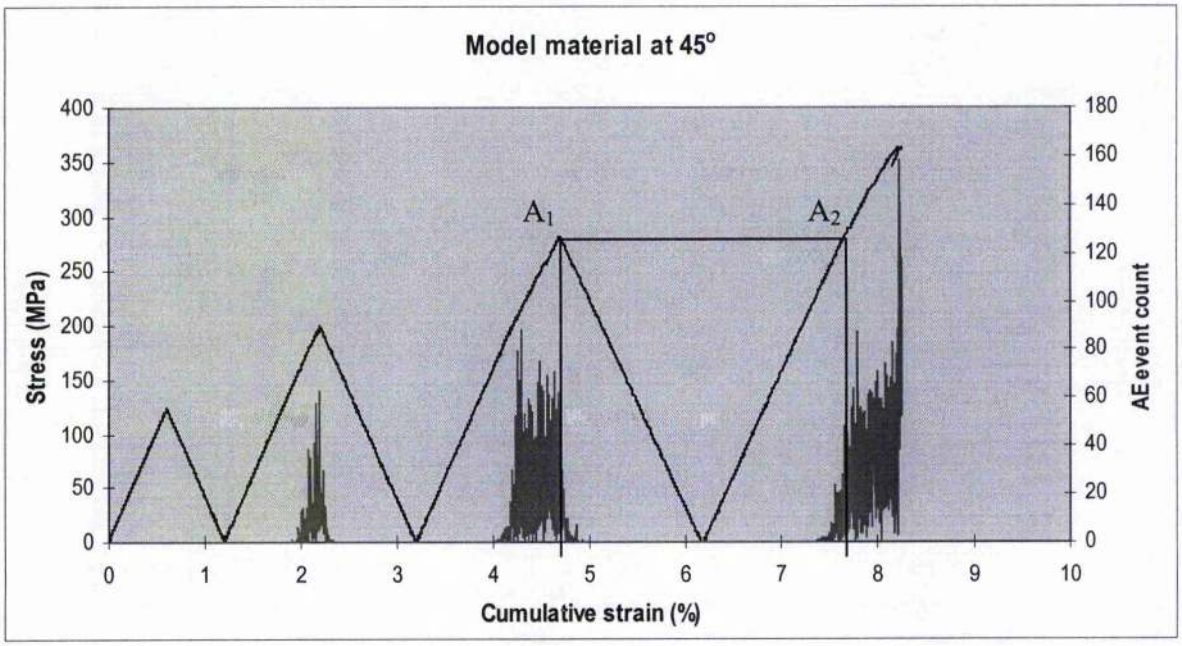

Figure 4.77.- Stress vs. cumulative strain curve in cyclic test for model material at 45°

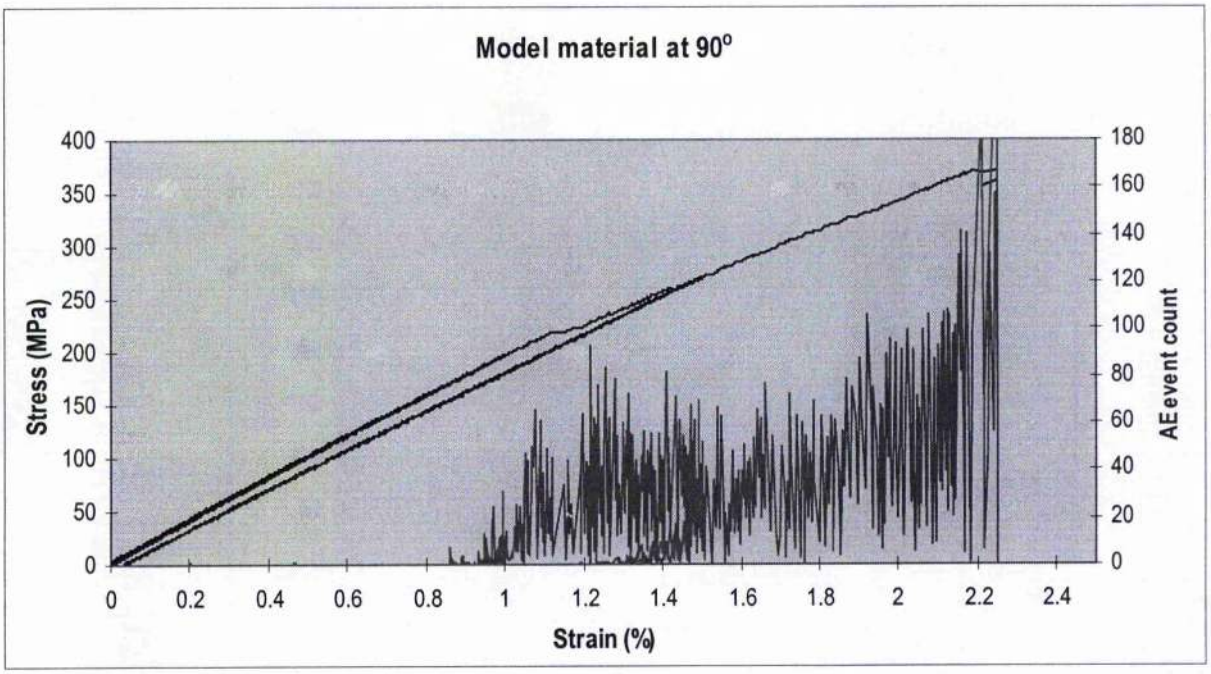

Figure 4.78.- Stress vs. strain curve in cyclic test for model material at 90° (Course direction).

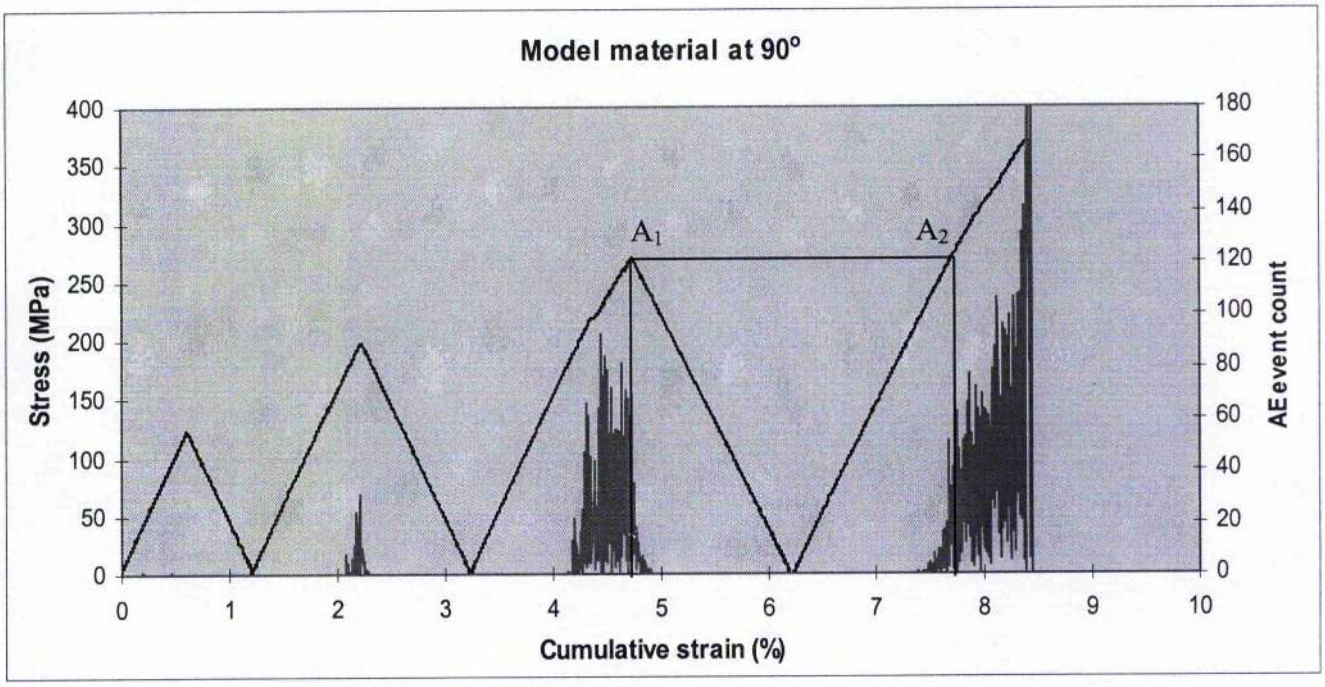

Figure 4.79.- Stress vs. cumulative strain curve in cyclic test for model material at 90° (Course direction).

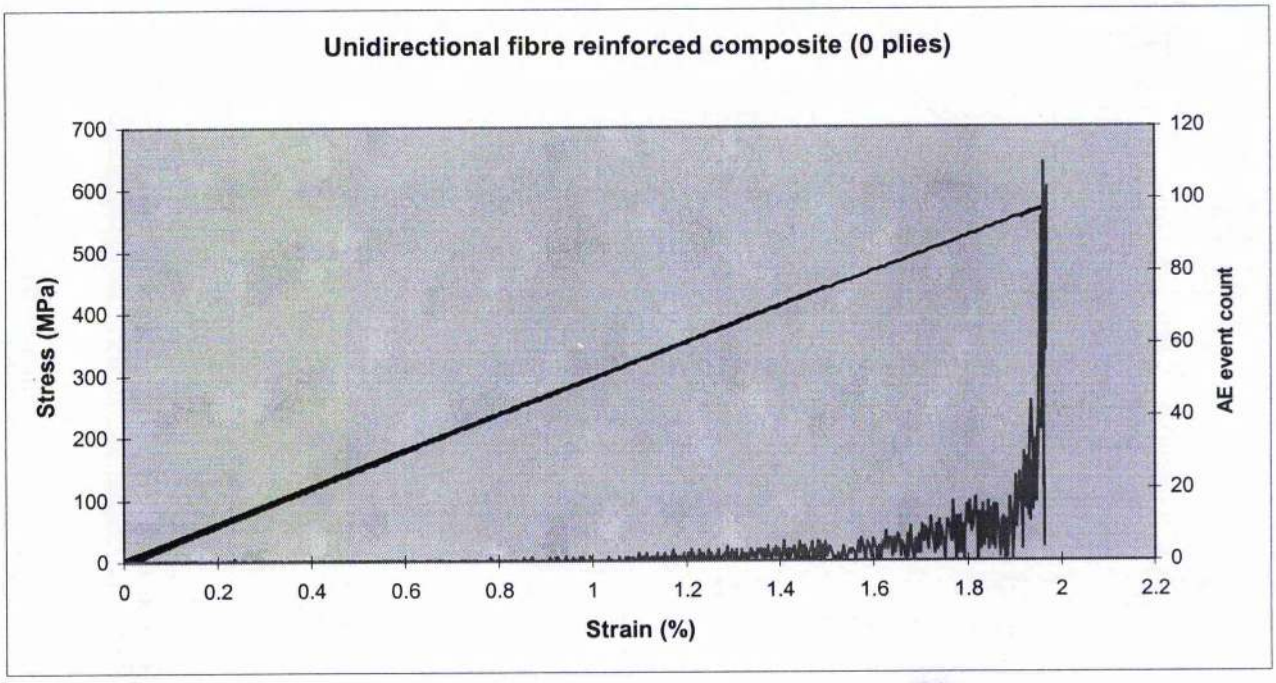

Figure 4.80.- Stress vs. strain curve for unidirectional reinforced sample.

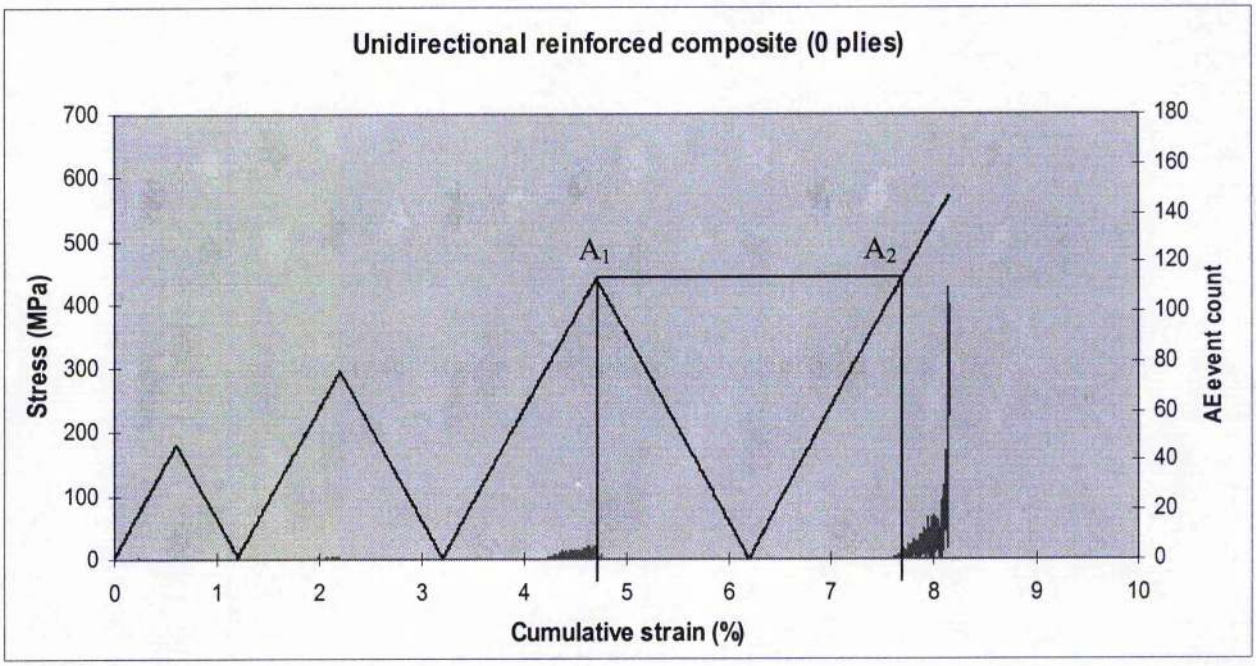

Figure 4.81.- Stress vs. cumulative strain curve for unidirectional reinforced sample.

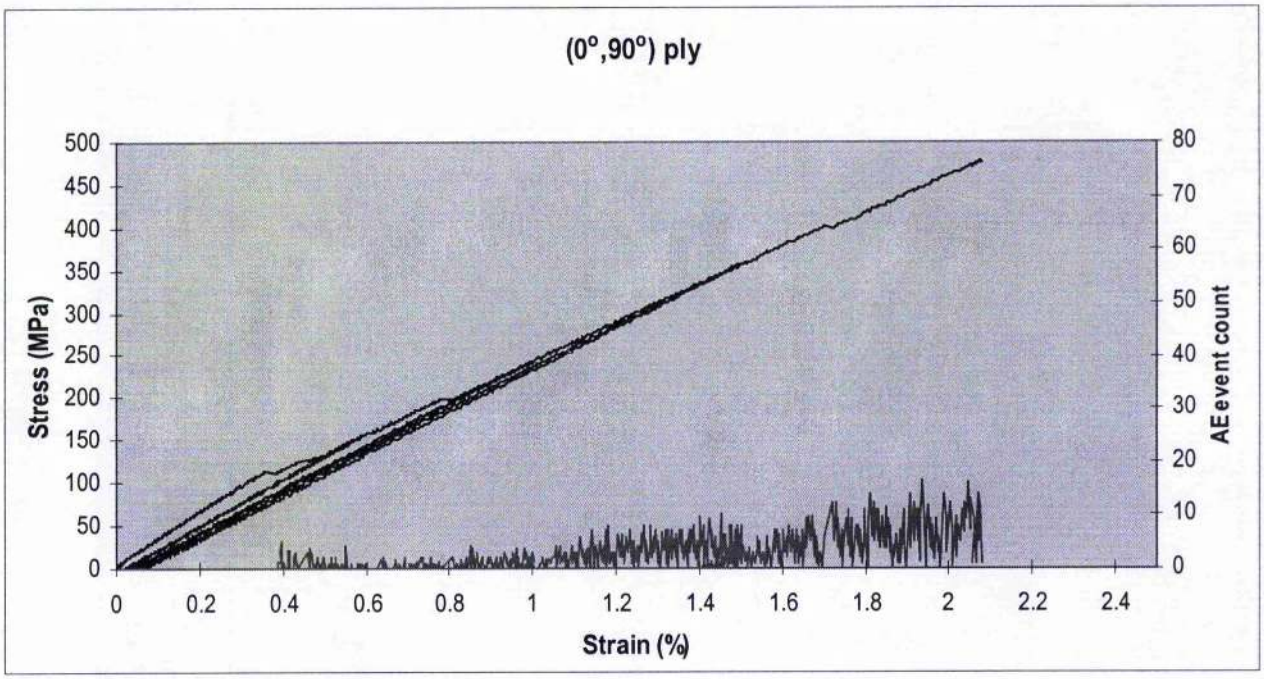

Figure 4.82.- Stress vs. strain curve for (0°, 90°) cross-ply.

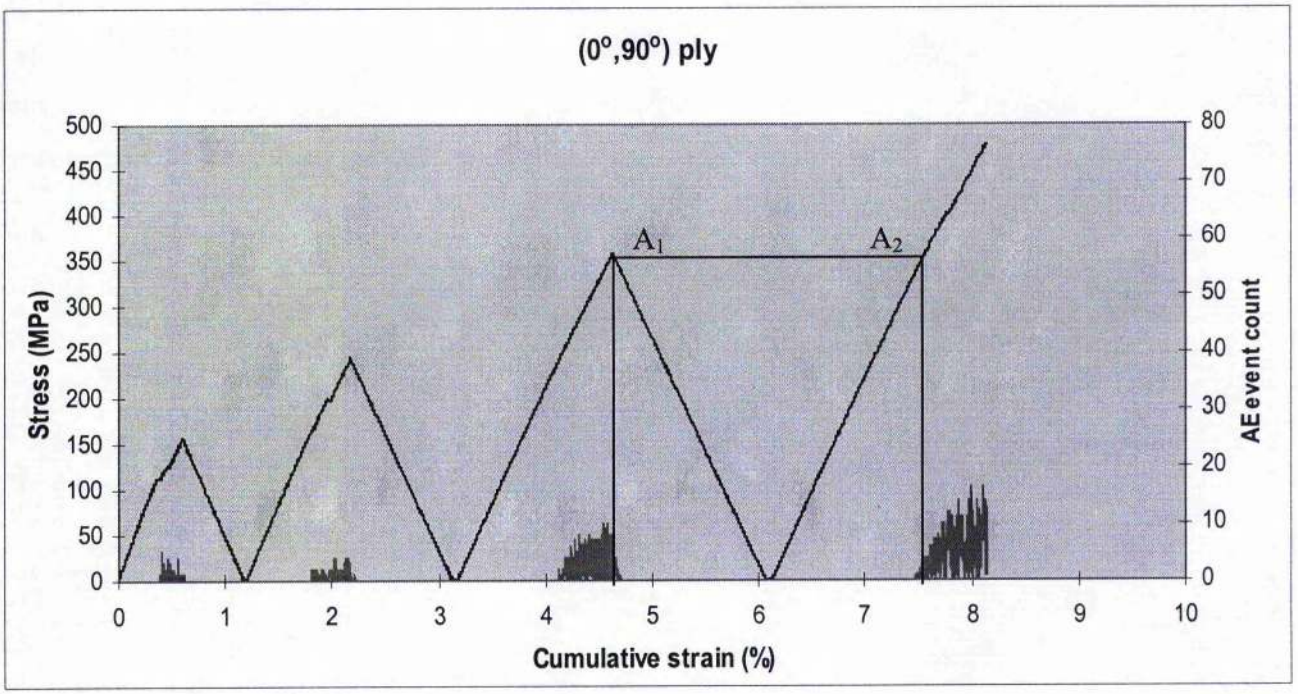

Figure 4.83.- Stress vs. cumulative strain curve for (0°, 90°) cross-ply.

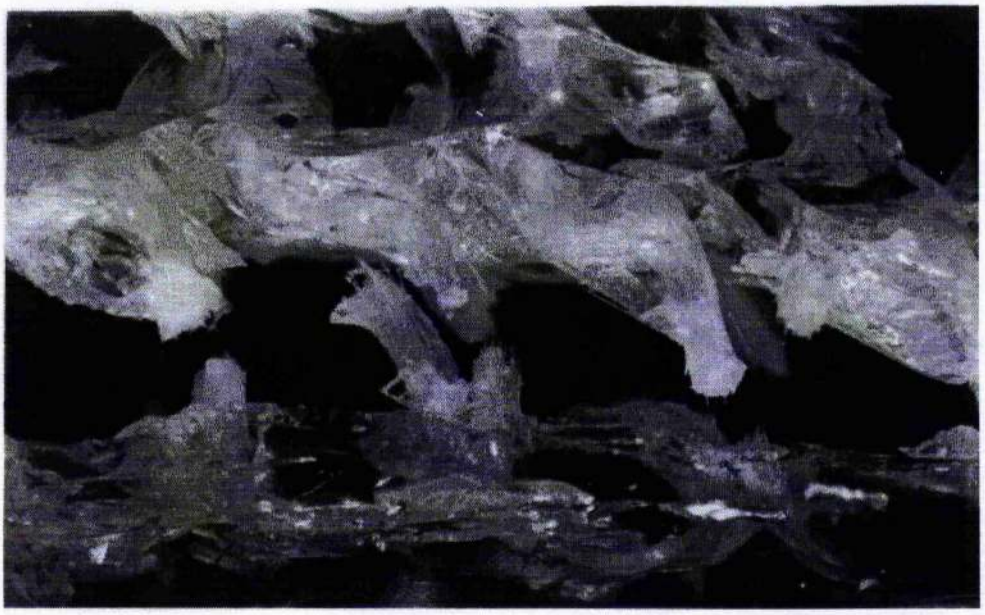

(a)

(b)

Figure 4.84.- Fracture area in (a) wale direction and (b) course direction

CHAPTER 5

EXPERIMENTAL RESULTS AND DISCUSSION ON THE COMMERCIAL MATERIAL (RTM)

5.1. INTRODUCTION.

This Chapter describes results on commercial knitted fabric composites. Two commercial composites manufactured with Milano 2x68 tex knitted fabric and Derakane vinyl ester resin as matrix were analysed. One panel consisted of 5 layers of fabric and the second panel, consisted of 4 layers of fabric. These materials were made by the Cooperative Research Centre for Advanced Composites Structures Limited in Australia using resin transfer moulding (RTM) in order to obtain an engineering material with high fibre volume fraction. The quasi-static behaviour of the materials has been investigated as a function of angle, including an investigation of the damage accumulation.

For the mechanical tests, coupons were tensile tested at 6 different angles (with at least four samples at each angle) with respect to the nominal wale direction of the knitted fabric. The angles used were -45°, 0°, 30°, +45°, 60 ° and 90° (it should be noted that the wale direction could only be defined to an accuracy of about ± 7°). The acoustic emission (AE) technique was used to monitor damage.

5.2. STRESS-STRAIN RESULTS FOR KNITTED FABRIC COMPOSITES RTM MANUFACTURED

The panels supplied consisted of 5 layers or 4 layers of 2x68 tex knitted fabric embedded in a matrix of Derakane epoxy vinyl ester 411-350. The fabric had areal densities of 742 g/m^2 and 940 g/m^2 respectively, and the panels were made by CRC-ACS using the resin transfer moulding (RTM) technique. Sections of the 5-layer panel were cut parallel and perpendicular to the wale direction, and microphotographs are shown in Figure 5.1(a) and Figure 5.1(b). These figures illustrate the complexity of the material. With careful observation, it was possible to identify the original five layers of cloth and these layers are labelled on the Figures. The fibre volume fraction determination is detailed in section 3.3. This first panel had a fibre volume fraction of 46±0.3% and the second had a fibre volume fraction of 48±0.5%.

5.2.1. KNITTED FABRIC WALE DIRECTION AT 0° TO THE LOADING DIRECTION

Typical stress-strain curves for samples with the wale direction of the fabric aligned parallel to the loading, 0^0-direction are shown in Figures 5.2 and 5.3 for 5 layers and 4 layers composite respectively. In general, the stress-strain curves appear non-linear from even very small strains. Overall the curves show a remarkable similarity to the stress-strain curves of ductile metals. Indeed, they even show a zero "work-hardening rate" region above a strain of about 1.7%, with failure at about 2%. In these opaque RTM materials, it was impossible to determine the onset of cracking visually and the acoustic emission (AE) technique was used to monitor damage. Acoustic emission (AE) activity is shown together with the stress-strain curves. AE activity begins at quite low strains (approximately 0.2% to 0.4%). From strains of about 0.2% to 1%, the AE event count rises slowly, but a dramatic increase is observed from about 1.0% strain. All coupons had strain gauges parallel and perpendicular to the loading direction so that the transverse strains were also measured. Figures 5.4 and 5.5 show the variation of the Poisson's ratio with strain ie the negative value of the ratio of the transverse strain to the longitudinal strain plotted as a function of the longitudinal strain.

Previously in Chapter 4, it was shown that an excellent indication of the onset of matrix cracking damage is given by the variation in the Poisson's ratio. Figures 5.4 and 5.5 show that the Poisson's ratio (-t/l) increases gradually (but not necessarily uniformly) to a strain of about 0.4%. Beyond this strain, the ratio decreases and hence it seems likely that matrix cracking began at approximately this strain. However it was not possible to verify this visually due to the opacity of the material. Also, because of the high complexity shown by the knitted fabric structure, it was impossible to detect matrix cracks in sections taken from the material until high strains, and high crack densities were reached (See Chapter 6)

Although matrix cracking was difficult to observe, there were indications of such damage on the surface of the sample in the form of lightly-coloured lines crossing the width of the coupon (see Figure 5.6 for example). These lines had the same spacing as expected from the study of the model sandwich laminates in the previous chapter. Hence, these lines had a spacing of 4 mm which corresponds to the spacing of the planes where the float stitches of courses 2 and 3 coincide. There was also some evidence of lines indicating matrix cracking on planes, which correspond to the needle points of course 1. These planes are approximately half way between the original planes. Detailed microstructural observations of failed coupons (in Chapter 6) show that cracks with these spacings can be found in sections taken near the surface of the specimens.

Figure 5.6 shows a failed coupon at 0° (wale direction) in which the fracture surface is perpendicular to the load direction. Damage in the outer plies can be seen in the photograph in the form of transversal white lines having a 4 mm spacing pattern, with fainter lines between them. It is important to notice that at failure, there was not a complete separation of the coupon. Fibres bridge the two fractured surfaces as loops are pulled out across the fracture plane. Higher magnification picture of the fractured region shows that some of the bundles of fibres have been fractured and been pulled out. The fibre bundles do not have resin adhering to them, suggesting that adhesion is poor between the glass fibres and the Derakane matrix (Figure 5.7).

5.2.2. KNITTED FABRIC WALE DIRECTION AT 30° TO THE LOADING DIRECTION

Figures 5.8 and 5.9 show typical stress-strain curves and AE activity for specimens loaded at 30° to the wale direction. As for the 0° results, it is difficult to detect a linear portion to the curves which appear non-linear from the origin. The stress-strain curves for the 5-layer and 4-layer material do appear slightly different in that the 4-layer material seems to show a sharp change in slope at a strain of about 0.6%. The 5-layer material, on the other hand, does not show such a sharp change in slope, although a smaller change is apparent at about 0.4%. Also, the AE emissions for the 5-layer material were recorded from about 0.3% to 0.4% strain whereas in the 4-layer material, the AE events were not recorded until about 0.5% strain. Again the stress-strain curve show a pronounced plateau, particularly for the 4-layer material, with failure at about 1.6%

Once more, it was difficult to observe cracks directly. If the change in the Poisson's ratio is taken as an indication of the onset of cracking, then in the 5-layer material (Figure 5.10), this began at very low strains. However, in the 4-layer material, the sharp change in the slope of the stress-strain curve at about 0.6% is accompanied by a sharp change in the Poisson's ratio (t/l) (Figure 5.11). These observations suggest that the onset of matrix cracking began at different strains in the 4-layer and the 5-layer material. Presumably this is related to the difference in areal density. In fractured specimens, indications of matrix cracks were observed running in the course direction of the knitted fabric (Figure 5.12). This direction is perpendicular to the 30° direction. In addition, the samples eventually failed parallel to this direction.

Figure 5.12 shows examples of a fracture surface and indications of matrix cracking seen in the surface of the specimens having a 4 mm spacing. A magnified section of the fracture surface can be seen in Figure 5.13 where pulled-out fibre bundles can be seen.

5.2.3. KNITTED FABRIC WALE DIRECTION AT 45° TO THE LOADING DIRECTION

The stress-strain curves for this angle showed similar behaviour to the behaviour of the 30^0 specimens (Figures 5.14 and 5.15). In this case, the Poisson's ratio data (Figure 5.16) seem to suggest the onset of matrix cracking damage at about 0.5% strain for the 5-layer material (Figure 5.16) and indeed, a small change in the slope of the stress-strain curve can be seen at this strain as well (Figure 5.14). As in the case of the 30^0 material, a substantial change in slope for the 4-layer stress-strain curves at about 0.6% (Figure 5.15) corresponds to a sharp change in the Poisson's ratio (Figure 5.17) In summary, the results suggest that predamage at this orientation began at strains of 0.4% and 0.5%, respectively for the 5-layer and 4-layer material, with matrix cracking beginning at 0.5% and 0.6%, respectively.

At this angle, two failure modes were identified. Figure 5.18a shows the fracture of a coupon at +45° in which the fracture plane follows the course direction. In the second mode, the fracture plane is closer to the wale direction of the specimen in which the crack develops running parallel to the legs of the loops. 60% of all the samples tested (both 4-layer and 5-layer) showed the first mode and 40% the second mode. The fracture surface for the first mode (ie parallel to the wale direction) can be seen in Figure 5.19.

5.2.4. KNITTED FABRIC WALE DIRECTION AT -45° TO THE LOADING DIRECTION

The behaviour of the coupons at -45^0 was similar to the behaviour at $+45^0$. Figures 5.20 and 5.21 show typical stress-strain curves at this angle. For this angle, the change in slope of Poisson's ratio occurs in both materials at about 0.6% strain (Figures 5.22 and 5.23). This also corresponds to a sharp change in slope of the 4-layer stress-strain curve. Again precracking damage was detected earlier in the 4-layer specimens, though this was not so apparent in the 5-layer material.

Final failure at –45° developed similarly to that observed at +45 ° due to the symmetry of the Milano knitted fabric whose face and back sides are similar. As occurred in the +45° orientation, the cracks are free to propagate either perpendicular to the wale direction or following the wale direction (Figure 5.24). Figure 5.24a shows the mode in which the fracture appeared trying to follow the wale direction. The damage in the outer fabric layer can be seen in the form of faint white lines having a 4 mm spacing. In Figure 5.24b the fracture is running roughly parallel to the course direction.

The fracture surface can be seen at higher magnification in Figure 5.25, which again shows fibre bundles pulled out of the fracture surface.

5.2.5. KNITTED FABRIC WALE DIRECTION AT 60° TO THE LOADING DIRECTION

Figures 5.26 and 5.27 show the stress vs. strain plot in which, again the non-linear behaviour dominates the curve. The acoustic emission signal registers damage from about 0.3% strain. The Poisson's ratio plots of Figures 5.28 and 5.29 suggest that matrix cracking damage begins at about 0.6% strain.

Cracking damage is clearly observed in the fractured specimen of Figure 5.30. The damage is in the form of faint white lines which can be seen in the surface of the sample. These lines follow the wale direction of the fabric and have a final spacing of about 2 mm. Figure 5.30 also shows that the composite samples failed by cracks running along this direction. Figure 5.31 shows the fractured area in more detail. The crack path follows the legs of the loops in the wale direction of the fabric. In figure 5.31, the legs of the loops can be clearly seen in the fracture surface.

5.2.6. KNITTED FABRIC WALE DIRECTION AT 90° TO THE LOADING DIRECTION

There is no general change in the stress-strain behaviour for the 90° specimens and the same non-linear behaviour is observed as before (Figures 5.32 and 5.33). At about 1.0% strain the stress seems to be stabilised and the increment is slowed down up to failure. Acoustic emission signals began at very low strains in this case, at about 0.2% strain. However, the evidence of the Poisson's ratio curves (Figures 5.34 and 5.35) suggests that matrix cracking damage did not begin until about 0.7% to 0.8% strain.

Figure 5.36 shows a fractured sample. The plane of the fracture was perpendicular to the load direction. The crack is bridged by unfractured fibre bundles and Figure 5.37 shows a magnified picture of the fractured surface where fibre bridging can be seen. Obviously, the failure runs parallel to the wale direction of the fabric. Figure 5.37 also shows that the fracture runs along the legs of the loops.

5.3. COMPARISON OF RESULTS FOR DIFFERENT ANGLES IN THE RTM MATERIAL

Despite the differences between the two RTM panels tested (i.e. areal density, number of layers), the cracking damage development and stress-strain curve behaviour were similar in both the 5 layer and the 4 layer composites. This similarity is presumably due to the importance of the fibre volume fraction which is almost the same in both cases (about 47%). Tables 5.1 and 5.2 show the mechanical parameters for all the angular orientations tested and Figures 5.38 to 5.41 show the variation of the mechanical properties with angle for both the 5 layer and 4 layer RTM composites. As found in the single layer material (see Chapter 4), the highest Young's modulus was found for the 0° and 30° directions although the highest strength is in the 0° direction in both cases.

The two-dimensional analysis on the loops carried out on single layer material suggested that the fibre distribution was roughly symmetrical about the 0^0 (wale) direction (see Figure 4.5). The fact that the mechanical tests results for both the single layer and RTM material show that the Young's modulus in the 0^0 and 30^0 directions are similar, suggests that a three-dimensional analysis of the fibre architecture is required (Gommers et al, 1998). This is likely to show that there is a significantly higher proportion of fibre oriented in the 30^0 direction than was detected in the two-dimensional analysis.

Tables 5.1 and 5.2 also show that the RTM material is more isotropic than the single layer laminates. The ratio of the Young's moduli in the 0^0 and 90^0 directions for the RTM material is about 1.2 (ie the Young's modulus in the 0^0 direction is about 20% higher). For the single layer material (Table 4.1), the ratio is 1.7. Similarly, the ratio of the strengths in the 0^0 and 90^0 directions for the RTM material is 1.3; for the single-layer material it is 1.9. Hence, the RTM material is much more isotropic and this is presumably because of the crushing together and rumpling of the layers of cloth to achieve the high fibre volume fraction in the RTM process. As Figure 5.1 shows, there is much distortion, and probably crushing, of the cloth layers leading to a more isotropic fibre orientation distribution.

Another similarity between the single layer material and the RTM material is the fracture path at failure. For both the single layer and RTM material, the fracture path in specimens with the wale direction oriented at 0^0 and 30^0 to the loading direction was along the course direction of the cloth. Observations of the fracture surface in the single-layer material showed this to be the plane of the head, or needle, of the loops. On the other hand, for both the single layer and RTM material, the 60^0 and 90^0 specimens fractured along a plane parallel to the wale direction of the cloth, along a path which linked the legs of the loops. The 45^0 angle specimens marked a transition in both cases between fracture along the course and wale directions.

The values of the mechanical properties found here for the RTM specimens are very similar to values found by Anwar et al, (1997). They also tested 2x68 tex, weft-knitted Milano fabrics with a Derakane vinyl ester resin matrix, but with six layers of fabric and a slightly higher fibre volume fraction. Anwar et al (1997) tested only the 0^0 and 90^0 directions, but a comparison with the results found here for those directions is shown in Table 5.3. The results for tensile strength, Young's modulus and strain to failure are all reasonably similar. The higher values found by Anwar et al (1997) in each case are probably due to the higher fibre volume fraction, in the case of the Young's moduli, and possibly to the increased number of layers, in the case of the strength and strain to failure.

Turning now to the damage accumulation, in the case of the RTM material, which fractured at high applied strains, it was possible to see evidence of matrix cracking in the form of fine white lines in the outer layer of the opaque specimens. This cracking damage appeared to extend across the width of the coupon, usually parallel to the course or wale direction which would be plane of final failure (except in the case of the 45^0 material). No such damage was evident in the single layer material since it failed as soon as any damage initiated. In the case of the model sandwich laminates, crack initiation at loop cross-over points was followed by the development of a cracking pattern which was dominated (for the 30^0, 45^0 and 60^0 angles) by the stiff outer 0^0 plies so that the matrix cracks grew mostly perpendicular to the loading direction for all angles of the fabric. However, the accentuated cracking in the model sandwich laminates followed the same behaviour as the RTM material. In the 0^0 and 30^0 model sandwich laminates, the accentuated cracking occurred around the head, or needle, of the loops in the course direction. In the 60^0 and 90^0 specimens, the accentuated cracking occurred along the legs of the loops in the wale direction. A difference was seen in the 45^0 specimens where the model sandwich laminates showed accentuated cracking around the heads of the loops, whereas in the RTM material, the faint white lines are indicative that matrix cracking could form in either the wale or course direction, with fracture also on either plane.

Finally, it should be mentioned that samples of the fractured RTM specimens were taken well away from the fracture surfaces and the matrix burnt away. Examination of the remaining fabric layers found that there were no indications of tow fracture or fibre fracture. The same result was found in the model sandwich laminate i.e. that the knitted fabric away from the fracture surfaces had not been damaged. This suggests that the tows in the knitted fabric were pulled out, unbroken, across any matrix cracking damage which occurred in the RTM composites. This suggestion is in line with the idea that yarns in the fabric are pulled out across matrix cracks, which are then bridged by fibre bundles (Huysmans et al, 2001). As in the case of the model sandwich laminates, it was decided to subject the RTM coupons to cyclic loading experiments to investigate whether the role of the fibre tows could be further understood.

5.4. CYCLIC TESTS OF RTM MATERIALS TO DIFFERENT STRAINS.

Samples cut at different angles from the 4 layer commercial composite (RTM) were tested in tensile loading by taking them to a certain strain and, after reaching this point, they were unloaded to zero load and reloaded again to a higher strain, and so on until fracture. The samples were tested at the same cross-head speed as in the earlier work (0.5 mm/s) and stress, strain and AE data were recorded (as before) by a datalogger..

5.4.1. KNITTED FABRIC WALE DIRECTION PARALLEL TO THE LOADING DIRECTION (0^o)

Samples at this angle were taken to 0.1% strain, unloaded, reloaded to 0.6%, unloaded, reloaded to 1.0%, unloaded, reloaded to 1.5% strain, unloaded and then reloaded to failure. Figure 5.42 shows the stress-strain behaviour for these cyclic tests, and Figure 5.43 shows the stress-cumulative strain results.

There are a number of features to be noted which were common to all the specimens cyclically loaded in this way. Firstly, there is elastic behaviour when the material is loaded to 0.1% and then unloaded. It is difficult to see this in Figure 5.42 since the two lines superimpose. Although there is elasticity, the curves do not appear to be entirely linear even at this low strain. Secondly, loading to 0.6% strain and unloading produces not only a small hysteresis loop, but also a residual strain (of about 0.03%). It should be noted, for comparison, that a strain of 0.6% is above the strain at which the change in the Poisson's ratio during the monotonic tests suggested is the strain for the onset of matrix cracking. Thirdly, when reloading the sample to 1% strain, the hysteresis loop is 'closed', in the sense that the stress passes through the previous peak stress value at a strain of 0.6% while the specimen is being loaded to a higher strain. Unloading from a strain of 1% produces a much larger residual strain (about 0.15%). Fourthly, when reloading the sample, now to a strain of 1.5%, the hysteresis loop is this time not 'closed'. During this reloading, the stress at 1% strain is lower (by about 3 MPa) than the value on the previous cycle. Fifthly, when unloading and reloading to failure, the hysteresis loop is again not closed, and the stress reduction at 1.5% strain is now larger (about 4.5 MPa). Finally, for each successive reloading to higher strains (above the initial strain of 0.1%) the hysteresis loops have a lower overall slope.

Figure 5.43 displays the stress-cumulative strain results curve of the same sample, together with the AE data. Similar constructions can be used (i.e. points A_1 and A_2) for this data as for the cyclic data in Chapter 4. Points A_1 and A_2 in figure 5.43 represent the peak stress reached when loading to a strain of 1.5% (point A_1), and the same stress reached after unloading and reloading (point A_2). Considering point A_1 first, it is clear that significant AE activity is recorded during unloading from the peak strain of 1.5% for a period equivalent to a strain of about 0.2%. However, on reloading to failure, there is significant AE activity for a period equivalent to a strain of about 0.4% before the same stress is reached (point A_2). This is perhaps not very surprising since the hysteresis loop is not 'closed' but undershoots the previous stress attained at the strain of 1.5% in the previous cycle.

5.4.2. KNITTED FABRIC WALE DIRECTION AT 30^0 TO THE LOADING DIRECTION

Samples at 30° were cycled to strains of 0.1%, 0.6%, 1.0% strain, and then up to fracture (Figure 5.44). The stress-cumulative strain behaviour is shown in Figure 5.45. The first load and unload to a strain of 0.1% again showed elastic behaviour, although again, it may not be linear elastic. Reloading, the curve followed the same path to a strain of 0.6%, and here unloading and reloading produced a small residual strain and a small hysteresis with the loop not quite 'closed.' The change in the Poisson's ratio during monotonic tests on this material suggested that matrix cracking would begin at about 0.6%.

5.4.3. KNITTED FABRIC WALE DIRECTION AT 45^0 TO THE LOADING DIRECTION

These samples were cycled to taken to three strains 0.6%, 1.0%, 1.5% strain and then to failure (Figures 5.46 and 5.47). The results here are very similar to the results for the 30^0 specimens. When cycled to a strain of about 0.6%, the hysteresis loop is not quite 'closed,' and when cycled to a strain of 1%, it is clearly not closed. All the previous general observations about residual strain, reduction in slope of the loops etc, apply here as well. Indeed, constructing points A_1 and A_2 shows again that significant AE activity occurs both on unloading and on reloading before the previous peak stress has been reached.

5.4.4. KNITTED FABRIC WALE DIRECTION AT -45^0 TO THE LOADING DIRECTION

In this angular orientation three peak strains were used, 0.6%, 1.0% and 1.5%. Typical results are shown in Figures 5.48 and 5.49. The results for the -45^0 angle are almost exactly the same as the results for 45^0. Again, the hysteresis loop for a peak strain of 0.6% is not quite closed. As in the case of the 45^0 specimens, the monotonic tests showed that the change in slope of the Poisson's ratio, and hence an indication of matrix cracking, occurred at about 0.6%.

5.4.5. KNITTED FABRIC WALE DIRECTION AT 60° TO THE LOADING DIRECTION

Typical stress-strain cyclic data for a sample at 60° are shown in Figure 5.50, with the cumulative strain data in Figure 5.51. In this case, peak strains of 0.5% and 0.9% were used since the strain to failure at this angle is lower than for the previous angles.

The general behaviour was as before. Figure 5.50 shows that when strained to 0.5% strain and unloaded, a small hysteresis occurred. On reloading to a strain of 0.9%, the hysteresis loop closed. On the other hand, when unloading from a strain of 0.9% and then reloading, the hysteresis loop did not close. In the monotonic tests, it was shown that the change in Poisson's ratio occurred at about 0.6% strain.

5.4.6. KNITTED FABRIC WALE DIRECTION AT 90° TO THE LOADING DIRECTION (LOADING IN THE COURSE DIRECTION)

The cyclic stress-strain curves and cumulative strain data for this angle are shown in Figures 5.52 and 5.53. These specimens were taken to peak strains of 0.1%, 0.3%, 0.6% and 0.8%. Loading/unloading to 0.1% was purely elastic (though not necessarily linear elastic) whereas loading to a peak strain of 0.3% and unloading showed a very small hysteresis. This hysteresis increased for peak strains of 0.6% and 0.8%. All of the hysteresis loops 'closed', except for the peak strain of 0.8% which showed evidence of not being completely closed. Interestingly, there was very little change in slope of the hysteresis loops compared to the previous angles tested. It should be noted that in the previous monotonic tests, the change in the Poisson's ratio (probably indicating the onset of matrix cracking) did not occur until a strain of about 0.8%.

5.5. COMPARISON OF RESULTS FOR CYCLIC TESTS AT DIFFERENT ANGLES IN THE RTM MATERIAL

In general, the results of the cyclic tests on the RTM material can be summarised as follows.

(i) For peak cyclic strains of 0.1%, all the materials tested showed an elastic response, though it is difficult to say whether this was linear-elastic. No residual strains occurred.

(ii) For higher strains, but below the onset of matrix cracking (as indicated by the change in Poisson's ratio), hysteresis loops form which are 'closed.' In all cases, a small residual strain occurred. The overall slope of the hysteresis loops is very similar to the original stress-strain curve.

(iii) For peak cyclic strains greater than the strain for the onset of matrix cracking (as indicated by the Poisson's ratio changes), the hysteresis loops do not 'close.' Indeed, as the peak cyclic strain increases, so the closure of the loops becomes poorer. In all cases, as the peak cyclic strain increases, so the residual strain on unloading increases. In addition, as the peak cyclic strain increases, so the overall slope of the loops decreases.

The only other work which the author has found on the cyclic behaviour of a knitted fabric composite in the literature is that by Gommers and Verpoest (1995). They tested a glass/epoxy warp knitted fabric composite which is quite different in fibre architecture to the material tested here, but useful comparisons can be made with their work. Although the fibre volume fraction is not stated in their paper, it must have been quite high since their data suggest a Young's modulus of about 15 GPa.

Firstly, when loading in the warp and weft directions, they found a very small cyclic hysteresis for a peak strain of 0.2%. Secondly, when loaded to peak strains of 0.5% and 1%, they found both an increased residual strain for the increased peak cyclic strain, and an increased hysteresis effect. Interestingly, the hysteresis loops in the paper by Gommers and Verpoest (1995) show residual strains, as here, and they are also 'closed' loops, but the loops do not show any overall reduction in slope compared to the initial stress-strain curve.

Gommers and Verpoest (1995) do not comment on the development of matrix cracking in their work, but they do show data for the change in Poisson's ratio with applied strain. These data appears to show a change in slope at a strain of about 1%. Hence, the fact that the Gommers and Verpoest (1995) loops are 'closed,' and that the cyclic loops have the same slope as the initial stress-strain curve, is consistent with a strain in their tests of 1% being equal to, or just below, the strain for the onset of matrix cracking. In other words, the results of Gommers and Verpoest (1995) are very similar to the results found here.

The following explanations are suggested for the behaviour of the RTM materials tested here. For very small peak cyclic strains (up to about 0.1%), the material is nonlinear elastic. Gommers and Verpoest (1995) suggested that the nonlinear elasticity is due to the nonlinear behaviour of epoxy in shear. It seems likely that a similar explanation is valid for the Derakane matrix used in these experiments for low peak cyclic strains. At higher strains, but below the strain for the onset of matrix cracking (as indicated by the Poisson's ratio changes), residual strains develop and the hysteresis loops are 'closed.' It is possible that within this strain range, precracking damage, in the form of cracking at the loop cross-over points occurs, but this damage does not seem to have a noticeable effect on the stress-strain behaviour except that it may contribute to the residual strain which occurs on unloading the specimens. The other contribution to the residual strain is presumably a nonlinear behaviour of the Derakane matrix. For peak cyclic strains above the onset of matrix cracking, the important changes are that the hysteresis loops no longer 'close,' and that the overall slope of the hysteresis loops decreases (an exception is the behaviour of the wale (0^0) specimens, for which the loops were closed up to a strain of 0.6% which is above the matrix cracking strain of 0.4% indicated by the Poisson's ratio changes). The reduction in the overall slope of the hysteresis loops is presumably due to the development of matrix cracking damage which reduces the modulus of the composite. To investigate further the non-closure of the hysteresis loops at high peak cyclic strains, some additional tests were carried out.

5.6. CYCLIC TESTS AT FIXED PEAK CYCLIC STRAINS.

Three angular orientations (30°, 45° and 90 °) were tested. In the case of the 30^0 sample, the sample was taken to a peak strain of 0.7% for three cycles, before being loaded to failure. The cyclic stress-strain curves and the stress-cumulative strain data are shown in Figures 5.54 and 5.55, respectively. In similar tests, a 45^0 sample was loaded to a strain of 1% for three cycles (see Figures 5.56 and 5.57) and the 90^0 specimen was loaded to a peak strain of 0.7% for four cycles (Figures 5.58 and 5.59).

For the 30^0 orientation, a peak strain of 0.7% is just above the strain at which the change in Poisson's ratio indicates that matrix cracking begins. When unloading from the strain of 0.7%, a residual strain occurs and on reloading the hysteresis loop does not quite close. In other words, the peak stress for the same peak strain has reduced. Cycling the specimen to the same peak strain suggests that the hysteresis loop is not quite stable since the peak stress falls, although the reduction is not very large.

For the 45^0 specimen, a peak strain of 1% is well above the strain at which matrix cracking occurs (the Poisson's ratio results suggested this occurred at about 0.6% strain). Here, there is a large reduction in peak stress after unloading and reloading to the same strain (ie the hysteresis loop does not 'close'), but a smaller reduction in peak stress for the third cycle. The residual strain appears to increase slightly in each cycle also.

For the 90^0 specimen cycled to a peak strain of 0.7%, this strain is again slightly below the expected matrix cracking strain (as indicated by the Poisson's ratio changes) of about 0.7% to 0.8%. In this case, there is only a very small reduction in the peak stress on reloading to 0.7% strain and the hysteresis loops are almost closed.

Comparison of the acoustic emission (AE) activity shown in the stress-cumulative strain curves for the three specimens shows the following. For the two specimens cycled above the expected onset of matrix cracking, significant AE activity was recorded each cycle, both on the approach to the peak stress reached each cycle, and as the stress was reducing from the peak value. In the case of the 90^0 specimen, very little AE activity was recorded either on the first cycle or on subsequent cycles. This is consistent with the monotonic tests (Figures 5.32 and 5.33) and the previous cyclic tests (Figure 5.52).

5.7. DISCUSSION OF THE IMPLICATIONS OF THE CYCLIC TEST DATA

In this section an attempt will be made to explain the cyclic tests data in the context of the previous results on the RTM material.

An interesting feature of the RTM material behaviour is the shape of the curves displayed in the stress-strain plots. In all cases, at high strains it is possible to identify a region of pseudo-plasticity where the slope of the stress-strain curves reduces, sometimes to zero. This behaviour, together with the cyclic stress-strain behaviour, suggests the following explanation. At low strains, this work has shown that damage initiation occurs at the cross-over sites of the knitted fabric. Gommers and Verpoest (1995) have suggested that there may be fibre/matrix debonding in such composites at low strain, but it seems more likely that there may be some yarn/matrix debonding. At a higher strain, which depends on the angle of loading, the predamage at the yarn cross-over points develops into matrix cracking. The observations in Chapter 4 suggest that this will occur first, for specimens loaded at angles between 0^0 and 45^0, on planes where the float stitches of courses 2 and 3 are held together. For higher angles, it is along the legs of the loops where the matrix cracking develops. When the matrix cracks form, it is likely that the fibre tows of the loops start to be pulled out to bridge the matrix crack fracture surfaces and also stretched. At sufficiently high strains when many matrix cracks have formed, the easy extension of the pulled out tows produces a stress-strain curve which goes flat since very little additional stress is needed to increase the strain, due to the stretchability of the knitted fabric.

Figure 5.60 and 5.61 are attempts to illustrate the loops being pulled out and stretched across the matrix cracks for the wale (0^0) and course (90^0) directions, respectively.

If the composite is loaded to failure, the tows of the loops are pulled out from the matrix and eventually they break during the total fracture. The cyclic tests provide additional confirmation of these suggestions. For low cyclic peak strains, below the onset of matrix cracking damage, the hysteresis loops are 'closed.' However, once matrix cracking occurs (as indicated by Poisson's ratio changes), the hysteresis loops do not close, in general. This appears to be an unusual result and it is believed that the non-closure of the loops is due to the effect of pulling fibre bundles out of the matrix. Hence, the same overall strain can be achieved for the composite on reloading, but at a lower applied load, because of the stretchability of the pulled-out fibre tows. The AE evidence would appear to confirm this suggestion since significant AE activity occurs both during reloading the specimens to the previous peak strain and during unloading. It is likely that this AE activity is due to the loops being stretched and pulled out of the matrix, probably with associated debonding at the tow/matrix interface and frictional rubbing. Hence, as soon as the sample is unloaded, the loops try to recover the strain and the tows re-enter the matrix sockets producing friction in the matrix wall which is detected by the acoustic emission. Similarly, during reloading, the tows are perhaps pulled out of the sockets, with possible further debonding, as well as being stretched, giving rise to AE activity before the previous maximum strain has been reached.

5.8 SUMMARY

Knitted fabric reinforced composites, consisting of five or four layers of cloth in a Derakane matrix, have been subjected to monotonic and cyclic loading experiments. Despite the differences between the two RTM panels tested (i.e. areal density, number of layers), the cracking damage development and stress-strain curve behaviour were similar in both the 5 layer and the 4 layer composites and the mechanical properties (Young's modulus and tensile strength) were also similar to previous work by others. The highest Young's modulus was found for the 0^{o} and 30^{o} directions, which is consistent with the results found for the single-layer knitted glass fabric/epoxy composites (see Chapter 4), confirming that the two-dimensional analysis on the angular distribution of the fibre reinforcement of the loops carried out on the single layer material (see Chapter 4) is insufficient to characterise the fibre distribution.

It has been found that the mechanical properties of the RTM material are much more isotropic than for the single-layer fabric, presumably because of the crushing together and rumpling of the layers of cloth to achieve the high fibre volume fraction in the RTM process. Fracture paths at failure in the single-layer and RTM material were found to be similar. The fracture path in specimens with the wale direction oriented at 0^{0} and 30^{0} to the loading direction was along the course direction of the cloth, whereas for the 60^{0} and 90^{0} specimens, the fracture path was parallel to the wale direction of the cloth. The 45^{0} angle specimens marked a transition between fracture along the course and wale directions.

Direct evidence of the onset of matrix cracking was difficult to obtain in these RTM specimens due to crushing and rumpling of the fabric layers, although cracking damage in the form of fine white lines in the outer layer of the opaque specimens could be observed. An indirect method of monitoring matrix cracking was used ie the change in the Poisson's ratio with applied strain. However, it should be noted that this technique requires further work to establish unambiguously that it is indeed matrix cracking in the RTM specimens which is giving rise to these changes.

Burning away the matrix of fractured RTM specimens showed that there were no tow fractures or fibre fractures within the composite away from the region of composite failure (the same result was found in the model sandwich laminates of Chapter 4).

Cyclic tests on the RTM specimens to progressively higher strains showed that for peak cyclic strains up to 0.1%, all the materials tested showed an elastic response, though it is difficult to say whether this was linear-elastic. No residual strains occurred. For higher peak cyclic strains, but below the onset of matrix cracking (as indicated by the change in Poisson's ratio), hysteresis loops formed which were 'closed,' and a small residual strain occurred. For peak cyclic strains greater than the strain for the onset of matrix cracking (as indicated by the Poisson's ratio changes), the hysteresis loops do not 'close,' the residual strain on unloading increases, and the overall slope of the hysteresis loops decreases. The behaviour of these cyclic loops, together with the large pseudo-plasticity of the monotonic stress-strain curves, have been explained in terms of the pulling out and stretching of knitted loops across matrix cracks.

The results in this Chapter, together with the results in Chapter 4, suggest that various types of damage occur in knitted fabric composites prior to fracture, including damage at loop cross-over points, matrix cracking, and possible tow/matrix debonding. The next Chapter presents microstructural observations (on both the model laminated knitted-fabric sandwich composite material of Chapter 4 and the commercial RTM material of Chapter 5) where attempts have been made to observe the different types of damage.

TABLES

Table 5.1.-Mechanical parameters for 5 knitted layers commercial material (RTM) showing the standard error.

Angle	#	E (GPa)	ν	UTS (MPa)	εf (%)
0°	1	14.4	0.32	103.3	2.04
	2	13.4	0.31	97.7	2.0
	3	14.3	0.32	101.6	1.04
	4	13.1	0.32	98.9	1.87
Average		***13.8±0.3***	***0.32±0.005***	***100.4±1.3***	***1.7±0.2***
30°	1	14.1	0.30	75.8	1.54
	2	14.2	0.29	76.9	1.04
	3	13.6	0.30	77.7	1.04
	4	14.4	0.30	77.3	1.56
Average		***14.1±0.2***	***0.30±0.003***	***76.9±0.4***	***1.3±0.2***
-45°	1	12.3	0.29	81.9	1.20
	2	12.8	0.29	70.8	1.48
	3	12.7	0.30	82.7	2.03
	4	12.5	0.29	81.8	1.19
Average	***x***	***12.6±0.1***	***0.29±0.003***	***82.1±0.6***	***1.5±0.2***
+45°	1	13.5	0.28	74.7	0.95
	2	13.1	0.28	76.6	1.31
	3	13.0	0.29	76.4	1.31
	4	13.5	0.29	74.5	1.29
Average		***13.2±0.1***	***0.28±0.003***	***75.6±0.6***	***1.2±0.2***
60°	1	11.8	0.29	76.9	1.23
	2	12.5	0.31	78.5	1.11
	3	12.0	0.29	76.4	0.95
	4	12.3	0.30	80.5	1.13
Average		***12.1±0.2***	***0.30±0.007***	***78.1±0.9***	***1.1±0.2***
90°	1	10.1	0.29	76.9	1.36
	2	11.5	0.30	76.3	1.42
	3	11.2	0.28	74.7	1.09
	4	11.9	0.32	74.3	1.24
Average		***11.2±0.4***	***0.30±0.012***	***75.6±0.6***	***1.2±0.1***

Table 5.2.-Mechanical parameters for 4 knitted layers commercial material (RTM) showing the standard error.

Angle	#	E (GPa)	ν	UTS (MPa)	εf (%)
0°	1	14.1	0.35	99.1	1.71
	2	13.7	0.34	98.3	1.62
	3	14.6	0.38	94.1	1.79
	4	14.7	0.35	97.3	1.71
Average		***14.3±0.2***	***0.35±0.01***	***97.5±1.2***	***1.6±0.04***
30°	1	14.7	0.31	76.2	0.97
	2	15.8	0.30	79.3	1.62
	3	14.7	0.32	77.7	1.21
	4	15.6	0.35	77.4	1.10
Average		***15.2±0.3***	***0.33±0.02***	***77.6±0.6***	***1.2±0.1***
-45°	1	14.1	0.30	74.3	1.55
	2	13.7	0.30	74.3	1.17
	3	14.2	0.31	74.3	1.43
	4	13.6	0.31	76.6	1.39
Average		***13.9±0.2***	***0.31±0.003***	***74.8±0.9***	***1.4± 0.1***
+45°	1	14.2	0.34	76.4	1.56
	2	13.5	0.32	76.2	1.55
	3	11.5	0.31	72.2	0.90
	4	13.4	0.36	75.7	1.74
Average		***13.2±0.6***	***0.33±0.01***	***75.1±1.0***	***1.4±0.2***
60°	1	13.8	0.30	76.1	1.00
	2	14.0	0.34	75.4	0.88
	3	14.2	0.34	82.3	1.21
	4	14.1	0.33	79.1	1.14
Average		***14±0.3***	***0.33±0.01***	***78.2±1.6***	***1.1±0.1***
90°	1	11.7	0.29	67.2	0.82
	2	11.5	0.31	72.2	0.90
	3	10.8	0.30	71.2	0.93
	4	11.5	0.31	72.2	0.90
Average		***11.4±0.2***	***0.30±0.005***	***70.7±1.2***	***0.89±0.02***

Table 5.2.- Comparison of results of Anwar et al (1997) with the present work

	σ_{TS} (MPa)	E (GPa)	ε_f (%)	V_f
Anwar et al				
0^0	128	14.6	2.3	≈ 0.52
90^0	83	12.8	1.4	≈ 0.52
This work				
0^0	99	14.1	1.7	≈ 0.47
90^0	74	11.3	1	≈ 0.47

FIGURES

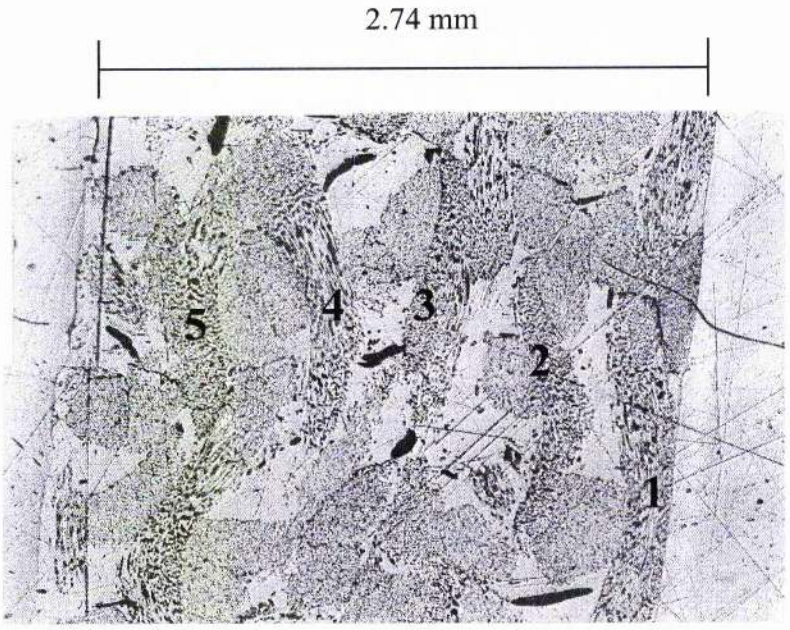

(a)

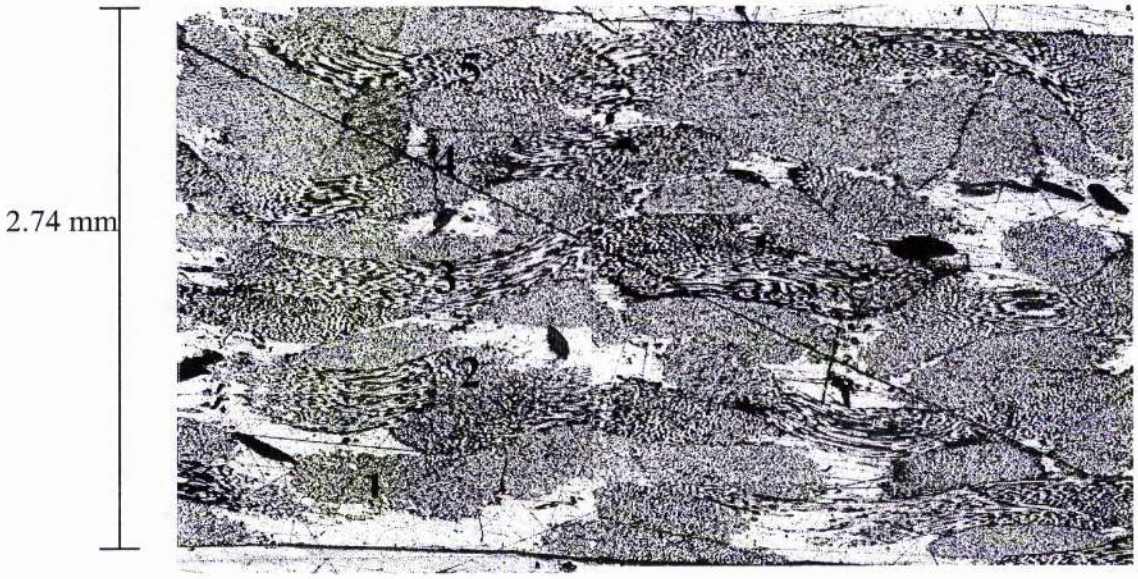

(b)

Figure 5.1.- Microphotographs of the 5 layers knitted fabric RTM composite. (a) longitudinal direction, (b) transversal direction

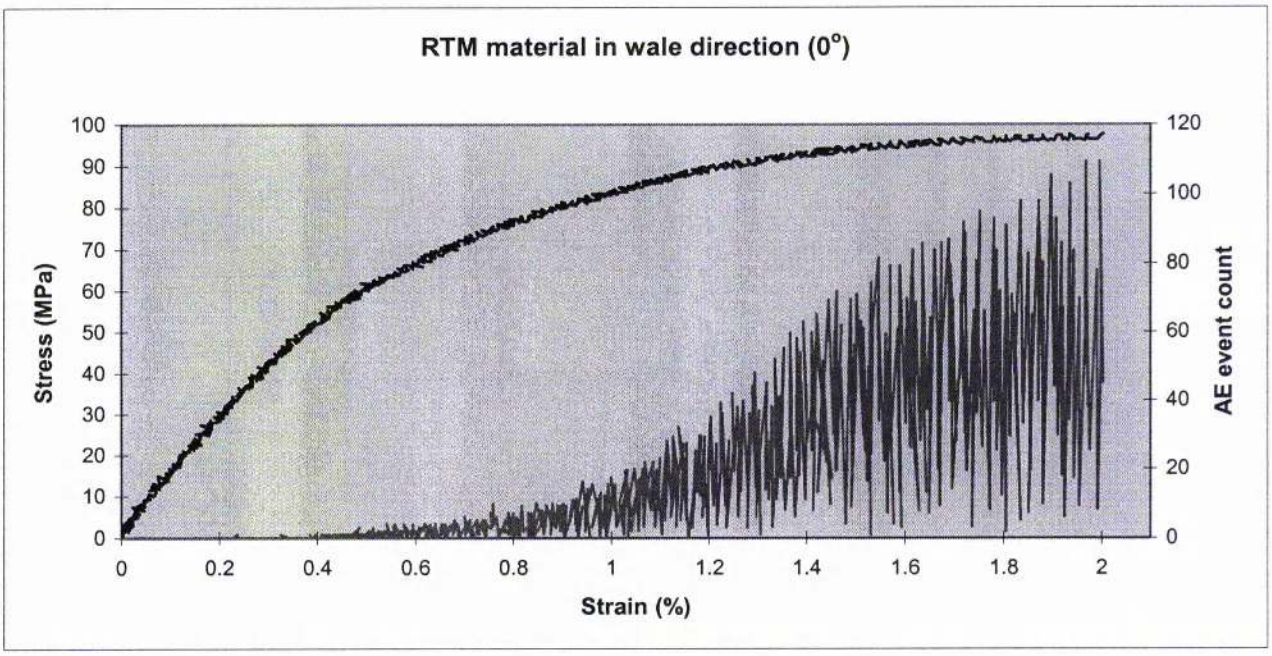

Figure 5.2.- Stress-strain curve for 5 layers RTM material tested at 0° direction (wale)

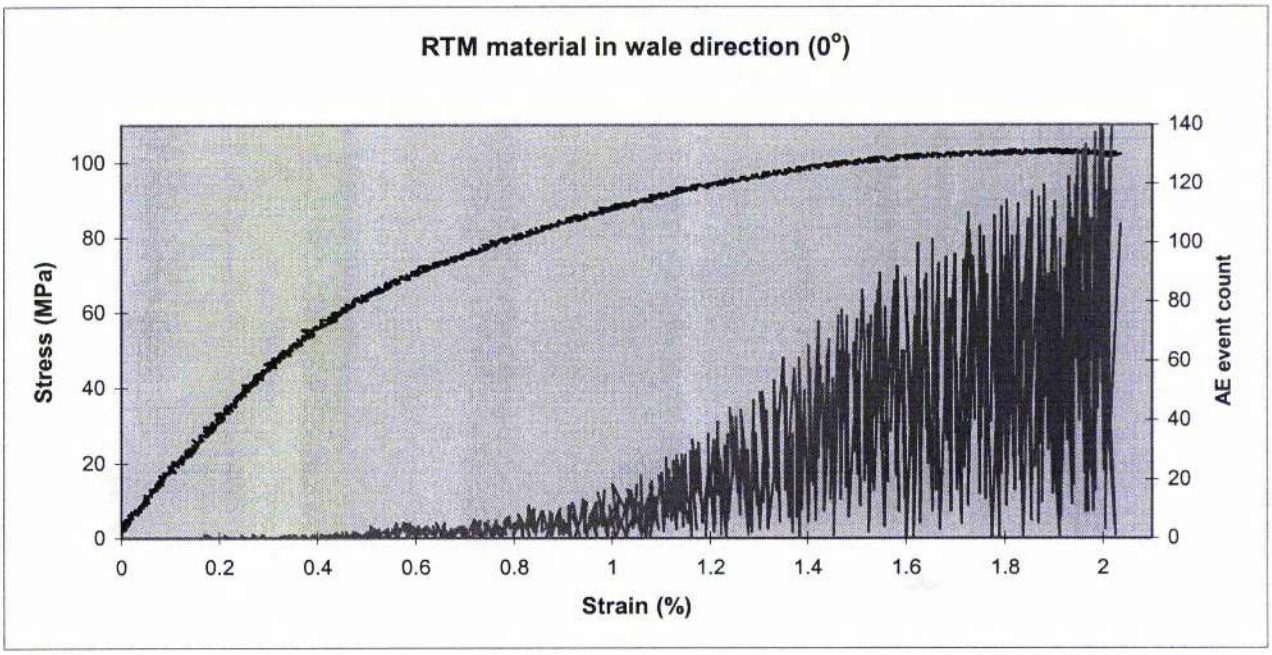

Figure 5.3.- Stress-strain curve for 4 layers RTM material tested at 0° direction (wale)

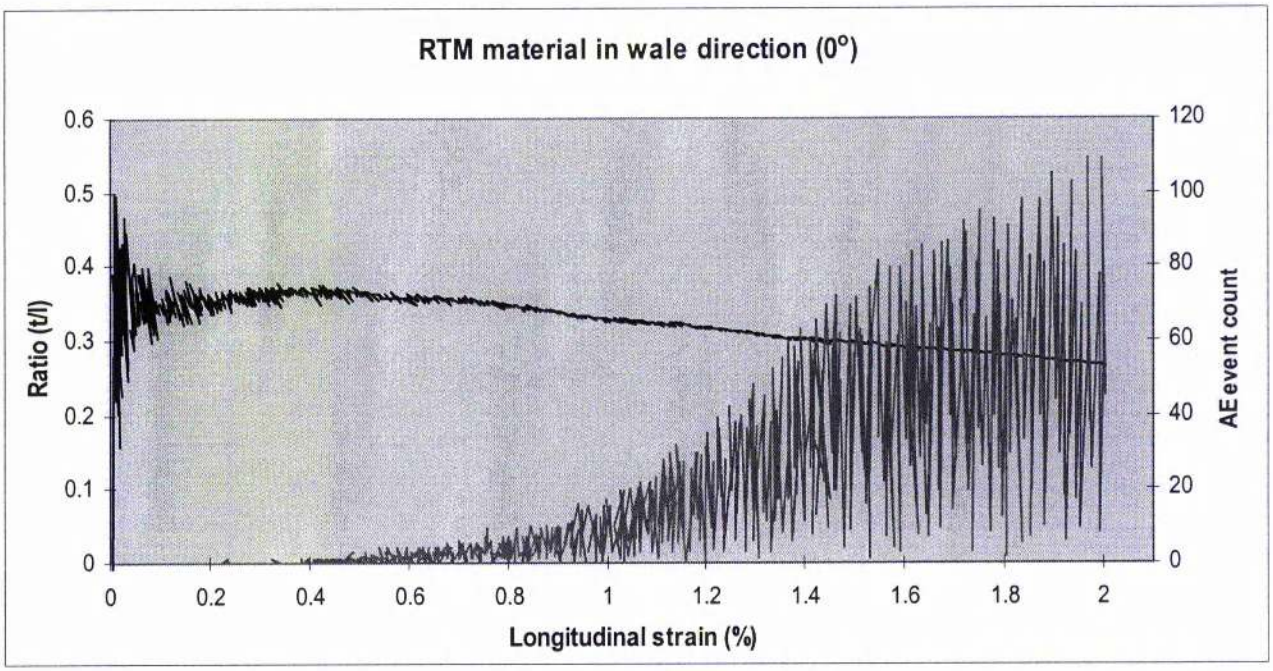

Figure 5.4.- Strains ratio (t/l) in 5 layers RTM material tested at 0° direction (wale)

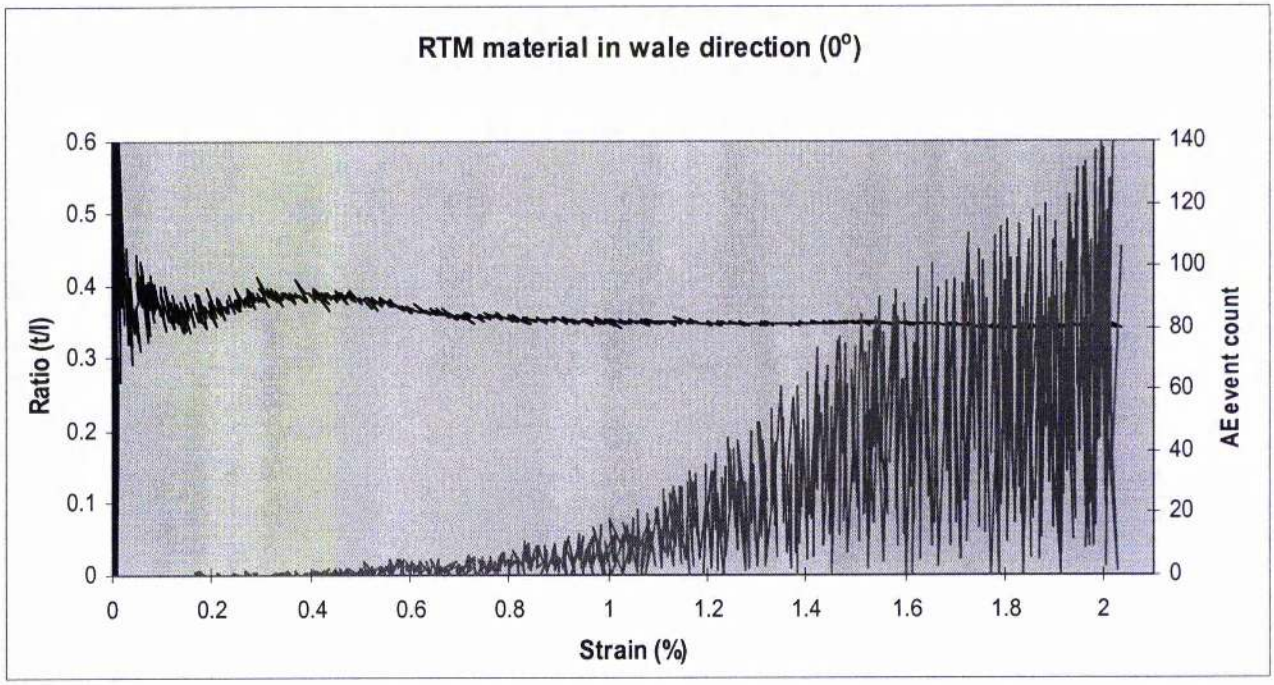

Figure 5.5.- Strains ratio (t/l) in 4 layers RTM material tested at 0° direction (wale)

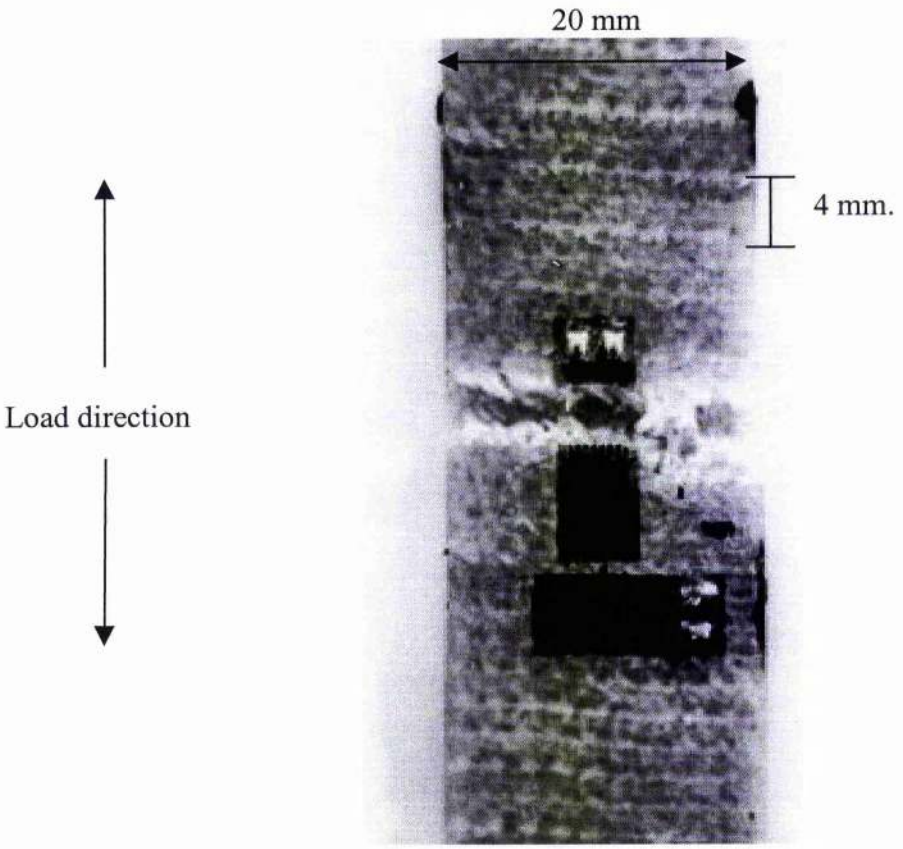

Figure 5.6.- Fractured specimen tested in the 0° (wale direction).

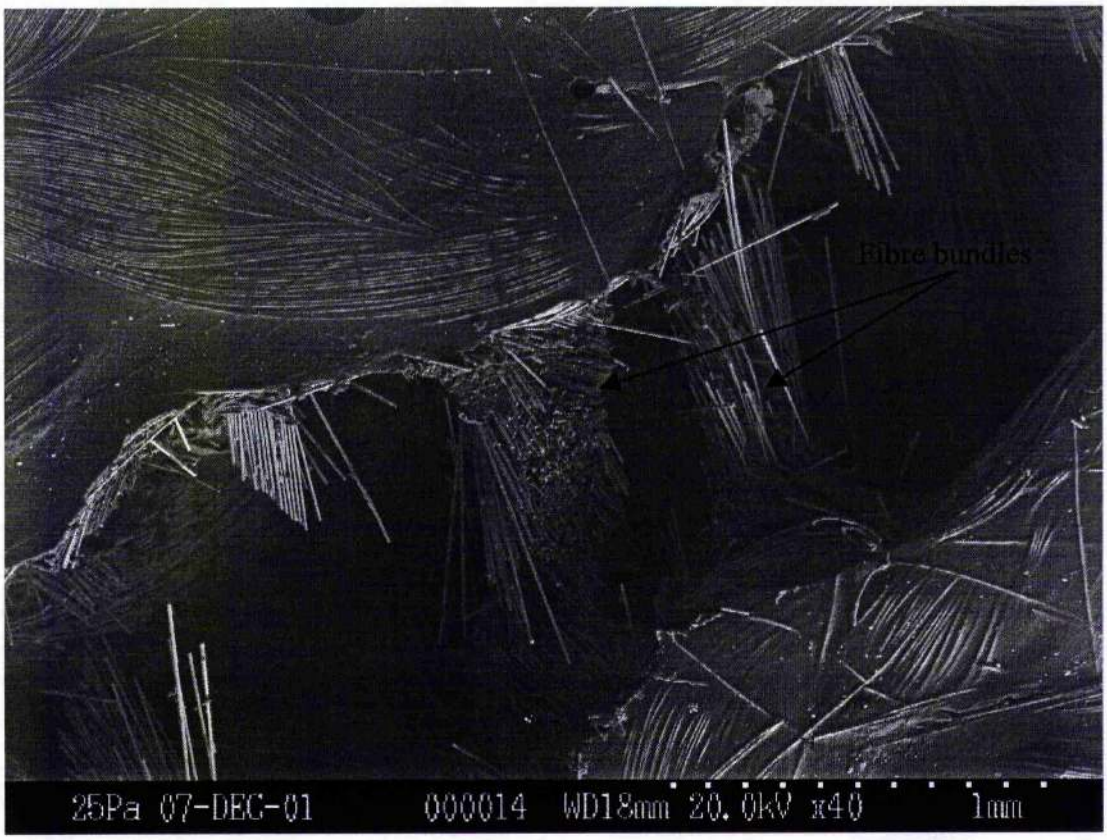

Figure 5.7.- Fractured surface of RTM sample tested in the 0° (wale) direction.

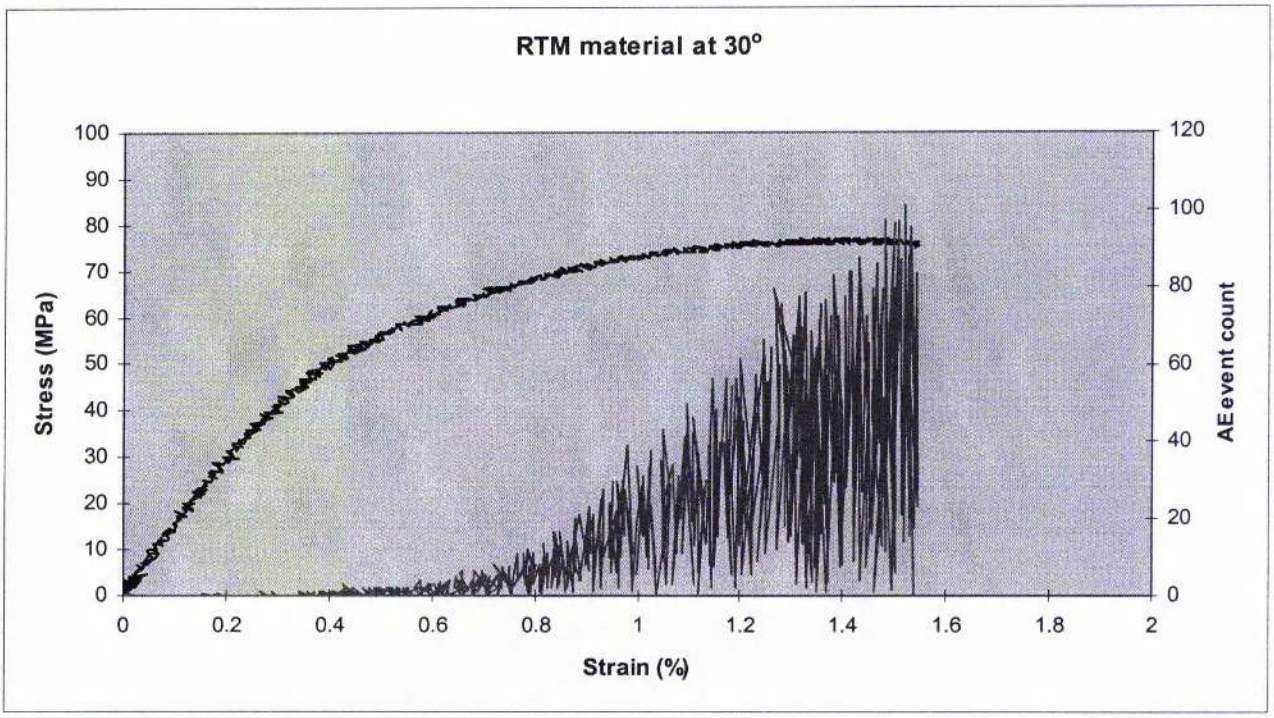

Figure 5.8.- Stress-strain curve for 5 layers RTM material tested at 30° direction.

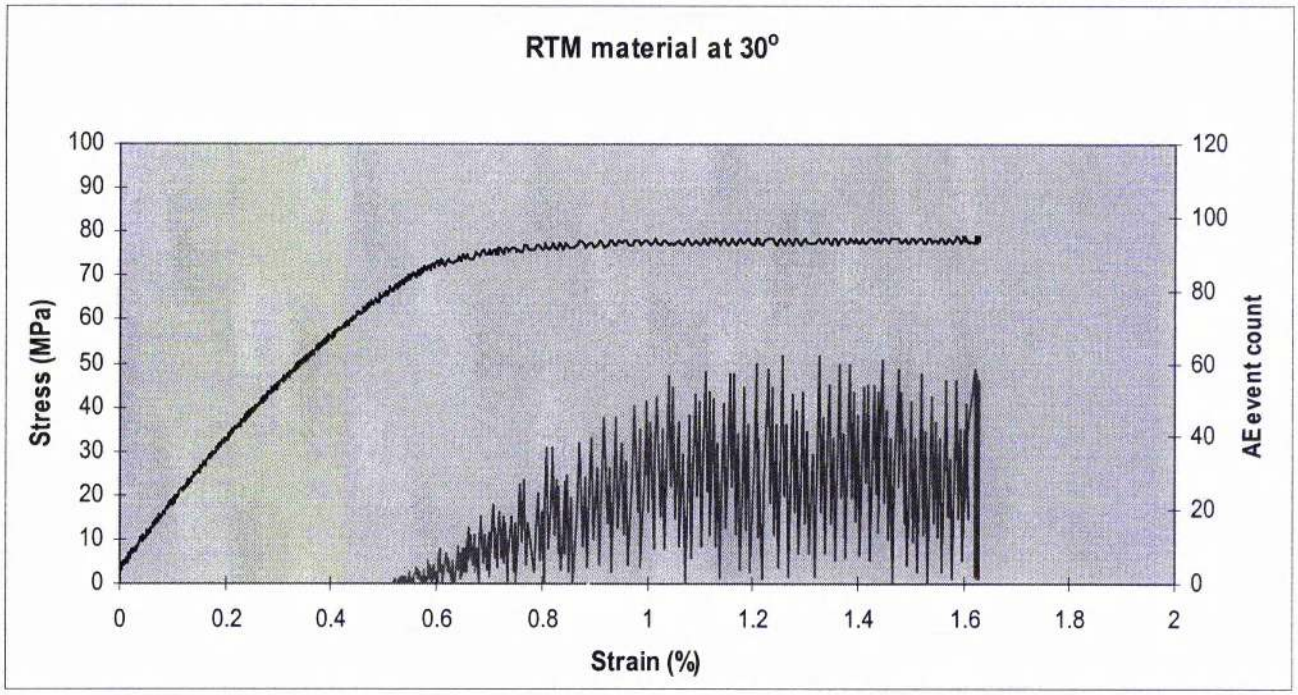

Figure 5.9.- Stress-strain curve for 4 layers RTM material tested at 30° direction.

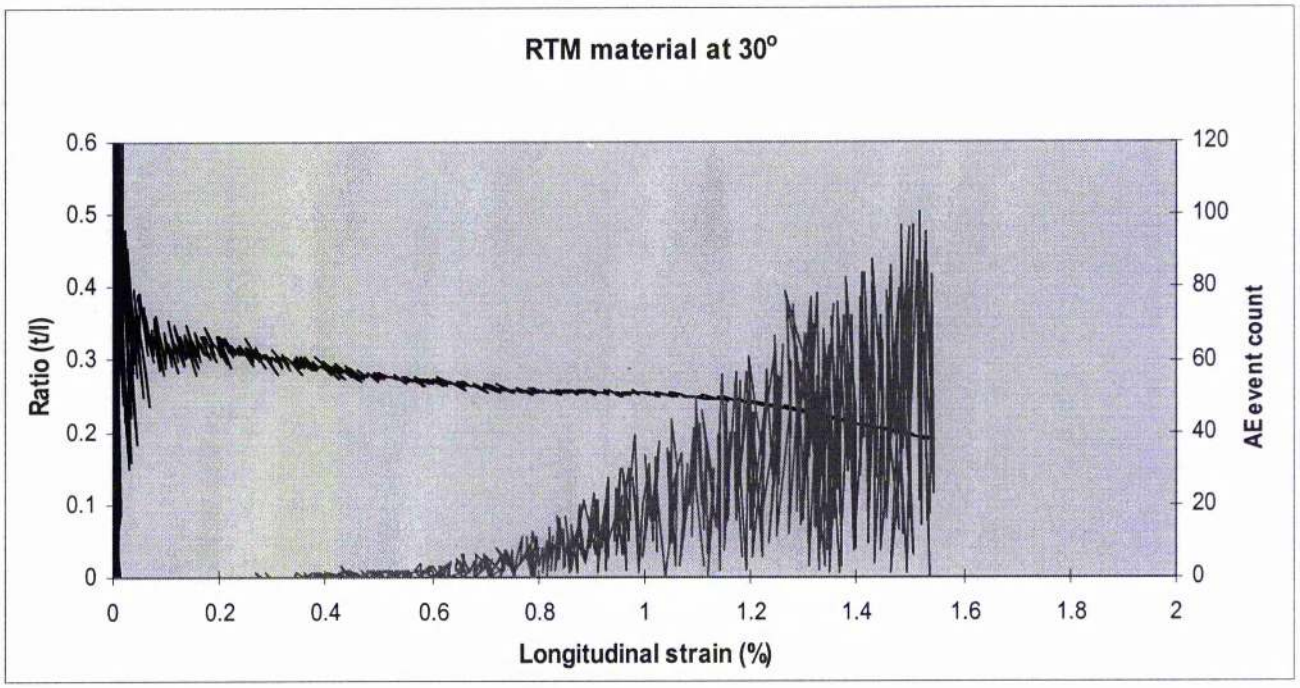

Figure 5.10.- Strains ratio (t/l) in 5 layers RTM material tested at 30° direction

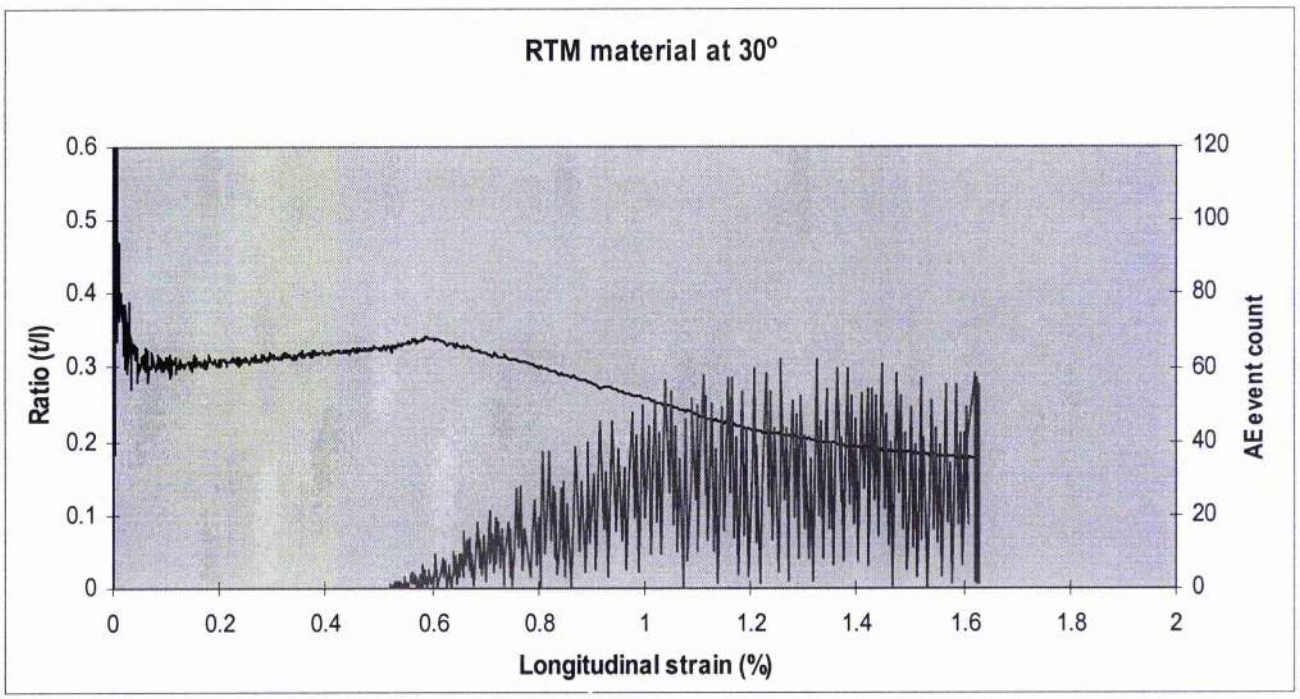

Figure 5.11.- Strains ratio (t/l) in 4 layers RTM material tested at 30° direction

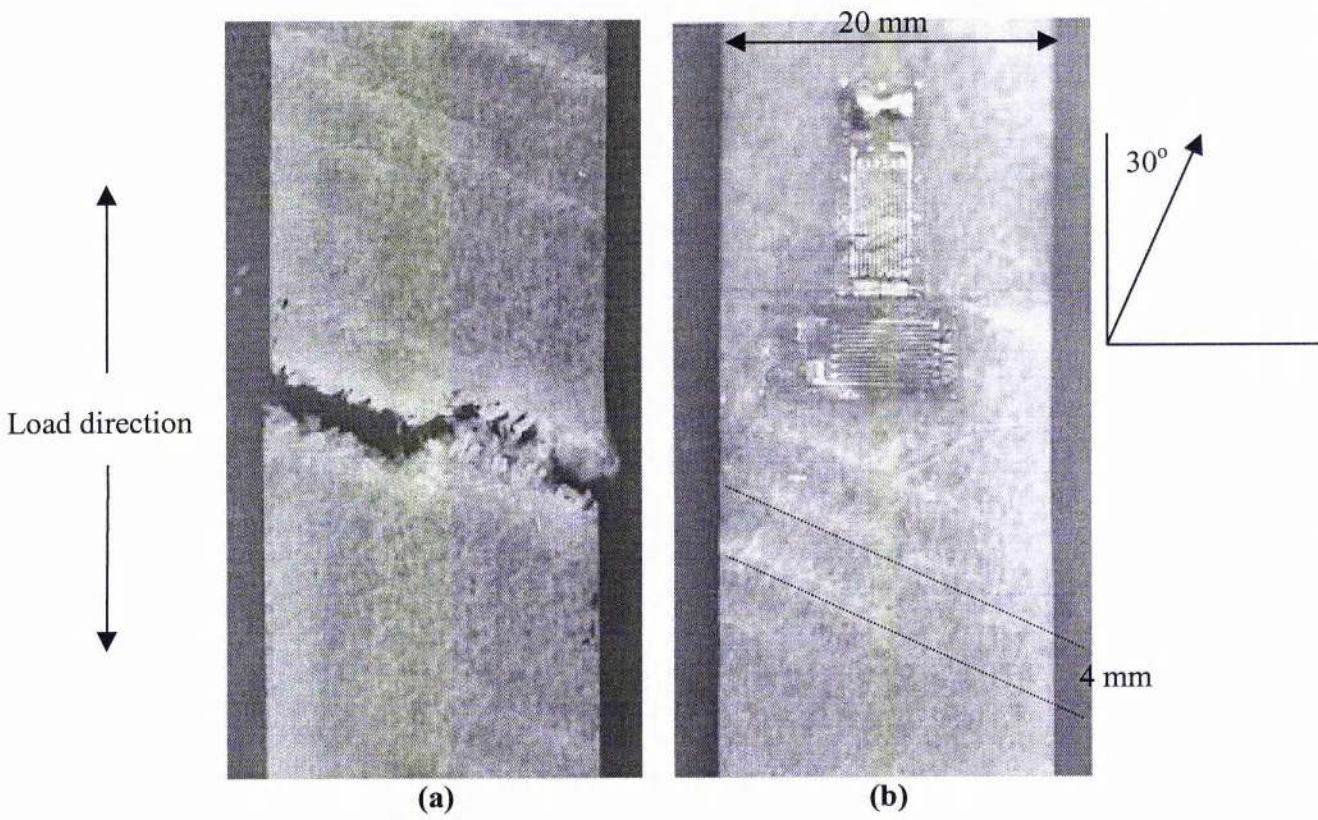

Figure 5.12.- Fracture sample tested in the 30° direction . (a) Fracture area (b) cracking pattern.

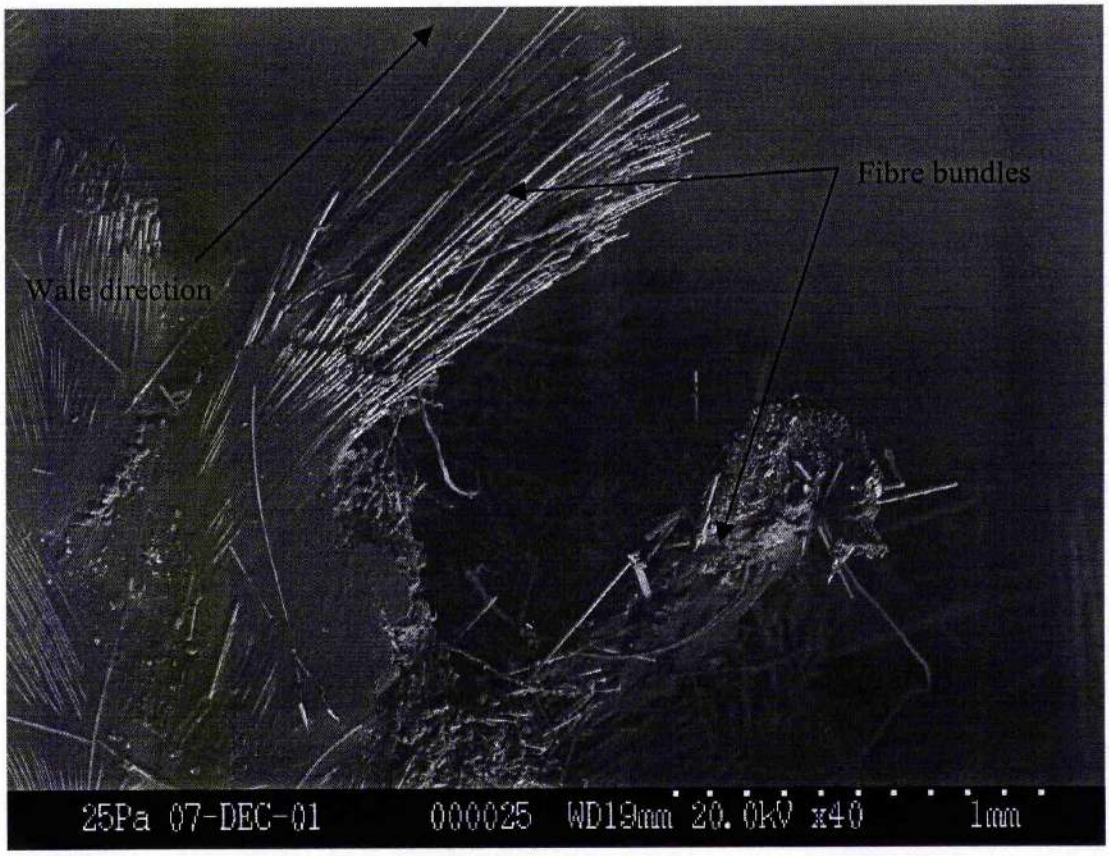

Figure 5.13.- Fractured surface of RTM sample tested in the 30° direction.

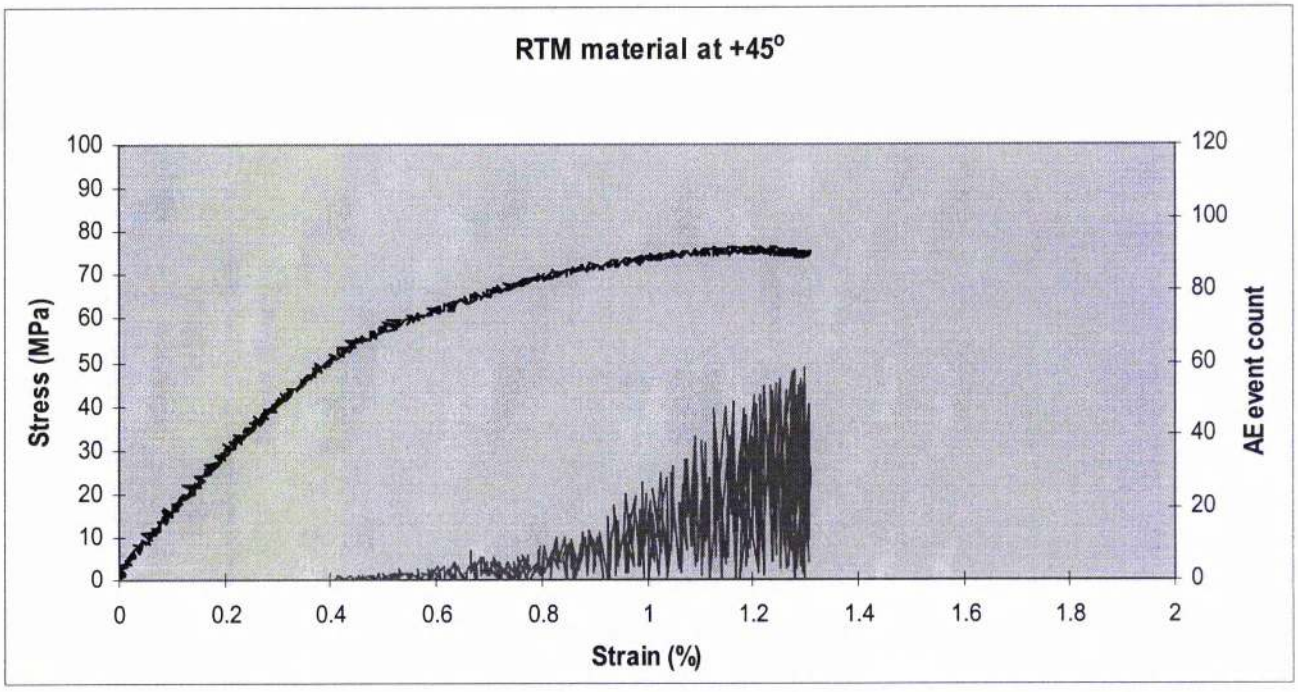

Figure 5.14.- Stress-strain curve for 5 layers RTM material tested at +45° direction.

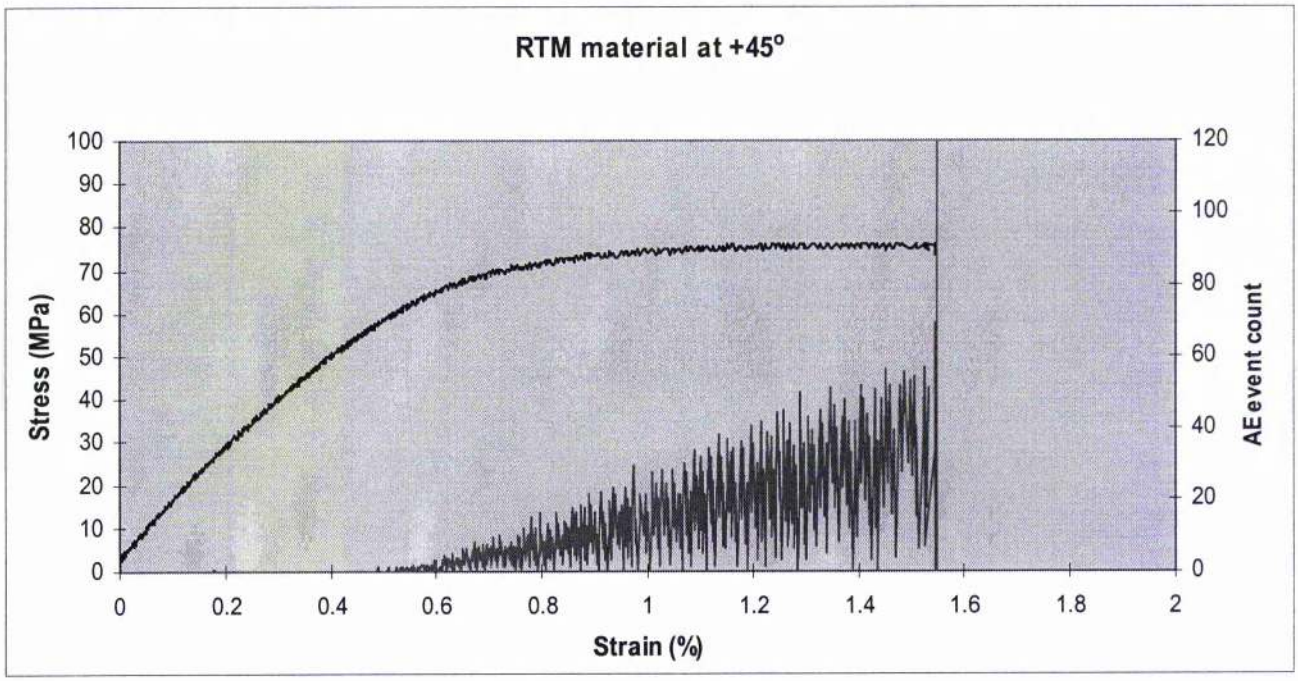

Figure 5.15.- Stress-strain curve for 4 layers RTM material tested at +45° direction.

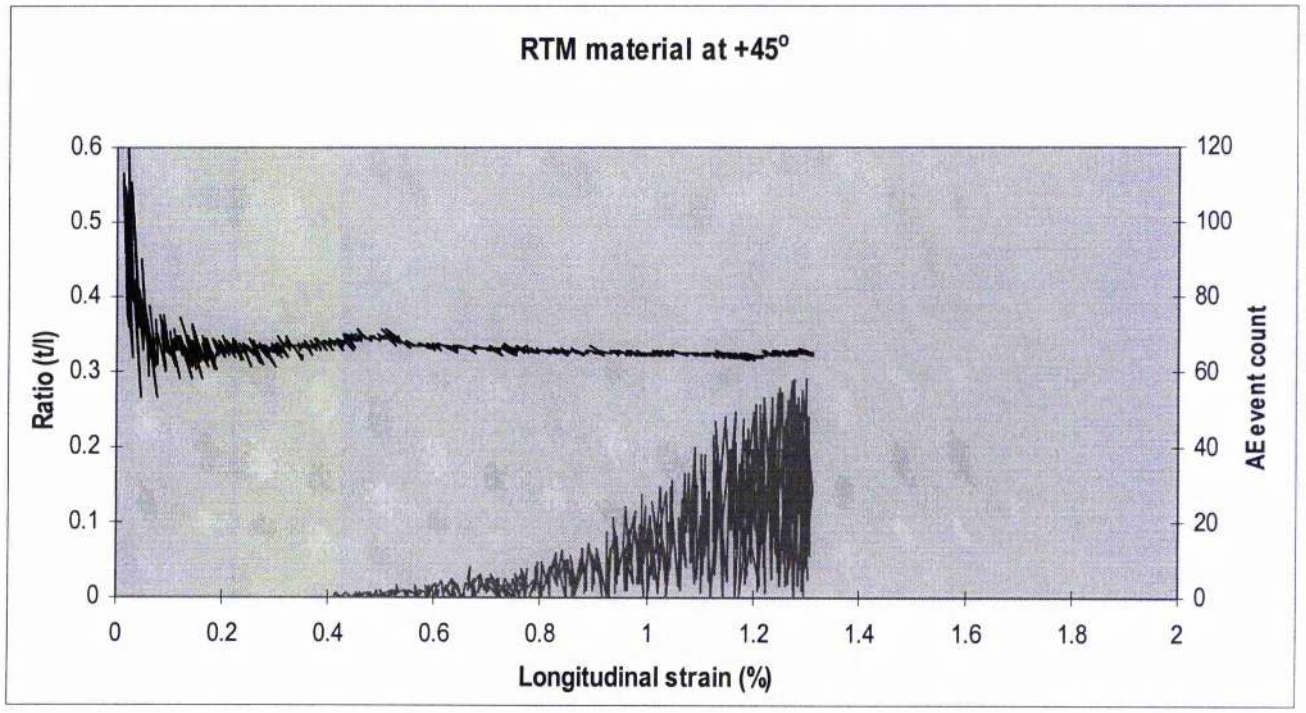

Figure 5.16.- Strains ratio (t/l) in 5 layers RTM material tested at +45° direction

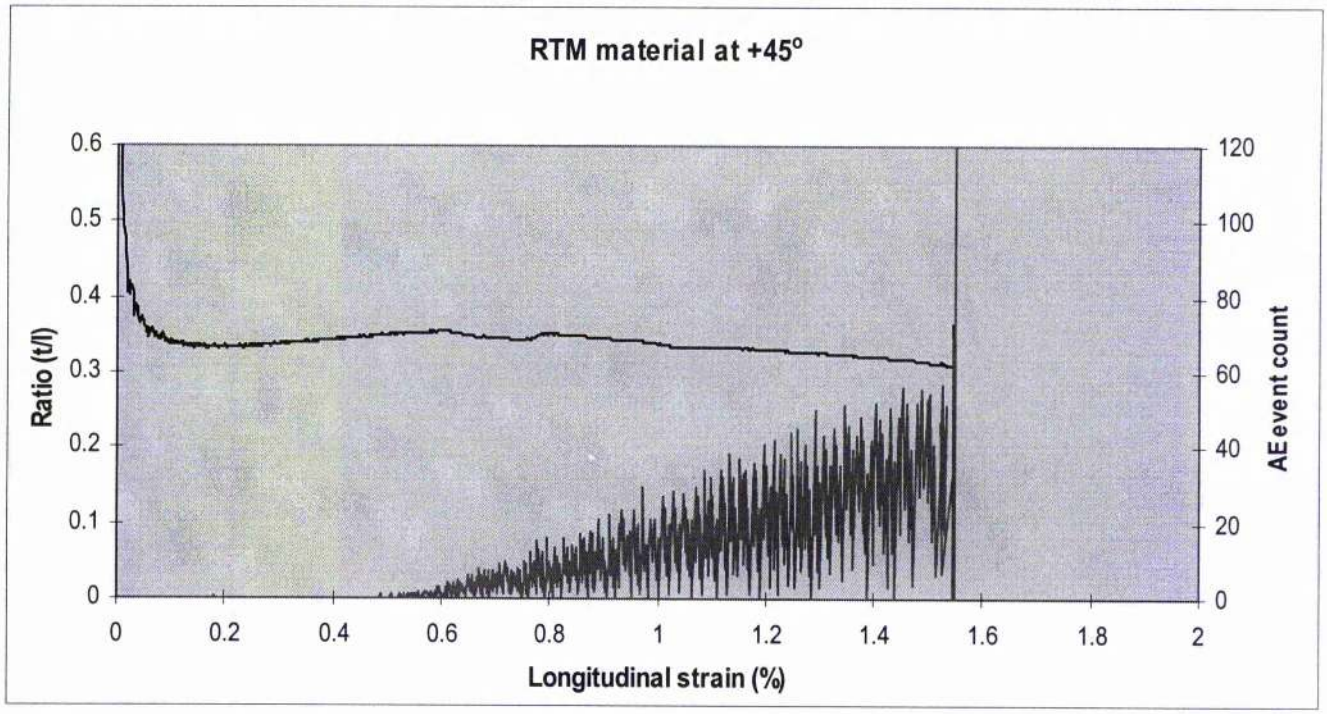

Figure 5.17.- Strains ratio (t/l) in 4 layers RTM material tested at +45° direction

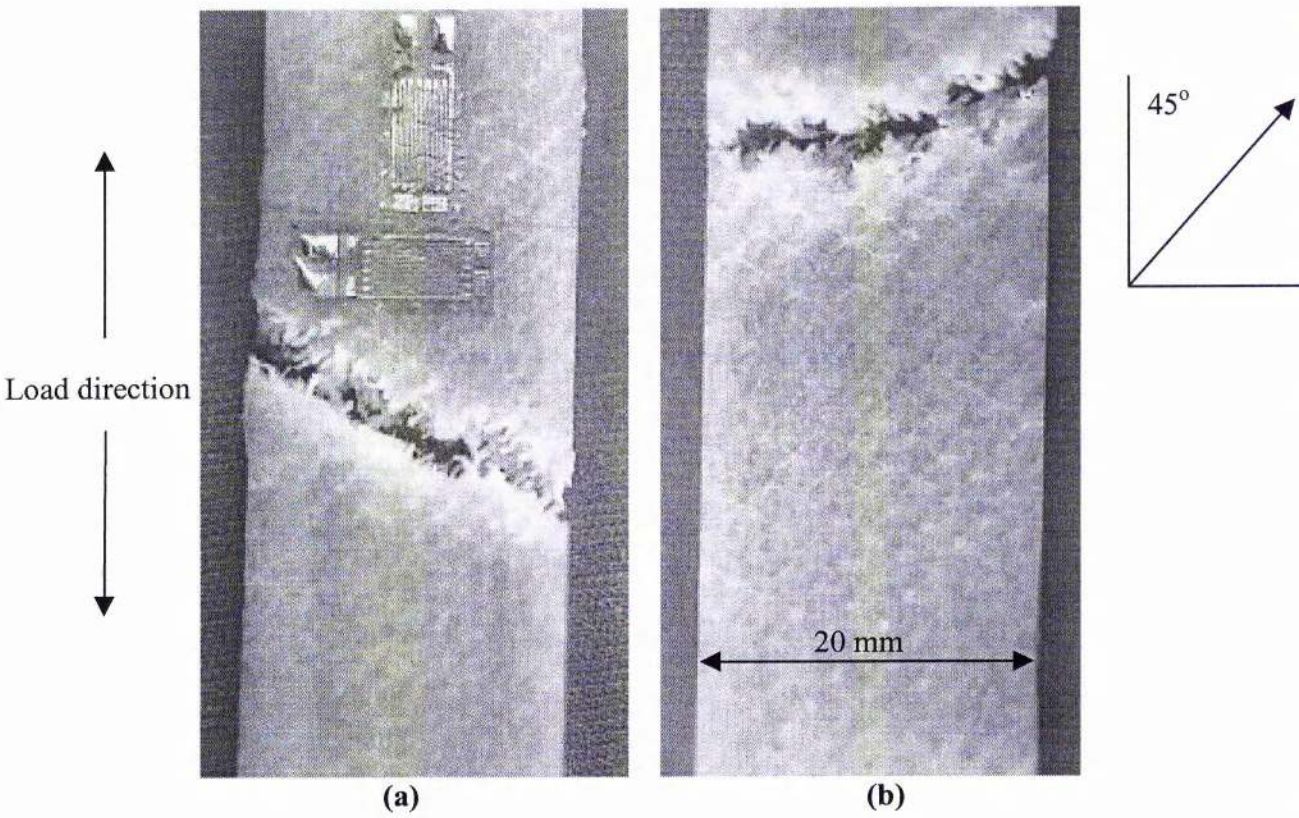

Figure 5.18.- Fracture sample tested in the +45° direction . (a) Perpendicular (b) Trying to follow wale direction.

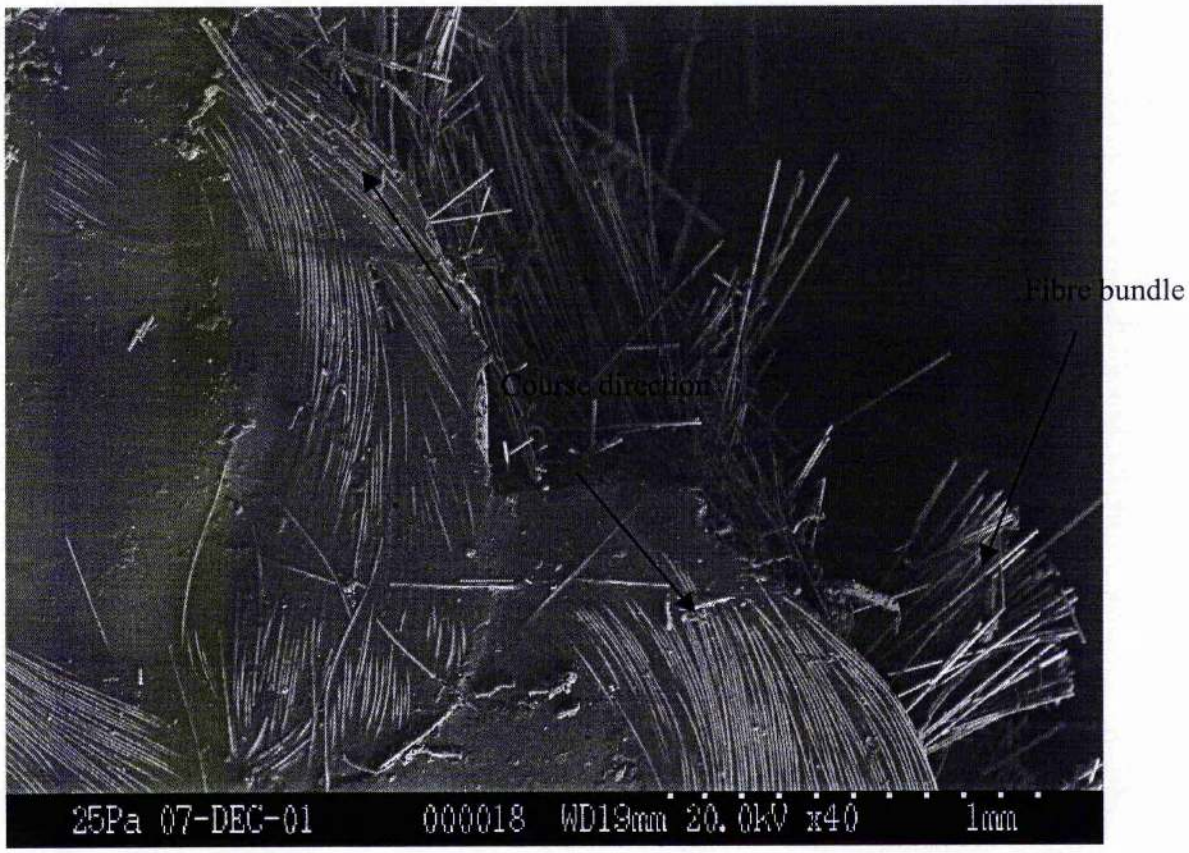

Figure 5.19.- Fractured surface of RTM sample tested in the +45° direction..

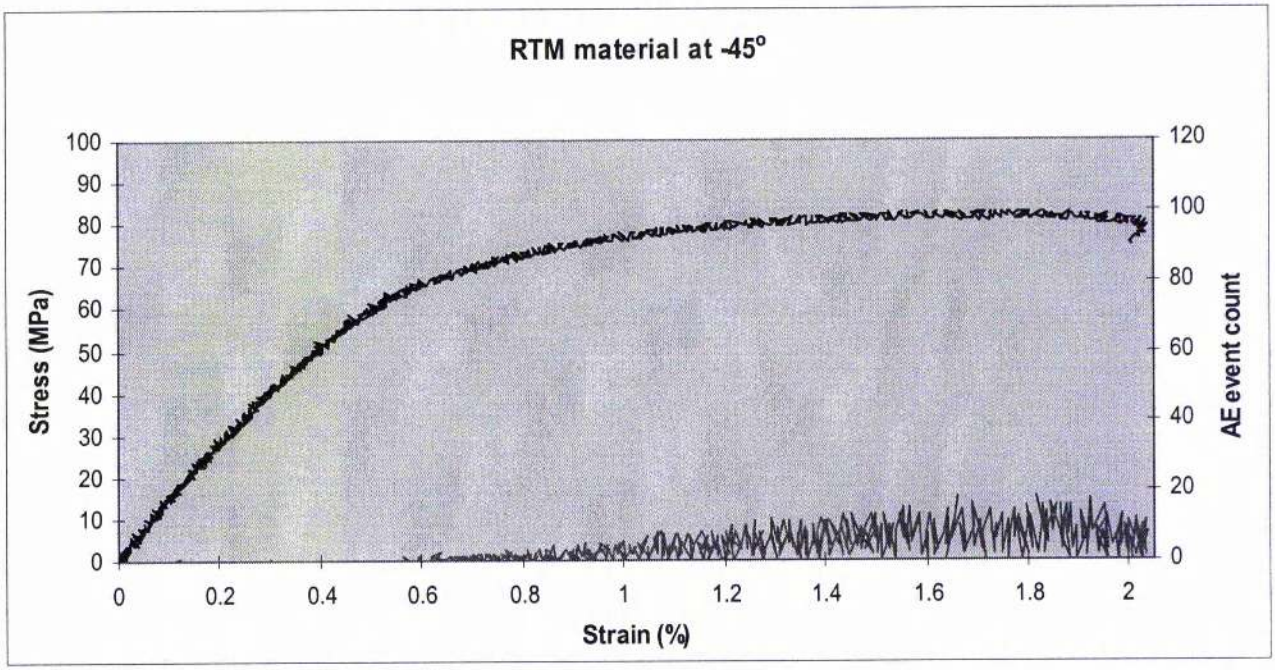

Figure 5.20.- Stress-strain curve for 5 layers RTM material tested at -45° direction.

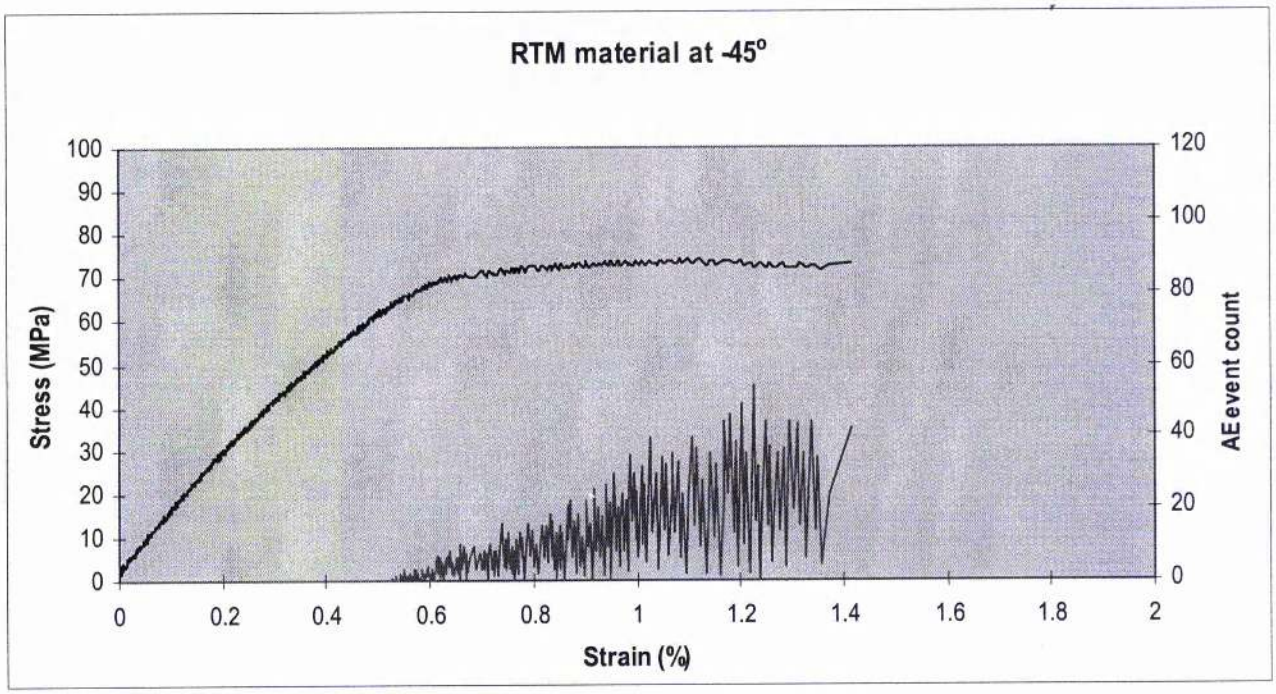

Figure 5.21.- Stress-strain curve for 4 layers RTM material tested at -45° direction.

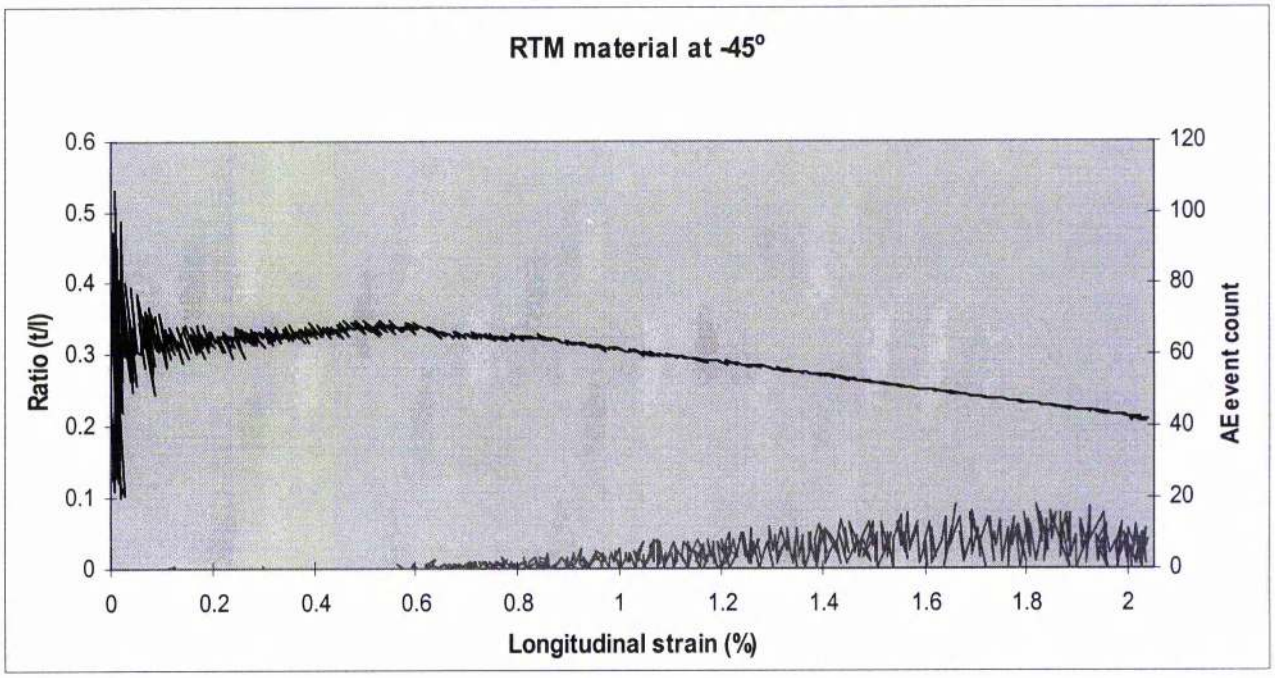

Figure 5.22.- Strains ratio (t/l) in 5 layers RTM material tested at -45° direction

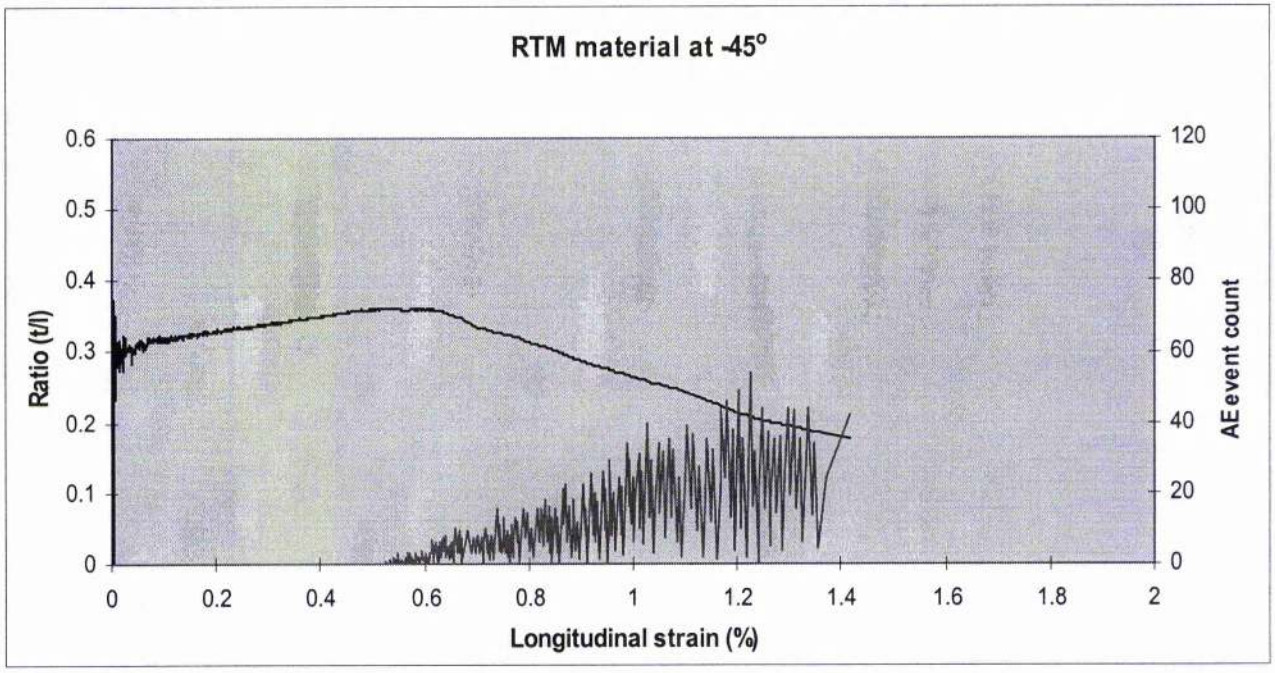

Figure 5.23.- Strains ratio (t/l) in 4 layers RTM material tested at -45° direction

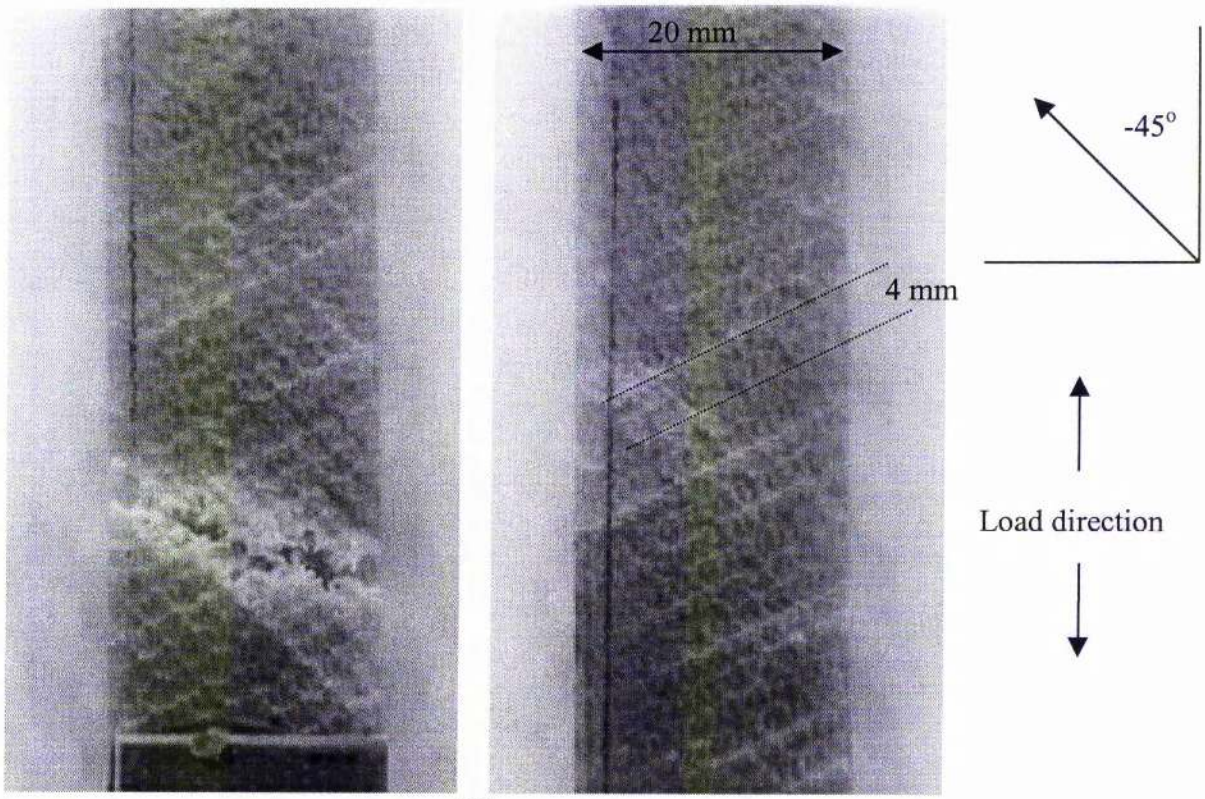

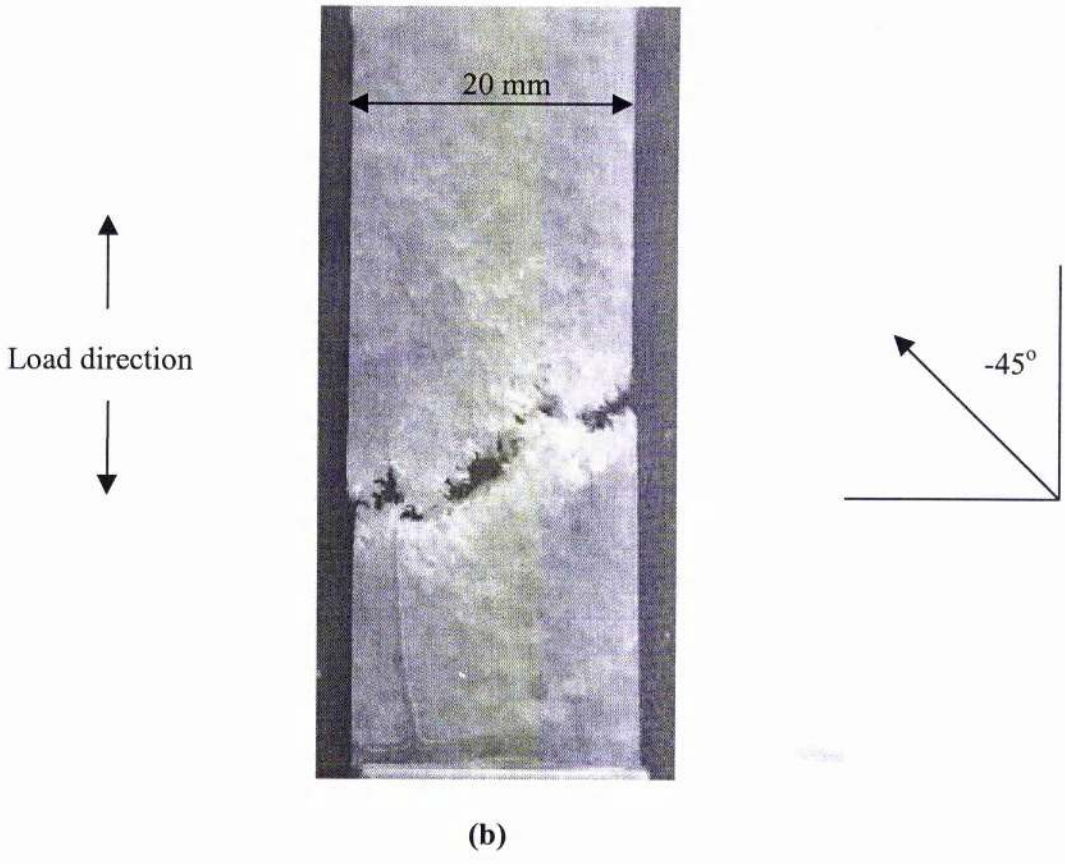

Figure 5.24.- Fractured specimen in the -45°. (a) parallel to loops direction (b) perpendicular to loops direction.

Figure 5.25.- Fractured surface of RTM sample tested in the -45° direction.

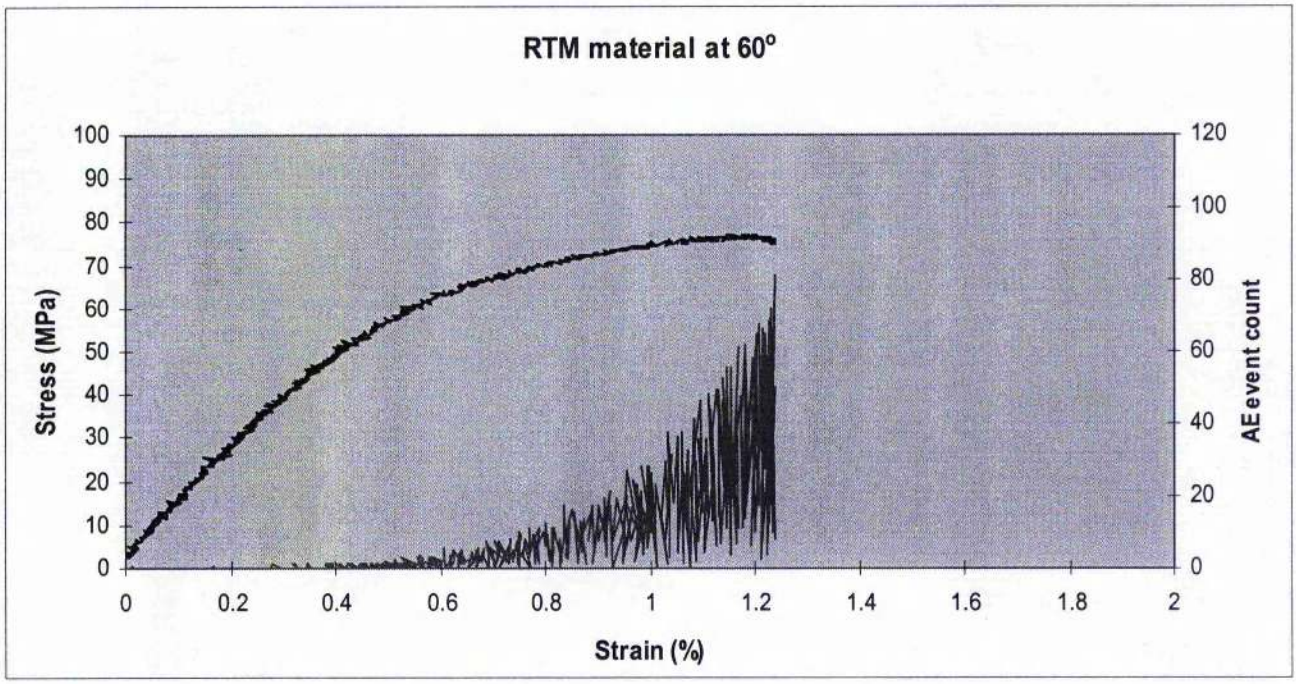

Figure 5.26.- Stress-strain curve for 5 layers RTM material tested at 60° direction.

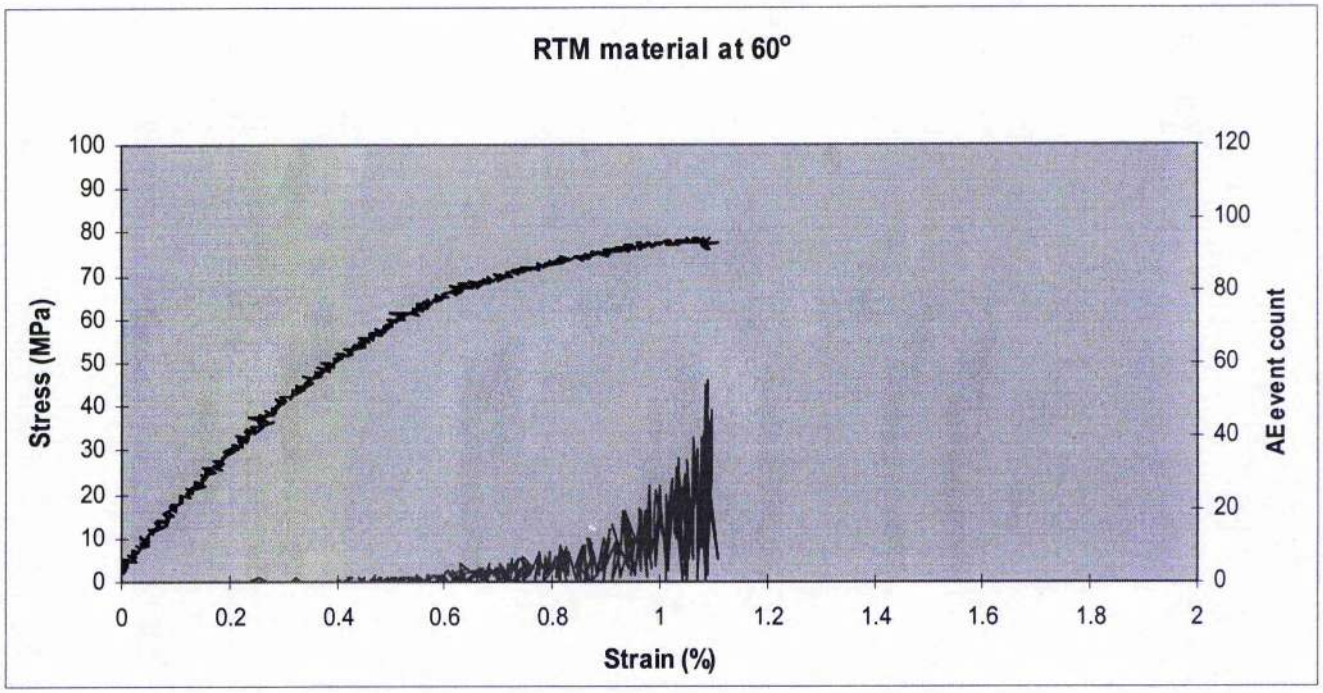

Figure 5.27- Stress-strain curve for 4 layers RTM material tested at 60° direction.

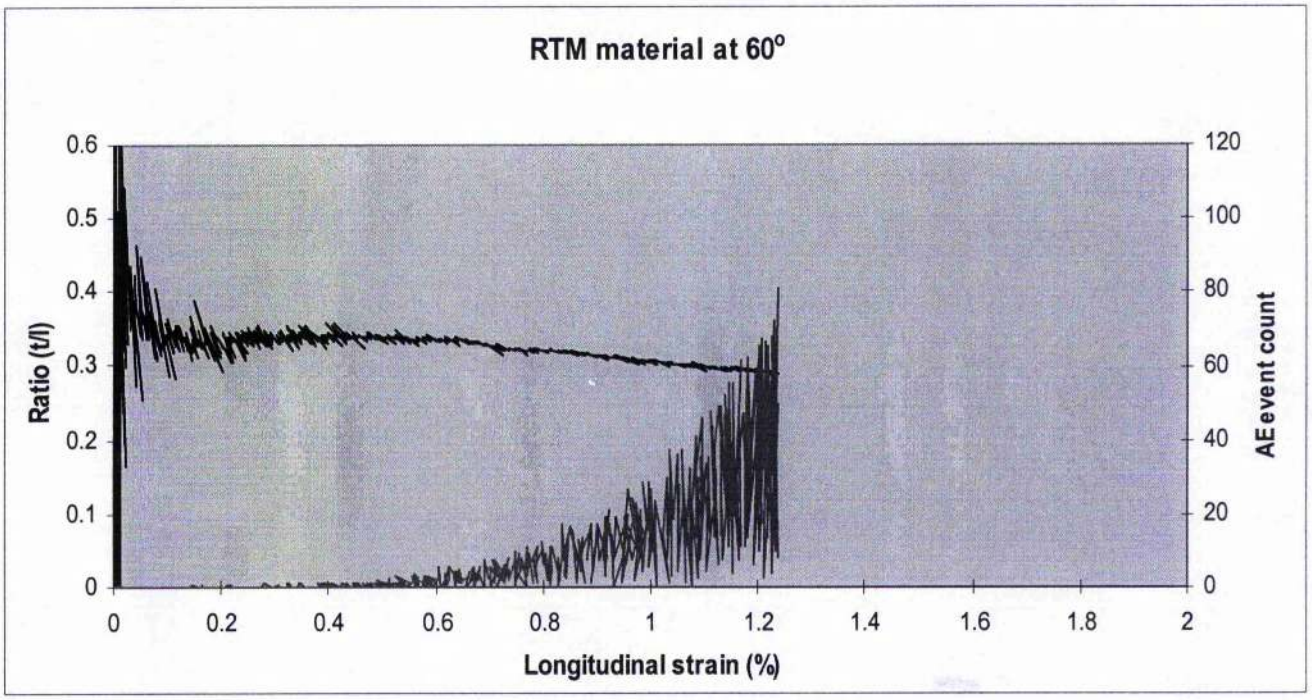

Figure 5.28.- Strains ratio (t/l) in 5 layers RTM material tested at 60° direction

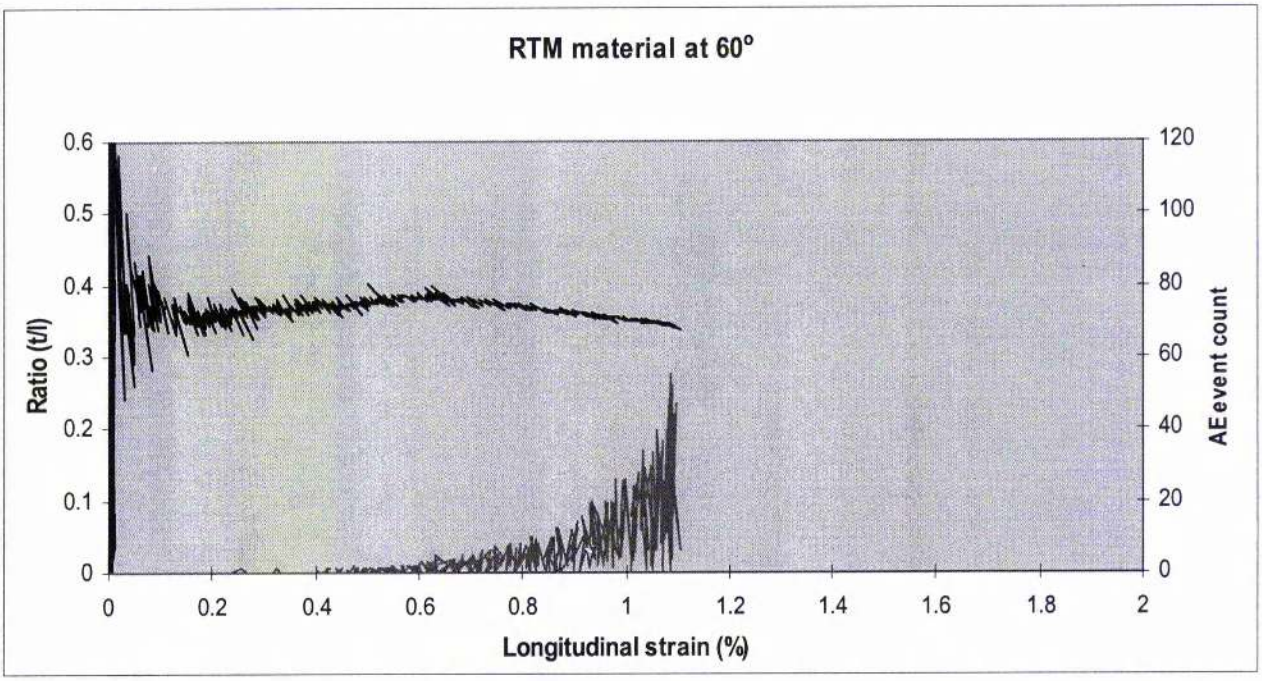

Figure 5.29.- Strains ratio (t/l) in 4 layers RTM material tested at 60° direction

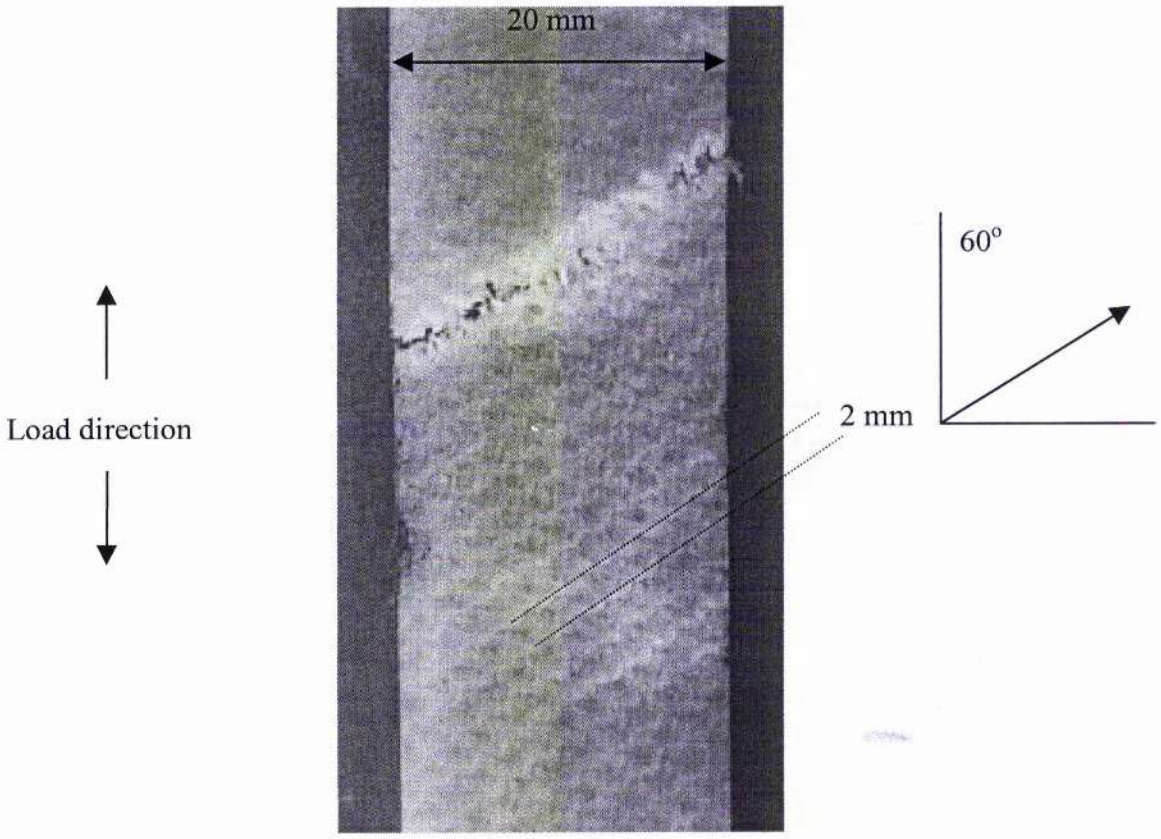

Figure 5.30.- Fractured specimen tested in the 60° direction.

Figure 5.31.- Fractured surface of RTM sample tested in the 60° direction.

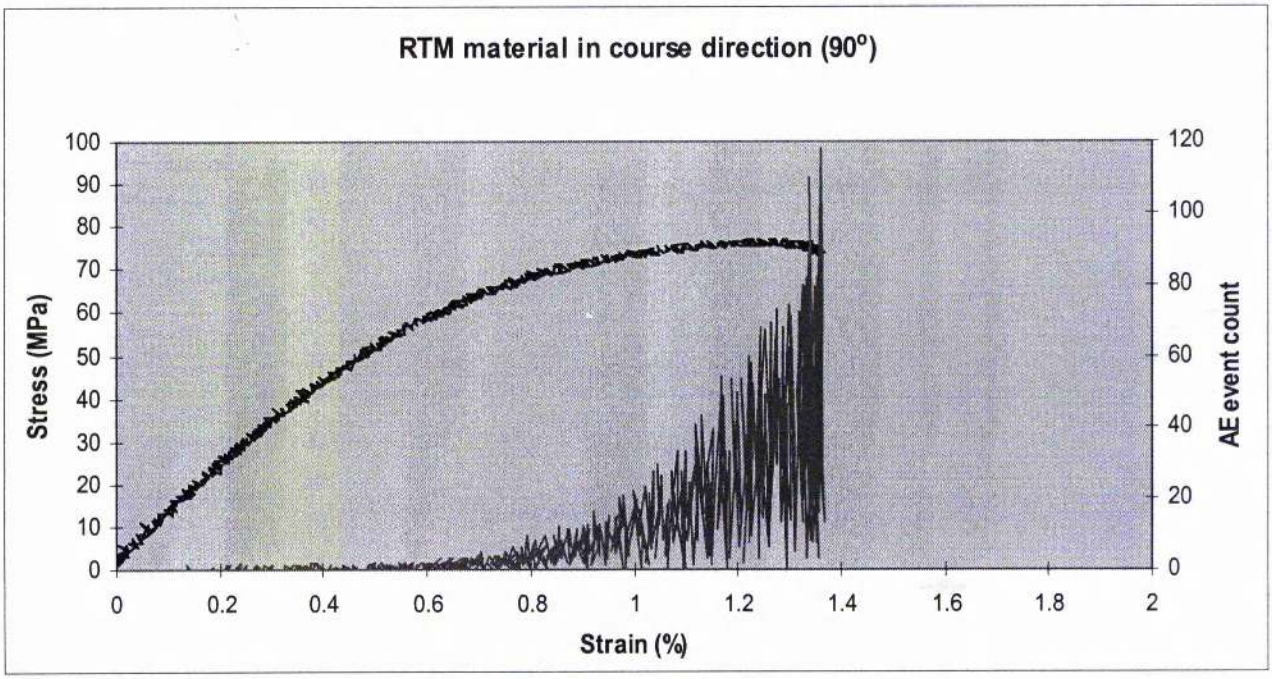

Figure 5.32- Stress-strain curve for 5 layers RTM material tested at 90° (course direction).

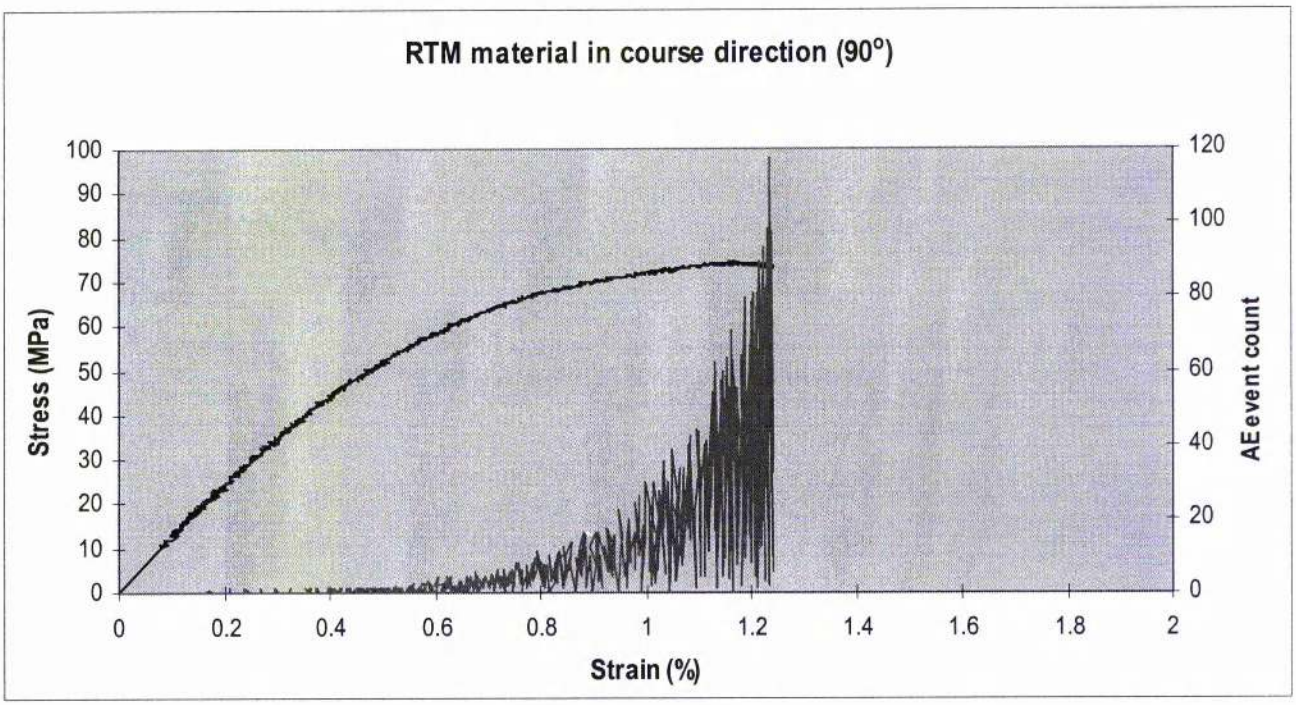

Figure 5.33- Stress-strain curve for 4 layers RTM material tested at 90° (course direction).

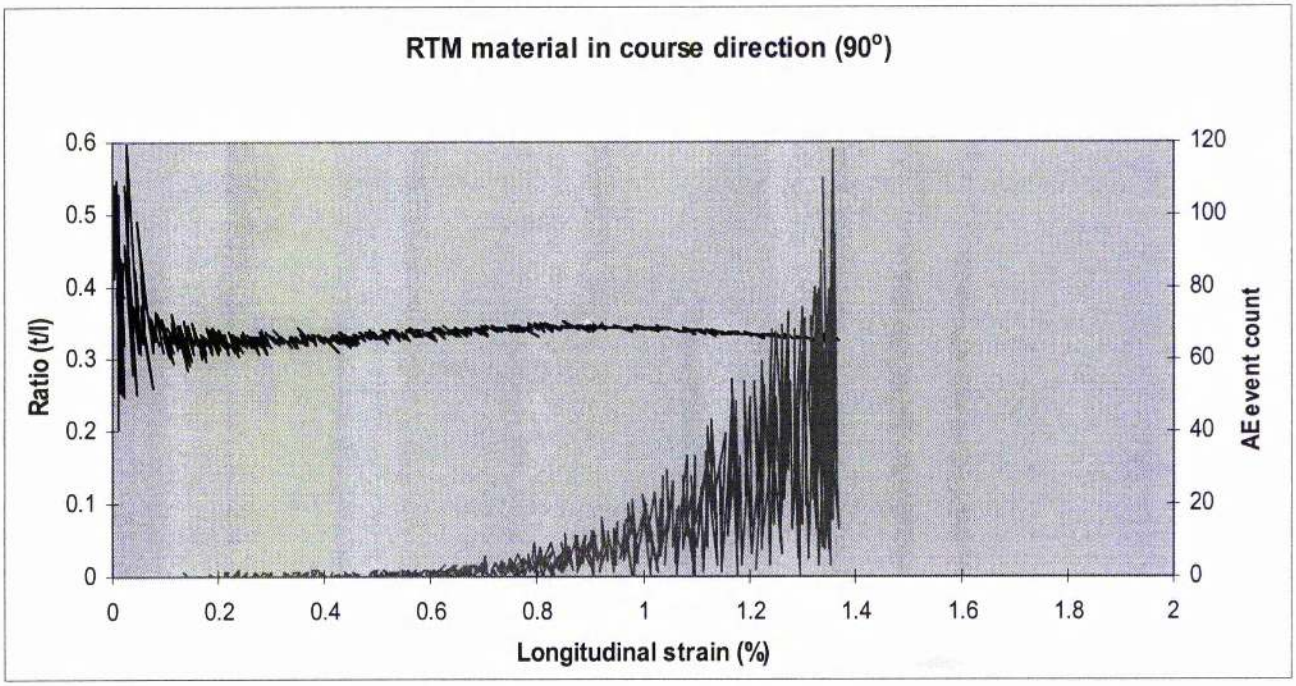

Figure 5.34.- Strains ratio (t/l) in 5 layers RTM material tested at 90° (course direction).

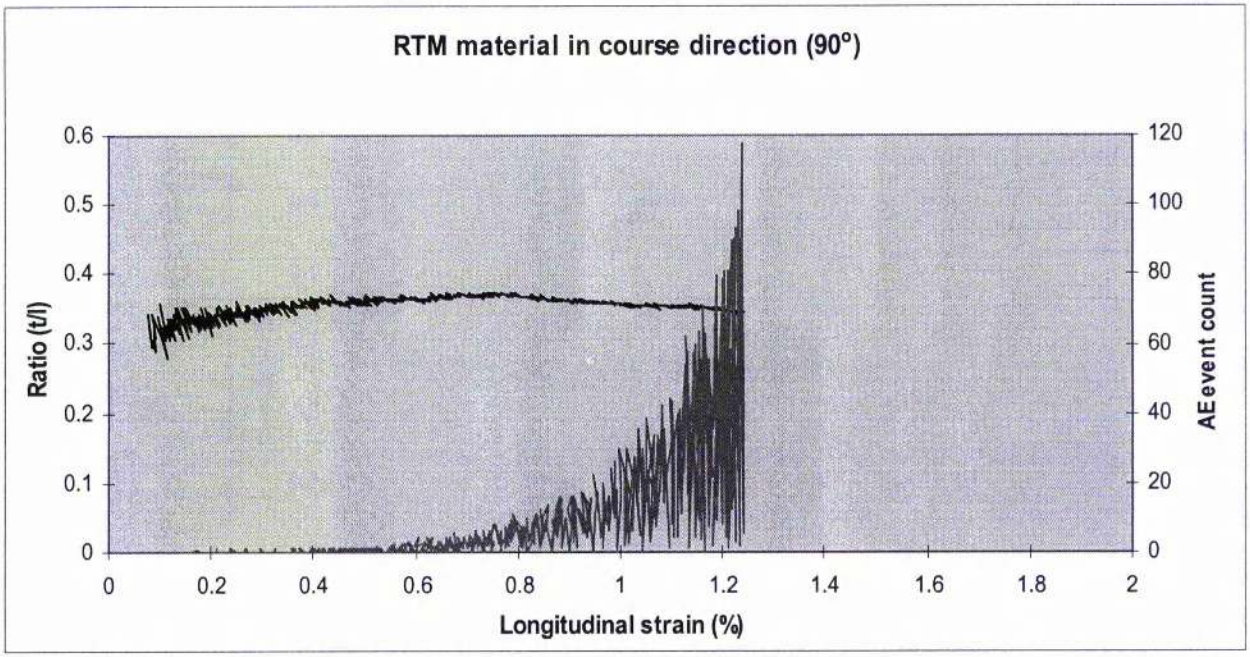

Figure 5.35.- Strains ratio (t/l) in 4 layers RTM material tested at 90° (course direction).

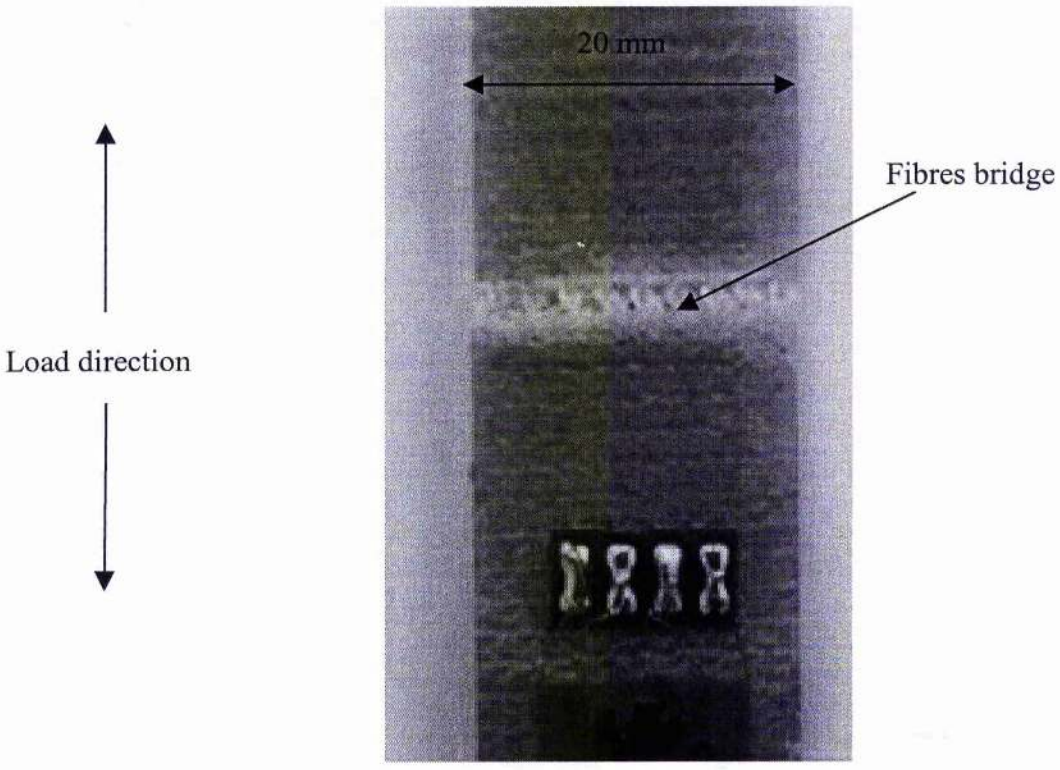

Figure 5.36.- Fractured specimen in the 90° (course direction).

Figure 5.37.- Fractured surface of RTM sample tested in the 90° (course direction)

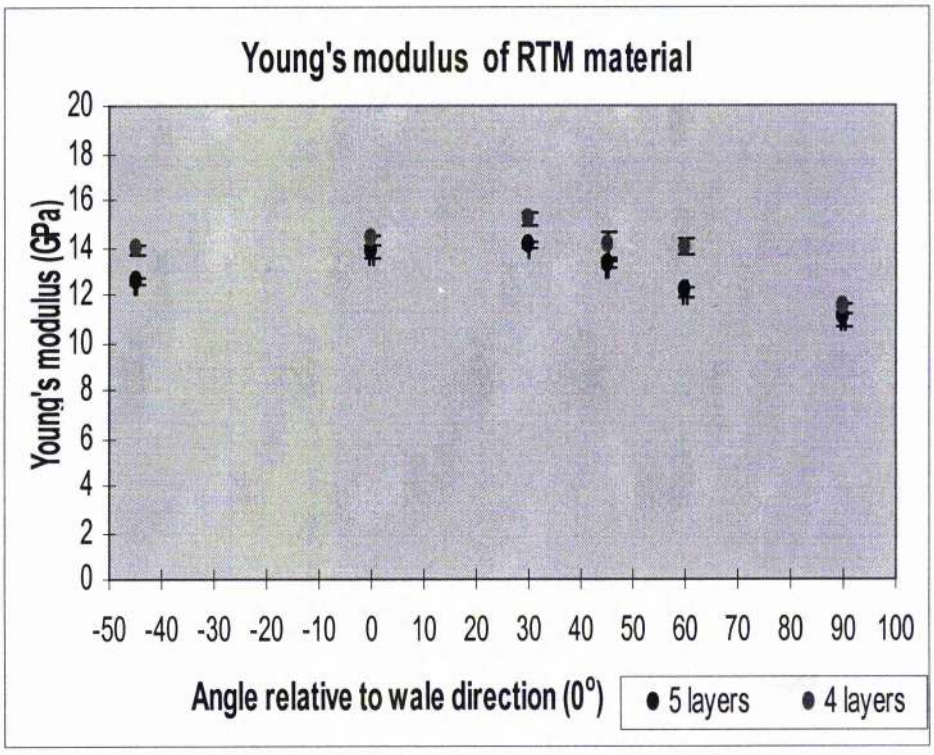

Figure 5.38.- Young's modulus of RTM material as function of angle. For some angles, the uncertainty is smaller than the symbol.

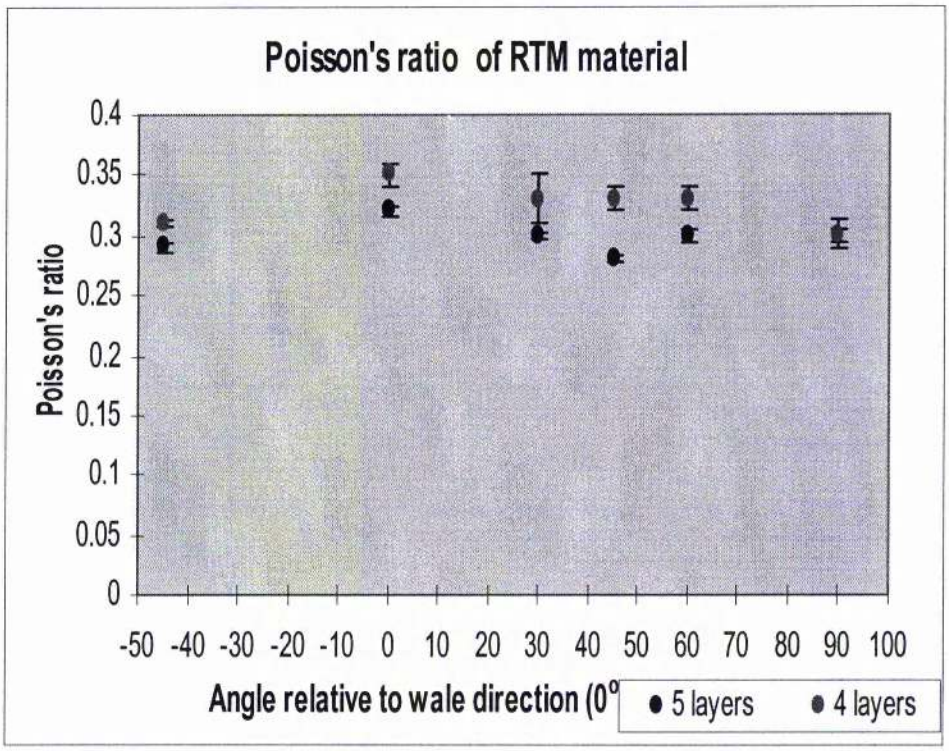

Figure 5.39.- Poisson's ratio of single RTM material as function of angle. For some angles, the uncertainty is smaller than the symbol.

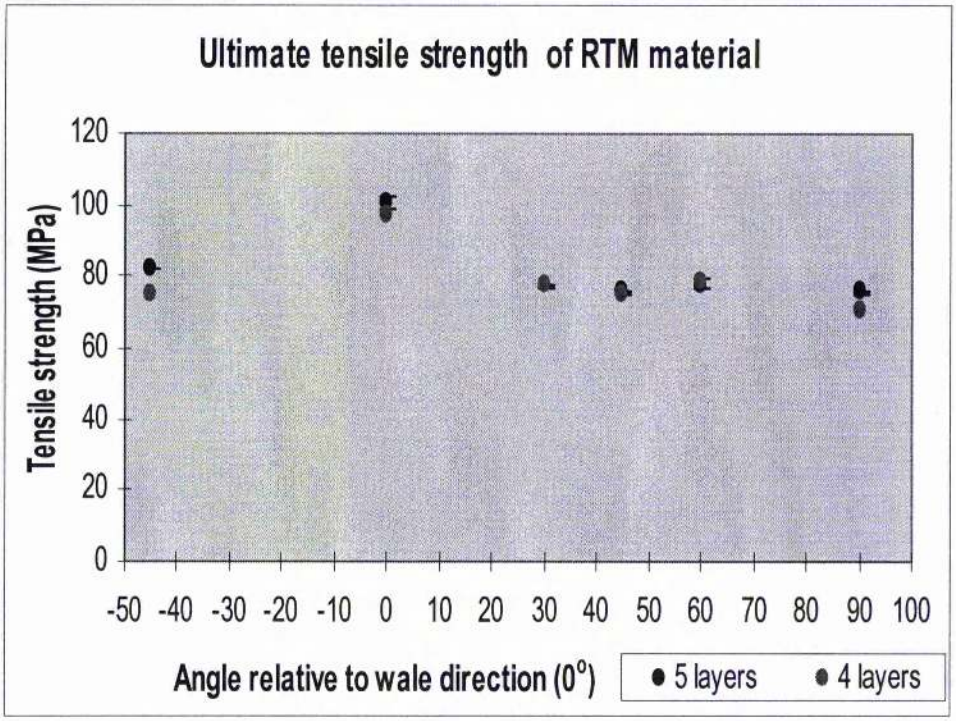

Figure 5.40.- Ultimate tensile strength of RTM material as function of angle. For some angles, the uncertainty is smaller than the symbol.

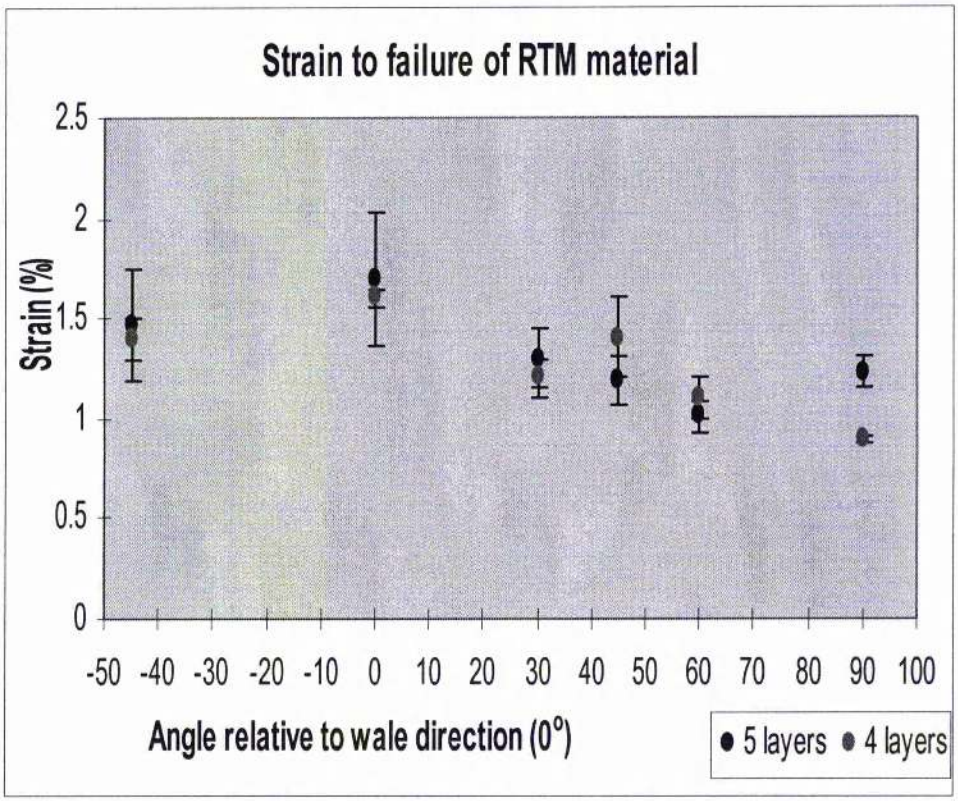

Figure 5.41.- Strain to failure of RTM material as function of angle. For some angles, the uncertainty is smaller than the symbol.

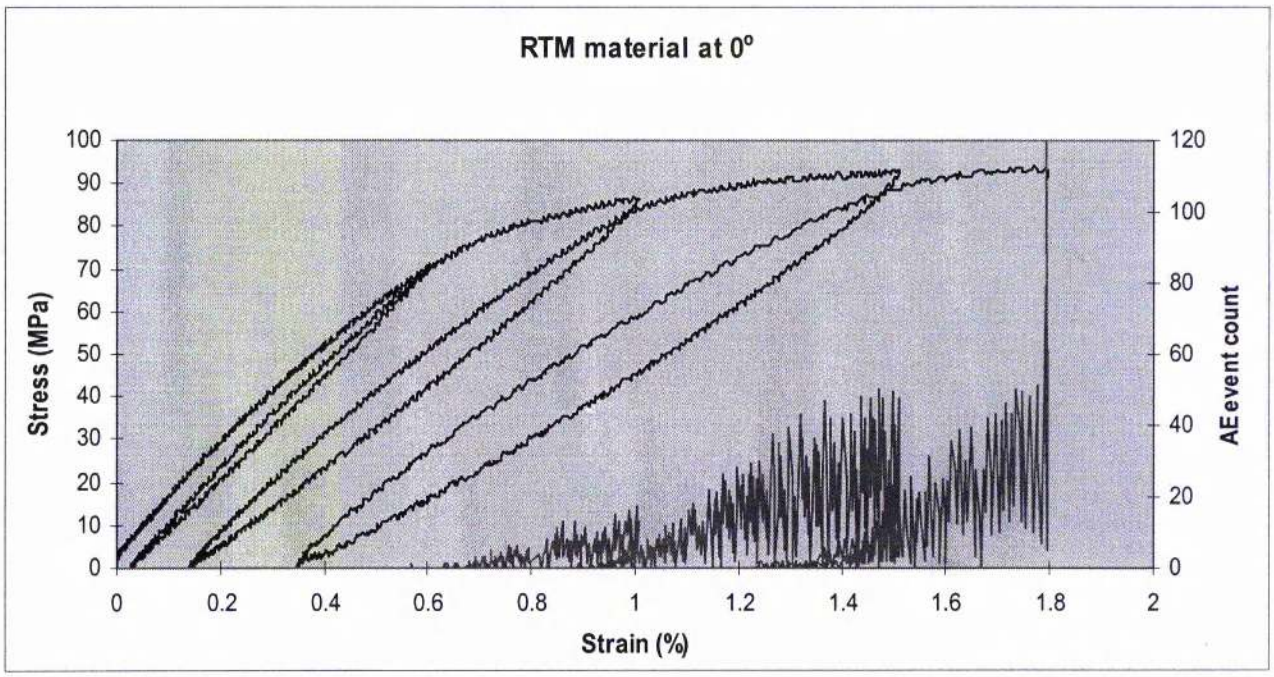

Figure 5.42.- Cyclic stress-strain curve for 4 layers RTM material at 0° (wale direction).

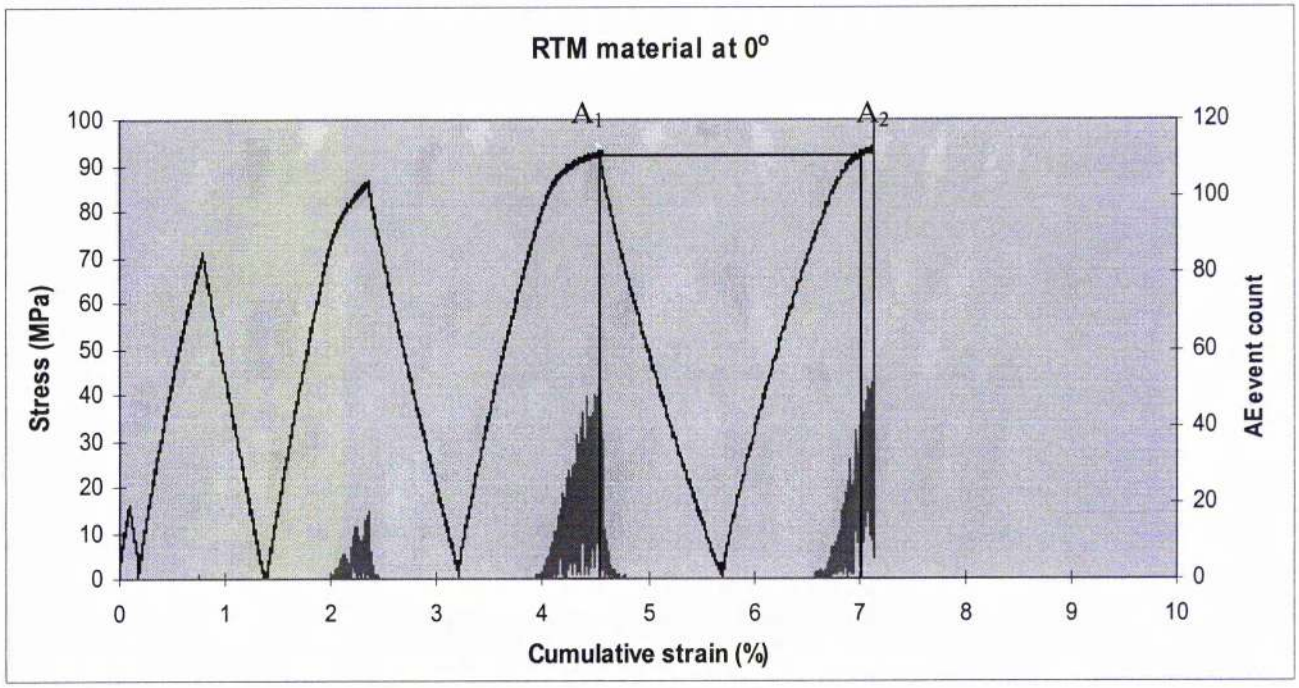

Figure 5.43.- Cyclic stress-cumulative strain curve for 4 layers RTM material at 0° (wale direction).

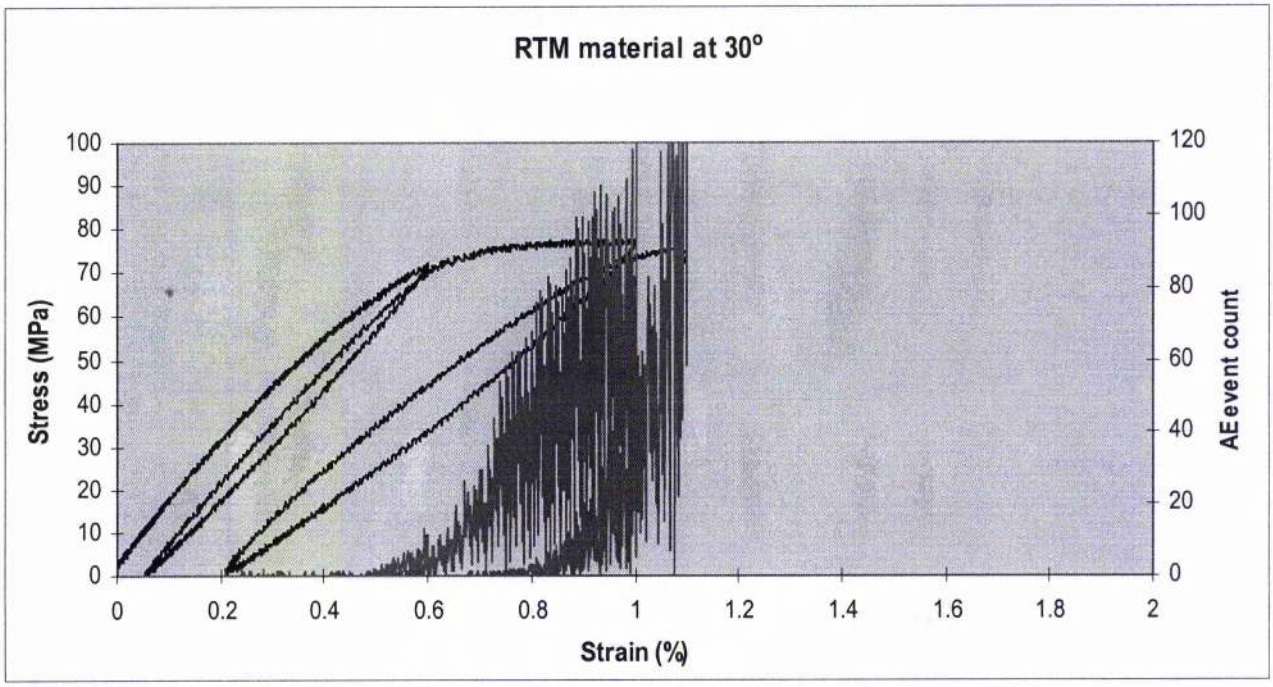

Figure 5.44.- Cyclic stress-strain curve for 4 layers RTM material at 30°.

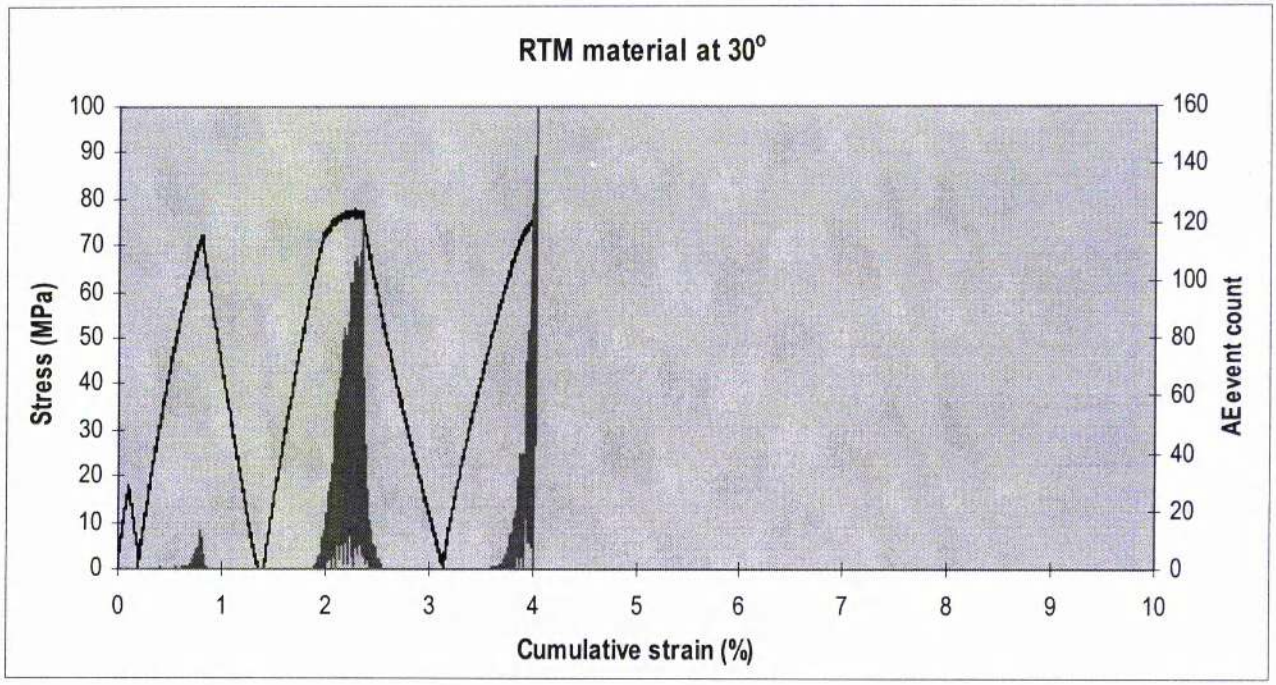

Figure 5.45.- Cyclic stress-cumulative strain curve for 4 layers RTM material at 30°.

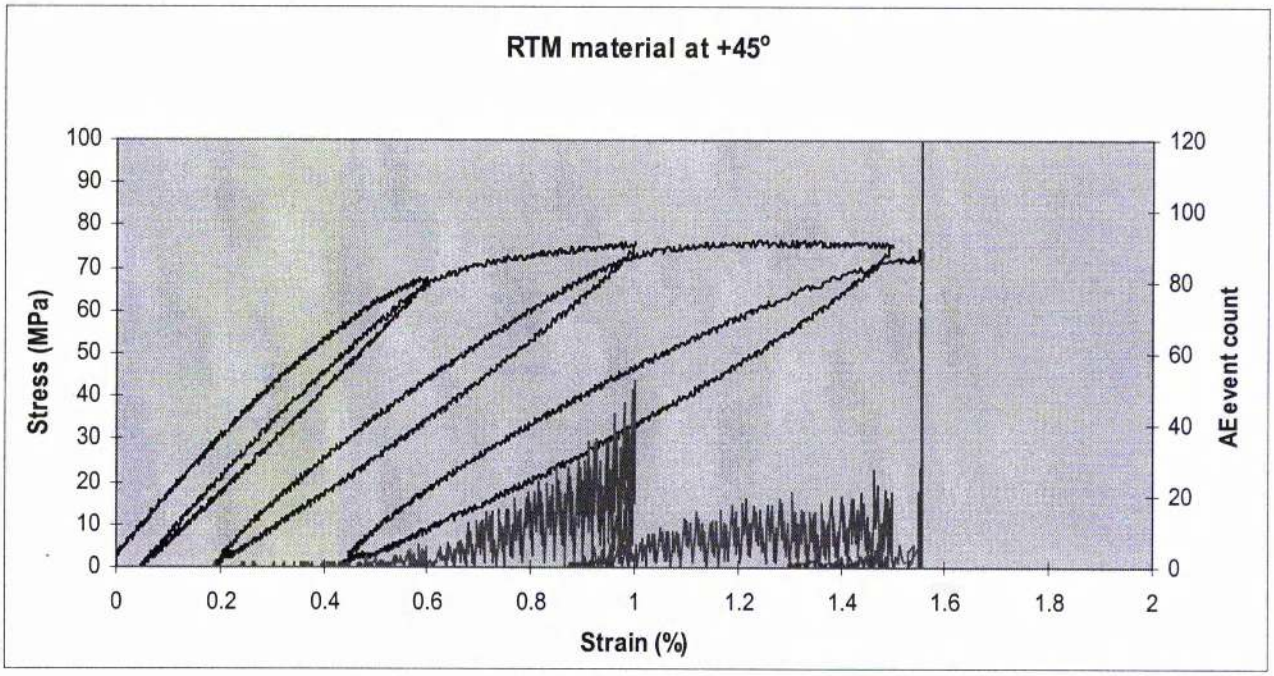

Figure 5.46.- Cyclic stress-strain curve for 4 layers RTM material at +45°.

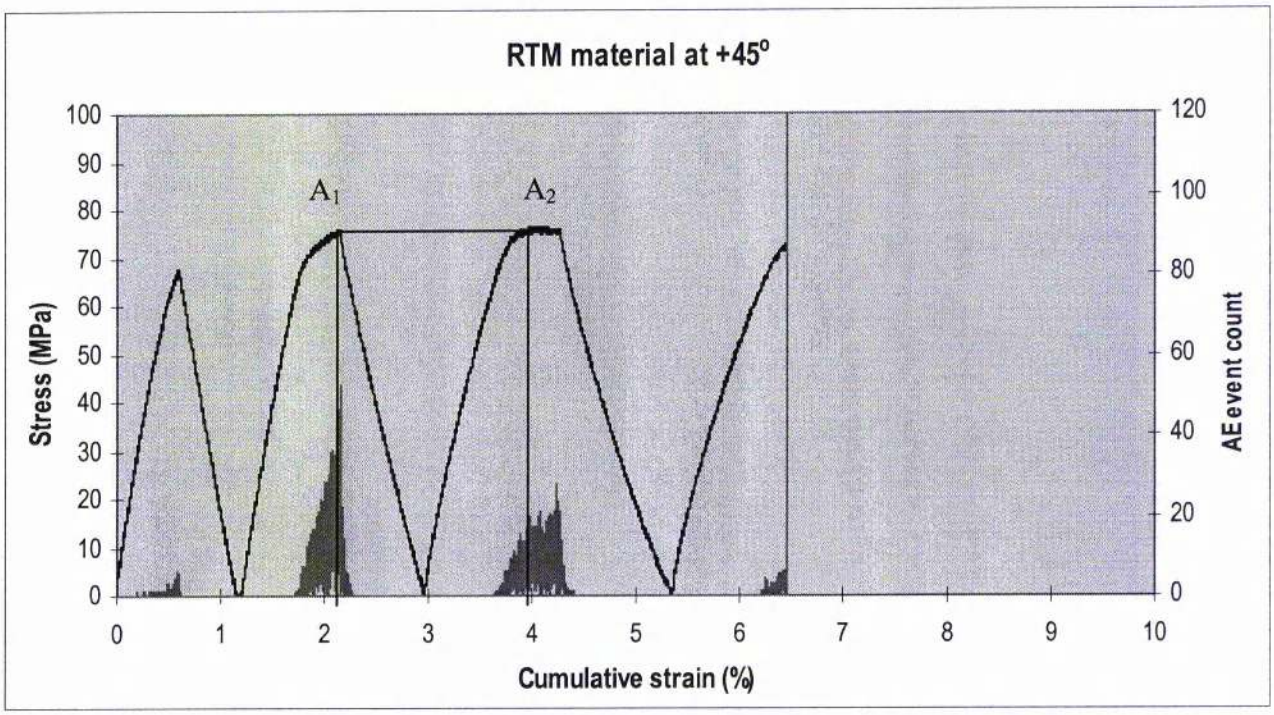

Figure 5.47.- Cyclic stress-time curve for 4 layers RTM material at +45°.

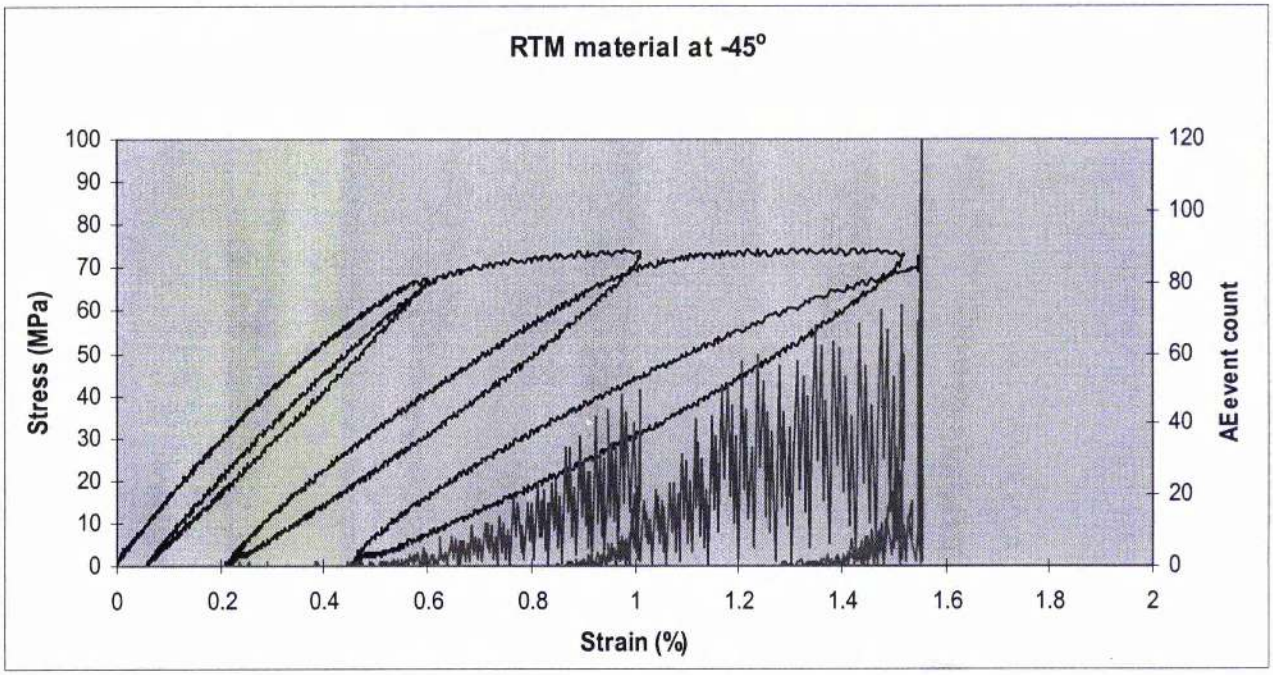

Figure 5.48.- Cyclic stress-strain curve for 4 layers RTM material at -45°.

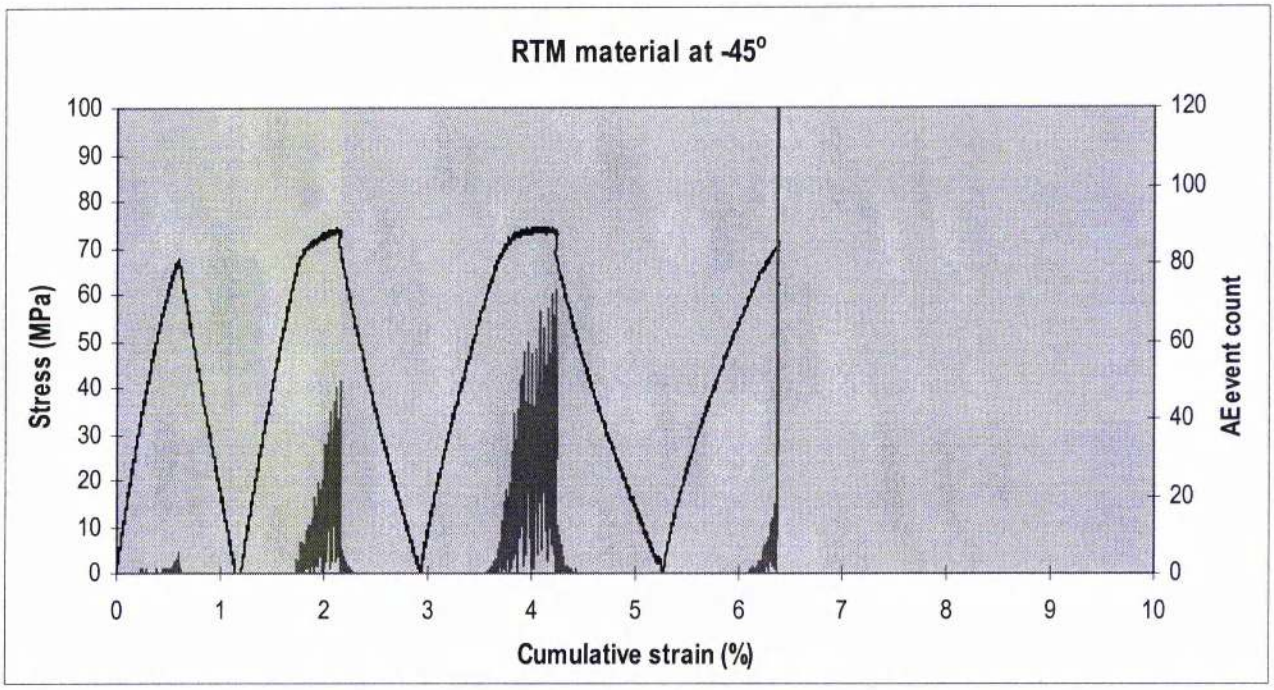

Figure 5.49.- Cyclic stress-time curve for 4 layers RTM material at -45°.

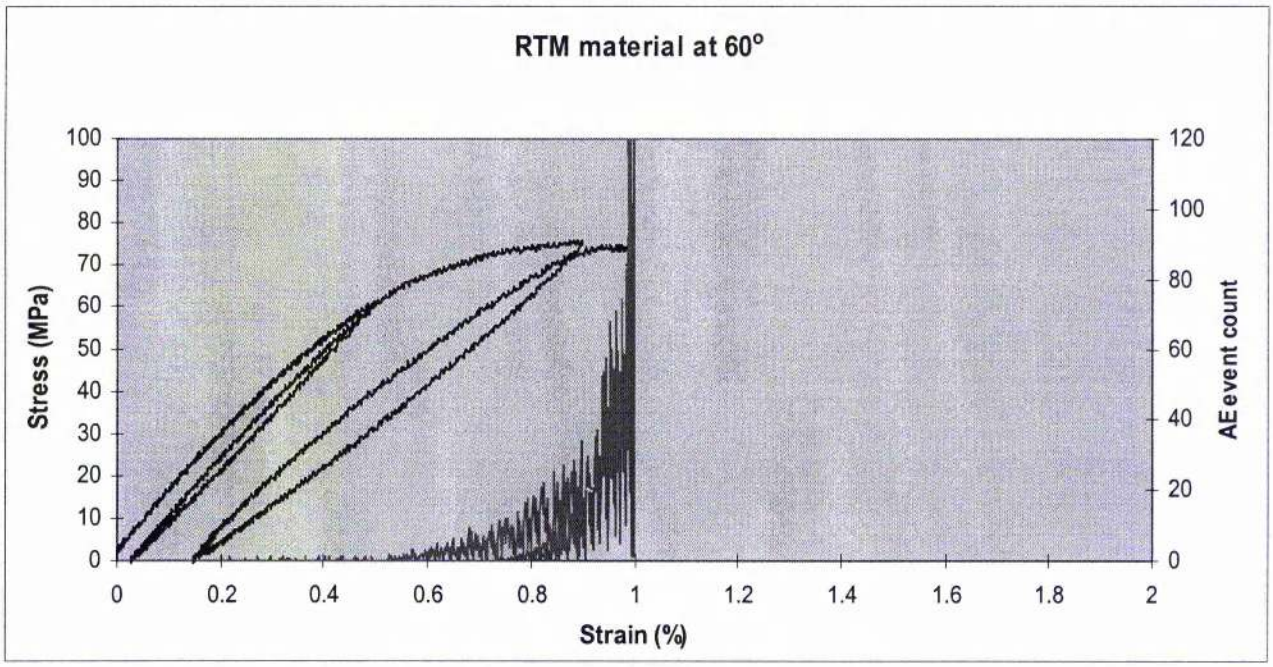

Figure 5.50.- Cyclic stress-strain curve for 4 layers RTM material at 60°.

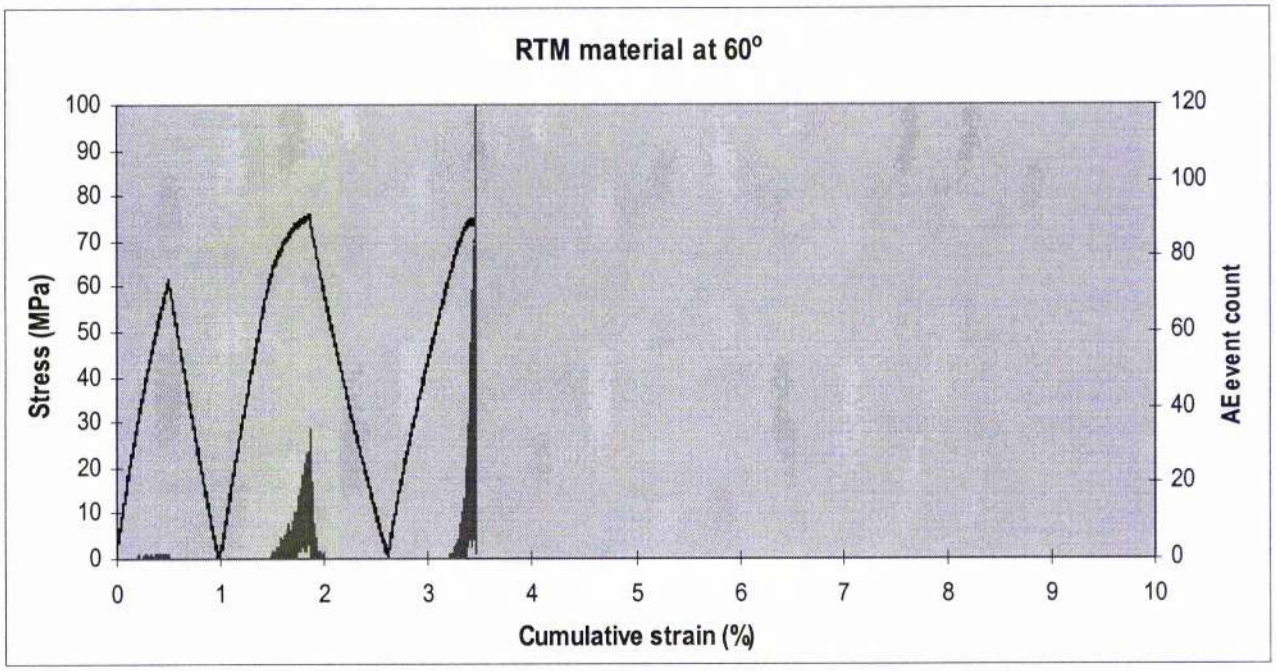

Figure 5.51.- Cyclic stress-time curve for 4 layers RTM material at 60°.

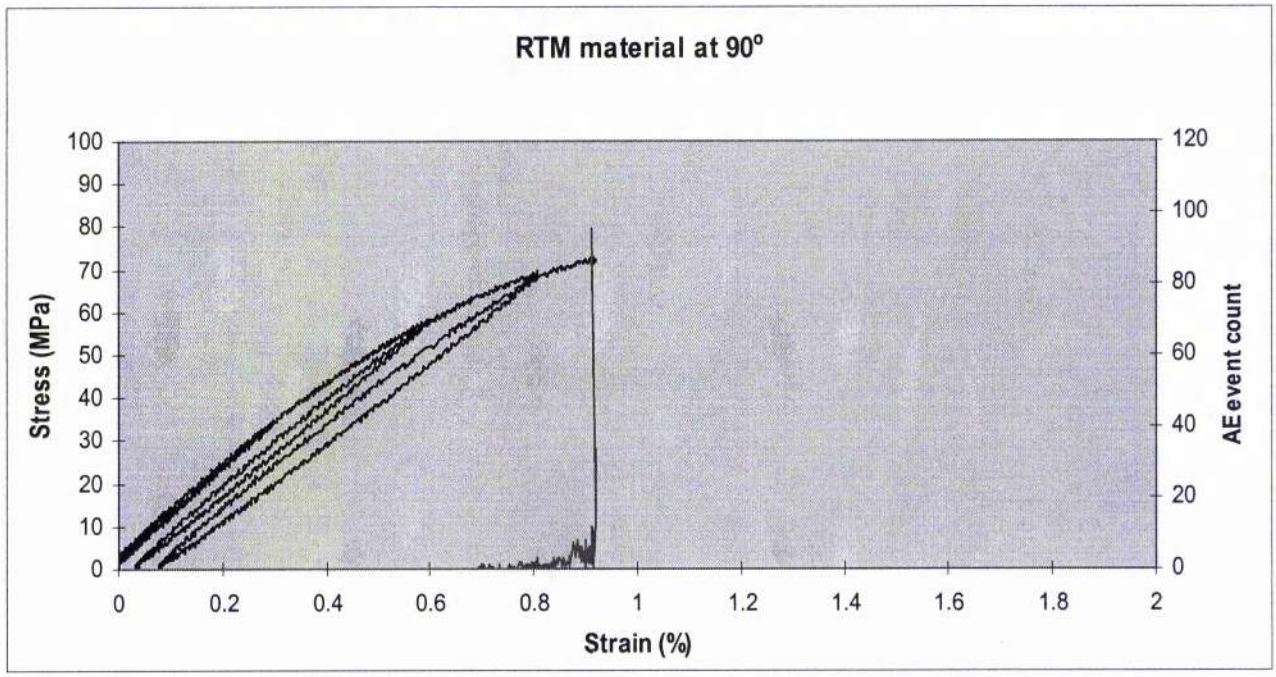

Figure 5.52.- Cyclic stress-strain curve for 4 layers RTM material at 90° (course direction)

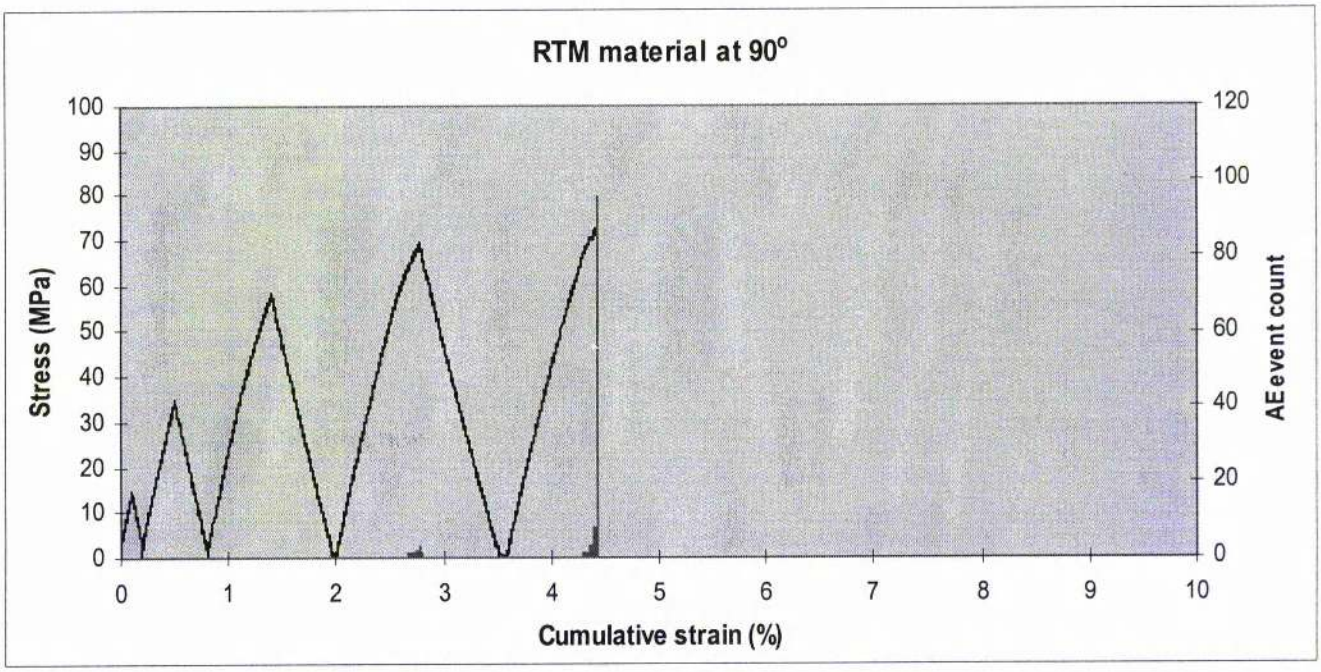

Figure 5.53.- Cyclic stress-time curve for 4 layers RTM material at 90° (course direction)

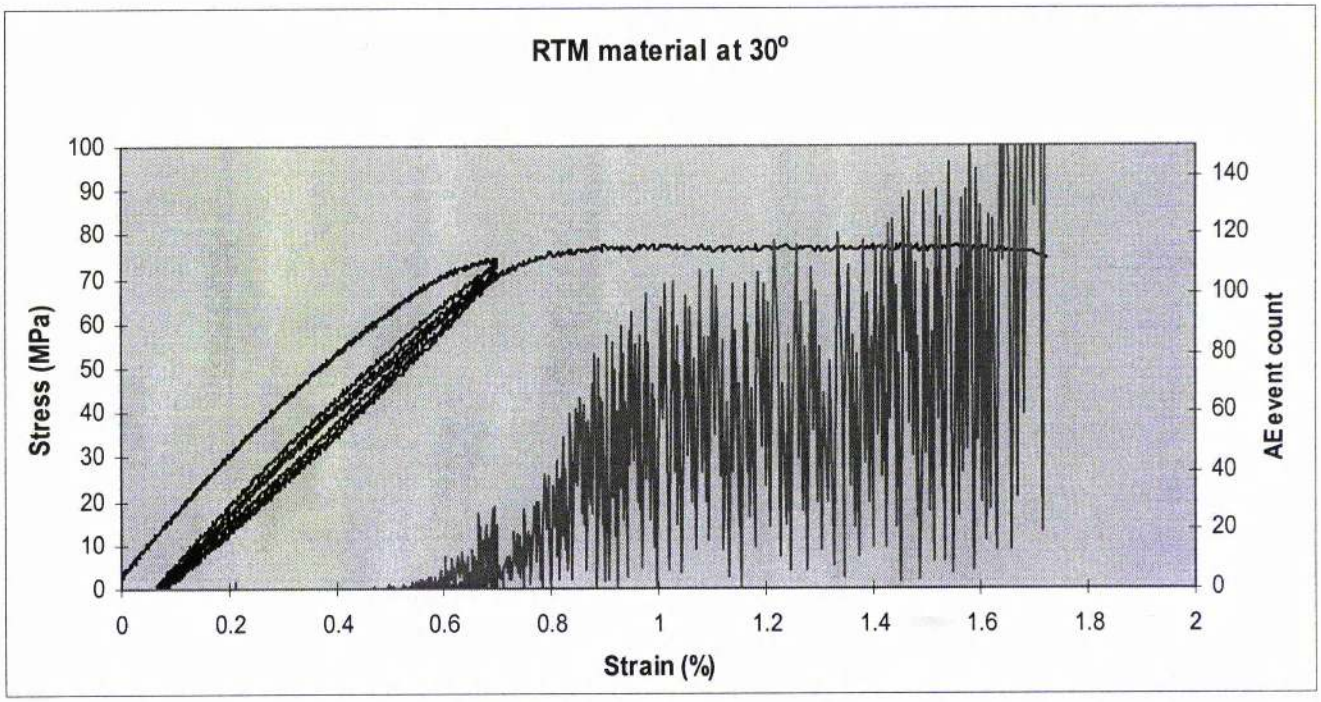

Figure 5.54.- Cyclic stress-strain curve for 4 layers RTM material at fixed strain for 30° direction.

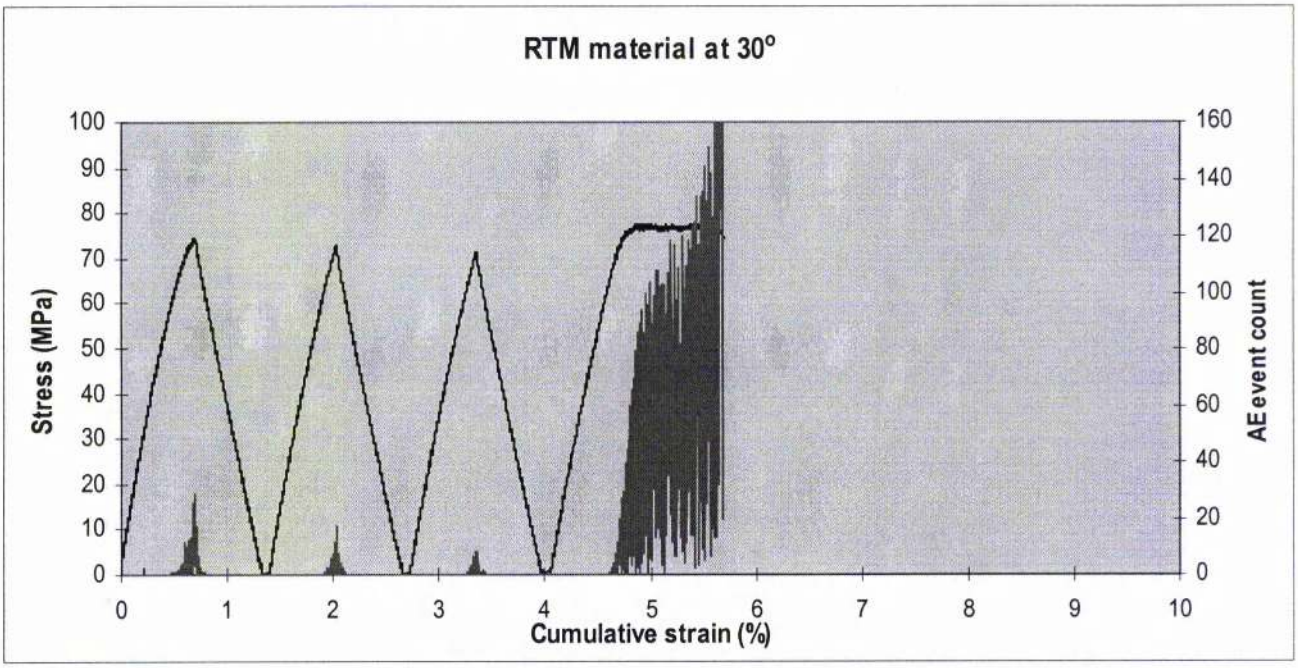

Figure 5.55.- Cyclic stress-time curve for 4 layers RTM material at fixed strain for 30° direction.

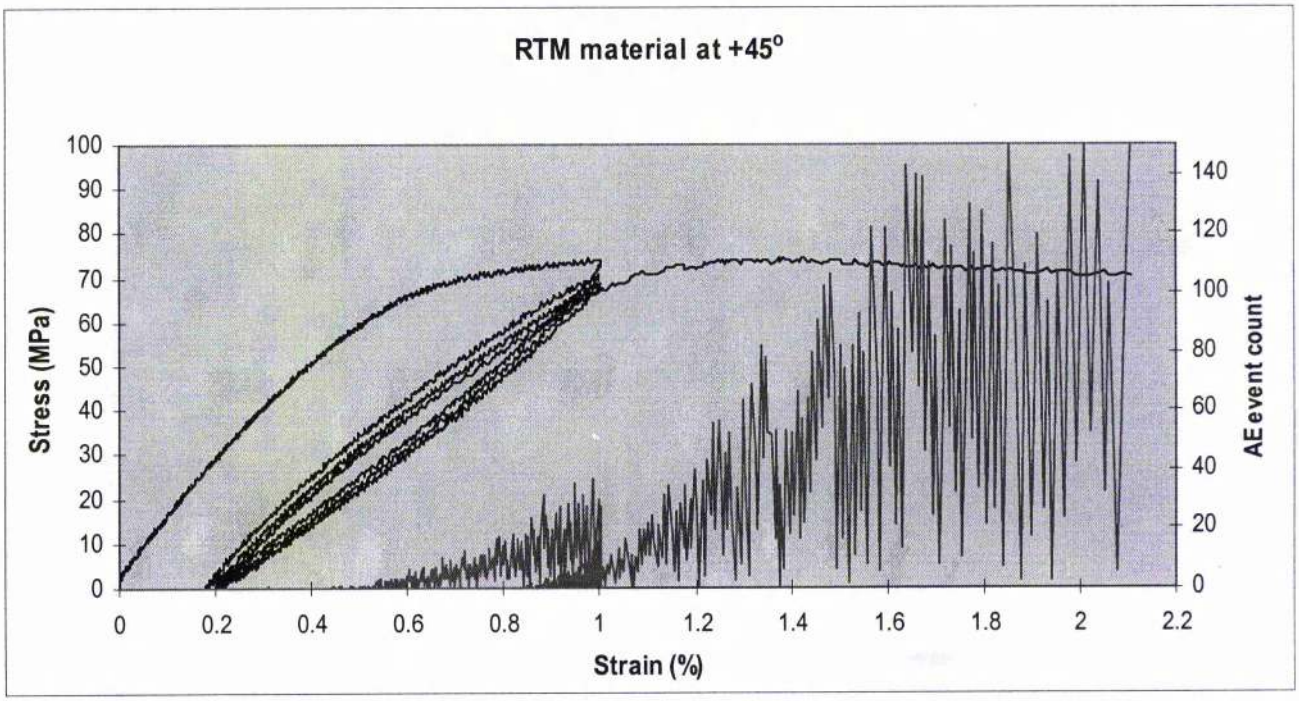

Figure 5.56.- Cyclic stress-strain curve for 4 layers RTM material at fixed strain for +45° direction.

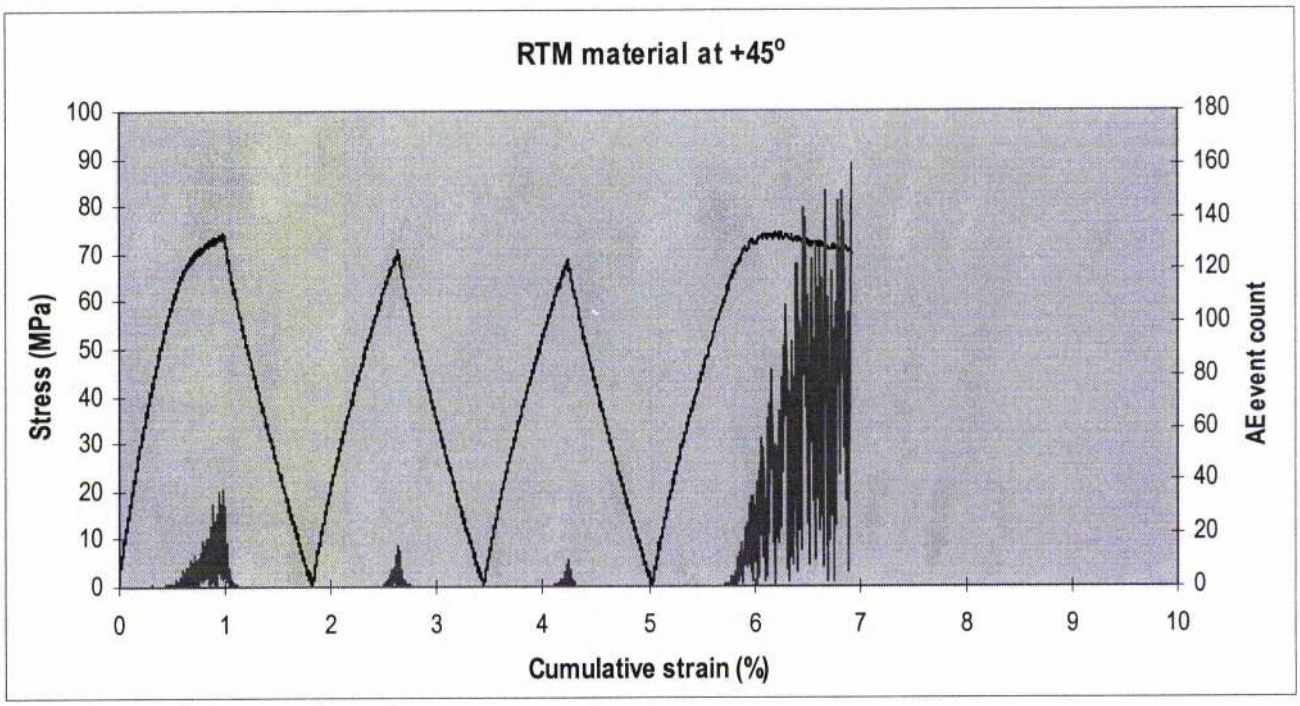

Figure 5.57.- Cyclic stress-time curve for 4 layers RTM material at fixed strain for +45° direction.

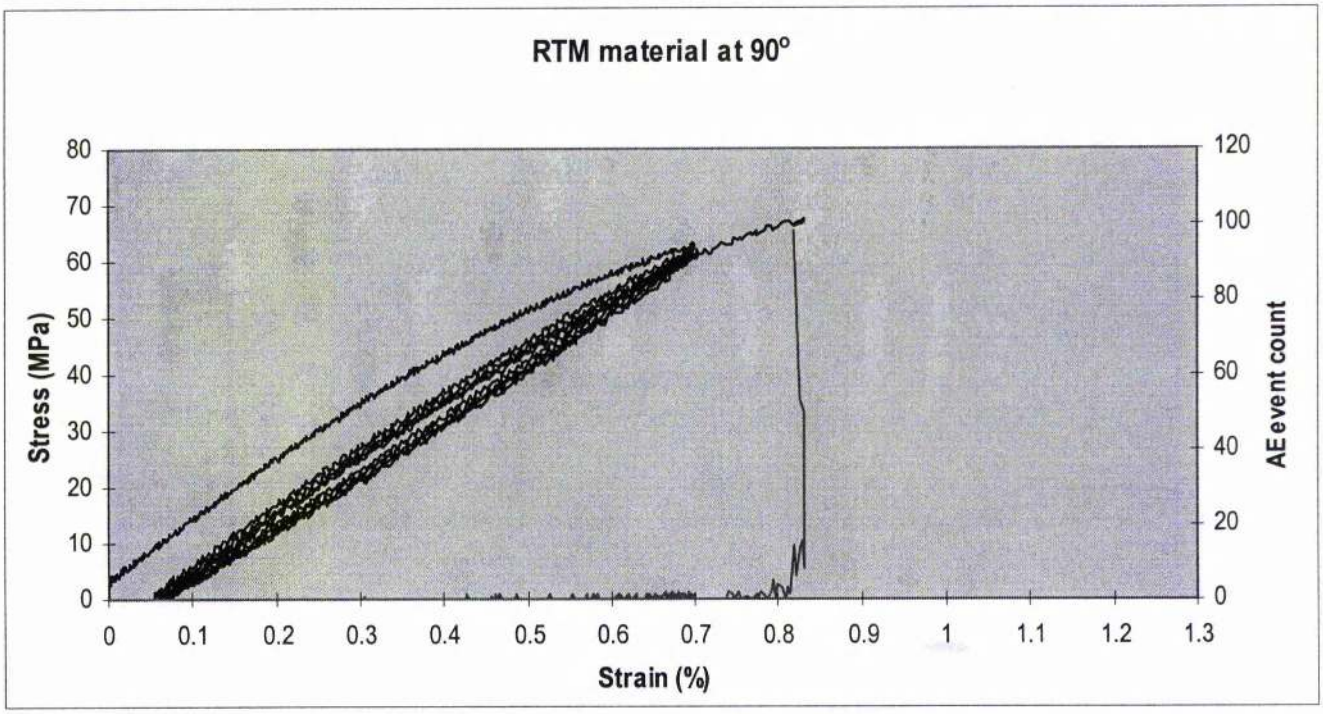

Figure 5.58.- Cyclic stress-strain curve for 4 layers RTM material at fixed strain for 90° direction.

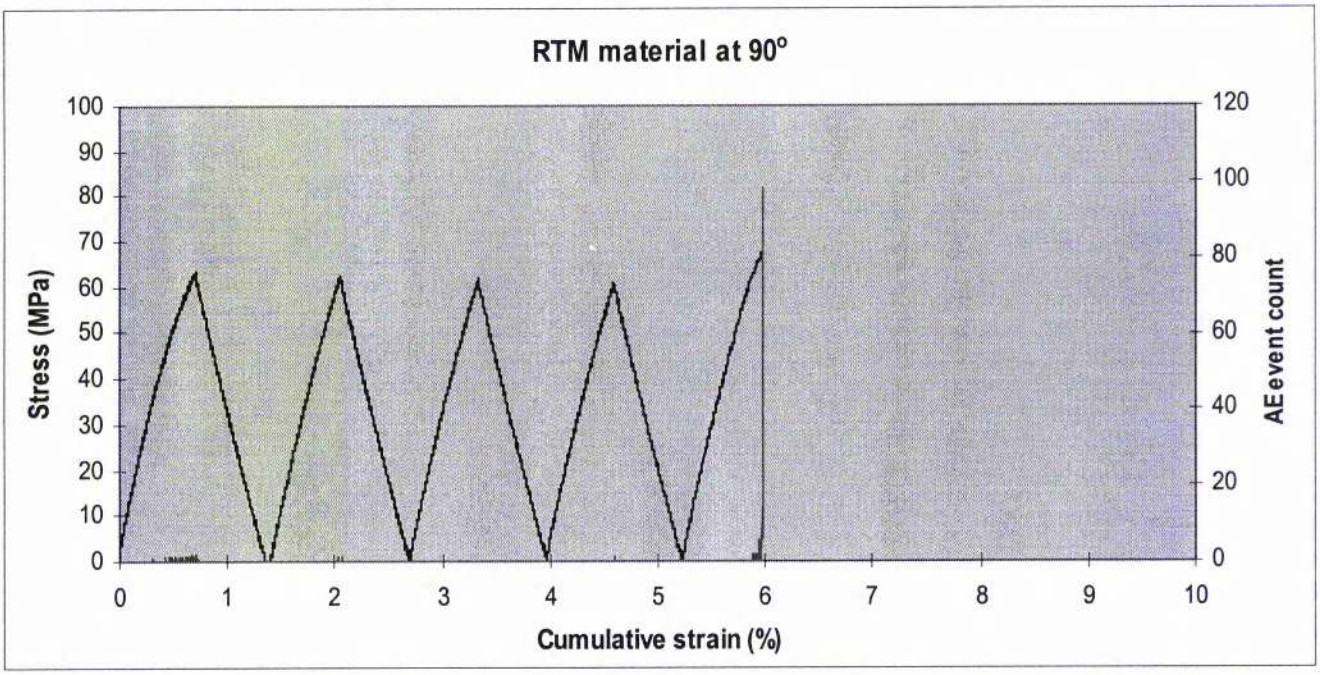

Figure 5.59.- Cyclic stress-time curve for 4 layers RTM material at fixed strain for 90° direction.

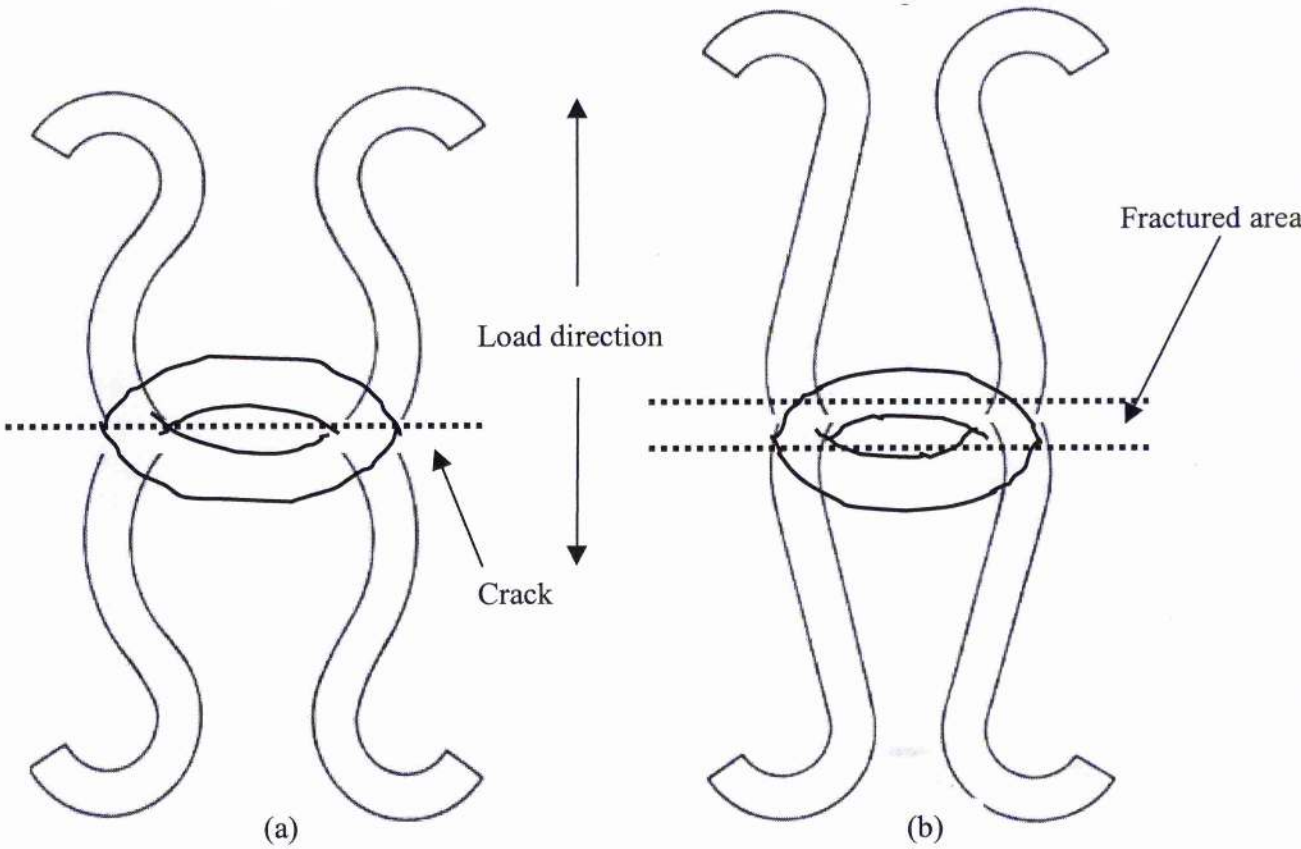

Figure 5.60.- Loop deformation in wale direction at (a) low strains and (b) high strains

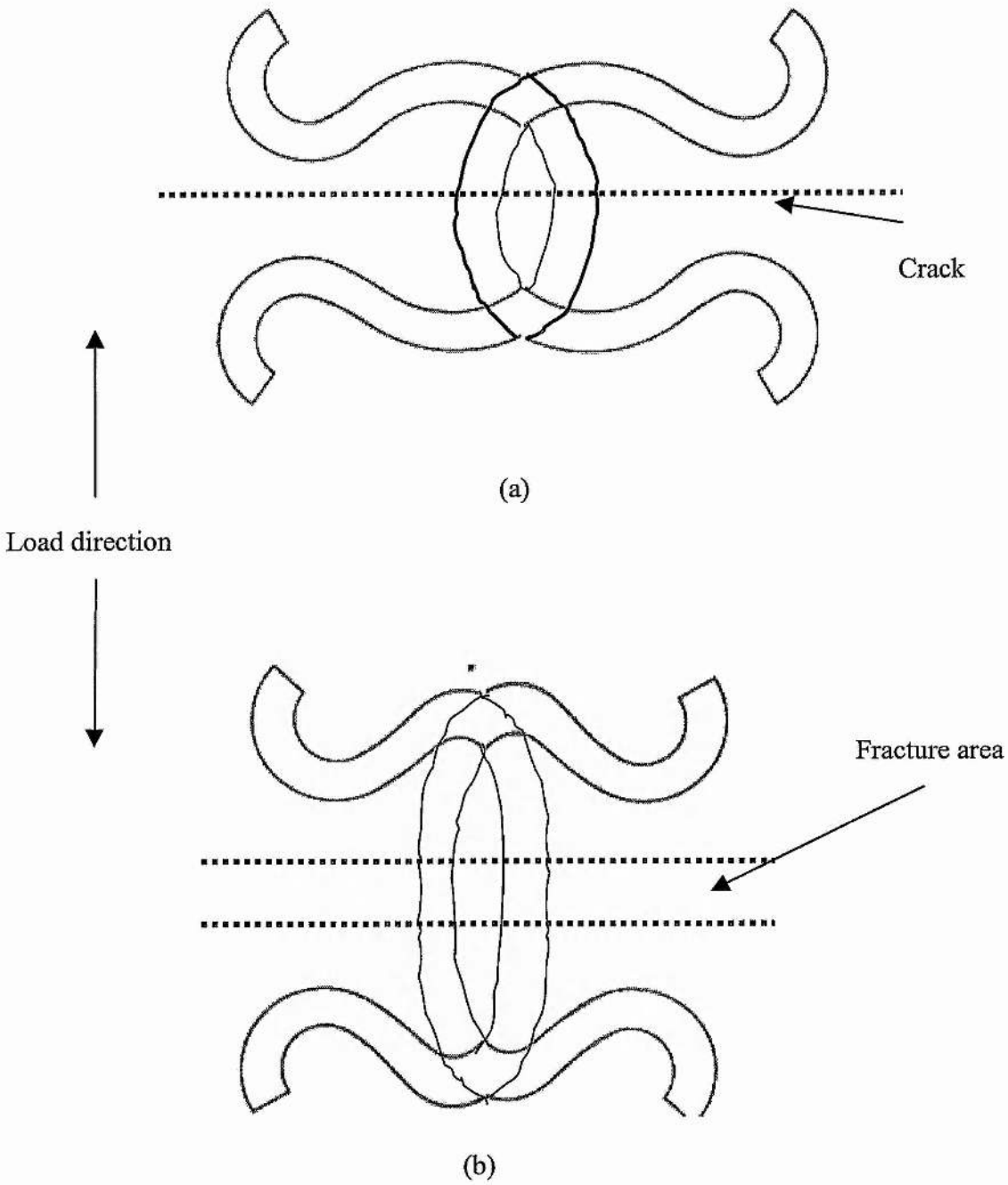

Figure 5.61.- Loop deformation in course direction at (a) low strains and (b) high strains

CHAPTER 6

RELATIONSHIP BETWEEN FABRIC ARCHITECTURE AND CRACKING DAMAGE DEVELOPMENT

6.1. INTRODUCTION.

Of particular interest in this work is the relationship of the complex fibre architecture of the knitted fabric composite to the damage accumulation under load. Earlier chapters have described this relationship at a macroscopic level. In this chapter, a more detailed study is presented of cracking development in relation to the knitted fabric architecture. The two principal material directions, wale and course, were investigated since they represent the two extremes in the orientation of the knitted fabric.

6.2. DAMAGE DEVELOPMENT IN MODEL SANDWICH LAMINATE MATERIAL.

Figures 6.1a and 6.1b show a plan view of the model sandwich specimens wale and course near failure where the difference in the cracking pattern is evident. As already mentioned (see Chapter 4), the cracks in the wale specimens develop initially with a crack spacing of about 4 mm, but subsequent loading produces a saturation crack spacing of about 2 mm, although occasional short cracks do initiate between the major cracks. The course specimens, on the other hand, show a much smoother increase in crack density up to coupon failure.

Figure 6.2 shows examples of the crack development in the wale direction specimens which has been discussed at length in Chapter 4. Figure 6.3 shows a polished section of such a specimen a crack saturation. This section is parallel to the loading direction and therefore the crack planes are perpendicular to it. In this view, the cracks can be seen every 2 mm. It should be noted that the repeating pattern of the fabric (every 4 mm) can not be seen clearly since a small misorientation of the polished surface allows different parts of the loops to be seen.

The micrographs show the large resin rich areas of the central (knitted fabric) part of the model sandwich laminate. Cracks labelled A to D can be seen and these cracks have an average crack spacing of 2mm. Such crack spacing is consistent with cracks forming at needle and sinker loops in the Milano fabric architecture (see Figure 4.1). It is possible to observe that the cracks are running from the tow/matrix interfaces and that they then propagate into the resin-rich regions (Figure 6.3).

Figure 6.4 shows examples of the crack development for the course direction test. At about 0.9 % strain (Figure 6.4a) it is possible to observe black spots in the photograph which appear at the cross-over points of the loops, as discussed in section 4.4.2. A cross-sectional view of such a course specimen taken to a strain close to failure and viewed parallel to the loading direction, Figure 6.5, shows that the average crack spacing is about 1 mm. This is consistent with the spacing of the sides or legs of the loops and is discussed in more detail in the following section. Figure 6.5 also suggests that, in general, the cracks in the course specimens do not extend in a planar manner across the knitted fabric layer. This effect, when viewed in the plan view (eg Figure 6.4), gives rise to the appearance of crack branching.

6.3. RELATIONSHIP BETWEEN KNITTED FABRIC ARCHITECTURE, DAMAGE AND COMPOSITE CROSS-SECTIONS FOR THE MODEL SANDWICH LAMINATE MATERIAL

Examination of micrographs from different planes of specimens loaded to different strains enabled the identification of each one of the tows forming the geometry of the knitted fabric with its appearance in a composite section. For example, Figure 6.6 shows a portion of the knitted fabric composite taken perpendicular to the wale direction. The course labelled number 1 indicates the rib, which holds the courses 2 and 3. This micrograph shows clearly that the repeating unit of the fabric occurs every 2mm. Figure 6.6b shows a micrograph of the corresponding portion of the fabric itself where each tow has been labelled in accordance with the schematic figure shown in Figure 6.6c. Note that the viewing direction of Figures 6.6a and 6.6b is indicated in Figure 6.6c. In Figure 6.6c, the front face and back face loops (courses 2 and 3) are clearly visible and connected by the rib (course 1).

The complexity of the structure shows that great care is required in the interpretation of micrographs such as Figure 6.6a. However, it is possible to identify the courses in such a micrograph and to label them in the same way. Figure 6.7 shows a different plane but the same viewing direction. In this case, the section of the rib course 1(head or needle of the loops), which holds courses 2 and 3 together, is visible as before, but the appearance of courses 2 and 3 is quite different.

Having interpreted the microstructure of the knitted fabric as seen in sections from the model sandwich composites, it is now possible to make a rigorous analysis of micrographs of tested coupons to relate the crack initiation and development to the structure of the knitted fabric. Figure 6.8 shows, for example, how the cracks are developed when the sample is tested in the wale direction. The fabric in this view is seen from the course direction (which is parallel to the loading direction) so the cracks run parallel to the course direction.

Figure 6.8a shows a section from a specimen in which the cracks were spaced 4 mm apart; it was found that at this stage, crack development occurs between courses 2 and 3. These locations are represented in Figure 6.8c by dotted lines. Crack initiation here is not surprising. In this plane, courses 2 and 3 are close together and can touch, giving raise to high strain magnifications between the tows. At higher applied strains the cracks are spaced every 2 mm as in Figure 6.8b. Dashed lines in Figure 6.8c represent a second set of cracks which are propagated along the line where course 1 is holding either course 2 or 3, giving the final crack pattern of about 2 mm.

In Chapter 4, it was frequently pointed out that matrix cracking was preceded by predamage in the form of cracking, perhaps better called microdebonding, at the loop cross-over points. Such damage appears as black spots in plan view photographs of the specimens (eg Figure 4.45). Figure 6.9 shows evidence of such microdebonding at a cross-over between two yarns. This wale direction sample (ie the wale direction is in the direction of loading and parallel to the outer 0^0 plies) had been loaded to a strain of 0.9% which is just below the onset of matrix cracking.

With the aid of these micrographs, it is possible to review the progression of damage for loading in the wale direction as follows. Crack initiation begins with debondings, or predamage, at the loop cross-over sites and each of these sites is a potential crack initiator. The first main cracks initiate in those places where the float stitches of courses 2 and 3 are in close proximity and cracks form here preferentially due to the strain magnification. These positions are shown by the dotted line in Figure 6.10. At higher strains, additional yarn/matrix debonding starts to appear at interfaces marked A or B in Figure 6.10, which is where course 1 holds threads 2 and 3. These debonds coalesce together forming a small crack without further propagation. Since course 1 crosses horizontally between the front face and the back face of the fabric, points A and B are in fact, in the same plane. Hence, cracks with a 4 mm spacing initiate in the plane where courses 2 and 3 are proximate (the plane of the dotted line going through point C in Figure 6.10). When these sites have been used, then cracks develop at points where course 1 holds courses 2 and 3 (points A and B), to give a final crack spacing of approximately 2 mm.

Considering now the course direction specimens, an edge section from a sandwich laminate specimen which has the knitted fabric loaded in the course direction is shown in Figure 6.11a. In this case, the specimen is viewed from the same direction as in Figure 6.6b. In this plane, the repeat spacing of the pattern is 2mm and the cracks grow parallel to the sides (legs) of the loops. At certain point they try to follow the twisted yarns and hence appear to be branched when viewed from the direction shown in Figure 6.4. The dotted lines in Figure 6.11b indicate the cracking geometry. Again course 1 corresponds to the rib holding courses 2 and 3. For loading in this direction, cracks initiate at the legs of the loops, and an initial characteristic crack spacing does not appear. However, eventually the crack pattern will approximate to the spacing of the legs of the loops which is about 1 mm

Finally, analysis of a course sample loaded to a strain of 0.7%, which is just below the onset of matrix cracking in these specimens (which occurs at about 0.8%) provided further evidence of early damage initiation in the form of cracking at the loop cross-over points. Figure 6.12 is a section from a course specimen with the section taken perpendicular to the applied load. As indicated earlier, it is possible to identify the various courses in such sections and these have been labelled course 1, 2 and 3 on the figure. This micrograph shows clearly the predamage, or microdebonding, at cross-over points between course 1 and courses 2 and 3.

6.4.- RELATIONSHIP BETWEEN KNITTED FABRIC ARCHITECTURE, DAMAGE AND COMPOSITE CROSS-SECTIONS FOR THE RTM MATERIAL

The establishment of the relationship between the architecture of the knitted fabric and damage in the model sandwich laminate composites was made easier because of the transparency of the matrix and the low fibre volume fraction. On the other hand, the commercial RTM material was more difficult to analyse since the Derekane matrix is not transparent and the fibre volume fraction was over three times higher. Despite these difficulties, some progress was made in relating the damage to the fibre architecture.

The wale direction specimens give the clearest cracking patterns in the model sandwich specimens and so it was decided to investigate the same loading direction for the RTM specimens. The analysis of the geometry of the knitted fabric was carried out by inspection of polished sections from both transverse and longitudinal directions for the wale (0^{o}) direction taken from fractured samples of five layers composites. The definition of the transverse and longitudinal sections is shown in Figure 6.13.

Figure 6.14 shows a micrograph through the full thickness of the commercial RTM material viewed using the longitudinal section. The individual layers of cloth are numbered 1 to 5 and, as has been mentioned earlier (see Chapter 5), the layers do not remain flat during manufacture. The labelled tows are in fact rib courses because these were the only courses it was possible to identify clearly. A view from the transverse direction of the same material is shown in Figure 6.15. Again the five layers can be seen through the thickness of the specimen, but it is too difficult to identify the individual courses of any one layer.

Although it was difficult to identify a regularity of cracking pattern, all samples from the RTM composites showed matrix cracking damage. In addition, debonding between yarn/matrix interfaces were also observed, as well as cracks which had propagated through resin-rich regions. Figure 6.16a, for example, shows matrix cracking which appears to extend into a microdebonding region between two yarns. Figure 6.16b shows what appears to be microdebonding, possibly at loop cross-over points. Figures 6.17a and 6.17b show similar regions of cracking damage.

6.5. SUMMARY

The relationship between the knitted fabric architecture and damage was analysed using edge sections and microscopy. For the model sandwich laminates, both wale and course direction were studied microscopically and the geometry and structure of the knitted fabric was first analysed in order to identify the components of the cloth, such as the rib (course 1) and courses 2 and 3. Then the cracked sections were related to the architecture.

The crack patterns in specimens loaded parallel to wale or course directions were related to the fibre architecture. In particular, evidence for the predamage, or microdebonding, at the loop cross-over points has been found.

The commercial RTM material was difficult to analyse in the same way due to the high fibre volume fraction and the tendency for the fabric layers to be crushed out-of-plane during manufacture. However, some features of the knitted fabric architecture were identified and related with the cracking damage. In particular, there was evidence of a cracking pattern in the outer layers of the composites which approximated to both the crack spacing seen in the model sandwich laminates (ie cracks every 2 mm or every 4 mm) and in the surface layer of the RTM coupons as faint white lines with the same spacing. Also, the microscopy showed evidence of cracking at loop cross-over points, similar to that found in the model sandwich laminate material.

FIGURES

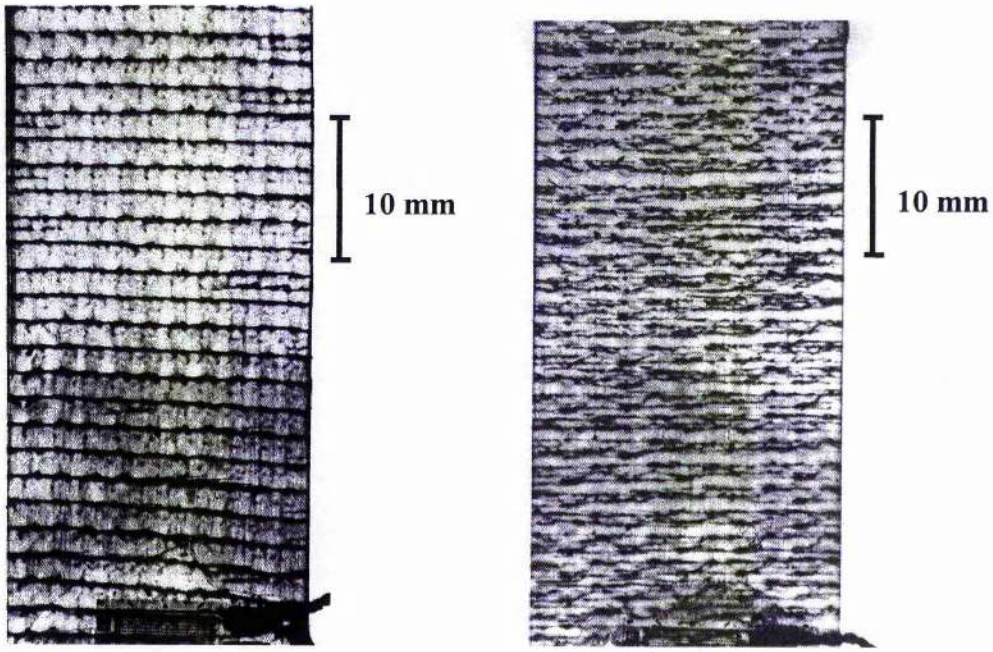

Figure 6.1.- Crack density prior to fracture. (a) wale specimen; (b), course specimen.

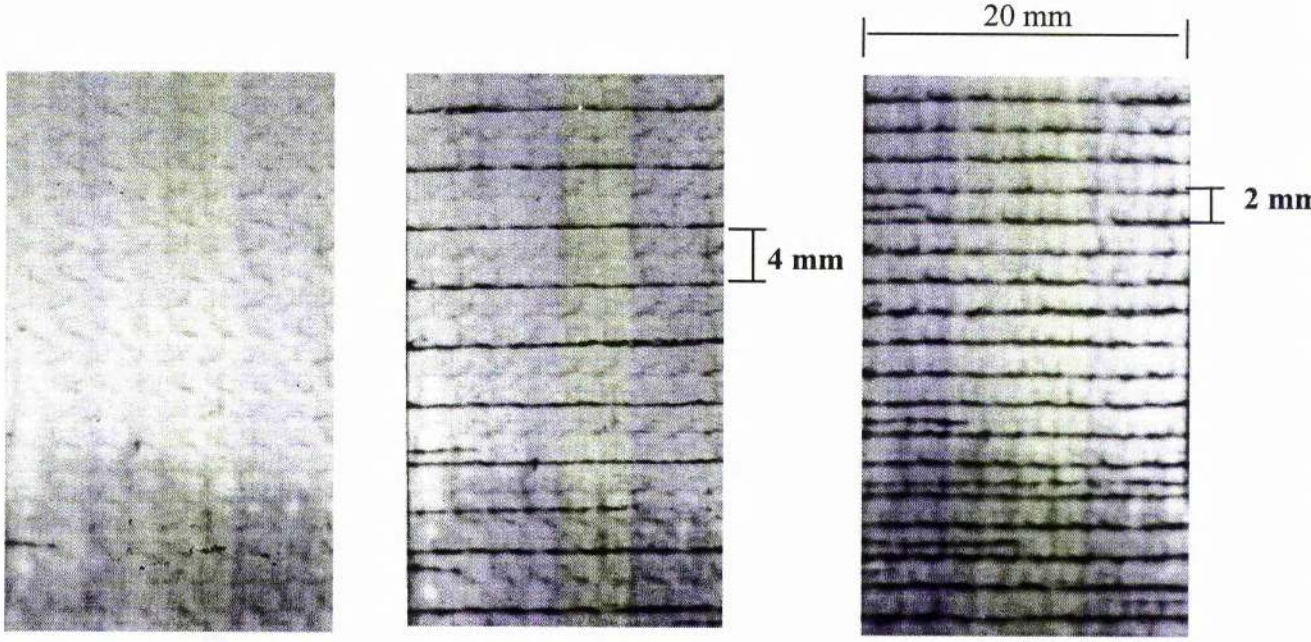

Figure 6.2.- Cracking developing along wale direction.

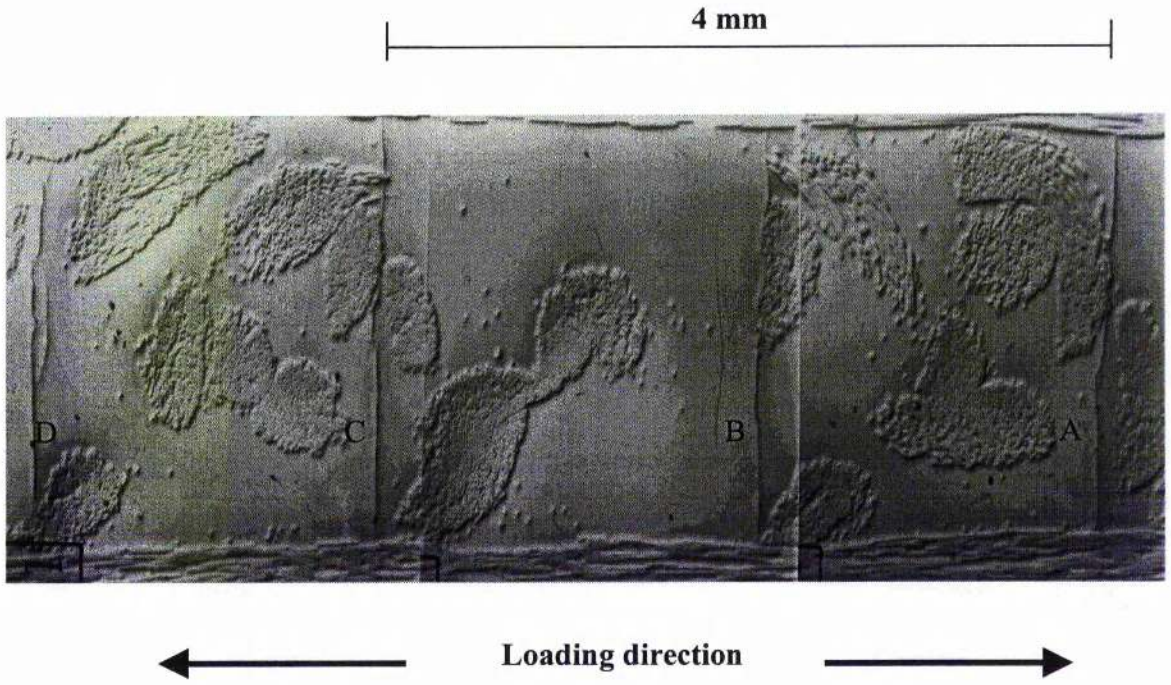

Figure 6.3.- Cracking pattern along sample in wale direction. Cracks can be seen at A, B, C, and D. Approximately 2 mm apart.

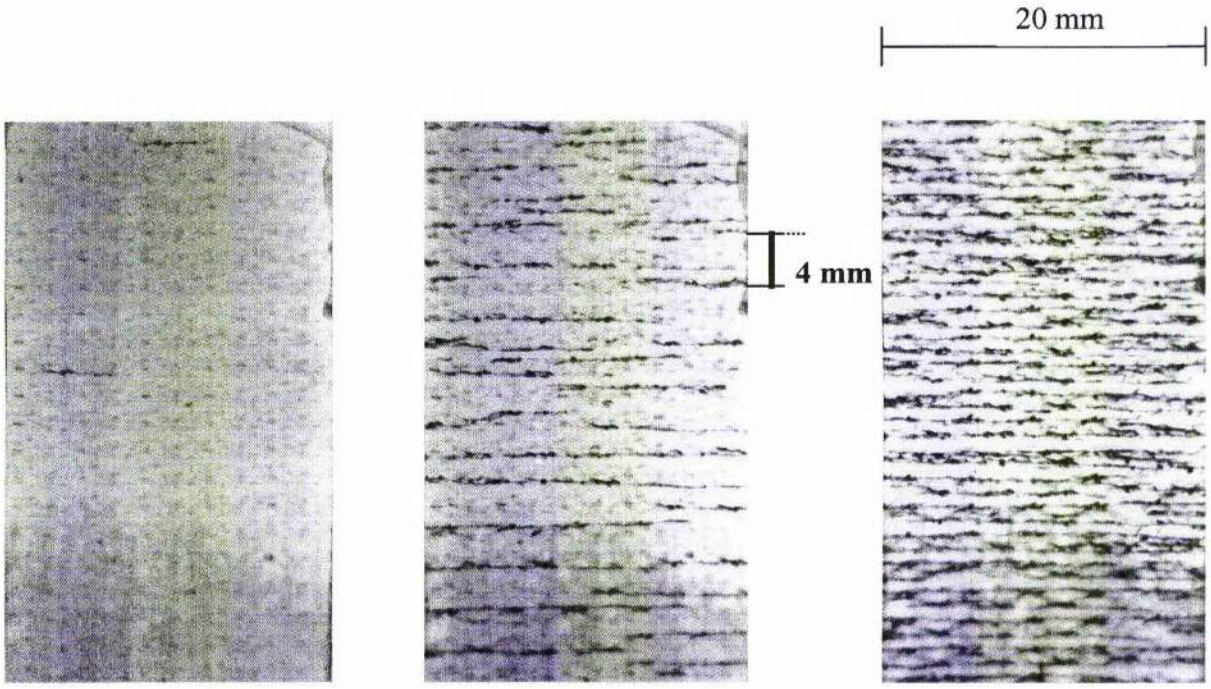

a) 0.9 % strain **b) 1.2% strain** **c) 2.0% strain**

Figure 6.4.- Cracking developing along course direction.

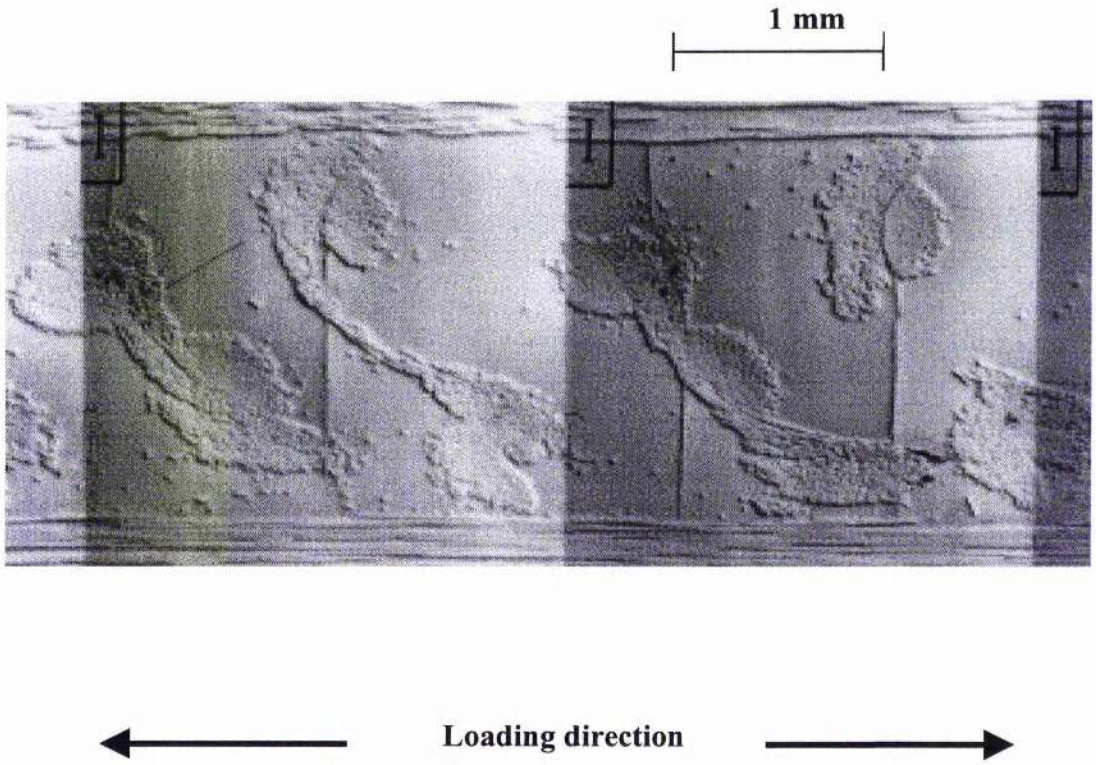

Figure 6.5.- Cracking pattern along sample in course direction.

Figure 6.6.- The structure of the knitted fabric composite- perpendicular to wale direction.

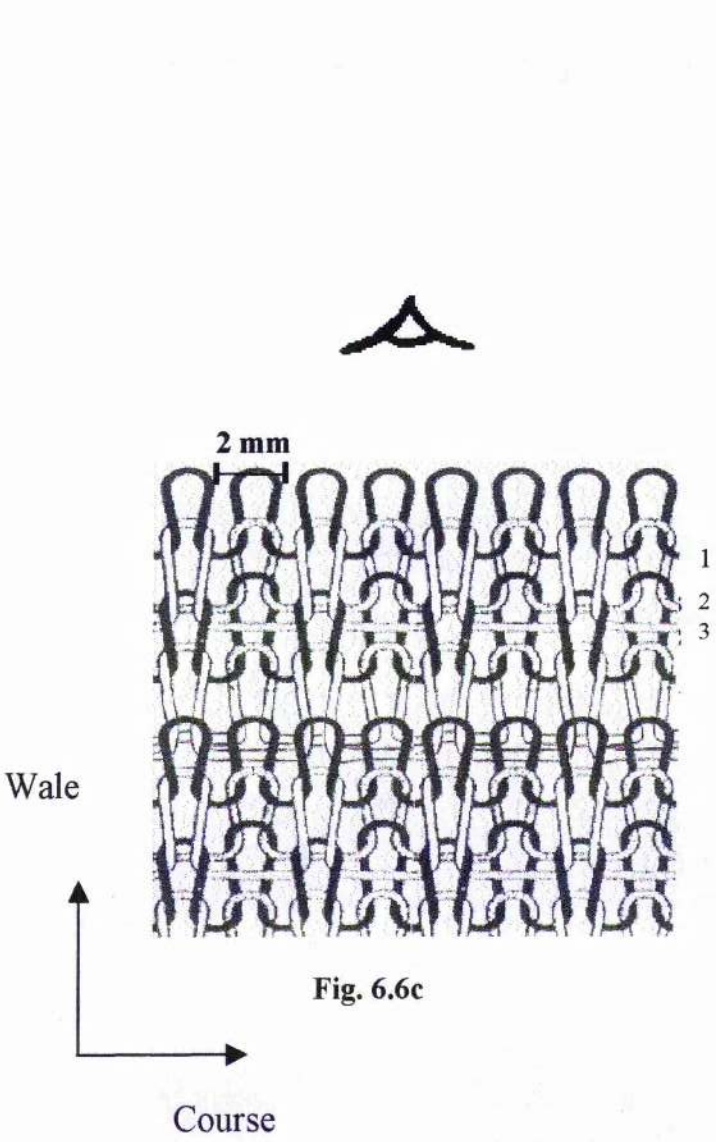

Fig. 6.6c

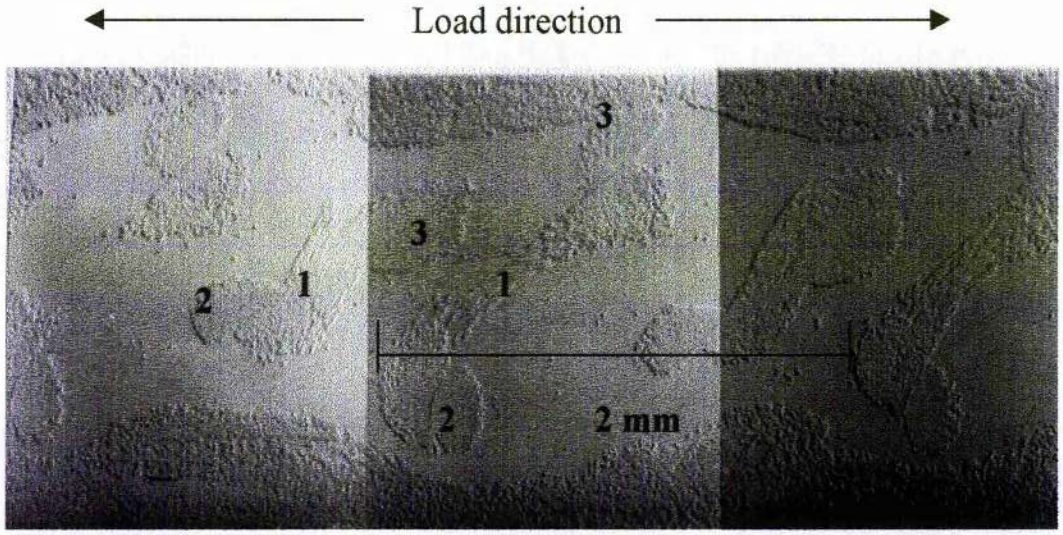

Fig. 6.6a

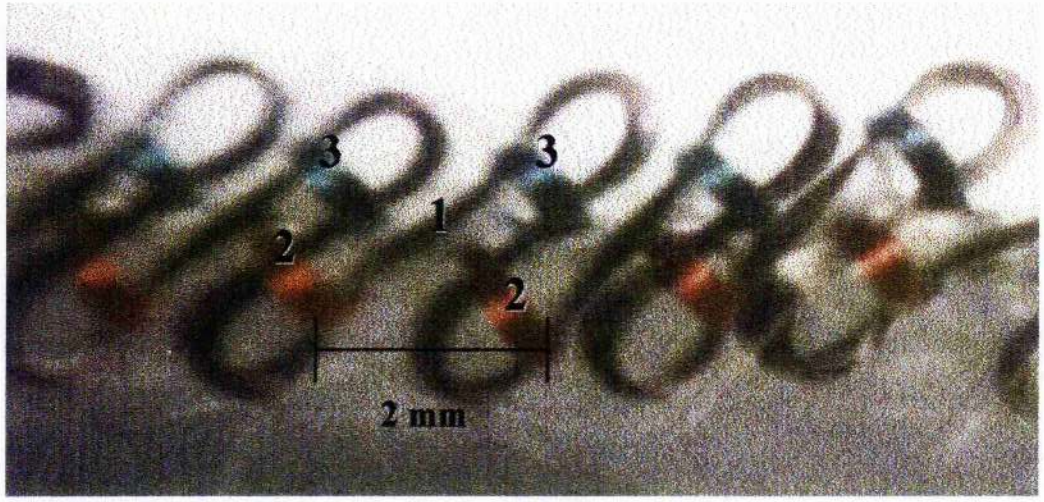

Fig. 6.6b

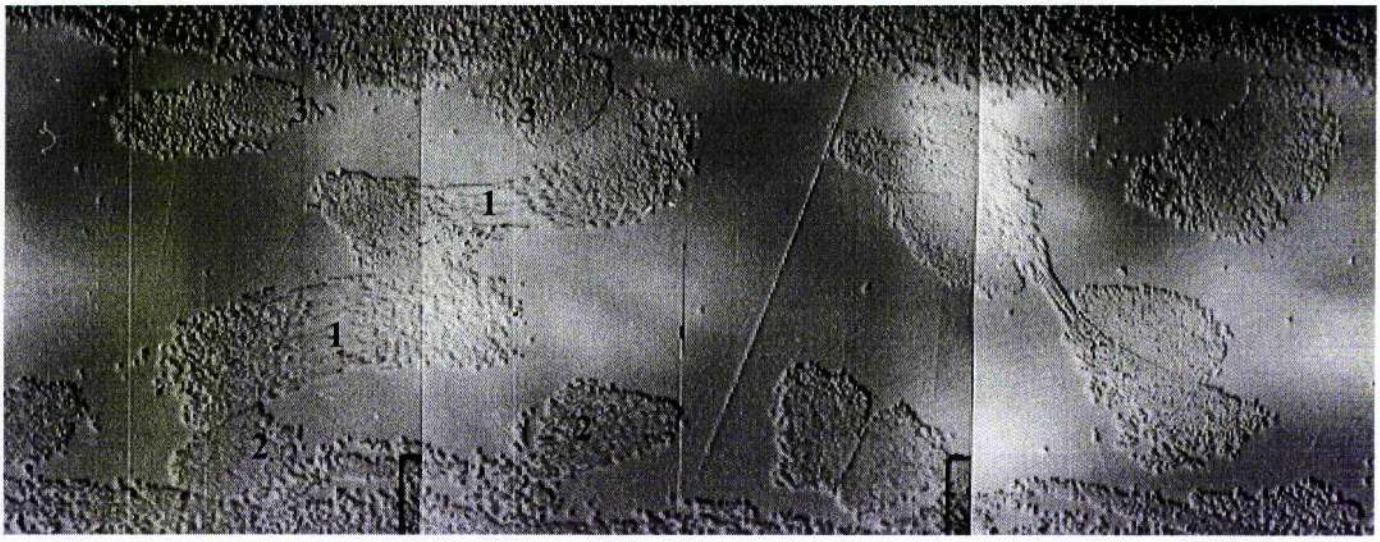

Figure 6.7.- Wale transversal section. The black single course (1) is holding together both sides of the fabric (courses 2 and 3). They are not superimposed as it is suggested by course 1.

Figure 6.8.- Cracking development in samples tested in wale direction.

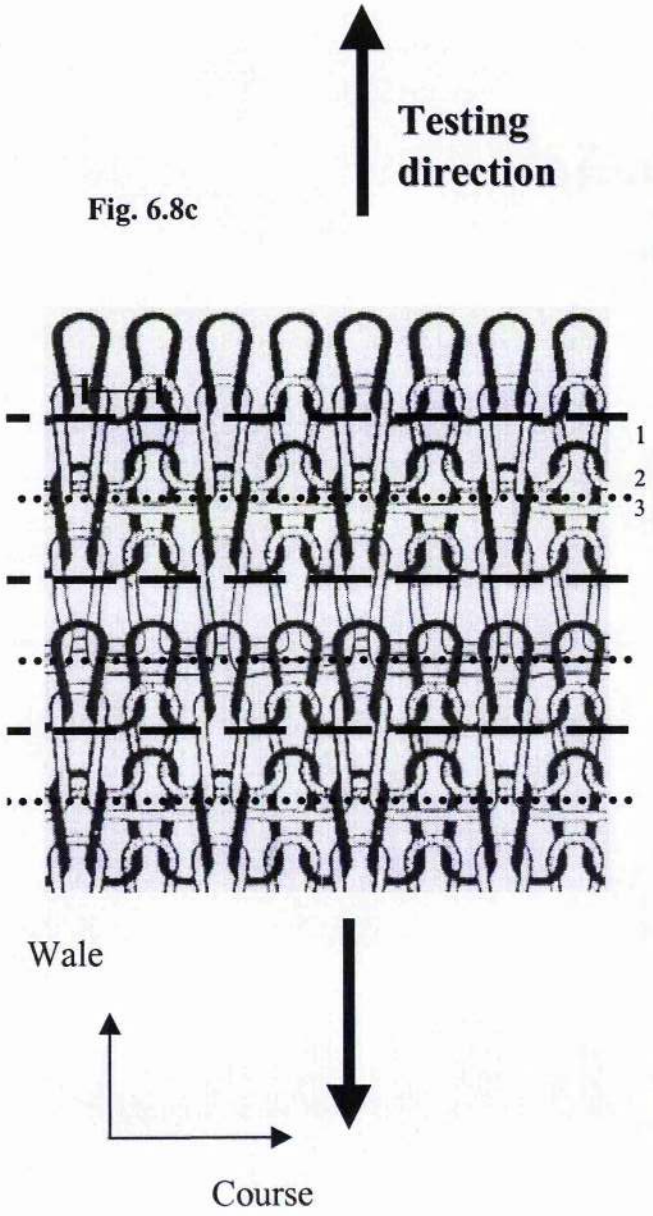

Fig. 6.8c

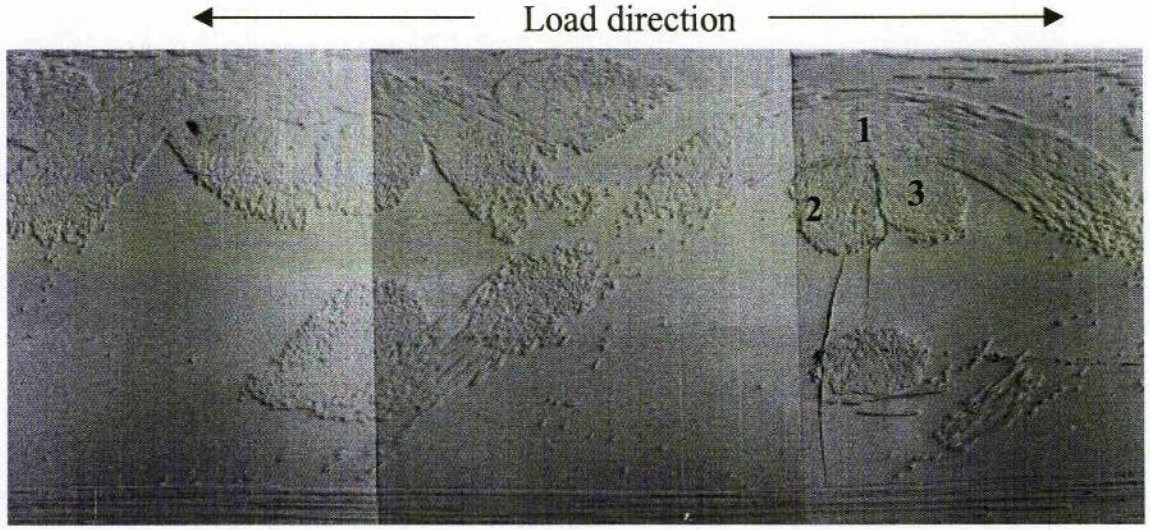

Fig. 6.8a

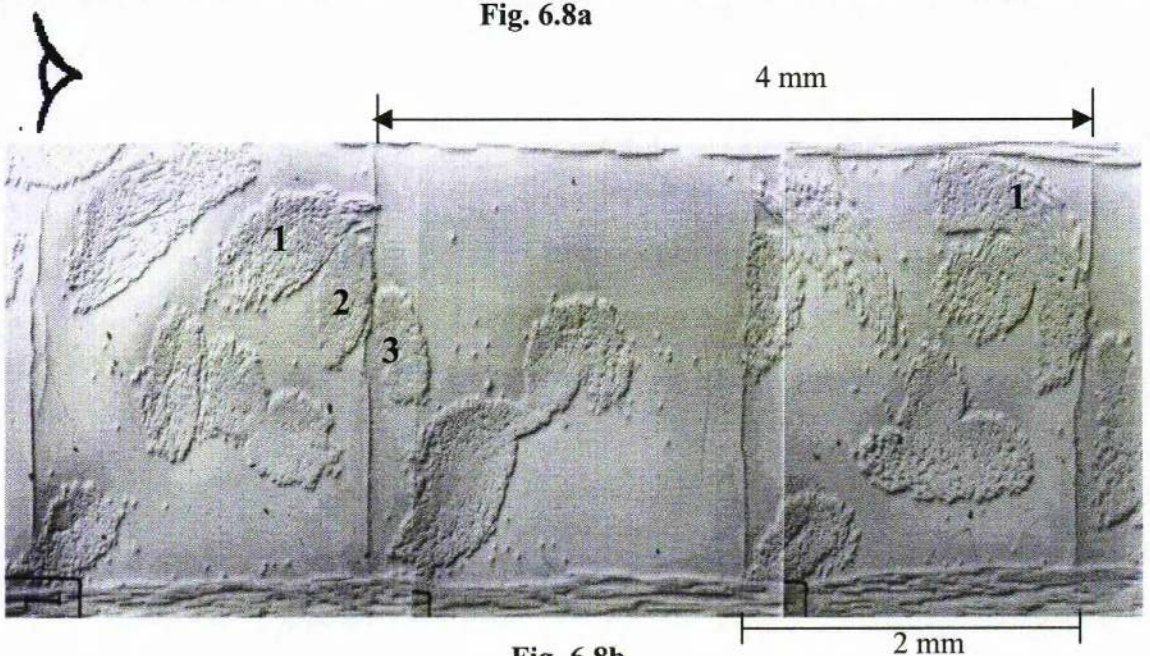

Fig. 6.8b

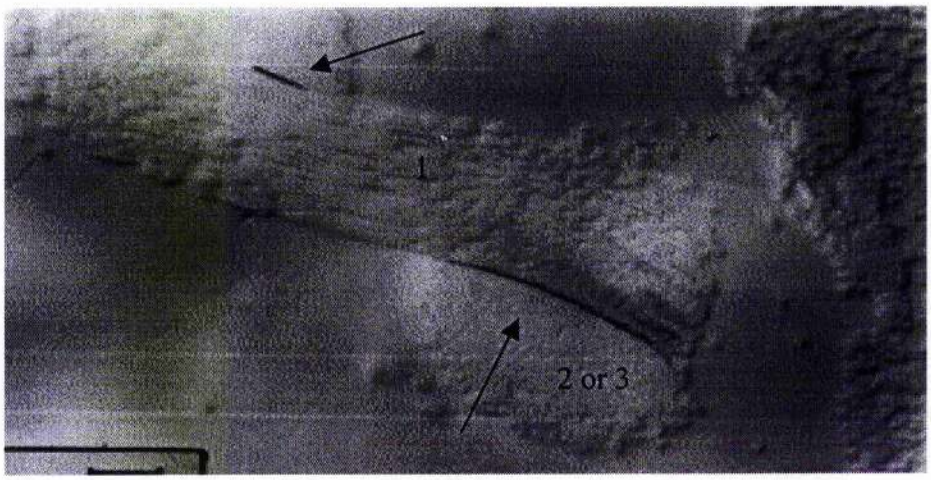

Figure 6.9.- Photographs showing microdebonding in samples tested in the wale direction.

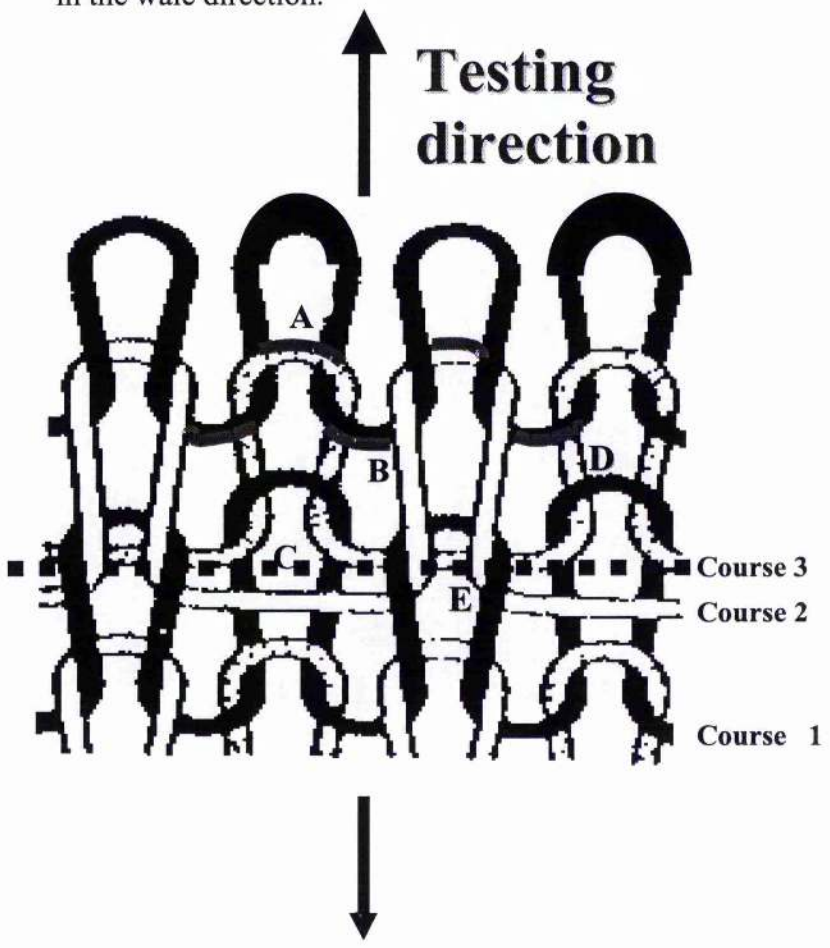

Figure 6.10.- Schematic of the fracture process in wale direction.

Figure 6.11.- Cracking development in samples tested in course direction.

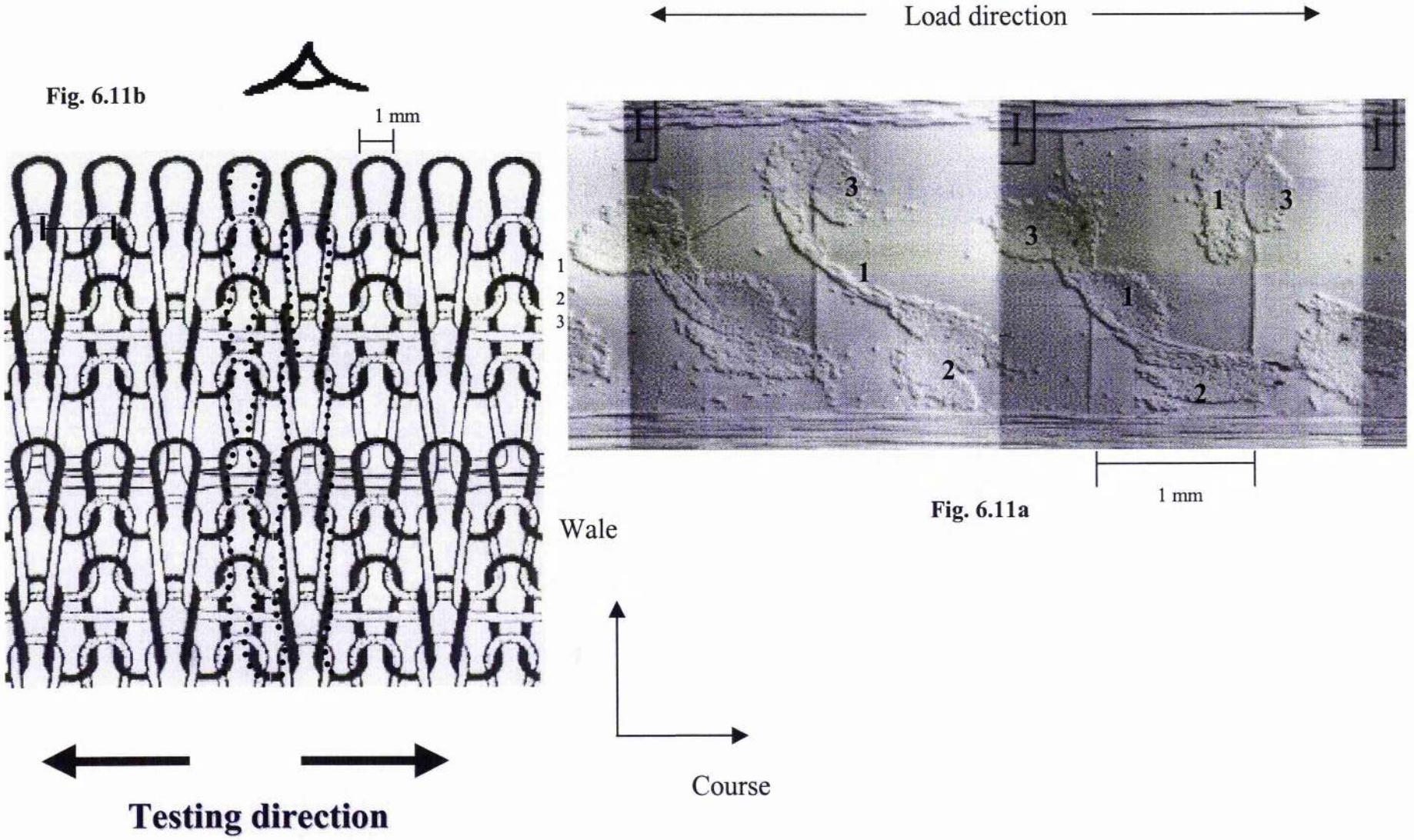

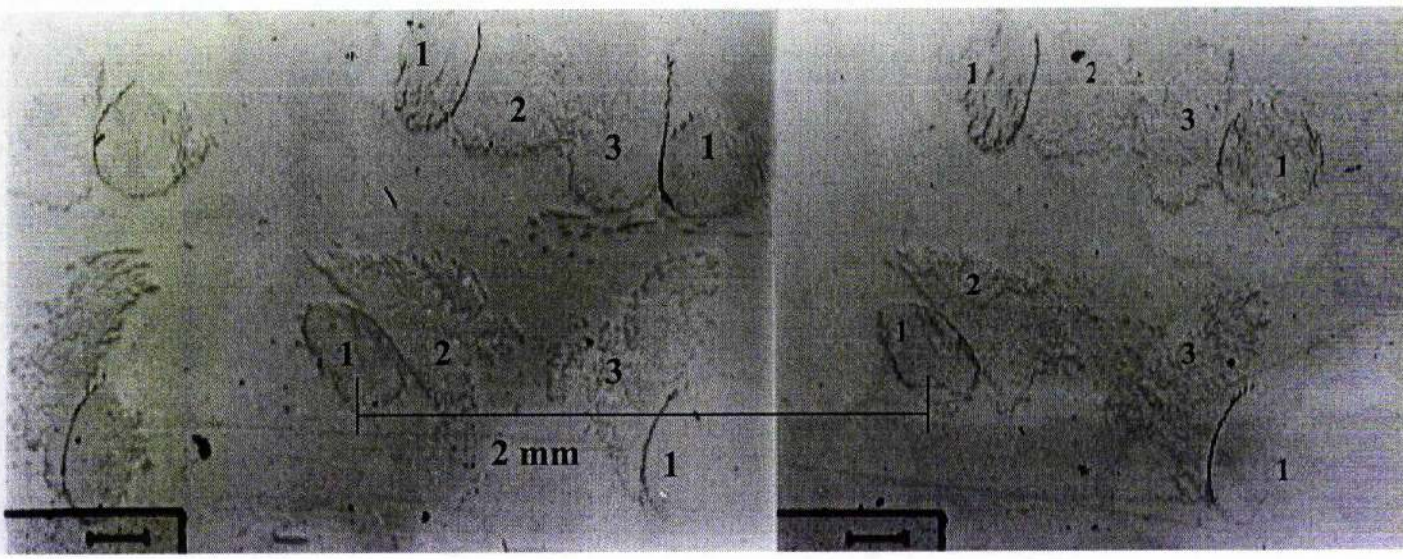

Figure 6.12.- Photographs showing microdebonding in the cross-over sites in a course sample loaded to 0.7% strain. Numbers correspond to each thread in the knitted fabric. Course direction sample, transverse section.

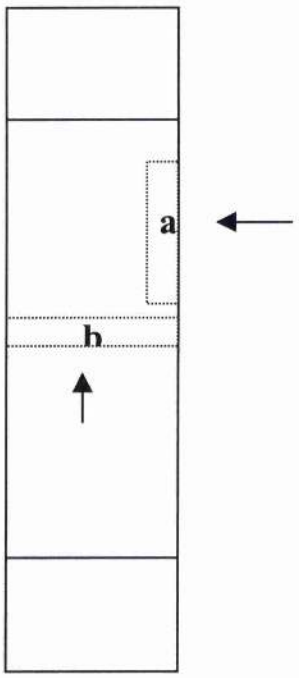

Figure 6.13.- Scheme of the pieces taken for the sample for polishing and microanalysis. a) indicates longitudinal direction, b) indicates transversal direction. Arrows indicate plane of view.

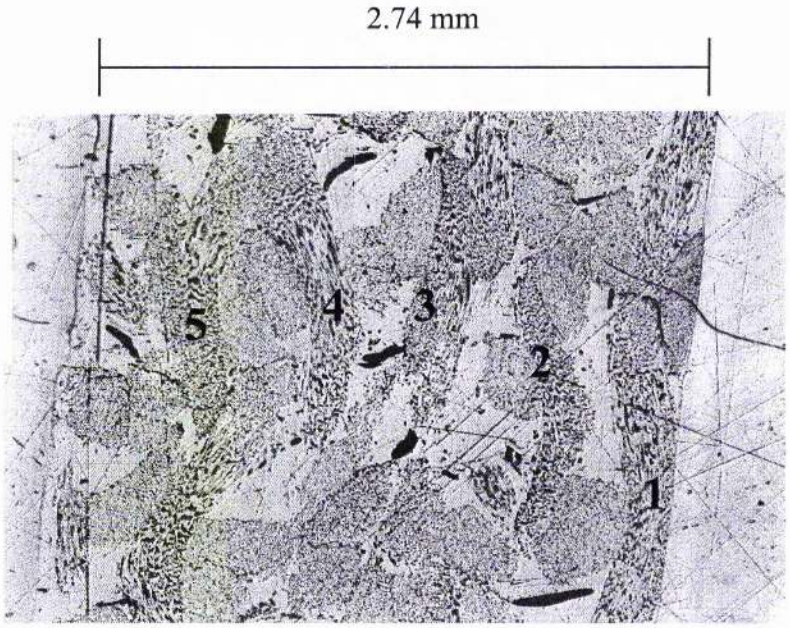

Figure 6.14..- Microphotograph showing the five threads. Sample: wale, longitudinal direction.

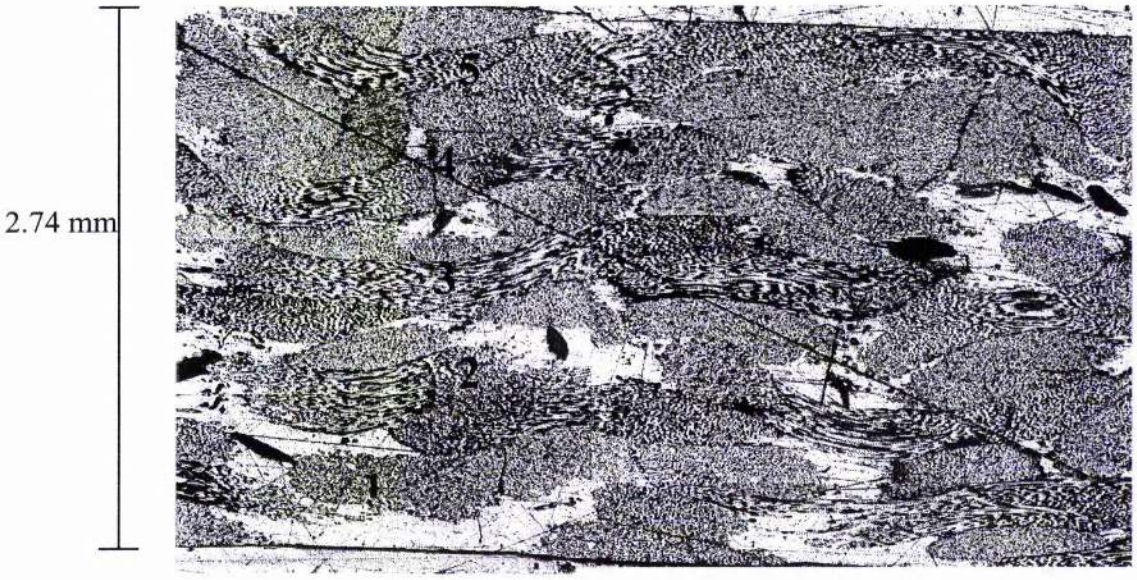

Figure 6.15..- Microphotograph showing the five threads, which can be identified and related to the knitted fabric geometry. Sample: wale, transversal direction.

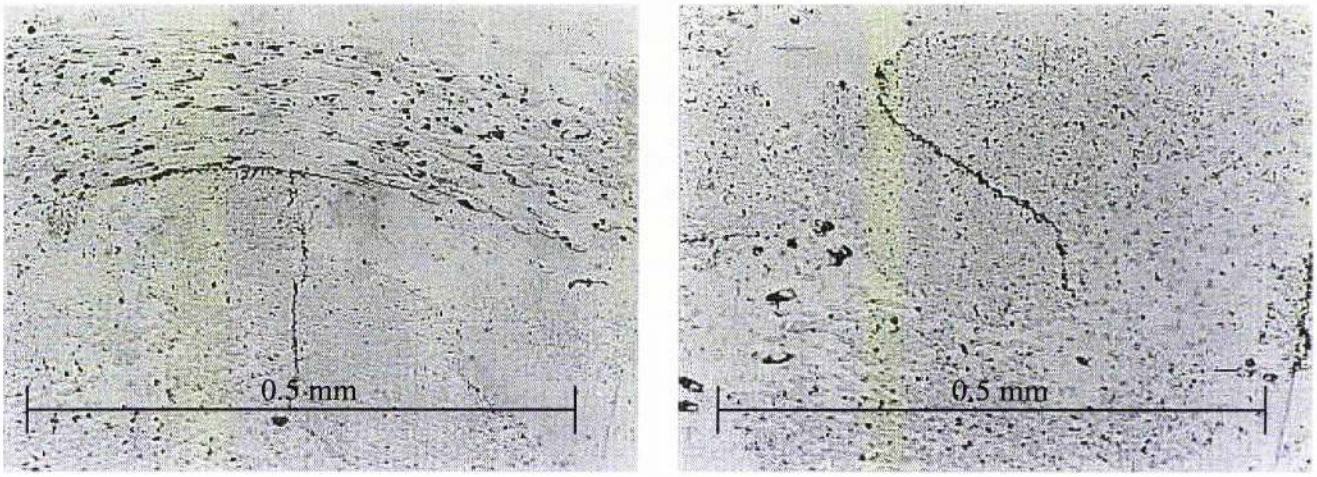

(a) (b)

Figure 6.16.- 0^{o} (wale direction) polished sample in (a) longitudinal and (b) transverse section.

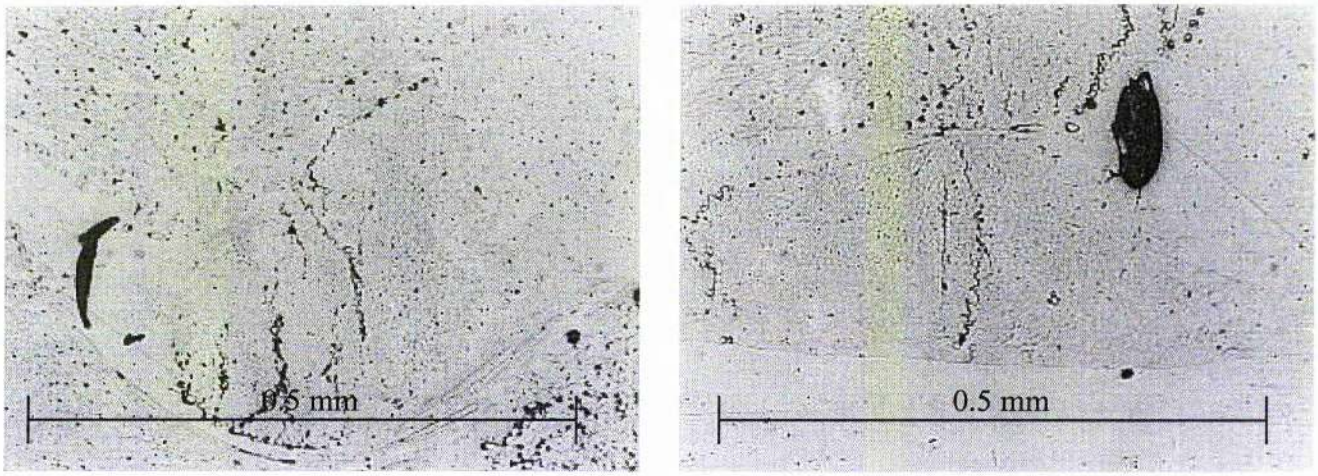

(a) (b)

Figure 6.17.- 30° polished sample in (a) longitudinal and (b) transverse section.

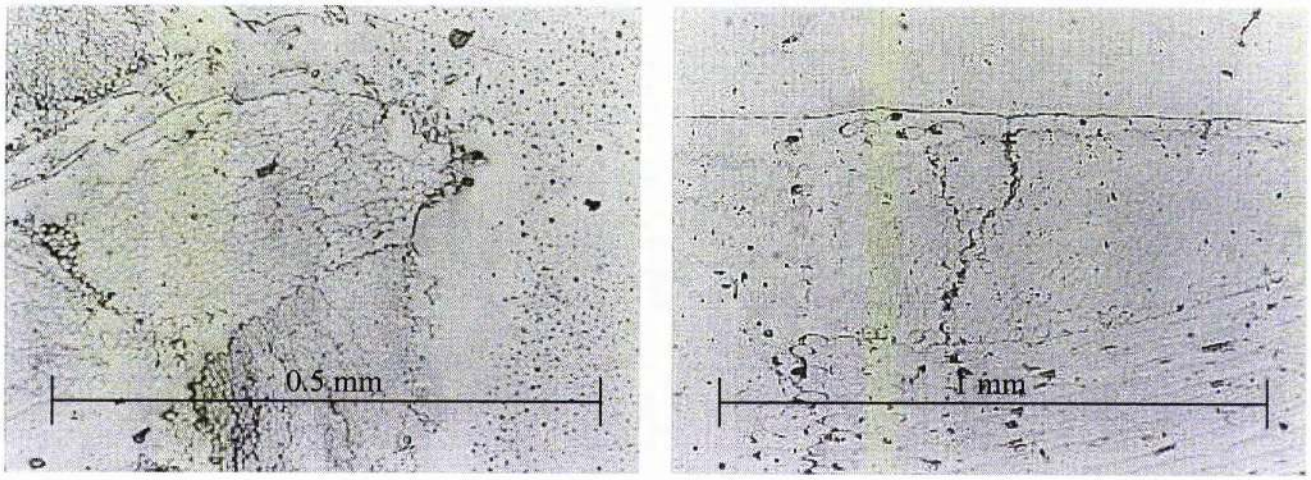

(a) (b)

Figure 6.18.- 45° polished sample in (a) longitudinal and (b) transverse section.

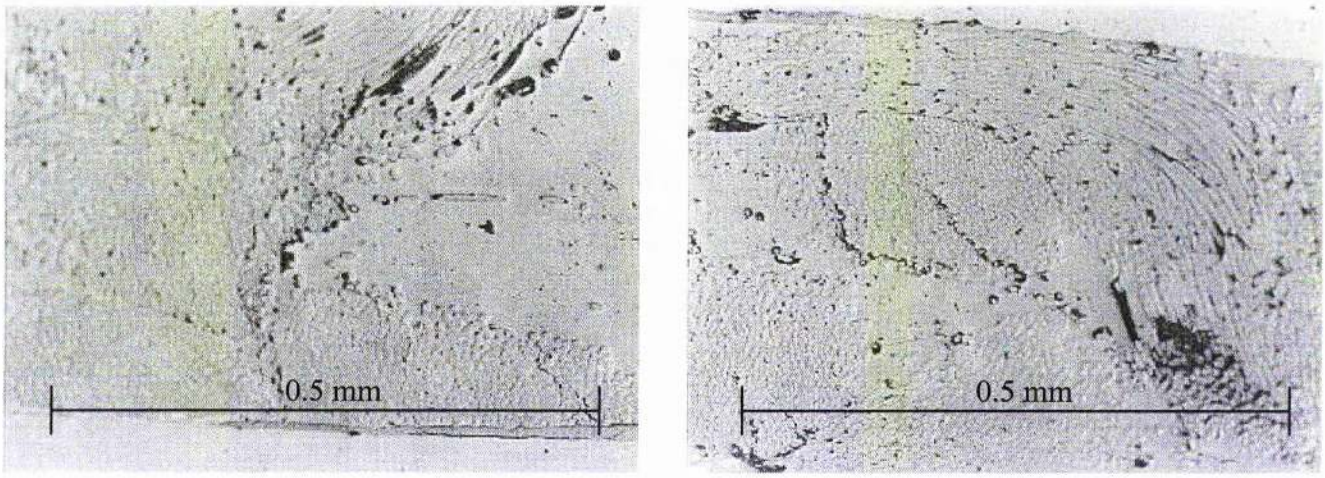

(a) (b)

Figure 6.19.- -45° polished sample in (a) longitudinal and (b) transverse section.

CHAPTER 7

CONCLUSIONS AND FURTHER WORK

7.1.- CONCLUSIONS.

Milano weft-knitted fabric, produced from E-glass yarns of 2x68 tex, was used to manufacture single layer knitted fabric composite panels. Specimens from these panels were tested under monotonic loading with the specimens cut at a range of angles to the wale (0^0) direction. The stress, strain and acoustic emission activity were monitored during loading and the transparent coupons enabled damage accumulation to be observed.

All the stress-strain results showed a small non-linearity for single layer samples tested at different orientations. From these results it was observed that the glass fabric/epoxy coupons failed suddenly and catastrophically when the first damage initiates, with the consequence that there was no acoustic emission activity recorded until very close to failure. It was clearly observed from the results that the Young's modulus and tensile strength are both higher close to the wale direction, as would be expected from a two-dimensional analysis of the loop shapes (this analysis was carried out to determine the orientation of the reinforcement due to the loop architecture). On the other hand, the Poisson's ratio and strain to failure were reasonably independent of the angle of loading.

Difficulties in analysing damage propagation in the single layer material were encountered due to the premature failure of the material. It was observed that the single layer samples failed catastrophically with the first sign of cracking without any prior indication of damage in the coupon. Therefore the accumulation of damage was impossible to monitor in this material.

A model material made up using a novel technique consisting of unidirectional glass fibre (0^0) plies, with the knitted fabric between the outer plies, was employed as a viable option to allow the knitted fabric composite to develop damage initiation and propagation. Analysis using this model material included tests on the 0^0 plies alone and tests where the knitted fabric within the sandwich laminate was oriented at different angles to the loading direction. These model sandwich laminates enabled the damage behaviour and failure mechanisms to be related to the angular orientation of the fabric.

A detailed examination by microscopy enabled the relationship between the fabric geometry and damage initiation to be found, using at the same time the acoustic emission technique to support the investigation. Two important methods for treating the data were introduced. Firstly, a methodology was introduced for extracting, from the results on the model sandwich panels, the stress-strain behaviour of the knitted fabric layer itself. Using this method, the onset of matrix cracking appeared in the stress-strain curve as a sharp discontinuity. Also, it was observed that precracking damage (which occurred at the loop cross-over points before matrix cracking begins) does not affect the derived stress-strain curves and that only the matrix cracking damage produces such an effect. Secondly, it was shown that a reduction in the Poisson's ratio occurred at the strain when matrix cracking began.

The sandwich laminates were used to investigate damage accumulation and hence their mechanical properties were not of particular significance since these parameters were dominated by the unidirectional fibres. However, their transparency enabled the following observations to be made. Firstly, the observed predamage in the knitted fabric layer was identified for the first time to be damage occurring at the loop cross-over points. Other authors have speculated that the first damage occurs around the head or needle of loops, but this work has shown the loop cross-over points to be the sites of the first damage. Debonds at the yarn/matrix interface develop from these sites and it has been shown that the most important sites for the further development of the damage are the fabric planes where the float stitch of courses 2 and 3 are held together by the rib stitch (course 1). This is probably because of the strain magnification here.

The influence of the knitted fabric architecture in determining the damage development in the composites was also shown in the results. The angle of the fabric to the loading direction determines whether damage is dominated by the head (or needle) of the loops, or by the legs of the loops.

During cyclic tests of the model sandwich laminates, the stress-strain behaviour was found to be linear elastic up to the onset of cracking. After this point, unloading produced a residual strain, due to the relaxation of the thermal residual strains in these laminates. Burning off the matrix from fractured samples showed that there was no tow fracture suggesting that fibre tows bridge the matrix cracks without fracturing except in the area of final failure of the coupon.

Following the tests on the single layer composites and the model sandwich laminates, two types of high volume fraction commercial RTM composites were analysed which had the same fabric architecture but a different matrix. Considering first the mechanical properties, the highest Young's modulus was found for 0^0 and 30^0 directions, although the highest strength is in the 0^0 direction in both cases. These results are consistent with the results for the single layer material. In addition, it was found that the mechanical properties of the RTM material are much more isotropic than for the single-layer fabric, presumably because of the crushing together and rumpling of the layers of cloth to achieve the high fibre volume fraction in the RTM process. In addition, fracture paths at failure in the single-layer and RTM material were found to be similar. As in the case of the model sandwich laminates, burning away the matrix of fractured RTM specimens showed that there were no tow fractures away from the region of composite failure.

An important difference between the RTM material and the model sandwich laminates was found to be the cracking damage development. The crack development in the RTM material was strongly dictated by the knitted fabric architecture. In the RTM material, the cracks are free to follow the paths in the knitted structure for all orientations, whereas in the model material crack propagation is dominated by the outer 0^0 fibre layers.

Since the RTM specimens were opaque, the cracking damage development was more difficult to be observed and crack densities were not measured. However, the reduction in the Poisson's ratio was used as an indication of matrix crack development.

Cyclic tests on the RTM specimens to progressively higher strains showed an elastic response for small strains, though it was difficult to say whether this was linear-elastic. For higher peak cyclic strains, hysteresis loops formed which were 'closed,' and a small residual strain occurred. For peak cyclic strains greater than the strain for the onset of matrix cracking (as indicated by the Poisson's ratio changes), the hysteresis loops do not 'close,' the residual strain increased on unloading, and the overall slope of the hysteresis loops decreased. The behaviour of these cyclic loops, together with the large pseudo-plasticity of the monotonic stress-strain curves, were explained in terms of the pulling out and stretching of knitted loops across matrix cracks.

Finally, cross-sections were taken from both model sandwich laminate specimens and RTM specimens, which were examined microscopically. Evidence of damage at loop-cross over points and debonding at yarn/matrix interfaces were found.

7.2.- FURTHER WORK.

An extensive research has been carried out here by obtaining detailed information on the knitted fabric reinforced composite. Mechanical properties and the mechanisms of damage accumulation and failure by tensile loading have been identified and analysed. However, there are many areas that could not be investigated at this time. Therefore some suggestions are made here for further work.

A two-dimensional analysis of the fibre architecture was carried out in this work, but is clear that this is not sufficient. It is suggested that a three-dimensional analysis is carried out and also that the unit cell of the fabric is identified. These two investigations will enable modelling of the mechanical properties to be attempted.

During monotonic testing of the RTM material, the reduction in the Poisson's ratio was taken as evidence of the onset of matrix cracking. At the moment, the evidence that the Poisson's ratio reduces when the matrix cracking begins in this material is indirect and based on observations of the model sandwich laminates used in this work (although other authors have also used the Poisson's ratio as a damage parameter). Hence, it would be valuable to attempt to show that changes in the Poisson's ratio are directly related to matrix cracking. To do this, it may be necessary to use a knitted carbon fabric with an epoxy resin matrix and to attempt to monitor the crack development using the dye-penetrant/X-ray technique.

The cyclic loading tests, which were carried out, showed that there were some unexpected effects with regard to the hysteresis loops (the loops did not close). These effects suggest that damage accumulation during cyclic loading, even to the same peak load, might be very rapid in these composites. However, there do not appear to be any studies in the literature of the fatigue performance of these materials. Hence, it would be useful to carry out some studies on their fatigue behaviour.

Finally, the experiments carried out here suggest that extensive pulling out of loops may occur across matrix cracks in these materials. If this is the case, then it would be interesting and important to investigate the knitted fabric composite degradation by the effect of external environment (particularly the effect of moisture).

REFERENCES

Agarwal, B. D and Broutman, L. J. ***"Analysis and Performance of Fibre Composites."*** Wiley Interscience Publication, 1980

Anwar, K.O., Callus, P.J., Leong, K.H., Curiskis, J.I. and Herszberg, I. ***"The Effect of Architecture on the Mechanical Properties of Knitted Composites."*** Volume 5, Textile Composites and Characterisation, pg. 328 –337, 1997.

Bannister, M. and Herzberg, I. ***"The Manufacture and Analysis of Composites Structures from Knitted Preforms".*** Fourth International Conference on Automated Composites, U.K., September 6-7, pg. 1 – 8, 1995.

Bassam, F., Boniface, L., Jones, K. and ogin, S.L. ***"On the Behaviour of the Residual Strain Produced by Matrix Cracking in Cross-ply Laminates."*** Composites Part A, 29A, Pg. 1425-1432, 1998.

Bishop, S.M. ***"Strength and Failure of Woven carbon-Fibre reinforced Plastics for High Performance Applications."*** Textile Structural Composites. Elsevier. 1989.

Boniface, L., Ogin, S.L. and Smith, P.A. ***"Damage Development in Woven Glass Fibre/Epoxy Laminates Under Tensile Loading."*** in Proceedings of the Second International conference on Deformation and Fracture of Composites, UMIST, pg 33.1-33.10, 1993.

Boniface, L., Ogin, S.L. and Smith, P.A. "***Strain Energy Release Rates and the Fatigue Growth of Matrix Cracks in Model Arrays in Composite Laminates.***" Proc Roy Soc, A432, pg 427-444, 1991.

Boniface, L.***"Damage Development in Fibre-reinforced Plastics Laminates".*** Thesis. University of Surrey, 1989.

Broutman, L. J. and Krock, R. H. "***Composite Materials, Volume 1: Interfaces in Matrix Composites***." Academic Press. 1974

Broutman, L. J. "***Modern Composite Materials***." Addison Wesley Publishing Company. 1967

Cox, B.N. and Davis, J.B. "***Knitted Composites for Energy Absorption Under Tensile Loading.***" Composites: part A 32, pg. 91-105, 2000.

Czigany, T; Ostgathe, M; Karger-Kocsis, J. "***Damage Development in GF/PET Composite Sheets with Different Fabric Architecture Produced of a Commingled Yarn***." Journal of Reinforced Plastics and Composites, Vol. 17, No. 3, pg. 251-267, 1998.

Daniel, I.M. and Ishai, O. ***"Engineering Mechanics of Composite Materials"***. Oxford University Press, 1994.

DeWalt, P.L. and Reichard, R.P. ***"Just How Good are Knitted Fabrics"*** Journal of Reinforced Plastics and Composites, Vol. 13, pg. 908- 917, October 1994

Fujii, T., Amijima, S. and Okubo, K. ***"Microscopic Fatigue Processes in a Plain-Weave Glass-Fibre Composite."*** Composites Science and Technology, vol 49, pg. 327-333, 1993.

Furness J. ***"Thermoset Composites".*** Materials Information centre, The Institute of Materials. 1999.

Gao, F., Boniface, L., Ogin, S.L., Smith, P.A. and Greaves, R.P. "***Damage Accumulation in Woven Fabric CFRP Laminates Under Tensile Loading: Part 1. Observations of Damage Accumulation.***" Composites Science and Technology 59, pg. 123-136, 1999a

Gao, F., Boniface, L., Ogin, S.L., Smith, P.A. and Greaves, R.P. ***"Damage Accumulation in Woven Fabric CFRP Laminates Under Tensile Loading: Part 2. Modelling the Effect of Damage on Macro-Mechanical Properties."*** Composites Science and Technology 59, pg. 137-145, 1999b

Garrett, K.W. and Bailey, J.E. ***"Multiple Transverse Fracture in 90° Cross-Ply Laminates of Glass Fibre-Reinforced Polyester."*** J Mater Sci, 12, pg. 157-164, 1997.

Gommers, B., Verpoest, I. and Van Houtte, P. ***"Determination of the Mechanical Properties of Composites Materials by Tensile Test. Part1. Elastic Properties."*** Journal of Composite Materials, Vol. 32, No. 4, pg. 129-136, 1998a.

Gommers, B., Verpoest, I. and Van Houtte, P. ***"Determination of the Mechanical Properties of Composites Materials by Tensile Test. Part II. Strength Properties."*** Journal of Composite Materials, Vol. 32, No. 2, pg. 453-460, 1998b.

Gommers, B., Verpoest I. and Van Houtte, P. ***"Analysis of Knitted Fabric Reinforced Composites: Part I. Fibre Orientation Distribution."*** Composites Part A 29A, pg. 1579, 1998c.

Gommers, B. and Verpoest I. ***"Tensile Behaviour of Knitted Fabric Reinforced Composites"*** ICCM-10, Vol IV, p. 309-316. 1995

Hamada, H., Sugimoto, K., Nakai, A., Takeda, N., Gotoh, S. and Ishida, T. ***"Mechanical Properties of Knitted Fabric Composites."*** Journal of Reinforced Plastics and Composites. Vol. 19, No. 05, pg. 364-376, 2000.

Harris, B. ***"Engineering Composite Materials."*** Second edition, IOM 1999.

Huang Z. M. and Ramakrishna S. ***"Micromechanical modelling approaches for the stiffness and strength of knitted fabric composites."*** Composites, Part A, vol 31, pg. 479-501, 2000.

Huang, Z. M., Ramakrishna, S., Dinner, H.P. and Tay, A.O. ***"Characterization of a Knitted Fabric Reinforced Elastomer Composite."*** Journal of Reinforced Plastics and Composites Vol. 18, No. 2, pg. 118-137, 1999(a).

Huang, Z. M., Ramakrishna, S. and Tay, A.O. ***"A Micromechanical Approach to the Tensile Strength of a Knitted Fabric Composite."*** Journal of Reinforced Plastics and Composites Vol. 33, No. 19, pg. 1758-1791, 1999(b).

Huysman, G., Verpoest, I. and Van Houtte, P. ***"A damage model for knitted fabric composites."*** Composites Part A, vol 32, pg. 1465-1475, 2001.

Huysmans, G. Verposet, I. and Van Houtte, P. ***"A Poly-Inclusion Approach for the Elastic Modelling of Knitted fabric Composites."*** Acta Mater. Vol 46, No.9, pg..3003-3013, 1998.

Kharrat, M., Chateuminoisgin, A., Carpentier, L. and Kapsa, P. ***"On the Interfacial Behaviour of a Glass/Epoxy Composite During a Micro-indentation Test; Assessment of Interfacial Shear Strength Using Reduced Indentation Curves."*** Composites Part A 28A, pg. 39-46, 1997.

Kinloch, A.J. and Young, R.J. ***"Fracture Behaviour of Polymer"*** Applied Science, London, 1983.

Lee, J. W. and Daniel, I. M. ***"Progresive Transverse Cracking of Crossply Composite Laminates."*** Journal of composite Materials. 24 (11) pg. 1225-1243, 1990.

Leong, K.H., Ramakrishna, S., Huang Z.M. and Bibo G.A. ***"The Potential of Knitting for Engineering Composites-A Review"*** Composites part A 31, pg.197-220. 2000

Leong, K.H., Falzon, P.J., Bannister, M. and Herszberg, I. ***"An Investigation of the Mechanical Performance of Weft Knitted Milano Rib Glass/Epoxy Composites."*** Composites Science and Technology. 58, pg. 239-251, 1998.

Leong, K.H., Ramakrishna, S. and Hamada, H. ***"The Potential of Knitting for Engineering Applications"*** 5th Japan SAMPE Symposium. Tokyo, Japan. pg. 623-632, 1997a.

Leong, K. H., Nguyen, M. and Herzberg, I. ***"The Effects of Deforming Knitted Glass Preforms on the Tensile Properties of resultant Composite Laminates."*** ICCM-11, Goald Coast, Australia, 14th -18th , pg. 201-210, July 1997b.

Leong, K. H., Bannister, M., Herzberg, I. and Falzon, P. J. ***"Bearing Strength of Glass/epoxy Composites Manufactured from Weft-Knitted E-glass Fabric."*** The First Australasian Congress on Applied Mechanics, ACAM-96. Australia, pg. 987-994, February 21-23, 1996.

Lim, T.C., Ramakrishna, S. and Shang H.M. ***"Effect of Textile Geometry on Axisymmetric Stretch Forming of Knitted Fabric Composites."*** Proc. Instn. Mech. Engrs. Vol 214 Part B. pg. 333-338, 2000.

Lim, T.C.; Ramakrishna, S.; Shang, H.M. ***"Optimisation of the Formability of Knitted Fabric Composite Sheet by Means of Combined Deep Drawing and Stretch Forming."*** Journal of Materials Processing Technology 89-90, pg. 99-103, 1999.

Marsden, W. ***"Damage Accumulation in a Woven Fabric Composite."*** PhD Thesis, University of Surrey, 1996.

Marsden, W., Boniface, L., Ogin, S.L. and Smith, P.A. ***"Quantifying Damage in Woven Glass Fibre/Epoxy Laminates."*** In proceedings FRC '94, Sixth International Conference on Fibre Reinforced Composites,. Newcastle upon Tyne, paper 31. 1994.

Matsumoto, T. ***"Fracture Mechanics Approach to Fatigue Life of Discontinuous Fibre Reinforced Composites."*** PhD Thesis, University of Michigan.2000

Matthews, F.L. and Rawlings, R.D. ***"Composite Materials: Engineering and Science".*** Chapman and Hall, 1994.

Miller E. ***"Introduction to Plastics and Composites: Mechanical Properties and Engineering Applications"*** Marcel Dekker, Inc. 1996

Mouritz. A.P., Leong, K.H. and Herszberg, I. ***"A Review of the Effect of Stitching on the In-plane Mechanical Properties of Fibre-Reinforced Polymer Composites."*** Composites Part A 28A, pg. 979-991, 1997.

Naik, R. A., Ifju, P. G. and Masters, J. E. ***"Effect of Fibre Architecture Parameters on Deformation Fields and Elastic Moduli of 2-D braided composites"***. Journal of Composite Materials, vol 28, pg. 656-681, 1994

Naik, N.K. and Shembekar, P.S. ***"Elastic Behaviour of Woven Fabric Composites: I-Lamina Analysis."*** Journal of Composite Materials, Vol. 26, pg. 2196-2225. 1992.

Nakai, A., Ohtani, A., Yamanouchi, M. and Hamada, H. ***"Fracture and Mechanical Properties of Knitted Fabric Composites."*** ICCM13. pg. 1265-1275, Beijing, China, May, 2001.

Naveen, V.P., Vani, A., Prakasha, V. and Rao, R.M. ***"Studies on Mechanical Behaviour of Knitted Glass-Epoxy Composites."***, Journal of Reinforced Plastics and Composites. Vol. 19, No. 05, pg. 245-250, 2000.

Nguyen, M., Leong, K.H. and Herszberg, I. ***"The Effects of Deforming Knitted Glass preforms on the Composite Compression Properties."*** 5th Japan SAMPE Symposium. Tokyo, Japan. October, pg. 765-769, 1997.

Ogin S. L.***"Textile-Reinforced Composite Materials."*** In Handbook of technical textiles," edited by Horrocks A R and Anand S C, published by Woodhead Publishing Limited, pg. 264-281, 2000.

Ogin S. L. ***"From Stiffness Reductions to Optical Fibre Sensors: The Usefulness of Shear-lag Analysis in Damage Accumulation Studies on Composite Laminates."*** In Proceedings of the International Conference on Advanced Technology in Experimental Mechanics '99, Yamaguchi, Japan, pg. 174-180, 1999

Ogin, S. L. ***"Textile-Reinforced Composite Materials."*** Composite Materials Technology, Course Notes. Lecture 8. University of Surrey. 1998.

Ogin, S. L., Smith, P. A. and Beaumont, P. W. ***"Matrix Cracking and Stiffness Reduction During the Fatigue of a $[0/90_2]_s$ GFRP Laminate."*** Composite Science Tecyhnology. 22, pg. 23-31. 1985.

Papargyris, A. D., Cooke, R. G., Papargyri, S. A. and Botis, A. I. ***"The Acoustic Behaviour of Bricks in Relation to their Mechanical Behaviour"***. Construction and Building Materials. Vol. 12, Issue 17. pg. 361-369, October 2001.

Peled, A. and Bentur, A. ***"Geometrical Characteristics and Efficiency of Textile Fabrics for Reinforcing Cement Composites."*** Cement and Concrete Research, 30, pg. 781-790. Pergamon. 2000.

Pink, E. and Campell, J.D. ***"The Low-Temperature Macro Deformation of an Epoxide Resin"***, Materials Science and Engineering, 15, pg. 187-196, 1974.

Raju, I. S., Foye, R. L. and Avva V. S. ***"A Review of Analytical Methods for Fabric and Textile Composites"*** in Proceedings of the Indo-US workshop on Composites for Aerospace Applications: Part 1, Bangalore, India, pg. 129-159, 1990.

Ramakrishna, S., Zheng Ming Huang, and H.M. Yew. ***"Development of a Novel Flexible Composite Material."*** Journal of Materials Processing Technology 89-90, pg. 473-477, 1999.

Ramakrishna, S., Coung, N. K. and Hamada, H. ***"Tensile Properties of Plain Weft Knitted Glass Fiber Fabric Reinforced Epoxy Composites."*** Journal of Reinforced Plastics and Composites, Vol, 16, No. 10, pg. 946-963, 1997a.

Ramakrishna, S. ***"Characterisation and Modelling of the Tensile Properties of Plain Weft-Knit Fabric-Reinforced Composites"*** Composites Science and Technology 57 pg. 1-22, 1997b.

Ramakrishna, S, and Hull, D. ***"Tensile Behaviour of Knitted Carbon-Fibre-Fabric/Epoxy Laminates. Part I: Experimental."*** Journal of Composites Science and Technology, Vol. 50, No. 2, pg. 237-247. 1994a

Ramakrishna, S. and Hull, D. ***"Tensile Behaviour of Knitted carbon-Fibre Fabric/Epoxy Laminates- Part II: Prediction of Tensile Properties. Composite Science and Technology."*** Vol. 50, pg. 249-258. 1994b

Rios, C. R. ***"Orientational Dependence of the Mechanical Properties, and Quantification of the Damage Accumulation of a Knitted Fabric Reinforcement Composite"*** MSc. Thesis. University of Surrey. 1998.

Rozant, O., Bourban, P. E. and Manson, J. A. E. ***"Warp Knit Laminates for Stampable Sandwich Preforms."*** Composite Science and technology 61, pg. 145-156. 2001.

Ruan, X. and Chou, T.W; ***"Failure Behaviour of Knitted Composites. Journal of Composite Materials,"*** Vol. 32, No. 31, pg. 198-221, 1998.

Savci, S. Curiskis, J.I. and Pailthorpe, M.T. ***"A Study of Deformation of weft-knit Preforms for Advanced Composite Structures. Part 1: Dry performs properties."*** Composites Science and Technology 60, pg. 1931-1942. 2000.

Savci, S. and Curiskis, J.I. ***"Weft-Knitted Glass-Fibre Preforms for Composite Materials."*** Volume V: Textile Composites and Characterisation. Pg. 338–347. 1997.

Scardino F. ***"An Introduction to Textile Structures and Their Behaviour. Textile Structural Composites,"*** Chapter 1, Composite Materials series vol.3, eds. Chou T.W. and Ko F.K, Elsevier. 1989.

Schaffer, J. P., Saxena, A., Antolovich, S. D., Sanders, T. H. and Warner, S. B. ***"The Science and Design of Engineering Materials".*** Mc Graw-Hill International. Second edition. 1999.

Smith, P. A. and Wood, J. R. ***"Poisson's ratio as a Damage Parameter in the Static Tensile loading of Simple Crossply Laminates."*** Composite Science and Technology. 38, pg. 85-93. 1990

Spencer, D. J. ***"Knitting Technology"*** Second Edition. Woodhead Publishing limited. 1998.

Stumpf, H., Mader, E., Baeten, S., Pisanikovski, T., Zah, W., Anderson, C.H., Verpoest, I. and and Schulte, K. ***"New Thermoplastic Composite performs based on Split-Film Warp-Knitting."*** Composites Part A 29A, pg. 1511-1523. 1998.

Stumpf, H. and Schutle, K. ***"QUICKTEMP – A New Short-Cycle-Time Manufacturing Method for Thermoplastic Composites Made from Low-Cost Textile Preform."*** Journal of Composites technology and Research, Vol. 19, No 4, pg. 222-227, October 1997.

Sugun, B. S. and Rao, M. V. ***"Drop Weight Impact Studies on Rib-Knit RTM Laminates."*** Journal of Reinforced Plastics and Composites. Vol. 19, No. 06, pg. 492-508, 2000.

Svensson, N., Shishoo, R. and Gilchrist, M. ***"Interlaminar Fracture of Commingled GF/PET Composite Laminates."*** Journal of Reinforced Plastics and Composites. Vol. 32, No. 20, pg. 1808- 1835, 1998.

Verpoest, I. and Dendauw, J. ***"Mechanical Properties of Knitted Glass Fibre/Epoxi Resin laminates."*** 37th International SAMPE Symposium, march 9-12, pg. 367-377, 1992.

Verpoest, I., Gommers, B., Huysmans, G., Ivens, J., Luo, Y., Pandita, S. and Philips, D. ***"The Potential of Knitted Fabrics as a Reinforcement for Composites"***. Proc ICCM-11, Gold Coast, Australia, vol 1, pg. 108-119. 1997

Wang. Y., Li, J. and Do, P.B. ***"Properties of Composite Laminates reinforced with E-Glass Multiaxial Non-Crimp Fabrics."*** Journal of Reinforced Plastics and Composites. Vol. 29, No. 17, pg. 2317- 2333, 1995.

Wu, W.L., Hamada, H., Kotaki, M. and Maekawa, Z. ***"Design of Knitted Fabric Reinforced Composites."*** Journal of Reinforced Plastics and Composites. Vol. 14. pg. 327- 332, October 1995.

Wu, W.L., Kotaki, M., Fujita, A., Hamada, H., Inoda, M. and Maekawa, Z. ***"Mechanical Properties of Warp-Knitted Fabric Reinforced Composites."*** Journal of Reinforced Plastics and Composites. Vol. 12. pg. 576- 581, October 1993.

Xue, P., Yu, T.X. and Tao, X.M. ***"Effect of Cell Geometry on the Energy-Absorbing Capacity of Grid-Domed Textile Composites."*** Composites: Part A 31, pg. 861-868. 2000.

Yu,T.X., Tao, X.M. and Xue, P. ***"The Energy-absorbing Capacity of Grid-domed Textile Composites."*** Composite Science and Technology 60, pg. 785-800, 2000.